ASSESSING A NOVEL APPROACH TO PHARMACEUTICAL REMOVAL FROM WASTEWATER: AEROBIC GRANULAR SLUDGE

by

Kylie Brigitta Bodle

A dissertation submitted in partial fulfillment
of the requirements for the degree

of

Doctor of Philosophy

in

Engineering

MONTANA STATE UNIVERSITY
Bozeman, Montana

May 2024

DEDICATION

Dedicated to Griffin, Brynna, and Mom and Dad.

But mostly dedicated to me, because in the words of the great Leslie Knope, “I am big enough to admit that I am [sometimes] inspired by myself.”

ACKNOWLEDGEMENTS

Thank you to my committee members for their advice, guidance, and support over the years: Dr. Catherine Kirkland, Dr. Ellen Lauchnor, Dr. Heidi Smith, and Dr. Craig Woolard. In particular, I am endlessly thankful to my advisor, Dr. Kirkland, for her time, personal and professional advice, and willingness to always lend an ear and talk things through with me. I could not have asked for a better advisor and friend and feel incredibly lucky to have learned from her.

Thank you to everyone at the Center for Biofilm Engineering for providing such an amazing place to work. The opportunities to learn, collaborate, and improve as a scientist were invaluable, and I feel so lucky to have worked in the CBE as long as I have.

Special thanks to Heidi Smith for her assistance with anything microscopy related. I am especially grateful to Rebecca Mueller, Hannah Goemann, and Chiachi Hwang for their assistance with 16S gene analyses. Thank you to all members of the Kirkland lab group and especially to Maddy Pernat for all of her help with lab work. I am also grateful to Merle de Kreuk at Delft University of Technology for her advice and troubleshooting help with granule growth. Thanks also to Terry Reid and Chris Roegner at the Rockford, IL AquaNereda® plant for their help with sampling and shipping granules. Many thanks also to Don Smith and Jesse Thomas at the MSU Mass Spectrometry Facility—thank you so much for teaching me about mass spectrometry and for providing advice on method development.

Lastly, thank you to my partner, Griffin Stevens, my family, and my friends for their constant support.

TABLE OF CONTENTS

1. INTRODUCTION 1

Background 1
Dissertation Overview 3
Funding and Collaborations 6

2. A BRIEF REVIEW OF WASTEWATER TREATMENT, EMERGING CONTAMINANTS, AEROBIC GRANULAR SLUDGE, AND PERTINENT ANALYTICAL TECHNIQUES 7

A Brief Summary of Wastewater Treatment 7
An Update to Wastewater Treatment: Aerobic Granular Sludge 10
Aerobic Granular Sludge: A Potential Solution to Pharmaceutical Contamination 13
Erythromycin 15
Diclofenac 16
Gemfibrozil 17
Methods Overview 18
UPLC-QTOF-MS 18
Fluorescence Microscopy 21
Nucleic Acid Sequencing 23
Conclusions 26

3. PHARMACEUTICAL SORPTION TO LAB MATERIALS MAY OVERESTIMATE RATES OF REMOVAL IN LAB-SCALE BIOREACTORS 27

Contribution of Authors and Co-Authors 27
Manuscript Information 28
Abstract 29
Introduction 29
Methods 31
AGS Reactor Operation 31
Pharmaceutical Compound Quantification 33
Lab Supply Sorption Tests 34
Pipette Tip Testing. 36
Syringe Filter Testing. 37
Tubing Testing. 37
Results and Discussion 38
Loss to Lab Supplies 38
Pipette Tips. 38
Syringe Filters. 40
Pharmaceutical Dosing into AGS Sequencing Batch Reactor 41

TABLE OF CONTENTS CONTINUED

Sorption to Tubing. 43
Conclusions 47
Declarations 47

4. TREATMENT PERFORMANCE AND MICROBIAL COMMUNITY STRUCTURE IN AN AEROBIC GRANULAR SLUDGE SEQUENCING BATCH REACTOR AMENDED WITH DICLOFENAC, ERYTHROMYCIN, AND GEMFIBROZIL 49

Contribution of Authors and Co-Authors 49
Manuscript Information 50
Abstract 51
Introduction 51
Methods 53
AGS Reactor Operation 53
Analytical Methods – Conventional Wastewater Analytes 55
Analytical Methods – Pharmaceutical Analyses 55
Bacterial Community Composition 59
DNA/RNA Extraction. 59
Metagenome Characterization. 59
16S Library Preparation and Sequencing. 61
Statistics and Data Analysis. 61
Results 63
Pharmaceutical Impacts on Granular Wastewater Treatment Performance 63
Pharmaceutical Removal 65
Diclofenac. 68
Erythromycin. 69
Gemfibrozil. 71
Functional Potential of Granules from Shotgun Metagenomics 73
Active Microbial Community Response to Pharmaceuticals 76
Discussion 80
Links Between Active Bacterial Community, Wastewater Treatment, and Pharmaceutical Degradation 80
Patterns in Taxonomic Shifts in Microbial Communities 84
Conclusions 85
Funding 85
Acknowledgements 86
Declaration of Competing Interests 86

TABLE OF CONTENTS CONTINUED

5. PHARMACEUTICAL IMPACTS ON AEROBIC GRANULAR SLUDGE MORPHOLOGY AND POTENTIAL IMPLICATIONS FOR ABIOTIC REMOVAL 87

Contribution of Authors and Co-Authors 87
Manuscript Information 88
Abstract 89
Introduction 89
Methods 92
Sequencing Batch Reactor Operation 92
Analytical Methods 94
Batch Experiments 96
Microscopic Analyses 98
Results 99
Reactor Performance 99
Batch Experiments / Adsorption Isotherms 101
Pharmaceutical Fate 103
Diclofenac. 104
Erythromycin. 104
Gemfibrozil. 105
Changes in Morphology 107
Discussion 110
Pharmaceutical Sorption in Batch Versus SBR 110
Potential Impacts of Declining Lipid Content on Sorptive Capacity and SVI_3 116
Conclusions 118
Funding 119
Acknowledgements 119
Declaration of Competing Interests 119

6. ENVIRONMENTALLY-GROWN AEROBIC GRANULAR SLUDGE RESPONSE TO PHARMACEUTICALS: IMPACTS ON WASTEWATER TREAMENT EFFICACY, ACTIVE MICROBIAL COMMUNITIES, AND PHARMACEUTICAL FATE 120

Contribution of Authors and Co-Authors 120
Manuscript Information 121
Abstract 122
Introduction 122
Methods 125
SBR Operation 125
Analytical Methods 128

TABLE OF CONTENTS CONTINUED

Wastewater Analytes and Pharmaceuticals. 128
Microscopy. 130
Bacterial Community Composition 131
DNA/RNA Extraction. 131
16S Library Preparation and Sequencing. 132
Statistics and Data Analysis. 132
Results and Discussion 133
Wastewater Treatment Performance 133
Pharmaceutical Fate and Removal 135
Diclofenac. 136
Erythromycin. 144
Gemfibrozil. 146
AGS Structural Characteristics 148
Active Microbial Community Shifts and Potential Links with Wastewater Treatment and Pharmaceutical Degradation 153
Conclusions 160
Funding 161
Acknowledgements 161
Declaration of Competing Interests 162

7. CONCLUSIONS AND FUTURE WORK 163

Conclusions: Lab- Versus Environmentally-Grown AGS 163
Recommendations for Future Work 167

CUMULATIVE REFERENCES CITED 174

APPENDICES 191

A: SUPPLEMENTARY MATERIALS FOR CHAPTER 4 192
Supplementary Methods – Pharmaceutical Extraction from Granules 195
Removal Calculation for All Analytes (Pharmaceuticals and Nutrients) 195
Results 196

B: SUPPLEMENTARY MATERIALS FOR CHAPTER 5 203
Recovery Calculation for Pharmaceuticals 204
Removal Calculation for All Analytes (Pharmaceuticals and Nutrients) 205
Test SBR Sorption Capacity Calculations 211
Key Terms. 211

TABLE OF CONTENTS CONTINUED

Calculations..... 211

C: SUPPLEMENTARY MATERIALS FOR CHAPTER 6..... 213
Spike-Recovery Testing..... 215
"Corrected Peak Area" Calculations for Degradation Products 216
Removal Calculations for All Analytes 217

D: MISC. METHODS USED IN PRELIMINARY EXPERIMENTS..... 224
Starved AGS Batch Tests..... 225
Fluorescence in situ Hybridization (FISH) 228

E: LABVIEW PROGRAM CODE USED FOR SBR CONTROL 231

LIST OF TABLES

Table Page

1. Table 2.1. Stains used to visualize different EPS components in granules [17]. 23

2. Table 3.1. Physical and chemical properties of tested pharmaceuticals. 32

3. Table 3.2. Lab supplies tested for pharmaceutical loss. Catalog numbers are included in parentheses. 35

4. Table 4.1. Physical and chemical properties of tested pharmaceuticals, as well as average extraction recoveries and retention times. 57

5. Table 5.1. Batch sorption experiment conditions. All concentrations listed are approximate and were measured immediately after adding AGS. High NH_3 and PO_4 concentrations were selected based on their average concentrations at the end of the fill phase in both reactors, as concentrations of each anion peaked at this point in SBR operation. Anaerobic phosphate release by phosphate accumulating organisms resulted in approximately 700 mg/L PO_4 at the end of the fill phase; dilution of the influent medium with liquid remaining in the SBR resulted in NH_3 concentrations of approximately 30 mg/L. 98

6. Table 5.2. Fitted constants and R^2 values for the Henry and Freundlich isotherms for each pharmaceutical. 103

7. Table 5.3. Average fractions of EPS components in 30 μm granule sections throughout the experiment. Values were calculated using granule sections taken from the approximate center of three different granules. One-tailed p-values were calculated from two-sample t-tests assuming unequal variance ($\alpha = 0.05$) and reflect comparisons of t0 and t80 values. Note that fractions sum to over 1 for reasons discussed in the text. 108

8. Table 6.1. Average fractions of EPS components in granules at day zero and day 66. Note that multiple components overlay each other, and therefore fractions sum to greater than 1. Values were calculated using 30 μm sections taken from the center of three different granules. 151

LIST OF TABLES CONTINUED

Table Page

9. Table A.1. Suspected degradation products screened for in all samples. This PCDL was constructed after reviewing relevant literature. Not all compounds listed were detected (indicated by "-"). Compounds with the same residence time could not be distinguished from one another and therefore were not reported. Both sodium and hydrogen adducts of gemfibrozil degradation products were often detected; for samples in which both adducts were present, peak areas were summed together and this total area was corrected as described in the main article. 194

10. Table A.2. Predicted toxicity of detected degradation products using EPA TEST software. A higher resolution version of this table can be found at https://www.frontiersin.org/articles/10.3389/frmbi.2023.1242895/full#supplementary-material 202

11. Table B.1. The composition of the influent media, adapted from [88]. 204

12. Table B.2. Physical and chemical properties of tested pharmaceuticals, as well as average extraction recoveries and retention times. 205

13. Table C.1. Physical and chemical properties of tested pharmaceuticals, as well as average extraction recoveries, retention times, and quantification limits. The method for recovery assessment is detailed below. 214

14. Table C.2. Suspected degradation products screened for in all samples. This PCDL was constructed after reviewing relevant literature. Not all compounds listed were detected (indicated by "-"). Compounds with the same residence time could not be distinguished from one another and therefore were not reported. Both sodium and hydrogen adducts of gemfibrozil degradation products were often detected; for samples in which both adducts were present, peak areas were summed together and this total area was corrected as described below. 215

15. Table D.1. FISH probes used in preliminary experiments, discussed in Chapter 7. *Indicates dual-labelled probe as described in [196]. 230

LIST OF FIGURES

Figure Page

1. Figure 1.1. Left: AGS from a full-scale treatment plant settled beneath a layer of floccular conventional activated sludge and clear water (image credit to Catherine Kirkland). Right: General schematic of oxic zones and bacterial population distributions within a single granule. Acronyms: AOB, ammonia oxidizing bacteria; NOB, nitrite oxidizing bacteria; PAOs, phosphate accumulating organisms; GAOs, glycogen accumulating organisms. 1

2. Figure 2.1. The modified Bardenpho process. The classic Bardenpho process does not utilize a second aerobic chamber [15]. 9

3. Figure 2.2. AGS-SBR schematic with each phase of operation shown. Both aerobic and anoxic conditions are possible during the aeration phase due to oxygen gradients within granules. Anaerobic conditions return during the settling and discharge phases; feeding new influent wastewater through the settled granule bed maintains these conditions as high organic carbon concentrations encourage consumption of any remaining oxygen by heterotrophs..... 13

4. Figure 2.3. Left: The EIC for compounds with an m/z approximately equal to 296.024. To determine which peak belongs to DCF, the mass spectra for compounds eluting at 1.5 and 8.5 minutes must be consulted. The mass spectrum for the compound eluting at 1.5 minutes does not match that for DCF (not shown); however, the mass spectrum for the compound eluting at 8.5 minutes matches that for DCF (right image). Therefore, the EIC peak area at 8.5 minutes can be correlated with DCF concentrations. 21

5. Figure 2.4. Granule sections stained to indicate different EPS components. Left, a granule from the AquaNereda® plant in Rockford, IL; right, a granule grown in the lab. Proteins (green), lipids (blue), alpha-polysaccharides (red), and beta-polysaccharides (pink) are indicated. EPS distributions differ widely between the two granule samples: lab-grown granules' EPS appear more stratified than those in the environmentally-grown granule. 23

LIST OF FIGURES CONTINUED

Figure Page

6. Figure 4.1. Total nitrogen and phosphate removal in the control and test SBR during the pharmaceutical dosing period. Note that N removal data in the control reactor is not plotted after day 40 because an acid overdose in the control reactor severely inhibited nitrifying populations. Given trends prior to the acid overdose, it is likely that nitrogen removal in the control would have proceeded at 100% if not for this issue. Nitrogen and phosphate removal in the test reactor averaged out at 73 ± 2% and 63 ± 6%, respectively, over the last 40 days of the experiment. 64

7. Figure 4.2. Pharmaceutical removal versus time. Removal was calculated based on a mass balance using measured influent and effluent concentrations (Appendix A equations A1 and A2). Negative removal percentages indicate that effluent concentrations were higher than predicted by the mass balance. 65

8. Figure 4.3. Top row, A-C: aqueous degradation products detected over time in the effluent (dashed and dotted lines) from the test reactor for DCF, ERY, and GEM, respectively. Y-axes all reflect corrected peak area but differ in scale. ERY-associated degradation products were temporarily detected in the influent (solid lines) to the test reactor. However, corrected peak areas of both ERY-associated products were generally higher in the effluent than influent, and therefore AGS-driven biodegradation of these compounds was likely occurring. Bottom row, D-F: solid phase degradation products for DCF, ERY, and GEM, respectively. Note that y-axes differ in scale though each reflects corrected peak area per g AGS. Points not connected by a line indicate detections in control granules. DCF3 was detected three times in control granules, likely due to cross-contamination during mass spectrometry analyses. Likewise, GEM1 was detected twice in control granules. Error bars, representing standard deviation of triplicate samples, are present for both aqueous and solid data on days 34, 56, and 80, and at times are smaller than sample points. Points on these days are averages. 66

LIST OF FIGURES CONTINUED

Figure Page

9. Figure 4.4. A multigene phylogeny of assembled MAGs and the level of completeness for nitrogen cycling pathways. Organisms identified from the assembled MAGs were from a range of families, with a large number in the Pseudomonadota (e.g., Competibacteraceae, Rhodocyclaceae) and the Bacteroidota. *Phyla, rather than family, are listed when the GTDB-provided family name corresponds to an uncultivated organism. None of the assembled MAGs contained the ammonia oxidation pathway, but multiple MAGs had complete denitrification pathways, primarily for dissimilatory nitrate reduction. Note that granule numbering is arbitrary and was simply used to differentiate different samples. 75

10. Figure 4.5. The relative abundance of active families in both reactors over time. Only families with relative abundance greater than or equal to 1% at at least one time point are plotted. Sampling times were matched across both reactors; for this reason, relative abundance data between days 31 and 55 are not plotted, since the control reactor was shut down during this time. 79

11. Figure 4.6. Semi-log plots of the relative abundance of active (A) and non-active (B) nitrifiers (summed Nitrosomonadaceae and Nitrospiraceae families) over time in control and test reactors. Over the first 38 days, active nitrifiers were more abundant in the test reactor than the control; however, from days 55-80, active nitrifiers were more abundant in the control SBR. Active nitrifiers also declined in relative abundance in the test reactor throughout the dosing period. The control SBR was shut down from days 40-50 and therefore data is not available in that timeframe; this is also likely why active nitrifiers in the control reactor are present at slightly lower relative abundances in the second half of the experiment than the first. Inactive nitrifiers were present at similar levels in both reactors throughout the test. 83

12. Figure 5.1. Effluent concentrations of ammonia and phosphate from the control and test reactors. Control effluent ammonia concentrations are not plotted past day 40 for reasons discussed in the text. Influent concentrations of both ammonia and phosphate were approximately 60 mg/L. Note that effluent phosphate concentrations peak above this value due to the activity of phosphate accumulating organisms, which release phosphate during the anaerobic phase of SBR operation. 101

LIST OF FIGURES CONTINUED

Figure Page

13. Figure 5.2. Batch adsorption data fit to (A) Henry and (B) Freundlich isotherms. Error bars all indicate standard deviation of triplicate samples and at times are smaller than sample points. Error bars in the x-direction indicate the standard deviation of C_e values for triplicates; those in the y-direction indicate the standard deviation of q_e values..... 103

14. Figure 5.3. Pharmaceutical concentrations in the aqueous (top row) and solid phase (bottom row) over time. Error bars represent the standard deviation of triplicate samples and are present on days 34, 56, and 80 for aqueous samples and days 34 and 80 for solid samples; points on these days are averages. Data in this image were originally published in [142] and are shown here with permission from the authors. 106

15. Figure 5.4. EPS component distributions in control and test granules over time. Green indicates proteins (fluorescein isothiocyanate stain); blue, lipids (nile red); red, alpha-PS (concanavalin A); pink, beta-PS (calcofluor white). All scale bars are 200 μm. 109

16. Figure 5.5. Sorbed masses of DCF, ERY, and GEM in batch tests versus time (based on a mass balance from aqueous measurements). Error bars indicate the standard deviation of triplicate samples and are at times smaller than sample points..... 113

17. Figure 6.1. Percent inhibition of nitrogen and phosphate removal versus time. Percent inhibition values below zero indicate that removal of nitrogen or phosphate was higher in the test reactor than the control. Phosphate removal was largely uninhibited throughout dosing; nitrogen removal was particularly inhibited between days 27-48. 134

18. Figure 6.2. Pharmaceutical removal in the test SBR. Removals below zero signify that effluent concentrations were higher than those predicted by a mass balance and should be interpreted as 0% removal. 136

LIST OF FIGURES CONTINUED

Figure Page

19. Figure 6.3. Influent and effluent pharmaceutical concentrations (top row) and solid phase pharmaceutical concentrations (bottom row) versus time. Error bars are present on days 28 and 67 for aqueous samples and day 67 for solid phase samples and reflect the standard deviation of triplicate sample extractions; values on these days are averages. Solid phase concentrations at day "-1" indicate background pharmaceutical concentrations in the granules. 140

20. Figure 6.4. A-C: Aqueous phase degradation products versus time. Dashed or dotted lines indicate products detected in the effluent; solid lines indicate those found in the influent. Note that all y-axis scales are different, though all reflect corrected peak area. Error bars are present on days 28 and 67 and indicate the standard deviation of triplicate samples; bars may be smaller than sample points. D: Solid phase GEM degradation products. Solid phase DCF and ERY degradation products were not detected throughout the experiment. 141

21. Figure 6.5. Aqueous parent pharmaceutical concentrations throughout a single SBR cycle on the final day of the experiment (day 67). Open symbols at time zero indicate influent concentrations. Filled symbols at time zero indicate mass-balance predicted final concentrations in the reactor at the end of the fill phase (calculated with Equation C4). The actual concentration measured at the end of the fill phase is shown at 70 minutes. Concentrations at 180 minutes reflect those in the effluent. Error bars on influent and effluent points reflect the standard deviation of triplicate samples and are smaller than sample points for some pharmaceuticals. 142

22. Figure 6.6. Aqueous phase degradation products detected throughout one SBR cycle on day 67. Open symbols at time zero for ERY1, ERY2, and GEM 3 indicate the presence of these degradation products in the influent. Note that y-axis scales are not equivalent, though all reflect corrected peak areas. Error bars on influent and effluent points reflect the standard deviation of triplicate samples and are smaller than sample points for some compounds. 143

LIST OF FIGURES CONTINUED

Figure Page

23. Figure 6.7. EPS component distributions in test granules at day zero (top row) and day 66 (bottom row). All scale bars are 200 μm. Statistically significant changes in fractions of each component were not found, excepting beta-polysaccharides, which decreased from 0.41 ± 0.04 of the total section biovolume at day zero to 0.27 ± 0.08 on day 66 ($p = 0.04$). Notably, beta-polysaccharide fractions in control granules also decreased to 0.35 ± 0.09—a concentration that was not statistically significantly different from beta-PS fractions in test granules at day 66. For this reason, declines in beta-PS fractions in test granules may be a consequence of AGS adaptation to the lab environment, not pharmaceutical exposure. 152

24. Figure 6.8. Relative abundances of active families versus time. Only families with relative abundance greater than or equal to 1% at at least one time point are plotted. ZOTUs that could not be classified at the family level with over 70% confidence were grouped by the next highest taxonomy level at which they could be confidently classified. The Control time zero sample reflects characteristics of the granular inoculum; the Test sample at time "13f" reflects characteristics of a sample of the floc washout that occurred on day 13. Families for which relative abundance was less than 1% were summed and are grouped as "Others" at each time point. 155

25. Figure 6.9. rRNA counts for phantom taxa, grouped at the family level, plotted versus time. Counts are only plotted for families in which over 50 counts occurred in at least 25% of samples. Taxa that could not be classified at the family level with over 70% confidence were grouped by the next highest taxonomy level at which they could be confidently classified. The Control time zero sample reflects characteristics of the granular inoculum; the Test sample at time "13f" reflects characteristics of a sample of the floc washout that occurred on day 13. 156

26. Figure 7.1. Pharmaceutical removal after 15 days versus initial dosed concentration in starved granule batch tests. AGS were capable of near-complete biodegradation (> 90% removal) of all three compounds at up to a 500 μg/L starting concentration. GEM was at least 95% biodegraded at up to a 2 mg/L starting concentration. 170

LIST OF FIGURES CONTINUED

Figure Page

27. Figure 7.2. FISH images of lab-grown (A-C) and environmentally-grown (D-F) AGS. Figures A and D show the whole granule section at 10x magnification; Figures B, C, E, and F are images collected at 100x magnification of different areas of the granules shown in A and D. Color key: green, all bacteria; blue, PAOs; red/orange, nitrifiers; lavender, GAOs. 172

28. Figure A.1. Schematic of the sampling port from which influent samples were taken. During the anaerobic feed phase, the influent sampling port tubing was briefly unclamped to allow collection of samples for influent pharmaceutical and nutrient concentrations..... 193

29. Figure A.2. Ammonia removal throughout the dosing period in the control and test reactor. Ammonia concentrations in the control reactor are not reported after day 40 due to a reactor operation issue, discussed in the main article body. Ammonia oxidation in the test reactor was the most inhibited nitrogen removal process—nitrite oxidation and denitrification proceeded at levels near equal to those in the control reactor, evidenced by equivalent nitrite and nitrate concentrations in both reactors (Figure A.3). 196

30. Figure A.3. Effluent concentrations of ammonia (NH_3), nitrite (NO_2), and nitrate (NO_3) versus time in the control and test reactors. Effluent ammonia concentrations are not reported past day 40 in the control reactor for reasons discussed previously (see Figure A.2 caption). 197

31. Figure A.4. Total dissolved organic carbon (DOC) removal throughout the dosing period in both SBRs. Note that excess DOC was accidentally fed in the first 10 days, resulting in lower DOC removal by the test reactor..... 197

32. Figure A.5. DOC consumption in the anaerobic feed phase of reactor operation. Though more DOC was consumed anaerobically in the control reactor than the test, most DOC consumption in the test SBR continued to occur anaerobically (70 ± 7%). 198

33. Figure A.6. Parent pharmaceutical concentrations in the aqueous (top row) and solid phase (bottom row) over time. Error bars represent the standard deviation of triplicate samples and are present on days 34, 56, and 80; points on these days are averages. 199

LIST OF FIGURES CONTINUED

Figure Page

34. Figure A.7. Non-metric multidimensional ordination of community similarity for the control (closed symbol) and test (open symbol) communities. The active community is delineated based on rRNA transcript to gene ratios (triangle symbols); the total community on DNA reads (circles); and lastly the total RNA pool is shown with diamond symbols. 200

35. Figure A.8. Phylogenetic tree of reference 16S sequences downloaded from GTDB (v 202) with environmental ZOTUs inserted into the tree. Reference taxa are identified with colored symbols. The ring active taxa show negative (orange), neutral (beige), or positive (blue) responses between sampling day 5 and 17, when removal of all pharmaceuticals showed a sharp decline. 201

36. Figure B.1. Schematic of the sampling port from which influent samples were taken. During the anaerobic feed phase, the influent sampling port tubing was briefly unclamped to allow collection of samples for influent pharmaceuticals and nutrient concentrations. 204

37. Figure B.2. Pharmaceutical removal versus time. Removal was calculated using equations S1 and S2. Removal percentages below zero indicate that effluent concentrations were higher than predicted by the mass balance. Data in this figure were originally published in [142] and are shown here with permission. 206

38. Figure B.3. Individual images of each EPS stain for a **control** granule at day 0 (top row) and day 80 (bottom row). From left to right: Red, alpha-polysaccharides; pink, beta-polysaccharides; green, proteins; blue; lipids; far right, the combined image of all stains. All scale bars are 200 μm. 207

39. Figure B.4. Individual images of each EPS stain for a **test** granule at day 0 (top row) and day 80 (bottom row). From left to right: Red, alpha-polysaccharides; pink, beta-polysaccharides; green, proteins; blue; lipids; far right, combined image of all stains. All scale bars are 200 μm. 208

LIST OF FIGURES CONTINUED

Figure Page

40. Figure B.5. Average fractions of various EPS components in granule sections versus time. Error bars represent the standard deviation of sections from triplicate granules. Triplicate sections from the same granule were also analyzed for each EPS component, and average values and standard deviations were similar to those plotted here at each time point (data not shown). Lipid concentrations in test granules declined linearly over time, evidenced by the linear trendline $R^2 > 0.9$. 209

41. Figure B.6. Sludge volume index versus time in both control and test reactors. The SVI_3 of AGS in the test reactor increased linearly over the 80-day exposure period, excepting the two points in which SBR-controlling software experienced an error (days 40 and 41, discussed in more detail in the main body of the text). Control AGS SVI_3 remained constant at approximately 12 mL/g. 209

42. Figure B.7. Granule size fractions versus time in both reactors. 10 mL AGS was sieved, and sieved portions were analyzed for VSS. “Fractional VSS” was calculated by dividing the VSS in each size bin by the total sample VSS. Sample points at t(-1) indicate samples taken from both reactors immediately before beginning pharmaceutical dosing. 210

43. Figure B.8. Solid phase pharmaceutical concentrations versus effluent (A) ammonia and (B) phosphate concentrations over days 10-23 only. 210

44. Figure C.1. Schematic of the sampling port from which influent samples were taken. During the anaerobic feed phase, the influent sampling port tubing was briefly unclamped to allow collection of samples for influent pharmaceutical and nutrient concentrations. 214

45. Figure C.2. Left, nitrogen removal; right, phosphate removal in the control and test reactors versus time. 218

46. Figure C.3. Effluent concentrations of ammonia-, nitrite-, and nitrate-nitrogen in the control and test reactors. Compounds are plotted as nitrogen to aid data visualization. Effluent nitrate was high in both SBRs over the first 10 days while organic carbon dosing was below 100 mg/L in the influent. 218

LIST OF FIGURES CONTINUED

Figure Page

47. Figure C.4. Nitrite and nitrate removal in the control and test SBRs. Control data is plotted with solid symbols and lines, test data with open symbols and dashed lines. A mass balance on the ammonia consumed was used to predict nitrite production. Predicted nitrite concentrations and effluent nitrite values were used to calculate nitrite removal and predict nitrate concentrations; effluent and predicted nitrate values were used to calculate nitrate removal. 219

48. Figure C.5. A: Total dissolved organic carbon (DOC) removal in both reactors. B: Anaerobic DOC removal. Approximately 20% of the influent carbon was fed as EDTA in the trace nutrient solution; EDTA is typically recalcitrant to biodegradation and therefore total DOC removals near 80% reflect almost complete removal of all biodegradable organic carbon. Most of the DOC fed was removed anaerobically after day 10. 219

49. Figure C.6. Pharmaceutical concentrations bound to all biomass (AGS and floc mixture) and just flocs (i.e., biomass that passed through a 0.2 mm sieve). Error bars represent the standard deviation of triplicate samples. An error bar is not present for all biomass for DCF because of an error during the mass spectrometry run of one triplicate; ERY and GEM could be quantified from this sample, but DCF could not. DCF all biomass data therefore represents the average of duplicate samples. GEM concentrations in all floc samples were below detection. 220

50. Figure C.7. Sludge volume index of biomass in both reactors measured after 10 minutes of settling (SVI_{10}) versus time. The large drop in SVI_{10} for biomass in the test SBR between days 6-15 is due to the floc washout that occurred on day 13. Notably, control biomass' SVI_{10} also dropped between days 0-27, and the SVI_{10} of biomass in both SBRs was equal on day 27. Both control and test biomass' SVI_{10} values remained near equal for the remainder of the experiment. 221

51. Figure C.8. Granule size distributions, as a fraction of the summed VSS of the sample, versus time in the control and test reactors. 221

LIST OF FIGURES CONTINUED

Figure Page

52. Figure C.9. Average fractions of various EPS components in granule sections versus time. Error bars represent the standard deviation of sections from triplicate granules. Triplicate sections from the same granule were also periodically analyzed for each EPS component and data followed trends similar to those shown above. 222

53. Figure C.10. Species' richness (as the number of active OTUs, or those with an rRNA to rDNA ratio greater than or equal to one) versus time in both SBRs. 222

54. Figure C.11. Top row: the relative abundance of active Azonexus and Sulfuritalea species versus time in both SBRs. Bottom row: rRNA counts for phantom taxa belonging to Azonexus (left) and Sulfuritalea species (right) versus time. Note that y-axis scales differ for all plots to improve data visualization. 223

55. Figure D.1. Starved AGS batch tests results at all pharmaceutical concentrations. Open symbols with no connecting line indicate control samples. Sample data at "t-2" and "t-1" reflects the concentration in bottles without any loss to filter material or AGS as described in the text. These samples were not analyzed from the 250 ug/L triplicates simply to reduce the number of analyses needed. 226

56. Figure D.2. Degradation products only detected on day 15 in starved AGS batch tests. Left, ERY-associated degradation products; right, DCF-associated degradation products. Note that y-axes both show corrected peak area but differ in scale. More detail on all molecules is provided in Chapters 4 and 6. 227

57. Figure D.3. GEM degradation products detected over time in starved AGS batch tests. Y-axes differ in scale, but both show corrected peak areas. GEM3 is discussed in more detail in Chapters 4 and 6; GEM5 was only detected in this study and is discussed in more detail in the above text. 228

NOMENCLATURE

AGS	Aerobic granular sludge
AOB	Ammonia oxidizing bacteria
CAS	Conventional activated sludge
CLSM	Confocal laser scanning microscopy
DCF	Diclofenac
EIC	Extracted ion chromatogram
EPS	Extracellular polymeric substances
ERY	Erythromycin
FISH	Fluorescence in situ hybridization
GAO	Glycogen accumulating organism
GEM	Gemfibrozil
NOB	Nitrite oxidizing bacteria
PAO	Phosphate accumulating organism
PHA	Polyhydroxyalkanoate
PPCPs	Pharmaceuticals and personal care products
SBR	Sequencing batch reactor
UPLC-QTOF-MS	Ultra-performance quadrupole time-of-flight mass spectrometry
VFA	Volatile fatty acid
WWTP	Wastewater treatment plant

ABSTRACT

Pharmaceutical concentrations in various environmental matrices are increasing across the globe. Effluent discharge from wastewater treatment plants is a major vector by which pharmaceuticals enter the environment, as many of these compounds are not biodegradable under conventional wastewater treatment conditions. Although concentrations are currently low (ng/L to µg/L levels), pharmaceutical contamination poses risks to both human and animal health, as many pharmaceuticals can have toxic effects on fish, birds, and small mammals, as well as contribute to the proliferation of antibiotic resistance genes in bacteria.

Aerobic granular sludge (AGS), an emerging biofilm-based wastewater treatment biotechnology and the subject of this dissertation, may be capable of enhancing pharmaceutical removal from wastewater. Scientific literature indicates that AGS uses a mixture of both biodegradation and adsorption to remove pharmaceuticals, but thus far, studies on this topic are limited. The research detailed herein investigated how AGS was affected by a mixture of three common, but relatively unstudied, pharmaceuticals: diclofenac (anti-inflammatory), erythromycin (antibiotic), and gemfibrozil (lipid regulator).

Studies described herein examined how AGS grown in two different environments—the lab versus a full-scale wastewater treatment plant—responded to pharmaceuticals. Pharmaceutical effects on wastewater treatment efficacy, active microbial populations, and biofilm structures were investigated. Pharmaceutical fates in both the aqueous and solid phases were also tracked.

In general, lab-grown AGS was more negatively impacted by pharmaceutical exposure, evidenced by reduced wastewater treatment efficacy, declines in key wastewater-treating microbial populations, and reductions in biofilm lipid content. Pharmaceuticals were also poorly removed by lab-grown granules. In contrast, key microbial populations and biofilm structures remained stable throughout dosing in environmentally-grown AGS, and gemfibrozil was completely biodegraded. An important caveat to comparison of the two studies, however, is that the pharmaceutical dose to lab-grown AGS was approximately double that to environmental granules.

Altogether, the research described herein demonstrates the promise of AGS as a dual wastewater and pharmaceutical treatment technology, but illustrates the importance of conducting experiments under conditions as environmentally relevant as possible.

INTRODUCTION

Background

This dissertation presents research on an emerging biofilm-based biotechnology and its capacity to remove several common pharmaceuticals from wastewater. Aerobic granular sludge (AGS) is a form of wastewater biofilm in which diverse communities of wastewater bacteria self-aggregate into dense spheres several millimeters in diameter. Oxygen gradients throughout each granule allow nitrifying, denitrifying, and phosphate accumulating organisms to coexist, thereby allowing complete wastewater treatment in a single reactor (Figure 1.1). In turn, this reduces the footprint and energy required for wastewater treatment processes. Furthermore, the complex, gel-like extracellular polymeric substances (EPS) secreted by bacteria in AGS enhance granule density, resulting in reduced settling times and higher biomass retention than conventional treatment systems [1, 2]. Studies also suggest the EPS in AGS provide a diffusive barrier that protects AGS-associated bacteria from shock loads or toxins [3, 4].

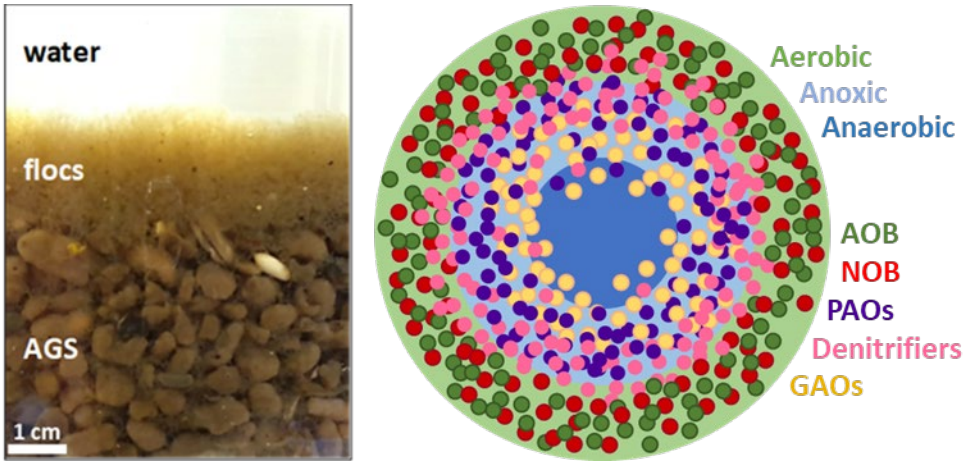

Figure 1.1. Left: AGS from a full-scale treatment plant settled beneath a layer of floccular conventional activated sludge and clear water (image credit to Catherine Kirkland). Right:

General schematic of oxic zones and bacterial population distributions within a single granule. Acronyms: AOB, ammonia oxidizing bacteria; NOB, nitrite oxidizing bacteria; PAOs, phosphate accumulating organisms; GAOs, glycogen accumulating organisms.

Emerging contaminants, such as pharmaceuticals and personal care products, are an example of toxins that can negatively impact wastewater bacteria. Emerging contaminants enter wastewater due to their ubiquitous daily use: soaps containing antimicrobial agents are washed down the drain, pharmaceutical compounds are partially metabolized, resulting in both unmetabolized and metabolized fractions entering sewage, and topically applied personal care products or pharmaceutically-active agents likewise rinse off, entering wastewater. Multiple studies have shown that pharmaceuticals can harm wastewater-treating bacteria, potentially reducing conventional contaminant treatment efficacy [5-7]. Furthermore, pharmaceuticals are generally not biodegradable, and therefore they enter the environment after passing, untreated, through wastewater treatment plants (WWTPs) [3].

Consequently, numerous pharmaceutical compounds are detected in environmental matrices across the globe. Various studies have detected pharmaceuticals at trace concentrations in drinking water sources [8] and treated drinking water [9, 10]. Pharmaceuticals have also been detected in plant and animal tissues, and therefore present hazards to both plant and animal health, as well as a potential pathway for bioaccumulation up the food chain [10]. Though current risks to human health appear low, the nebulous, ever-changing nature of pharmaceutical mixtures in water sources makes it difficult to accurately determine impacts on human health. In particular, the effects of chronic exposure to these complex pharmaceutical mixtures are unknown [8].

To ensure water sources remain safe for humans and animals alike, treatment methods that sustainably remove pharmaceuticals and other emerging contaminants while simultaneously treating wastewater are needed. AGS shows promise in this area: studies indicate that AGS outperforms conventional activated sludge (CAS) systems at pharmaceutical removal [3, 11]. However, the body of literature available on this subject is limited. In particular, the removal mechanisms—sorption and/or biodegradation—utilized by AGS are poorly understood, as are the effects of pharmaceuticals on AGS biofilm structures and microbial populations. The research presented in this dissertation contributes to improved understanding of these topics. The following chapters detail studies in which both lab- and environmentally-grown AGS are exposed to pharmaceuticals, and changes to abiotic and biotic granule characteristics are tracked. The fates of dosed pharmaceuticals are also detailed, as are pharmaceutical impacts on granules' ability to perform conventional wastewater treatment.

Dissertation Overview

Chapter 2 provides important background information on the chemistry and microorganisms responsible for conventional wastewater treatment. A brief literature review on AGS in general and AGS-driven treatment of pharmaceuticals and other emerging contaminants is also presented. Lastly, more detail is provided on key analytical research methods used throughout this research: ultra-performance liquid chromatography quadrupole time-of-flight mass spectrometry (UPLC-QTOF-MS) is discussed, as well as confocal laser scanning microscopy (CLSM) and nucleic acid sequencing techniques.

Chapter 3 presents research findings obtained as a prerequisite to conducting accurate pharmaceutical dosing experiments with AGS. This chapter is a manuscript titled

"Pharmaceutical sorption to lab materials may overestimate rates of removal in lab-scale bioreactors" and published in *Water, Air, and Soil Pollution*. Many pharmaceuticals are hydrophobic and readily partition to various plastic lab supplies. It is therefore essential to use lab materials that are well-suited to the compound(s) tested. Pharmaceutical losses to different types of essential lab materials, such as pipette tips, tubing, etc., are presented in this chapter, as well as dosing methods that more accurately deliver desired pharmaceutical concentrations. This information is essential for accurately determining the extent to which pharmaceuticals are removed by the target process, rather than overestimating removal due to incidental sorption.

Chapters 4 and 5 present the results of an experiment in which pharmaceuticals were continuously fed to lab-grown granules. "Lab-grown" granules refers to granules cultivated from planktonic CAS in lab-scale bioreactors for over a year. Chapter 4 is a manuscript titled "Treatment performance and microbial community structure in an aerobic granular sludge sequencing batch reactor amended with diclofenac, erythromycin, and gemfibrozil" and published in *Frontiers in Microbiomes*. In this chapter, the biotic effects of the pharmaceutical mixture on AGS are summarized: impacts on wastewater treatment efficacy, active microbial communities, and pharmaceutical biodegradation are detailed. Chapter 5, in contrast, focuses on abiotic pharmaceutical removal processes and abiotic impacts on AGS morphology. This chapter is a publication titled "Pharmaceutical impacts on aerobic granular sludge morphology and potential implications for abiotic removal" and published in *Chemosphere*. The sorptive capacity of AGS for the tested pharmaceuticals is documented as well as each compound's sorption isotherm. Changes in the distribution of EPS in granules throughout dosing are also discussed, as these changes likely impacted granules' sorptive properties.

Chapter 6 presents the results of a similar study with environmentally-grown granules. In this study, granules were sampled from a full-scale AGS treatment plant in Rockford, IL and inoculated directly into lab-scale bioreactors. Pharmaceutical dosing then began immediately. The goal of this study was to document if environmentally-grown AGS responded differently to pharmaceuticals than lab-grown AGS, and, by extension, if lab-grown AGS are an accurate model for full-scale granules. Environmentally-grown AGS is exposed to a more diverse body of substrates than lab-grown AGS [12], and therefore may be better able to degrade complex substrates such as pharmaceuticals. Similarly, AGS from full-scale plants likely forms in the presence of trace pharmaceuticals, and therefore may possess characteristics that enhance its ability to perform wastewater treatment throughout pharmaceutical exposure. Studies have also shown that substrate composition affects microbial diversity and granule structure [13, 14]. This chapter is titled "Environmentally-grown aerobic granular sludge response to pharmaceuticals: impacts on wastewater treatment efficacy, active microbial communities, and pharmaceutical fate" and has been submitted to the *Journal of Environmental Management*. It documents the impacts of the same pharmaceutical mixture on full-scale granules' structures, active microbial communities, and wastewater treatment efficacy, as well as tracks pharmaceuticals' fate in aqueous and solid phases.

Lastly, Chapter 7 presents conclusions drawn from the prior four studies and recommendations for future research. Pharmaceutical impacts on lab- and environmentally-grown AGS are compared, with special attention given to the effect that pharmaceutical dosage may have had on observations in all studies. The roles of key microbial communities are summarized, as well as potential relationships between these communities and wastewater

treatment efficacy and biofilm structures. Future research directions for AGS-driven pharmaceutical treatment are recommended. Lastly, results from two preliminary studies, which could not be further investigated due to time constraints, are presented, in order to demonstrate both the potential of AGS as a treatment option and the need for further research.

Appendices A, B, and C provide supplementary materials for the manuscripts in Chapters 4, 5, and 6, respectively. Appendix D provides supplemental methods and background information for experiments discussed in Chapter 7. Appendix E provides the LabVIEW program used for sequencing batch reactor control in all experiments.

Funding and Collaborations

Work presented in this dissertation was supported by the Montana IDeA Network of Biomedical Research Excellence (INBRE), which is funded by the National Institute of General Medical Sciences of the National Institutes of Health under Award Number P20GM103474. Additional support was also provided by the Montana Water Center Graduate Student Water Resource Fellowship, the Warren L. Jones Memorial Scholarship, and the Robert and Mary Sanks Graduate Fellowship. Conference travel support was provided by the Montana State University (MSU) graduate school's Professional Advancement Grant.

This work was performed at the Center for Biofilm Engineering at MSU. Field samples were obtained from the AquaNereda® AGS demonstration plant in Rockford, IL and the Nereda® wastewater treatment plant in Utrecht, The Netherlands.

CHAPTER TWO

A BRIEF REVIEW OF WASTEWATER TREATMENT, EMERGING CONTAMINANTS, AEROBIC GRANULAR SLUDGE, AND PERTINENT ANALYTICAL TECHNIQUES

A Brief Summary of Wastewater Treatment

Effective wastewater treatment is essential to protect environmental health. Wastewater contains nitrogen, carbon, and phosphorus species that, if left untreated, would be consumed by algae and other microbiota in natural water bodies. Concurrent consumption of these nutrients with oxygen can result in algal blooms and oxygen depletion, leading to fish die-off and toxin production. Toxins produced during overgrowth of algae can bioaccumulate up the food chain, potentially poisoning humans and animals and contaminating drinking water sources. For all of these reasons, complete conversion of these compounds to inert, non-biodegradable forms during wastewater treatment is vital for both human and environmental health. The following details regarding wastewater treatment are based on widely accepted knowledge and practice, as presented in the text *Wastewater Engineering: Treatment and Resource Recovery*, 5th edition, by Metcalf and Eddy, Inc [15].

Wastewater treatment plants (WWTPs) utilize a series of bioreactors with carefully maintained oxygen and organic carbon concentrations to control the microbial conversion of contaminants to inert forms. The diverse microbial communities that perform wastewater treatment are generally referred to as conventional activated sludge (CAS). Nitrogen typically enters plants as ammonia (NH_3), which is converted to nitrite (NO_2^-) and then nitrate (NO_3^-) by aerobic autotrophic bacteria. Nitrate is then converted to nitrogen gas (N_2) by heterotrophic

bacteria, under anoxic conditions and in the presence of organic carbon. Phosphorus enters WWTPs as phosphate (PO_4^{-3}), which is either removed through biological processes or converted to inert phosphorus via chemical precipitation with iron or alum salts. Biological conversion of phosphate is the process pertinent to this dissertation and therefore chemical precipitation will not be discussed further.

Phosphate accumulating organisms (PAOs) are the bacteria responsible for phosphate removal in wastewater treatment. PAOs remove phosphate in a cyclical fashion: under anaerobic conditions, these organisms consume volatile fatty acids (VFAs), which are typically present in influent wastewater or produced by other bacteria via fermentation processes. PAOs store VFAs as polyhydroxyalkanoates (PHAs); conversion and storage require energy, which is generated by the hydrolysis of intracellularly stored polyphosphates. PAOs release phosphate during hydrolysis of polyphosphate bonds, and therefore phosphate concentrations in anaerobic reactors are typically higher than those in other reactors. However, PHA storage and polyphosphate release are important prerequisites for eventual phosphate consumption, which occurs aerobically [15].

Under aerobic conditions, PAOs utilize stored PHAs for growth. Energy generated from PHA oxidation is used for polyphosphate storage, resulting in greater phosphate removal from solution than was released during anaerobic metabolism. Net phosphate removal occurs because a portion of biomass is wasted throughout the wastewater treatment process, resulting in removal of stored polyphosphates; continued PAO growth further sustains phosphate removal [15]. Glycogen accumulating organisms (GAOs) are a group of nuisance bacteria that may outcompete PAOs for VFAs. GAOs store glycogen under aerobic conditions, not phosphate, and therefore do

not provide a valuable function during wastewater treatment. Slightly basic pH values (pH > 7.5) can be used to favor PAO growth over that of GAOs; temperature and solids retention time can also be used for GAO control [15].

Biological phosphate removal influences the design of biological nutrient removal systems, since strictly anaerobic conditions are required for the phosphate accumulation process. A common treatment process schematic is shown in Figure 2.1. This system, referred to as a "Bardenpho process", utilizes influent rich in organic carbon to establish anaerobic conditions in the first bioreactor chamber. Thereafter, wastewater flows to an anoxic chamber, in which any remaining carbon should be consumed by denitrifying organisms. Low organic carbon concentrations in the following aerobic chamber are important in order to prevent the overgrowth of opportunistic heterotrophic organisms, which would otherwise outcompete wastewater-treating autotrophic organisms and PAOs in this chamber [15].

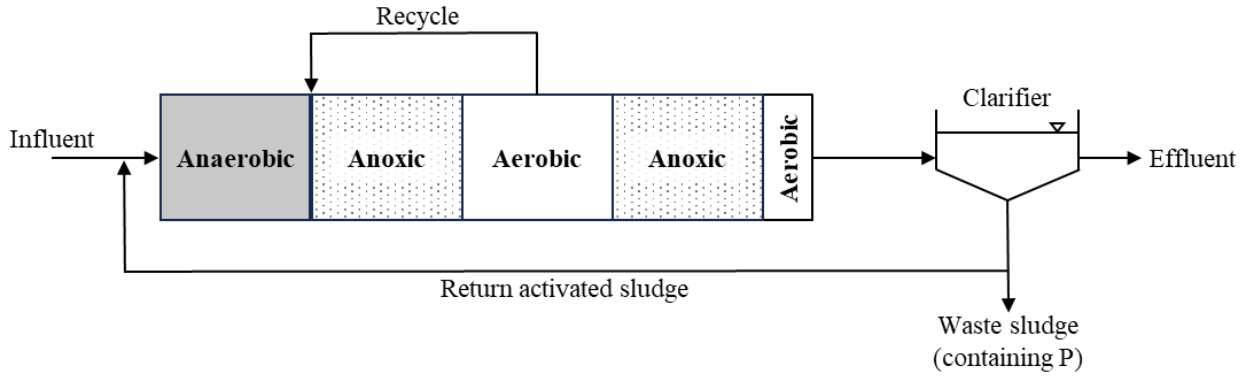

Figure 2.1. The modified Bardenpho process. The classic Bardenpho process does not utilize a second aerobic chamber [15].

The key autotrophic organisms grown in the aerobic chamber of a Bardenpho system are ammonia- and nitrite-oxidizing bacteria (AOB and NOB, respectively). AOB, typically of the genera *Nitrosomonas* or *Nitrosospira*, perform stepwise oxidation of ammonia to nitrite. NOB,

typically of the *Nitrobacter, Nitrococcus, Nitrospina,* or *Nitrospira* genera, then oxidize nitrite to nitrate. Both AOB and NOB utilize inorganic carbon in the form of carbon dioxide. The overall conversion of ammonia to nitrate is termed “nitrification”.

Nitrate-rich wastewater produced in the aerobic chamber of the Bardenpho process flows to a second anoxic chamber, in which mixing without aeration allows heterotrophic organisms to reduce nitrate to nitrogen gas. Numerous bacterial genera are capable of performing this step, termed “denitrification”; many are facultative heterotrophs and therefore possess the ability to use oxygen instead of nitrate as an electron acceptor when it is available. For this reason, the absence of dissolved oxygen is critical for successful denitrification to occur—oxygen is more energetically favorable than nitrate, and therefore when present, bacteria will preferentially reduce oxygen rather than nitrate [15]. A portion of wastewater from the prior aerobic stage is also recycled back to the first anoxic stage, which helps ensure complete removal of all nitrogen species. Exogenous carbon is often added to the second anoxic stage to provide sufficient carbon for denitrifying organisms.

A final aerobic chamber is located after the second anoxic reactor. Aeration in this chamber helps to strip any remaining nitrogen gas from the liquid. Aerobic conditions also help ensure that PAOs uptake any phosphate that may have been released in the previous anoxic stage.

An Update to Wastewater Treatment: Aerobic Granular Sludge

Aerobic granular sludge (AGS) is an emerging biotechnology in which all key wastewater-treating bacteria coexist in biofilm “granules”. Biofilms are a bacterial growth phenotype in which bacteria live enmeshed in a complex, self-secreted matrix of extracellular

polymeric substances (EPS); EPS typically consist of proteins, lipids, and long chain sugars such as alpha- or beta-polysaccharides [16-18]. Bacteria generally form biofilms by attaching to a surface and secreting EPS, which further aids in their attachment and provides a protective diffusive boundary layer between bacteria in the biofilm and potentially toxic substances outside of the biofilm [16]. AGS is unique in that bacteria aggregate together to form biofilm granules without any carrier material—instead, conditions in sequencing batch reactors (SBRs) encourage activated sludge bacteria to adhere to one another, and over time, granules several millimeters in diameter will form (as pictured in Figure 1.1) [19].

The phases of SBR operation are shown in Figure 2.2. The anaerobic phase is analogous to that occurring in an anaerobic Bardenpho reactor, except that influent wastewater is fed in a plug flow fashion and the reactor is not stirred. Most of the influent organic carbon is consumed anaerobically by PAOs in this phase. After a certain filling time (Figure 2.2 lists the fill time used in lab experiments discussed herein), aeration occurs, and both aerobic and anoxic conditions occur simultaneously due to granules' sizes: oxygen is plentiful at granules' outer edges, and therefore nitrifying bacteria proliferate in this region and consume oxygen before it can diffuse to deeper layers of the granule. Nitrate produced by nitrifying organisms is consumed by denitrifiers living deeper within the granule, where oxygen concentrations are low (Figure 1.1). Any remaining organic carbon will also be consumed by denitrifers at this phase in the SBR cycle; PAOs will also consume phosphate at this time.

After aeration, the SBR acts as its own primary clarifier; granules settle quickly and treated wastewater is decanted off the top of the settled granule bed. This process then repeats itself.

The processes underlying granule formation in SBRs are not fully understood. Shear stresses and operational conditions that select for slow-growing organisms appear to be the main drivers of granulation [19, 20]. Aeration causes collisions between planktonic microorganisms; this cell-to-cell contact is hypothesized to encourage EPS secretion and cellular aggregate formation [19]. Short settling times then selectively retain denser organisms in the SBR, and shear stresses during aeration encourage cell aggregates to become even denser [19]. Slow-growing organisms, such as PAOs and nitrifiers, have also been shown to enhance AGS' density and stability; low carbon concentrations during aeration prevent fast-growing organisms from outcompeting these communities for essential nutrients [20]. In conjunction with aeration and the washout of less dense biomass, SBRs therefore selectively retain self-aggregating, dense bacterial communities; in other words, aerobic granular sludge.

Wastewater treatment using AGS is advantageous because both energy and footprint requirements are smaller: unlike the commonly utilized Bardenpho process (Figure 2.1), for example, complete wastewater treatment can be obtained in a single SBR using AGS [20]. SBRs also only require aeration for a portion of their operating time, whereas conventional systems require constant aeration in at least one reactor [15, 21]. Aeration typically consumes 50-60% of the energy associated with wastewater treatment, and therefore reducing its use can have a major impact on WWTP energy costs [22]. Other AGS advantages include improved settleability—granules are denser than CAS flocs, and therefore settling times are shorter and more biomass is retained during settling, resulting in more efficient wastewater treatment—and AGS are more resistant to shock loads, due to the mass transfer barrier provided by EPS in AGS [1-4, 19]. Lastly, unlike other biofilm treatment technologies, AGS form without carrier materials, which is

also beneficial as these materials break down over time and can act as a source of plastic pollution [23].

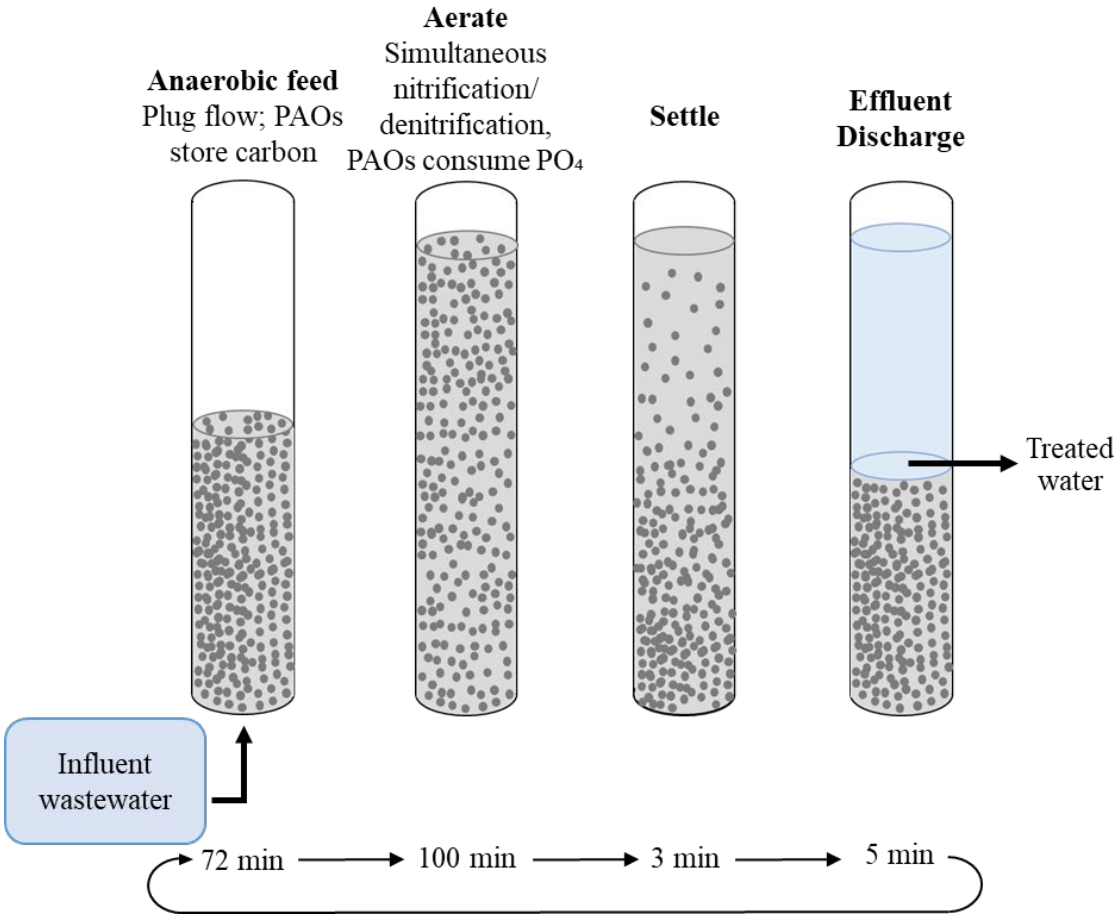

Figure 2.2. AGS-SBR schematic with each phase of operation shown. Both aerobic and anoxic conditions are possible during the aeration phase due to oxygen gradients within granules. Anaerobic conditions return during the settling and discharge phases; feeding new influent wastewater through the settled granule bed maintains these conditions as high organic carbon concentrations encourage consumption of any remaining oxygen by heterotrophs.

Aerobic Granular Sludge: A Potential Solution to Pharmaceutical Contamination

As stated briefly in Chapter 1, pharmaceuticals and personal care products (PPCPs) pose a threat to complete wastewater treatment because they can negatively impact wastewater-

treating bacteria [5-7]. These contaminants are present in wastewater due to their ubiquitous daily use, and because of their poor biodegradability, PPCPs are generally not removed during wastewater treatment processes [3, 24]. Altogether, these compounds threaten environmental health in numerous ways: they can harm treatment of traditional contaminants (nitrogen and phosphorus species), and their presence alone can harm plants, animals, and microbiota [24-28]. Although current environmental concentrations of these compounds are low (ng/L to μg/L levels), multiple studies have still documented negative impacts at these levels. For example, a study by Murack *et al.* (2011) found that environmentally-relevant concentrations (0.3 μg/L) of progesterone, a common ingredient in birth control, reduced fertility in fathead minnows [27]. Likewise, multiple antibiotics (at concentrations as low as 5 μg/L) have been shown to act synergistically to inhibit growth of cyanobacteria and algae [28], and various painkillers bioaccumulate and/or impair development in aquatic species and plants at concentrations under 100 μg/L [26, 29-31].

Given WWTPs' position as a collection point for PPCPs, the most logical solution to PPCP contamination is improved removal of these compounds during wastewater treatment. Aerobic granular sludge may provide this enhanced removal capacity. The diffusive barrier supplied by EPS in AGS protects bacteria from toxins, such as PPCPs [1-4, 19], and may also provide a material for PPCP sorption [3, 32, 33]. Taken together, AGS may be capable of simultaneous treatment of conventional contaminants and PPCP removal. Studies thus far suggest this is possible: for example, Kent and Tay (2019) observed over 99% removal of ammonia and phosphate during pharmaceutical dosing to AGS, and average pharmaceutical removals ranged from 10-93%, depending on the compound [3]. Pharmaceutical removal rates in

this study were typically higher than those of conventional activated sludge [3]. Other studies have shown similar results (e.g., [32, 34]); however, relative to the numerous types of PPCPs in the environment, there is little research available on these compounds' impacts on AGS. In particular, the removal mechanisms (sorption versus biodegradation) utilized by AGS are poorly understood, as are the effects of pharmaceuticals on AGS structures and microbial populations.

In this dissertation, three common, albeit relatively unstudied, pharmaceuticals were selected for further investigation. Compounds were selected based on their prevalence in the environment, their expected risk to plants, animals, and microorganisms (based on documented toxic effects on each), and the likelihood for AGS-driven treatment. Treatment likelihood was judged partially based on the hydrophobic properties of each pharmaceutical, as it was expected that more hydrophobic compounds will adsorb to the organic EPS in AGS. For this reason, each compound selected has an octanol-water partition coefficient greater than 10^3, indicating a preference for organic phases rather than water [35-37]. AGS treatability was also estimated based on existing studies of similar pharmaceuticals' effects on, and/or removal by, AGS or CAS. Lastly, pharmaceuticals were excluded from consideration if three or more studies existed on their interactions with AGS to ensure the proposed research advanced scientific knowledge.

Erythromycin

ERY is a macrolide antibiotic commonly used in both human and veterinary medicine [38]. Approximately 5% of dosed ERY is excreted in its active form after consumption [38]. Despite the large portion of ERY metabolized, ERY and its metabolites are often detected in WWTP and septic system effluents, as well as ground- and surface waters across the US [8, 39-42]. ERY has been shown to bioaccumulate in multiple aquatic species [38], implicated in

proliferation of antibiotic resistance genes [43], and exhibited high toxicity to photosynthetic aquatic microorganisms [28].

At the time of study development, just one publication explored whether AGS could remove ERY from wastewater, with promising—if limited—results [44]. Wang *et al.* (2019) monitored aqueous and adsorbed concentrations of ERY and found that most ERY removal occurred via adsorption (influent concentrations ranged from 0.85 to 1.65 µg/L) [44]. However, the authors did not monitor ERY degradation products, and ERY may be biodegradable by AGS: a study by Pasquini *et al.* (2013) documented ERY biodegradation by conventional activated sludge over a 24-hour dosing period [45]. AGS-driven removal of macrolide antibiotics other than ERY has been reported in several other studies, though the effects of each antibiotic on AGS varied widely and the removal mechanism was not investigated [11, 46, 47]. No studies have investigated how ERY exposure impacts microbial communities or spatial EPS distributions in AGS.

Diclofenac

DCF is a good candidate for study for many of the same reasons as ERY. It was the 61st most prescribed drug in 2021, the most recent year for which data is available [48]. DCF is administered orally or topically. Approximately 94% of topically applied DCF washes off, thus a presenting a pathway for DCF to readily enter wastewater [49].

DCF is widely detected in the environment [26] and poorly removed by conventional WWTPs: several studies indicate removals under 40% [42, 50, 51]. DCF is also toxic to various aquatic plants and animals at environmental concentrations [26]. Though diclofenac is a non-steroidal anti-inflammatory drug, it has been shown to inhibit bacterial DNA synthesis at higher

concentrations and act synergistically with antibiotics to prevent biofilm formation [52, 53]. Antimicrobial effects due to chronic exposure at lower concentrations are unknown, but observations thus far indicate that DCF could contribute to antibiotic resistance [26, 52, 53].

At the time of study design, just one study existed on DCF-AGS interactions at environmental concentrations: Margot *et al.* (2016) explored how a mixture of 36 different pharmaceuticals and pesticides at 1 µg/L impacted AGS and observed less than 20% removal of DCF specifically [46]. However, exposure only lasted five days, and total suspended solids (TSS) concentrations in the study were five to ten times lower than those in full scale granular sludge treatment reactors [46, 54]; therefore, results may not be representative of those in a more realistic system. This study also did not investigate DCF degradation products, adsorbed DCF concentrations, or changes to granular morphology.

Encouragingly, a study by Falas *et al.* (2012) compared DCF removal by CAS flocs with that by CAS biofilm carriers and observed approximately 90% removal by the biofilms, despite no removal by flocs [55]. Floccular biomass concentrations in Falas *et al.* (2012) were near equal to granular biomass concentrations reported in Margot *et al.* (2016); poor DCF removal was reported in both studies [46, 55]. In contrast, biofilm carriers' biomass concentrations in Falas *et al.* (2012) were closer to those in full scale AGS systems (over 10 g/L) [54, 55]. Increased DCF removal may therefore be linked with higher biomass concentrations.

Gemfibrozil

GEM is a lipid-regulating drug. Though just 2% of dosed GEM is excreted in its active form, the mass of GEM typically dosed per person is 1200 mg, resulting in up to 24 mg excreted into wastewater with every dose [56]. GEM has been detected in WWTP influents across the US

from 1-10 µg/L, but in some cases as high as 63 µg/L [42, 57, 58]. GEM is also often measured in ground- and surface waters across the globe [42, 57, 59, 60]. Environmental concentrations (1 µg/L or less) can inhibit growth, induce oxidative stress, and cause endocrine disruption in various aquatic organisms [61, 62].

Margot *et al.* (2016) also included GEM in the mixture of 1 µg/L pharmaceuticals exposed to AGS and observed approximately 50% removal [46]. To date, this is the only publication in which lipid regulators' impacts on AGS are explored; however, a few studies have investigated CAS-driven removal of lipid regulators with encouraging results [50, 55, 63]. Inyang *et al.* (2016) observed near 100% degradation of 1 µg/L GEM under aerobic conditions in batch tests with activated sludge [63]. The same study discussed previously by Falas *et al.* (2012) also observed better GEM removal by CAS biofilm carriers than flocs [55].

The overarching goal of research presented in this dissertation was to investigate the effects of these three pharmaceutical compounds on aerobic granular sludge. Pharmaceutical fates and impacts on AGS bacteria and EPS were evaluated, as were pharmaceutical effects on conventional contaminants' removal.

Methods Overview

UPLC-QTOF-MS

Identification and quantification of the pharmaceuticals tested herein was performed with ultra-performance quadrupole time of flight mass spectrometry (UPLC-QTOF-MS). UPLC-QTOF-MS is a highly sensitive and accurate technique for the identification and quantification of various molecules, and was therefore well suited for measurement of low pharmaceutical concentrations. It was also used to identify daughter products formed during biodegradation of

these compounds. A brief description of how mass spectrometry identifies and quantifies different molecules is provided in the following paragraphs.

Liquid chromatography occurs prior to mass spectrometry to aid in separation of different molecules from each other. In short, a liquid mobile phase carries liquid samples through a chromatography column to a detector. The chromatography column is typically packed with a polar or nonpolar material, which causes molecules of different polarities to bind to the material with different affinities. This difference in affinities translates to different binding times, and therefore molecules will separate from each other through the column and elute at different times. This "retention time" can be used to tentatively identify the specific molecule, with mass spectrometry adding further confidence to the identification. Separated molecules flow to a detector, which in this research was a mass spectrometer.

Mass spectrometry, in general, is an analytical technique in which molecules in a sample are first ionized and converted to the gas phase. Ionized molecules are either protonated or deprotonated by an adduct, which is most commonly hydrogen or sodium. Ionized molecules then pass through a mass analyzer, which separates molecules based on their mass-to-charge (m/z) ratio. M/z ratios reflect exact isotopic masses—molecules with the same elements but different isotopes, or isotopologues, will be separated from each other.

Separated molecules then flow to a mass detector, which counts the number of ions per m/z per unit time (i.e., a three-dimensional plot of counts vs. m/z vs. time is generated). In this research, a quadrupole time-of-flight (QTOF) mass detector was used. In short, this method determines the m/z of an ion based on the time the ion takes to fly through an electric field of known strength and distance; heavier ions travel slower than lighter ones. A two-dimensional

plot of counts versus time for a specific m/z is called an Extracted Ion Chromatogram (EIC); this chromatogram can be used to quantify the concentration of a specific molecule. Counts will increase and diminish, forming a peak, as molecules pass through the detector. The area of this peak will change in proportion to the molecule's concentration, allowing standard curves to be generated using samples of known concentration. Many different molecules may have similar m/z values, however; therefore, to confirm that an EIC actually represents a specific molecule, mass spectra must be used (an example is shown in Figure 2.3).

Two-dimensional plots of each isotopologue's relative abundance versus m/z are also known as "mass spectra" and are unique to each molecule. Relative abundance is calculated by normalizing the amount of each isotopologue to the amount of the most abundant isotopologue. In this way, the proportion of isotopologues to each other is determined. For example, the pharmaceutical diclofenac (DCF, $C_{14}H_{11}Cl_2NO_2$), after ionization with hydrogen, can be separated into seven different isotopologues at the relative abundances shown in Figure 2.3. The highest peak, at an m/z of 296.024, indicates that most of the DCF molecules detected are made up of the isotopologue containing each element's most common isotopes (i.e., $^{12}C_{14}$ $^{1}H_{11}$ $^{35}Cl_2$ ^{14}N $^{16}O_2$). The second most abundant molecule, with an m/z of 298.021, reflects diclofenac molecules containing the ^{37}Cl isotope. Its relative abundance is approximately 65%, meaning there are 35% less ^{37}Cl-containing DCF molecules than there are of the most abundant isotopologue. In essence, analysts can identify molecules by linking the relative abundances of different isotopologues with knowledge of each elements' isotope ratios [64].

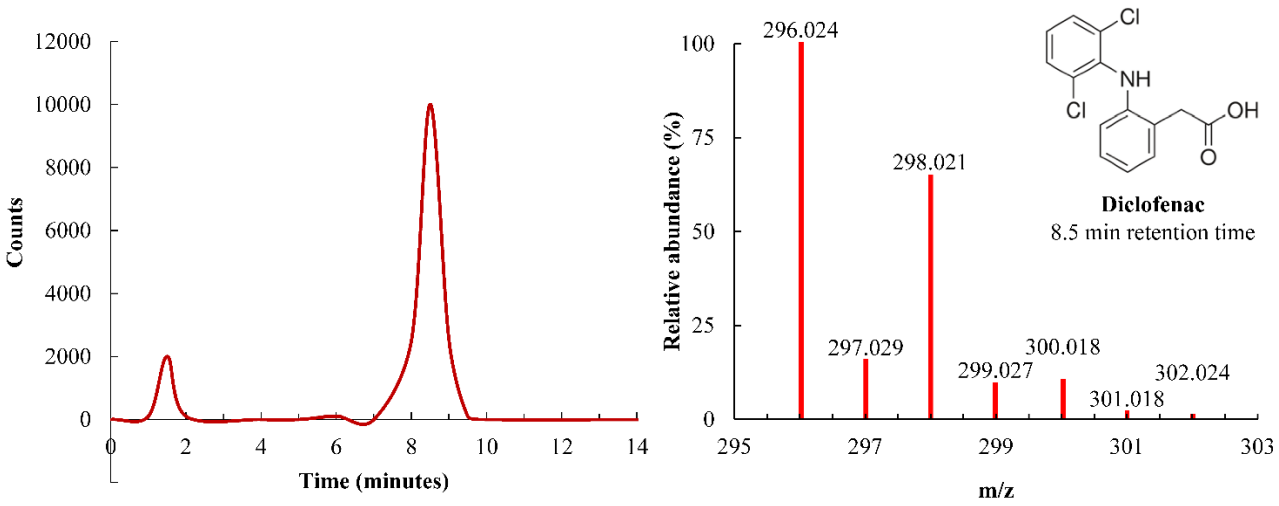

Figure 2.3. Left: The EIC for compounds with an m/z approximately equal to 296.024. To determine which peak belongs to DCF, the mass spectra for compounds eluting at 1.5 and 8.5 minutes must be consulted. The mass spectrum for the compound eluting at 1.5 minutes does not match that for DCF (not shown); however, the mass spectrum for the compound eluting at 8.5 minutes matches that for DCF (right image). Therefore, the EIC peak area at 8.5 minutes can be correlated with DCF concentrations.

Databases, such as enviPat [65], provide mass spectra based on a molecule's chemical formula and the adduct formed, and together with the mass spectra generated during analysis can be used to identify the specific molecule. It is important to note that the ionization source can majorly impact each molecules' mass spectra: some ionization sources cause molecules to fragment into many smaller molecules ("hard" ionization), whereas others simply charge the molecule, allowing it to be separated into its isotopologues ("soft" ionization). Electrospray ionization, a soft ionization source, was used throughout research presented herein, and therefore mass spectra generated from molecular fragmentation were not considered.

Fluorescence Microscopy

Confocal laser scanning microscopy (CLSM) was used to visualize the distributions of various extracellular polymeric substances (EPS) in AGS biofilms throughout pharmaceutical

dosing. CLSM was also used to visualize bacterial distributions in AGS. EPS components were identified using a staining scheme adapted from [17]; stains and their respective targets are listed in Table 2.1. In brief, the four major components of EPS—proteins, lipids, and alpha- and beta-polysaccharides—were targeted and visualized. Bacterial distributions were visualized using fluorescence in situ hybridization (FISH). Both techniques are discussed further in the following text, as well as CLSM.

Unlike conventional widefield laser microscopy, CLSM allows light from only one plane of focus to be collected at a time. This results in improved image quality, as out-of-focus light is neglected [66]. In brief, laser light at a specific wavelength is focused on a point, fluorophores at that point in the sample are excited, and they then re-emit light at a different wavelength. The re-emitted light, or fluorescence signal, is detected, and an image can be built, one point at a time, by scanning in the x- and y-directions. This technique enhances images' optical resolution because only fluorescence from the focal plane is collected [66]. Furthermore, high-resolution images can be collected deeper within the sample by changing the focal plane; images collected within the same sample at multiple depths can be reconstructed into a three-dimensional image.

The staining and CLSM imaging technique used herein utilized the different excitation and emission wavelengths of four different stains: calcofluor white, fluorescein isothiocyanate (FITC), nile red, and concanavalin A conjugated with tetramethylrhodamine (Con A-TRITC). Table 2.1 summarizes the different excitation and emission wavelengths of each stain, as well as the EPS targeted. Figure 2.4 shows CLSM images of stained granules grown in two different environments; staining allows visualization of the different EPS distributions occurring in both granules.

Table 2.1. Stains used to visualize different EPS components in granules [17].

Stain	Excitation (nm)	Emission (nm)	Target
Calcofluor white	400	410-480	β-1,4- and β-1,3 polysaccharides
FITC	488	500-550	Proteins, amino sugars
Nile red	514	625-700	Lipids, hydrophobic sites
Con A-TRITC	543	550-600	α-mannopyranosyl, α-glucopyranosyl sugars (α-polysaccharides)

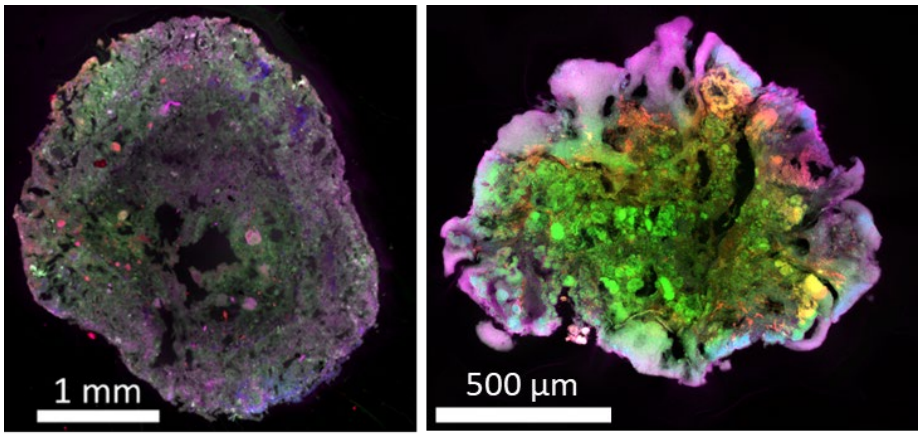

Figure 2.4. Granule sections stained to indicate different EPS components. Left, a granule from the AquaNereda® plant in Rockford, IL; right, a granule grown in the lab. Proteins (green), lipids (blue), alpha-polysaccharides (red), and beta-polysaccharides (pink) are indicated. EPS distributions differ widely between the two granule samples: lab-grown granules' EPS appear more stratified than those in the environmentally-grown granule.

Nucleic Acid Sequencing

Nucleic acids (DNA and RNA) were extracted from AGS and sequenced in order to identify members of the bacterial community and track the effects of pharmaceuticals on active microbial populations. More specifically, the V4 region of 16S ribosomal RNA (rRNA) genes and transcripts were targeted for sequencing. 16S rRNA genes, or rDNA, are DNA sequences that provide code for the 16S subunit of the bacterial ribosome. The 16S rDNA sequence is highly conserved across bacterial species, i.e., it does not change as bacteria evolve, and it is also

present in all bacterial species [67], meaning that it can reliably be targeted in samples with diverse communities. Properties of this gene allow for accurate identification of bacteria down to the species level: conserved regions reflect phylogenetic relationships between bacterial species; variable regions are specific to the species itself [67]. It is therefore not necessary to sequence the entire gene for bacterial identification. The V4 region of this gene is variable and approximately 254 base pairs long; consequently, sequencing this region provides accurate bacterial identification using less computing power [68].

Importantly, the detection of bacterial DNA does not always signify that bacteria were active or alive at the time of sampling. DNA sequences can remain intact for thousands of years in dead organisms [69]; likewise, DNA may be present extracellularly, as a biofilm component or from lysed cells [70]. Furthermore, many bacterial communities contain dormant organisms, and DNA from dormant organisms may be more abundant than that from active ones [71, 72]. For this reason, bacterial communities constructed solely from 16S rDNA sequencing are unlikely to accurately represent the active bacterial community. To address this, bacterial 16S rRNA can be sequenced: used to target active organisms: only translationally-active bacteria produce ribosomes, or molecules consisting mostly of RNA sequences [73]. RNA is much less stable in the environment; thus, its detection signifies recent metabolic activity [72, 73]. Like the gene encoding for the 16S ribosomal subunit, 16S rRNA sequences are highly conserved across all bacterial species, and the V4 region of this sequence can similarly be used for bacterial identification. rRNA instability necessitates reverse transcription of extracted sequences to complementary single-stranded DNA sequences (“cDNA”); cDNA formed from rRNA is referred to as “rRNA transcripts”. Sequencing is ultimately performed on rRNA transcripts.

Both rDNA and rRNA transcript sequencing were performed in this dissertation because rRNA transcript sequencing alone would have been insufficient for identification of active community members. rRNA content varies between species, meaning that higher rRNA reads do not necessarily indicate a more abundant active organism [73]. Furthermore, reverse transcription of rRNA to cDNA can introduce multiple biases into the data—some rRNA sequences may be reverse transcribed better than others, resulting in artificially lower rRNA read numbers for certain taxa [74]. Instead, transcript-to-gene ratios were calculated after sequencing: for each identified taxon, the number of transcript reads was divided by the number of gene reads, per the method in [72]. Taxa with ratios greater than or equal to 1 were considered "active", as it was assumed that active bacteria would have at least as many rRNA transcripts as genes. Ratio thresholds for activity determination in the literature range from 0.5 to 2 [72]. The active community consisted of taxa meeting the forementioned criteria (i.e., rRNA/rDNA $\geq$ 1); rDNA read numbers for active taxa were used to calculate relative abundances within the active community.

"Phantom" taxa, or those with detected rRNA but without detected rDNA, were frequently found throughout research described herein. It is physically impossible for bacteria to have rRNA without rDNA encoding for ribosomes; however, this phenomenon is commonly documented throughout the literature (e.g., [72, 75]). One theory for the presence of phantom taxa is that these taxa are very low in abundance relative to the total community, but are much more active than others, overall resulting in preferential amplification of rRNA transcripts but poor rDNA amplification [75]. Phantom taxa likely play an important role in microbiome function, but their rDNA numbers are zero and therefore their abundance cannot be plotted as

part of the active community. To address the potential roles of phantom taxa, changes in the number of rRNA transcript copy numbers were used to approximate changes in phantom taxa activity levels. More detail on this approach can be found in Chapter 6.

Conclusions

Altogether, aerobic granular sludge is an emerging biotechnology worthy of further investigation. Its potential application as a sustainable treatment technique for pharmaceutical removal from wastewater is particularly promising. The forementioned analytical techniques were used throughout research described herein to explore how pharmaceutical exposure impacted both lab- and environmentally-grown granules. Pharmaceutical impacts on wastewater treatment efficacy, active microbial communities, and biofilm structures within granules cultivated under the two different conditions were examined. Pharmaceutical fates in both the solid and aqueous phases were also documented. This research enhances understanding of the mechanisms used by AGS to remove pharmaceuticals, as well as pharmaceutical impacts to essential wastewater-treating bacteria. Findings from research detailed here contribute to the developing body of knowledge on AGS-driven treatment of PPCPs.

CHAPTER THREE

PHARMACEUTICAL SORPTION TO LAB MATERIALS MAY OVERESTIMATE RATES OF REMOVAL IN LAB-SCALE BIOREACTORS

Contribution of Authors and Co-Authors

Manuscript in Chapter 3

Author: Kylie B. Bodle

Contributions: Designed and conducted study. Collected and analyzed data, wrote and revised manuscript.

Co-Author: Madeline R. Pernat

Contributions: Helped conduct the study, collected data, and provided feedback and comments on the manuscript.

Co-Author: Catherine M. Kirkland

Contributions: Helped conceive and design study, aided in data interpretation, aided in revision of the manuscript and provided comments.

Manuscript Information

Kylie B. Bodle, Madeline R. Pernat, Catherine M. Kirkland

Water, Air, and Soil Pollution

Status of Manuscript:
☐ Prepared for submission to a peer-reviewed journal
☐ Officially submitted to a peer-reviewed journal
☐ Accepted by a peer-reviewed journal
☒ Published in a peer-reviewed journal

Springer
Vol. 233 Issue 12 Page 505
https://doi.org/10.1007/s11270-022-05974-2

Abstract

Environmental contamination from pharmaceuticals has received increased attention from researchers in the past 20 years. As such, numerous lab-scale studies have sought to characterize the effects of these contaminants on various targets, as well as determine improved removal methods. Many studies have used lab-scale bioreactors to investigate pharmaceutical effects on wastewater bacteria, as wastewater treatment plants often act as reservoirs for pharmaceuticals. However, few—if any—of these studies report the specific lab materials used during testing, such as tubing or pipette tip type. In this study, the pharmaceuticals erythromycin, diclofenac, and gemfibrozil were exposed to different micropipette tips, syringe filters, and tubing types, and losses over time were evaluated. Losses to tubing and syringe filters were particularly significant and neared 100%, depending on the pharmaceutical compound and length of exposure time. Results discussed herein indicate that pharmaceutical sorption to various lab supplies results in decreases to both dosed and quantified pharmaceutical concentrations. Studies that fail to consider this source of loss may therefore draw inaccurate conclusions about pharmaceutical effects or removal efficiencies.

Introduction

Pharmaceutical compounds are increasingly detected in environmental matrices around the globe [39, 76]. The presence of these compounds can be traced, in large part, to their release from wastewater treatment plants [46]. Wastewater treatment plants (WWTPs) are generally not designed to remove non-biodegradable compounds like pharmaceuticals; therefore, WWTPs act as reservoirs for pharmaceuticals prior to releasing them, minimally treated, to the environment.

Numerous pharmaceuticals have toxic effects on plants, wildlife, and microbiota at part per billion concentrations [24-26]. Additionally, pharmaceuticals can harm wastewater-treating bacteria, potentially resulting in decreased treatment efficacy as these compounds accumulate [77].

Aerobic granular sludge (AGS) is a promising emerging biotechnology for wastewater treatment. AGS consists of nitrifying, denitrifying, and phosphate-accumulating organisms that self-aggregate into dense, spherical biofilms 1-2 mm in diameter. The high concentration and variety of extracellular polymeric substances (EPS) in AGS confer protection from various toxins and likely provide a sorptive medium for hydrophobic compound removal [3, 4, 78]. Altogether, granules may be capable of simultaneously treating conventional wastewater contaminants while biodegrading or adsorbing recalcitrant compounds, such as pharmaceuticals. However, the body of literature available on granule-driven pharmaceutical treatment is limited, and therefore more information is needed on how granules respond to a wide range of pharmaceuticals.

The initial objective of this study was to evaluate the effects of three model pharmaceuticals on lab-grown AGS. Erythromycin (ERY, antibiotic), diclofenac (DCF, NSAID), and gemfibrozil (GEM, lipid regulator) are three pharmaceuticals commonly found in the environment [26, 38, 41, 42, 57, 76, 79, 80]. However, few studies have investigated the interaction between each compound and AGS.

After analysis of preliminary results, a new objective—and prerequisite—for this study became apparent: understanding, quantifying, and mitigating pharmaceutical losses to various lab supplies. Pharmaceutical losses to influent tubing were particularly evident. A search of the

literature found only one relevant publication in which pharmaceutical sorption to tubing and filter materials was tested, and results were not directly applicable to the study conditions and materials described herein [81]. Likewise, although multiple studies investigate AGS exposure to pharmaceuticals [3, 4, 11, 32, 34, 44, 46, 47, 82-88], several do not report influent concentrations [4, 11, 86-88]. None describe the specific materials used to ensure that desired influent pharmaceutical concentrations were achieved. Several report only overall pharmaceutical removal or effluent concentrations [4, 11, 86-88]. After measuring significant pharmaceutical losses through the influent tubing, we questioned if the removals reported were due entirely to AGS-driven sorption or degradation, or if removals could partially be attributed to losses to lab supplies. We therefore assessed pharmaceutical losses to various micropipette tips, tubing types, syringes, and syringe filters.

Methods

AGS Reactor Operation

AGS were grown in two identical double-walled glass laboratory-scale sequencing batch reactors (SBRs). Both SBRs had an internal diameter of 60 mm and working volume of 3.4 L and were operated in repeating three-hour cycles: 72 minutes anaerobic feed from the bottom of the reactor, 100 minutes aeration at a rate of 5 L/min, three minutes settling, and five minutes effluent discharge from a port 47 cm above the bottom reactor flange. Approximately 50% of the reactor liquid was withdrawn in each cycle, resulting in a hydraulic residence time of 6.4 hours. The solids residence time was controlled at approximately 25 ± 5 days.

An automatic timer (Chrontrol) controlled influent, effluent, and aeration pumps. Labview software (National Instruments) controlled pH (7.0 ± 0.3) and dissolved oxygen (1.75 ±

0.25 mg/L) during the aeration phase. Influent media were identical to those described by [89], except that the concentration of sodium acetate in the influent was increased to 10.3 mM, resulting in an organic loading rate of 2.5 g C/L*d. Both SBRs were initially seeded with AGS from an AquaNereda® treatment plant in Utrecht, The Netherlands and operated at steady state for over 200 days prior to starting experimentation.

For 30 days, the test reactor received 23 mL of pharmaceutical medium with the influent media during the feed phase, resulting in nominal influent concentrations of approximately 10 ug/L of each pharmaceutical. The pharmaceutical medium consisted of 705 ug/L each of erythromycin (TCI Chemicals), diclofenac sodium (Acros Organics), and gemfibrozil (Acros Organics) in nanopure water. Pharmaceutical properties are summarized in Table 3.1. Pharmaceutical stock solutions were prepared first in methanol at 1 g/L and then diluted into water; therefore approximately 7.9 mg/L methanol was also present in the influent medium. The pharmaceutical medium was protected from light to prevent photolytic degradation, prepared fresh every 8-10 days, and sampled directly to quantify pharmaceutical concentrations. Influent samples were taken from a sampling port in the tubing located at the base of the reactor and were extracted and quantified per methods detailed in the following section.

Table 3.1. Physical and chemical properties of tested pharmaceuticals.

	Erythromycin	**Diclofenac**	**Gemfibrozil**
Chemical formula	$C_{37}H_{67}NO_{13}$	$C_{14}H_{11}Cl_2NO_3$	$C_{15}H_{22}O_3$
Molecular weight (g/mole)	733.9	296.1	250.3
Water solubility (mg/L at 25ºC)	2000 [38]	1418 [90]	29.1 [57]
Octanol-water partition coefficient (Log K_{ow})	3.06 [38]	4.51 [91]	4.77 [57]
Acid dissociation constant (pKa)	8.89 [38]	3.99 [91]	4.7 [57]

Pharmaceutical Compound Quantification

Influent and effluent samples were prepared for HPLC-QtoF-MS analyses by solid phase extraction (SPE). Waters Oasis HLB cartridges (30 mg, 20 mL) were preconditioned with 1 mL methanol, dried, and equilibrated with 1 mL nanopure water. 75 mL influent or 150 ml effluent sample were then filtered with a 1.5 µm glass fiber filter (Hach) to remove solids and loaded on the cartridges at 10 mL/min using a vacuum manifold system. Loaded cartridges were washed with 1 mL 5% vol/vol methanol in water, dried for 30 minutes, then frozen at -18°C until elution (no longer than 14 days).

Pharmaceuticals were eluted at 5 mL/min using 2 x 5 mL methanol followed by 2 x 5 mL methanol:acetone (1:1, v/v) mixture. Eluents were evaporated to dryness under a gentle nitrogen stream at 40°C, reconstituted in 1 mL methanol, and stored at -18C until HPLC-QtoF-MS analysis.

To account for possible pharmaceutical losses during the extraction process, influent and effluent pharmaceutical samples were taken in duplicate. One sample from each duplicate set was pre-spiked with pharmaceutical stock solution to a final nominal concentration of 10 µg/L prior to performing any extraction steps. After extraction, the unspiked sample was split in half, and one half was post-spiked to a final nominal concentration equal to 10 µg/L multiplied by each samples' respective concentration factor. Recovery was then determined as follows:

$$Recovery = \frac{Prespike\ concentration - unspiked\ concentration}{Postspike\ concentration - unspiked\ concentration} \quad (1)$$

Measured pharmaceutical concentrations in unspiked samples were thus corrected for recovery of each analyte. Recovery was consistently over 60% for ERY and over 95% for DCF and GEM.

Mass spectrometry was performed with an Agilent 6538 UHD Accurate-Mass QtoF HPLC-MS (Agilent Technologies) in positive ion mode. Chromatographic analysis methods were adapted from [92]. In brief, pharmaceuticals were separated with an Agilent Eclipse Plus C18 column (2.1 x 100 mm) at 30ºC under gradient elution. Methanol and ultrapure water, both enriched with formic acid (0.1% v/v), were used as mobile phases at 0.7 mL/min. Gradient elution was achieved by increasing the concentration of organic solvent from 1% initially to 95% at 10.1 minutes, then returning to initial conditions and re-equilibrating for 3 minutes (total run length of 13 minutes). Sample injection volume was 8 µL. Retention times for ERY, DCF, and GEM were consistently 6.6, 8.4, and 9.1 minutes, respectively.

Analyte concentrations were determined based on a calibration curve relating peak area with nominal concentration in analytical standards in both methanol and water. The instrument limits of quantification were 10 µg/L for ERY and 50 µg/L for DCF and GEM. As a check for biodegradation, all samples were also screened for ERY, DCF, and GEM biodegradation products using a personal compound database and library (PCDL). However, degradation products were not detected in any of the samples described in the following sections, and therefore pharmaceutical losses were likely abiotic in nature.

Lab Supply Sorption Tests

To identify the source of pharmaceutical losses and determine possible mitigating actions, pharmaceutical losses to various micropipette tips, syringe filters, and tubing types were assessed by repeated washing of each with pharmaceutical solution. The lab supplies tested are listed in Table 3.2. Losses to different micropipette tips were quantified first after initial analyses

of standards prepared with Axygen tips resulted in noisy, unpredictable data (not shown). The best-performing micropipette tips identified in this test were used in all future tests.

Table 3.2. Lab supplies tested for pharmaceutical loss. Catalog numbers are included in parentheses.

<table>
<tr><th>Pipette tips</th><th>Syringe filters</th><th>Tubing (all Masterflex)</th></tr>
<tr><td>Ayxgen Maxymum Recovery (AXYTF1000LRS)</td><td rowspan="2">Sartorius MiniSart Regenerated Cellulose (17765K)</td><td>Tygon size 14 (06404-14)</td></tr>
<tr><td rowspan="2">USA Scientific TipOne (1122-1730)</td><td rowspan="2">Puriflex size 14 (96419-14)</td></tr>
<tr><td rowspan="3">Mettler-Toledo Rainin RC-1000LR (17014398)</td><td rowspan="3">FisherBrand PTFE membrane (09-719H)</td></tr>
<tr><td>PharmaPure size 13 and 14 (06435-13, 06435-14)</td></tr>
<tr><td>Platinum-cured silicone size 14 (96410-14)</td></tr>
</table>

Pharmaceutical losses to syringe filters were evaluated next. Many pharmaceutical extraction protocols utilize a final syringe filtration step to remove particulates after reconstituting extracted samples [44, 83, 93-95]; likewise, samples taken directly from the AGS reactor required syringe filtration before analyses. In both cases, filtration volumes were small (under 2 mL) and therefore pharmaceutical loss to the filtration material could have a large impact on measured concentrations. It was therefore important to determine if pharmaceutical loss to syringe filters could be occurring and decreasing measured concentrations. Syringes were also tested for pharmaceutical loss and losses were not detectable (data not shown).

Lastly, pharmaceutical losses to different tubing types were evaluated after preliminary data showed that pharmaceutical concentrations declined as solution travelled through influent tubing.

Mixed solutions of ERY, DCF, and GEM were prepared by diluting a 1 g/L stock solution in methanol into nanopure water. Glassware that had recently been baked in a muffle furnace (550^{o}C x 5 hours to remove all carbon-based contaminants) was used to store all pharmaceutical solutions. Glassware was also tested for pharmaceutical loss and losses were not detectable (data not shown). All pharmaceutical samples taken during lab supply sorption tests were analyzed directly (i.e., not extracted). Losses were calculated as follows:

$$Loss = 100\% \times \left(1 - \frac{Current\ Concentration}{Initial\ Concentration}\right) \quad (2)$$

Pipette Tip Testing. A solution containing each pharmaceutical at 100 µg/L was prepared ("pharmaceutical solution"). This concentration was selected to ensure that pharmaceutical concentrations would remain detectable after losses to tips. One milliliter micropipette tips from Axygen, USA Scientific, and Mettler-Toledo (Table 3.2) were tested for losses. For each tip brand tested, two glass flasks were filled with 50 mL pharmaceutical solution, and samples were immediately taken from both with fresh pipette tips. One flask ("rinse") was then used to pull and discharge 1 mL solution into the pipette tip repeatedly four times. The other flask ("sample") was then used to collect 1 mL of solution for analysis, thereby representing the fifth usage of the pipette tip. In this way, the 0th, 5th, 10th, and 15th "washes" of each tip were sampled. This method ensured that measured concentrations reflected actual pharmaceutical losses to the pipette tip, not declining concentrations in the rinse flask. The test was conducted in triplicate for each pipette tip except the Axygen tips, as initial analyses of standards prepared with Axygen tips showed noisy, unpredictable relationships between peak area and concentration. The goal of this test, therefore, was to determine if USA Scientific or Mettler-Toledo tips performed better than Axygen tips.

Syringe Filter Testing. Regenerated cellulose syringe filters (Sartorius Minisart, 0.45 um x 25 mm) and PTFE membrane syringe filters (Fisherbrand, 0.45 um x 25 mm) were used to test pharmaceutical losses. 500 µg/L pharmaceutical solution was prepared and sampled directly with Mettler-Toledo tips (previously identified as the best-performing micropipette tips). This concentration was selected to ensure that pharmaceutical concentrations would remain detectable after losses to the high surface area material in filters. A 3 mL syringe was used to flush 1.5 mL solution through each filter to flush out any organic contaminants that may have been attached to the syringe filter material. The next mL filtered was then collected and analyzed. Tests were conducted in triplicate with new filters and syringes.

Tubing Testing. The tubing types listed in Table 3.2 were exposed to the target pharmaceuticals in two separate tests. In a short-term test, 30 cm long tubing samples provided by ColeParmer (Table 3.2) were connected to a 1 RPM peristaltic pump. The tubing residence time was approximately two minutes. PTFE tubing was connected to the influent end of each type of tubing to increase the tubing length and submerged in separate pharmaceutical solutions, all at approximately 705 µg/L. Reasoning for the concentration of pharmaceutical solution is provided in the AGS Reactor Operation section. Pharmaceutical losses to PTFE tubing were assumed to be minimal, as this type of tubing was also used during the pharmaceutical extraction and concentration process with good recovery of each analyte. Pump heads compatible with PTFE tubing were not available for this research. Pumping was continuous for 24 hours. Samples were taken with Mettler-Toledo pipette tips from each influent immediately prior to starting pumping, and then collected from the effluent end of each tube type after 24 hours.

The best-performing tubing type identified in the short-term was then utilized for longer-term, higher concentration testing. Triplicate 90 cm lengths of size 13 PharmaPure tubing were connected to a 1 RPM pump, yielding an approximate residence time of six minutes. Influent ends were submerged in separate flasks containing 12.5 mg/L pharmaceutical solution (nominal concentration). Pharmaceutical concentrations were increased with an eye to future testing, as it was desired that influent pharmaceutical concentrations in forthcoming AGS exposure tests would be 50 µg/L. Dilution of 6.5 mL pharmaceutical solution at 12.5 mg/L with 1600 mL influent media would result in the desired 50 µg/L influent concentration.

Pumping was continuous for seven days. Influent samples were taken with Mettler-Toledo pipette tips and effluent samples were collected directly from the effluent end of each tube. After seven days, PTFE tubing was connected to the influent end of one tubing section, and only the PTFE portion was submerged in influent solution. Influent and effluent samples were then collected for the next three days to determine if sorption was occurring preferentially to the inside or outside of the tubing section.

Results and Discussion

Loss to Lab Supplies

Pipette Tips. Pharmaceutical losses to different pipette tips varied from -10 to nearly 20%, depending on the compound and tip used (Figure 3.1). Positive losses after washing indicate that pharmaceutical sorption to the tip was still occurring; negative losses indicate that sorption decreased significantly, resulting in higher pharmaceutical concentrations in the sample released from the pipette tip than were measured in the initial sample. A negative loss may therefore indicate equilibrium-induced desorption. Variation among replicate samples was high

for both tips tested in triplicate; however, Mettler Toledo (MT) tips performed more consistently when exposed to DCF and GEM, as evidenced by lower standard deviation among sample replicates. After the 5th wash, DCF and GEM losses to MT tips were -5.5 ± 2.6% and -9.8 ± 3.5%, respectively. DCF and GEM losses to USA Scientific tips were -6.2 ± 4.4% and 11.9 ± 6.7%, respectively. ERY losses to both tip types were similar and below 1% on average.

Despite the high variability seen in this test, results show that pharmaceutical sorption to different brands of micropipette tips may significantly influence measured sample concentrations—and the number of tip uses is also likely to have a large impact. It is also difficult to conclude why certain tips perform better than others. All tips' manufacturers list virgin polypropylene as the pipette tip material, and all tips had similar geometries. Likewise, it is difficult to correlate the properties of each pharmaceutical (listed in Table 3.1) with losses. ERY has the lowest octanol-water partition coefficient (K_{ow}) of the three compounds tested, which may explain why ERY losses were generally lower than those for DCF or GEM. However, this behavior was not consistent, as ERY and DCF losses to Axygen tips were near equal (-8% and -10%, respectively), despite large differences in K_{ow} values.

Altogether, pharmaceutical losses due to either parameter—tip reuse or brand—may have a large impact on measured concentrations, and the variability associated with pharmaceutical loss may make impacts difficult to predict.

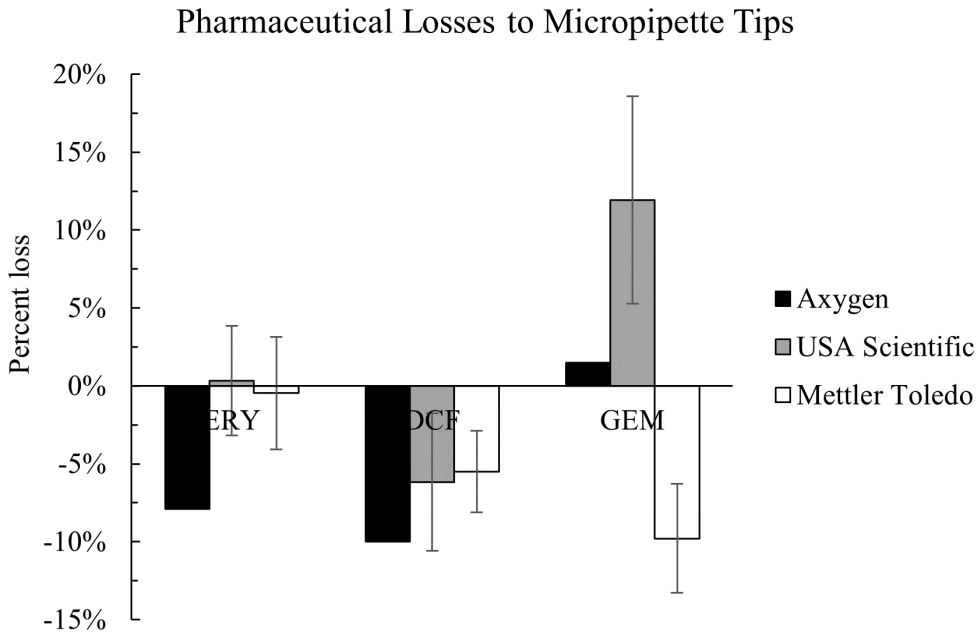

Figure 3.1. Pharmaceutical losses to different brands of 1 mL micropipette tips after five washes. Mettler-Toledo tips performed best of the three brands tested, as losses to these tips were less than those to other brands and variability within replicates was smallest. As previously mentioned, Axygen tips were not tested in triplicate and therefore standard deviation bars are not included for these data.

Syringe Filters. PTFE filters performed much worse than regenerated cellulose (RC) filters during syringe filter testing (Figure 3.2). ERY losses to PTFE filters were 92 ± 2.8%; losses to RC filters had greater variability (46 ± 19%) but were still significantly less than those to PTFE filters ($p = 0.03$). DCF losses to both filter types were not significantly different ($p = 0.09$), but GEM losses to PTFE filters were again greater than those to RC filters ($p = 0.002$). All losses to filters greatly exceed those to pipette tips, excepting DCF loss to RC filters (0.2 ± 5.8%). These results further demonstrate that the use of specific lab supplies may have a non-trivial impact on pharmaceutical quantification.

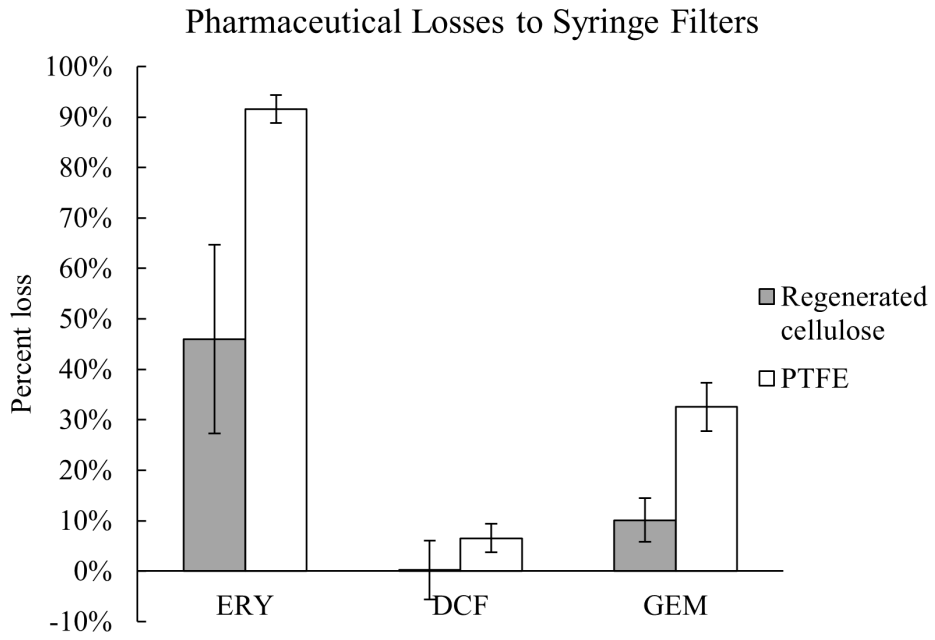

Figure 3.2. Pharmaceutical losses after flushing 1.5 mL through RC or PTFE syringe filters. Regenerated cellulose filters far outperformed PTFE filters, as indicated by much smaller losses to these filters.

Pharmaceutical Dosing into AGS Sequencing Batch Reactor

Figure 3.3 shows the influent and "theoretical influent" concentrations into the test sequencing batch reactor (SBR). Theoretical concentrations were calculated by measuring the concentration of each pharmaceutical in the pharmaceutical medium, and then multiplying it by the influent dilution factor of 0.014. For all pharmaceuticals, theoretical influent (TI) concentrations are much greater than actual influent concentrations, which indicates a loss of each compound somewhere in the influent tubing to the reactor.

Both DCF and GEM TI concentrations are relatively constant for the test period, excepting day 33, which may be an outlier; this may indicate that sorption of DCF and GEM to the Tygon tubing submerged in the pharmaceutical medium was minimal. Most sorption of these

compounds likely occurred to platinum-cured silicone ("silicone") tubing located past the feedstock bottle. Actual influent concentrations of DCF and GEM were consistently 2.5 and 4.7 times lower than TI concentrations, respectively.

Conversely, TI ERY concentrations decreased over time and recovered each time fresh pharmaceutical medium was prepared, indicating ERY sorption to the Tygon tubing in the pharmaceutical medium. ERY also adsorbed to silicone tubing located past the feedstock bottle, as evidenced by up to seven times lower ERY concentrations in the actual influent.

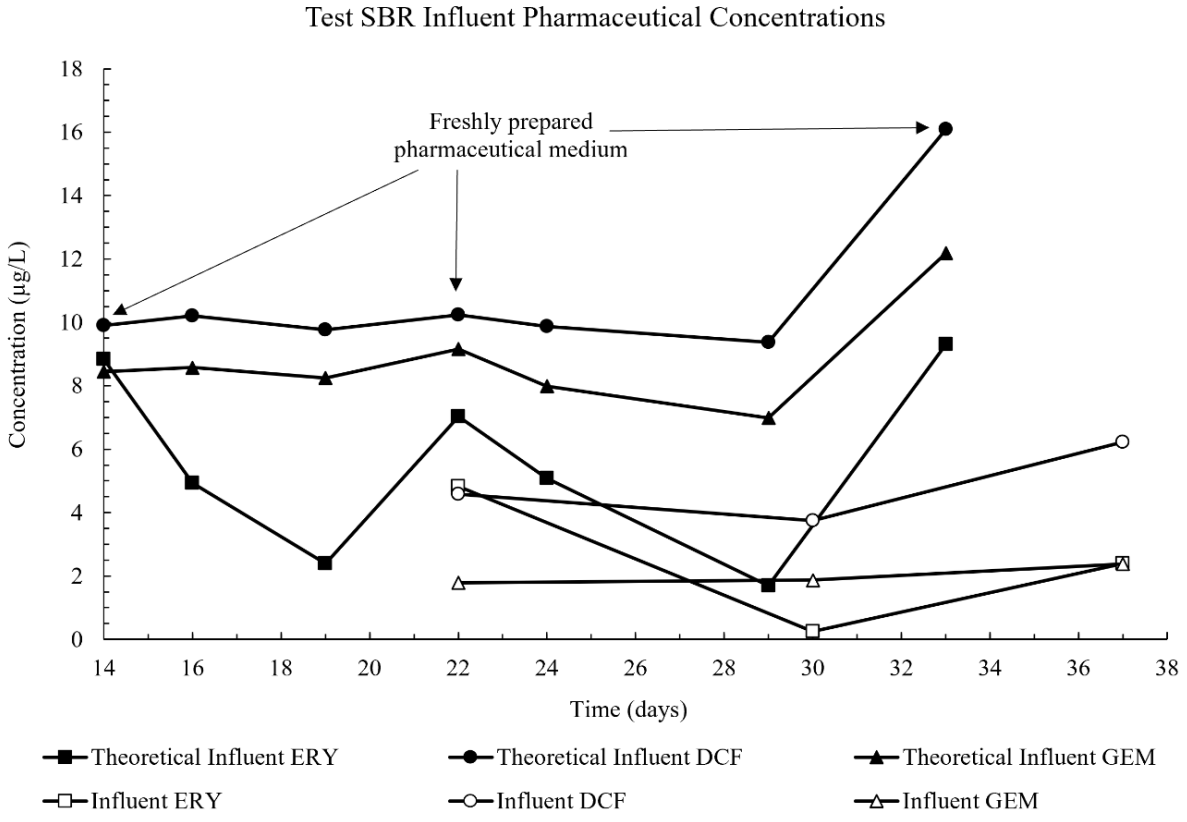

Figure 3.3. Theoretical influent and actual influent pharmaceutical concentrations to the test AGS SBR. Theoretical influent concentrations (solid lines) were calculated by measuring pharmaceutical concentrations in the feed medium and then multiplying those by a dilution factor. Theoretical influent concentrations should equal actual influent concentrations (dashed lines); the discrepancies shown here indicate losses of all three compounds to the influent tubing to the reactor.

Sorption to Tubing. Pharmaceutical losses to different tubing types in short-term tests are shown in Figure 3.4. Loss of each pharmaceutical to the silicone tubing roughly imitated actual influent results shown in Figure 3.3: DCF loss was smallest, followed by ERY, then GEM. Likewise, pharmaceutical losses to Tygon tubing followed the pattern seen in theoretical influent samples in Figure 3.3, with large ERY losses, near zero DCF losses, and fairly small GEM losses. PharmaPure tubing performed best of the tubing types tested, with only 6, 3, and 7% of ERY, DCF, and GEM lost from influent to effluent over 24 hours, respectively. Again, losses to pipette tips were generally less than those to tubing.

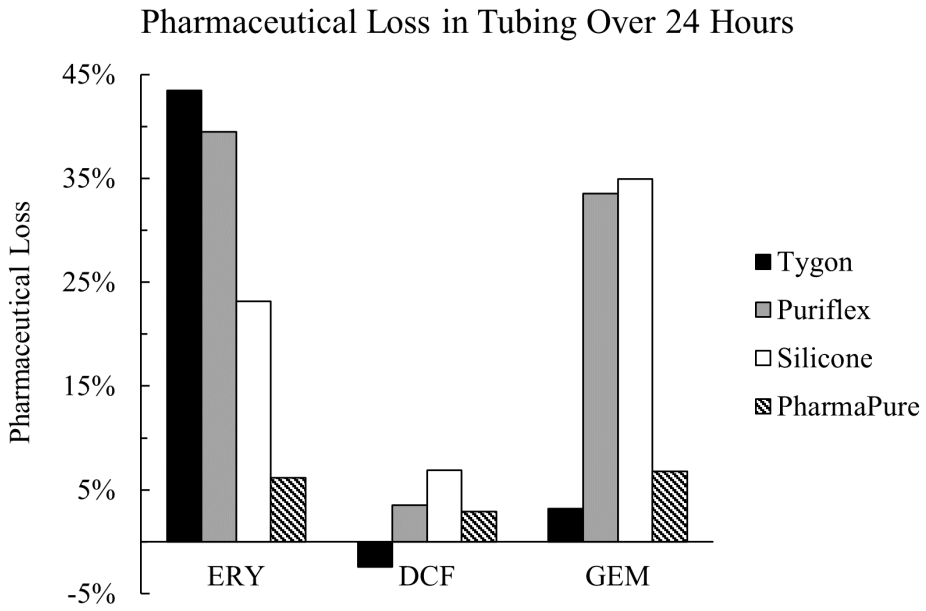

Figure 3.4. Pharmaceutical losses to different brands of size 14 tubing after 24 hours of constant exposure to 705 µg/L pharmaceutical solution. Losses to PharmaPure tubing were generally smallest and most consistent of the four tubing types tested, as ERY, DCF, and GEM losses were all under 7%.

Figure 3.5 shows results from a longer-term test with PharmaPure tubing. In this test, the influent end of each tubing replicate was submerged in pharmaceutical medium until day seven, after which PTFE tubing was connected to the influent end and submerged instead. Immediately

after this change, effluent GEM concentrations increased to near equal influent ones. GEM may have adsorbed preferentially to the outer, uncoated portion of the submerged tubing, causing lower concentrations at the tubing-liquid interface to enter the tubing, despite higher concentrations in the bulk influent liquid. Upon removing the tubing from the liquid, higher bulk GEM concentrations were then able to enter and exit the tubing, unchanged. This may have occurred due to the different surface properties of PTFE and PharmaPure tubing—in addition to chemical resistance, PTFE is known to be generally smoother and less porous than other materials [96], and therefore may have provided less surface area for GEM sorption than the outer surface of the PharmaPure tubing.

DCF sorption was minimal throughout testing, with effluent concentrations consistently not statistically different from influent ones, except for the initial exposure on day zero ($p = 0.13$-0.3).

Likewise, despite declining ERY concentrations throughout the entire test, influent and effluent ERY concentrations were not significantly different at any time point ($p = 0.37$-0.94). This indicates that, from day zero to seven, ERY sorption was occurring solely to the outer, uncoated portion of the PharmaPure tubing, because additional losses to the inner portion would have resulted in different influent and effluent concentrations. Sorption was also great enough to decrease bulk influent liquid concentrations, not just those at the liquid-tubing interface. Interestingly, connecting PTFE tubing to the influent end of the PharmaPure tubing did not stop ERY loss. ERY concentrations continued to decline, albeit at a slightly lower rate, from day eight to 11. The reasons for this are unknown—ERY may have adsorbed to the PTFE tubing. Degradation products were not detected in any samples, and therefore losses were likely abiotic.

Results from this test also highlight the importance of testing materials under lab-relevant conditions: the existing study of pharmaceutical sorption to tubing soaked small pieces of tubing in pharmaceutical solution, and therefore was unable to distinguish if sorption occurred to the inside or outside of tubing types [81].

Although the residence time of pharmaceutical solution in the size 13 PharmaPure tubing was approximately three times longer than that of the size 14 tubing, and the concentration of pharmaceutical solution tested was much higher, similar loss trends in both short- and long-term tests were observed when PTFE tubing was submerged. DCF and GEM losses were near zero from day eight to 11. However, although influent and effluent ERY concentrations were equal on days eight and 11, approximately 54% of ERY was lost from the influent on day eight to the effluent at day 11. It is possible that the increased residence time, combined with higher ERY concentrations, resulted in greater ERY sorption to the submerged PTFE tubing, which may explain why ERY concentrations continued to decline. Altogether, results suggest that DCF and GEM sorption to tubing is not highly concentration- or residence time-dependent, but ERY sorption likely is. It is also worth noting that, although submerged PTFE tubing appeared to partially mitigate pharmaceutical losses, losses to PTFE syringe filters were high. This may be due to the increased surface area of the membrane within each syringe filter.

It is difficult to conclude why certain tubing types sorb more pharmaceuticals than others. The surface roughness and pore size distribution of each tubing material are likely to have a large impact on the sorptive properties of each [97]; however, these data are not publicly available from Masterflex. Different functional groups on the tubing material itself may have also impacted sorption [97], though this data is also unavailable. Furthermore, the chemical properties

of the pharmaceuticals tested do not always correlate with observed sorptive behaviors. For example, GEM has the highest K_{ow} and lowest molecular weight of the pharmaceuticals tested (Table 3.1), which should translate to a higher affinity for carbonaceous materials and an ability to penetrate pores more easily in each tubing type [98], resulting in greater sorption. However, GEM losses to tubing were not consistently higher than those of other pharmaceuticals. Similarly, ERY has the largest molecular weight and lowest K_{ow} of the compounds tested (Table 3.1), but long-term losses to PharmaPure tubing far exceeded those of DCF or GEM (Figure 3.5). Altogether, these results indicate that review of materials' chemical and physical properties alone may not be sufficient for rigorous experimental designs—testing is necessary to confirm compatibility.

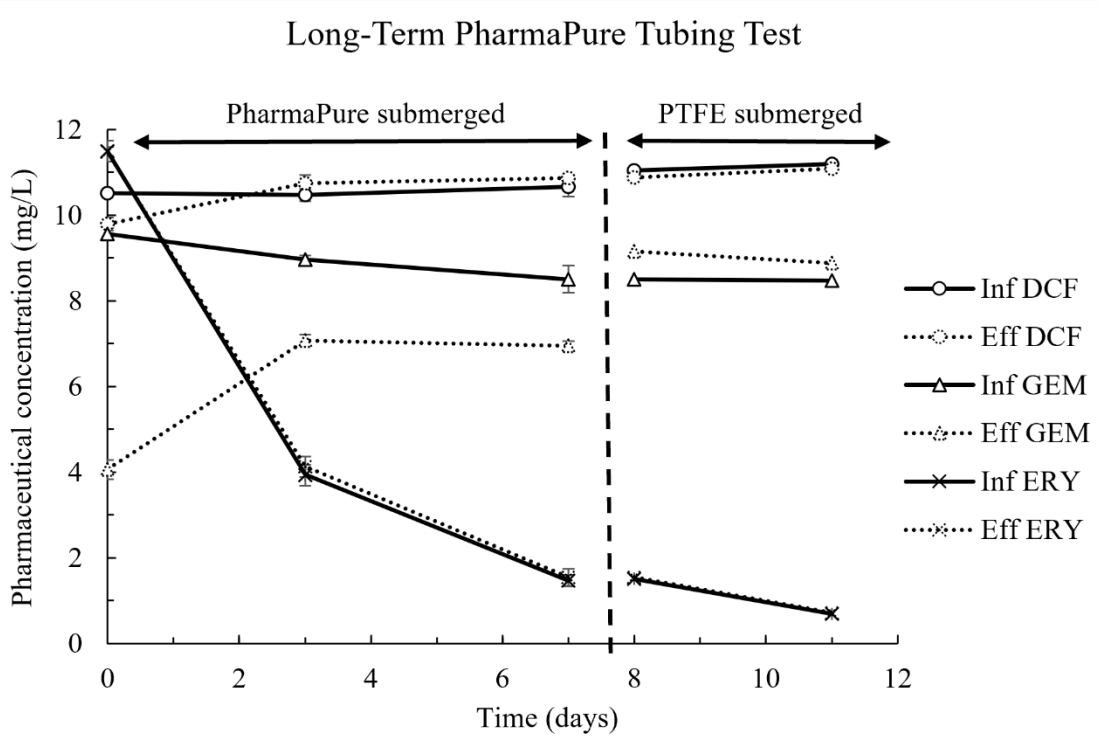

Figure 3.5. Results of a longer-term pharmaceutical exposure test with size 13 PharmaPure tubing and 12.5 mg/L pharmaceutical solution. Error bars represent standard deviation of triplicate samples and are at times smaller than points. DCF losses were negligible over time and GEM losses stopped after PTFE tubing was submerged in the influent pharmaceutical solution.

ERY losses were largest when PharmaPure tubing was submerged, but continued to decline slightly after PTFE tubing was submerged in the influent solution.

Conclusions

ERY, DCF, and GEM losses due to adsorption to various tubing materials, brands of 1 mL pipette tips, and syringe filter materials were quantified and were significant. Depending on the pharmaceutical and the material, losses were at times over 90%. In particular, pharmaceutical sorption to the influent tubing to a test AGS reactor greatly reduced the concentrations of pharmaceuticals dosed.

Results from these tests show that failure to consider pharmaceutical adsorption to various lab supplies may result in overestimation of pharmaceutical removal rates in bioreactors, as well as underestimation of pharmaceuticals in environmental samples. This issue is particularly problematic in cases where pharmaceutical removal is attributed solely to adsorption to biological materials, as is often the case in experiments with aerobic granular sludge: many studies assume that decreasing aqueous concentrations of the tested compounds are due to adsorption to AGS [3, 4, 32, 46, 47, 82, 84]. However, results from the tests discussed herein indicate that it is essential to first confirm that various lab materials do not significantly sorb the dosed contaminants—otherwise, concluding that AGS, or other biological materials, are the sorptive medium may be inaccurate.

Declarations

This research is supported by Montana INBRE, which is funded by the National Institute of General Medical Sciences division of the National Institutes of Health under Award Number

P20GM103474. Special thanks also to staff at the Mass Spectrometry Facility at Montana State University (MSU) for training and assistance. Funding for the Proteomics, Metabolomics and Mass Spectrometry Facility used in this publication was made possible in part by the MJ Murdock Charitable Trust, the National Institute of General Medical Sciences of the National Institutes of Health under Award Numbers P20GM103474 and S10OD28650, and the MSU Office of Research, Economic Development and Graduate Education. The content is solely the responsibility of the authors and does not necessarily represent the official views of the National Institutes of Health.

The datasets generated and/or analyzed during the current study are available from the corresponding author on reasonable request.

The authors have no relevant financial or non-financial interests to disclose. Study conceptualization and methodology: Kylie B. Bodle; Formal analysis and investigation: Kylie B. Bodle, Madeline R. Pernat; Writing – original draft preparation: Kylie B. Bodle; Writing – review and editing: Catherine M. Kirkland, Madeline R. Pernat, Kylie B. Bodle; Funding acquisition, resources, and supervision: Catherine M. Kirkland.

CHAPTER FOUR

TREATMENT PERFORMANCE AND MICROBIAL COMMUNITY STRUCTURE IN AN AEROBIC GRANULAR SLUDGE SEQUENCING BATCH REACTOR AMENDED WITH DICLOFENAC, ERYTHROMYCIN, AND GEMFIBROZIL

Contribution of Authors and Co-Authors

Manuscript in Chapter 4

Author: Kylie B. Bodle

Contributions: Designed and conducted study. Collected and analyzed data, wrote and revised manuscript.

Author: Rebecca C. Mueller

Contributions: Analyzed data, provided supervision, and wrote and revised manuscript.

Co-Author: Madeline R. Pernat

Contributions: Helped conduct the study, collected data, and provided feedback and comments on the manuscript.

Co-Author: Catherine M. Kirkland

Contributions: Helped conceive and design study, aided in data interpretation, aided in revision of the manuscript and provided comments.

Manuscript Information

Kylie B. Bodle, Rebecca C. Mueller, Madeline R. Pernat, Catherine M. Kirkland

Frontiers in Microbiomes

Status of Manuscript:
☐ Prepared for submission to a peer-reviewed journal
☐ Officially submitted to a peer-reviewed journal
☐ Accepted by a peer-reviewed journal
☒ Published in a peer-reviewed journal

Frontiers
Vol. 2 Issue 1242895
https://doi.org/10.3389/frmbi.2023.1242895

Abstract

This study characterizes the effects of three commonly detected pharmaceuticals—diclofenac, erythromycin, and gemfibrozil—on aerobic granular sludge. Approximately 150 μg/L of each pharmaceutical was fed in the influent to a sequencing batch reactor for 80 days, and the performance of the test reactor was compared with that of a control reactor. Wastewater treatment efficacy in the test reactor dropped by approximately 30-40%, and ammonia oxidation was particularly inhibited. The relative abundance of active *Rhodocyclaceae, Nitrosomonadaceae,* and *Nitrospiraceae* families declined throughout exposure, likely explaining reductions in wastewater treatment performance. Pharmaceuticals were temporarily removed in the first 12 days of the test via both sorption and degradation; both removal processes declined sharply thereafter. This study demonstrates that aerobic granular sludge may successfully remove pharmaceuticals in the short term, but long-term tests are necessary to confirm if pharmaceutical removal is sustainable.

Introduction

Pharmaceutical consumption has increased concomitantly with population growth [99]. A natural consequence of this is increasing pharmaceutical contamination in the environment, due in part to incomplete metabolism by humans, followed by poor removal by conventional wastewater treatment systems [76, 99]. As such, improved wastewater treatment methods are worthy of investigation, as exposure to pharmaceuticals can cause antibiotic resistance gene proliferation as well as numerous other adverse effects on plants, animals, and microbiota [10, 24, 31].

Aerobic granular sludge (AGS) is an emerging wastewater treatment biotechnology that may be capable of enhancing pharmaceutical removal from wastewater [32, 84]. AGS is highly diverse with populations of nitrifying, denitrifying, and phosphate-accumulating organisms that self-aggregate into spherical biofilms. The gel-like extracellular polymeric substances (EPS) secreted by bacteria in AGS confer protection from toxins and enhance AGS density, resulting in short settling times and high biomass retention [1]. Furthermore, the EPS in AGS may provide a sorptive medium for organic compound removal [3, 4]. However, the body of literature on AGS-driven pharmaceutical treatment is limited, and therefore more information is needed on how granules respond to a wide range of pharmaceuticals.

The pharmaceuticals diclofenac (DCF), erythromycin (ERY), and gemfibrozil (GEM) were selected for use in this study because, though each is frequently detected in the environment [26, 38, 57], few studies exist on each compound's interaction with AGS. Diclofenac is a commonly used non-steroidal anti-inflammatory drug (NSAID) that is poorly removed (under 40%) in conventional wastewater treatment systems [50]. It has also been shown to act synergistically with antibiotics to prevent biofilm formation [53]. Erythromycin is a macrolide antibiotic commonly used in both human and veterinary medicine, and has been shown to bioaccumulate in multiple aquatic species [38]. Lastly, gemfibrozil is a fibrate, or lipid regulator, that has been shown to inhibit growth and cause endocrine disruption in various aquatic organisms [62]. All three compounds have been detected in wastewater treatment plant influents at concentrations as high as 64 μg/L [26, 38, 57].

There were three objectives of this study: (1) Identify how the three common, but relatively unstudied, pharmaceuticals listed above impact conventional wastewater treatment by

lab-grown AGS; (2) investigate the fate of each pharmaceutical by tracking aqueous and solid phase parent compounds and degradation products; and (3) track microbial community and activity changes throughout exposure. To our knowledge, no studies have confirmed pharmaceutical biodegradation by AGS using detection of degradation products. Notably, the byproducts formed during degradation of pharmaceuticals may be more toxic than the parent pharmaceuticals, and therefore it is vital to improve understanding of the intermediates and products formed. Abiotic removal of the dosed pharmaceuticals was monitored in this study but is not discussed in order to allow sufficient discussion of biotic processes here. In particular, this study sought to link shifts in the active microbial community in pharmaceutical-exposed granules with changes in wastewater treatment efficacy and pharmaceutical fate.

Methods

AGS Reactor Operation

AGS sequencing batch reactor (SBR) operation is detailed in [100]. In brief, AGS was grown in two identical glass SBRs with a working volume of 3.4 L. Both SBRs were operated in repeating three-hour cycles: 72 minutes anaerobic feed, 100 minutes aeration at a gas flow rate of 5 L/min, three minutes settling, and five minutes effluent discharge. The hydraulic residence time in both reactors was approximately 6.4 hours, and the solids residence time was controlled at approximately 25 ± 5 days. SBR operating parameters are consistent with those in other lab-scale studies (e.g., [4, 11, 46]. During aeration, pH and dissolved oxygen were controlled with LabVIEW software (National Instruments) at 7.0 ± 0.3 and 1.75 ± 0.25 mg/L, respectively. Influent media were identical to those described by [89], except that influent sodium acetate was increased to 10.3 mM, resulting in an organic loading rate of 2.5 g C/L*d. Both SBRs were

initially seeded with AGS from an AquaNereda® treatment plant in Utrecht, The Netherlands and operated at steady state (i.e., complete nitrogen and phosphate removal) for over 300 days prior to beginning experimentation. Immediately before starting experimentation, both SBRs were emptied and AGS was combined, mixed, and redistributed so that granule qualities would be as similar as possible in both reactors.

For 80 days, the test reactor received 46 mL of pharmaceutical media with the influent medium, resulting in an influent concentration of approximately 150 µg/L of each pharmaceutical. Individual stock solutions of each pharmaceutical were prepared first in methanol at 10 g/L, then diluted into nanopure water to obtain two pharmaceutical media: one solution ("DG") containing 17.86 mg/L each of diclofenac sodium (Acros Organics) and gemfibrozil (Acros Organics), and a second solution ("ERY") containing 35.8 mg/L erythromycin (TCI Chemicals). Twenty-three mL of each solution (46 mL total) were delivered with the influent medium throughout the anaerobic feed period. Approximately 0.13 mg/L methanol was also present in the combined influent stream. The pharmaceutical media were protected from light to prevent photolytic degradation and prepared fresh every 8-10 days.

Results discussed in [100] showed that the pharmaceuticals tested herein sorbed to different lab materials with different affinities; therefore, to ensure the accuracy of pharmaceutical dosing, ERY solution was pumped into the reactor using silicone tubing (Masterflex). DG solution was pumped into the reactor using PharmaPure tubing (Masterflex). Despite different pharmaceutical stock solution concentrations, sorption to tubing resulted in fairly stable influent concentrations of approximately 150 µg/L of each pharmaceutical. Although each pharmaceutical is typically measured in wastewater treatment plant influents at

approximately 1-10 µg/L [26, 38, 57], pharmaceutical sorption to tubing drove usage of this elevated influent concentration: 150 µg/L was the minimum concentration of pharmaceuticals that could be consistently dosed to the test reactor without significant losses from sorption. Influent samples were taken from a sampling port in the tubing located at the base of the reactor (reactor schematic available in Appendix A, Figure A.1) and were extracted and quantified per methods detailed in the following sections.

Analytical Methods – Conventional Wastewater Analytes

Influent and effluent samples from both reactors were regularly taken and filtered through 0.45 µm regenerated cellulose filters prior to analyses for ammonia, nitrite, nitrate, phosphate, and dissolved organic carbon. Ammonia was quantified with Hach kit TNT 832 and a Hach DR 3900 spectrophotometer, equivalent to US EPA Method 350.1. Other anions listed were quantified with a Dionex ICS-1100 anion chromatography system equipped with an IonPac AS22 RFIC column (4 x 250 mm) and IonPac guard column (4 x 50 mm). Dissolved organic carbon (DOC), defined as that which could pass through a 0.45 µm filter, was measured with a SKALAR Formacs^{HT} Total Organic Carbon analyzer system.

Analytical Methods – Pharmaceutical Analyses

Aqueous influent and effluent samples were prepared for mass spectrometry (MS) analyses by solid phase extraction (SPE) as detailed in [100]. It is important to note that the periodic flow conditions that are characteristic of SBR systems allow constant sorption and desorption of pharmaceuticals within influent tubing. For this reason, the most accurate method of quantifying influent concentrations would have required extraction of the entire influent volume, which would been too destructive to reactor operation. For that reason, 100 mL influent

or effluent sample were filtered with a 1.5 μm glass fiber filter (Hach) to remove solids and loaded on preconditioned Waters Oasis HLB cartridges (30 mg, 20 mL) at 10 mL/min using a vacuum manifold system. Loaded cartridges were washed, dried, and frozen at -18°C until elution (no longer than 14 days). Pharmaceutical losses to the lab materials used during extraction (glassware, syringes, pipette tips, and glass fiber filters) were tested for and were found to be minimal [100].

Influent and effluent pharmaceutical samples were periodically taken in duplicate to account for possible pharmaceutical losses during the extraction process, as detailed in [100]. In brief, one sample from each duplicate set was pre-spiked with pharmaceutical stock solution to a final nominal concentration of 100 μg/L prior to extraction. After extraction, the unspiked sample was split in half, and one half was post-spiked to a final nominal concentration equal to 100 μg/L multiplied by each samples' concentration factor. Recovery was then determined as follows:

$$Recovery = \frac{Prespike\ concentration - unspiked\ concentration}{Postspike\ concentration - unspiked\ concentration}$$

Measured pharmaceutical concentrations in unspiked samples were thereby corrected for recovery of each analyte. Recovery was 97 ± 9% for DCF, 117 ± 17% for ERY, and 98 ± 11% for GEM (Table 4.1). Triplicate influent and effluent samples were taken once per month to assess accuracy. Pharmaceutical quantification and detection were performed with an Acquity I Class Plus ultra-performance liquid chromatograph (UPLC) coupled to a Waters Synapt XS quadrupole time-of-flight mass spectrometer (QToF-MS) in positive ion mode. Chromatographic analysis methods were adapted from [92]. In brief, pharmaceuticals were separated with an Agilent Eclipse Plus C18 column (2.1 x 100 mm) at 30°C under gradient elution. Formic acid-

enriched methanol and ultrapure water (0.1% v/v) were used as mobile phases at 0.7 mL/min, and the concentration of organic solvent was increased from 1% initially to 95% at 10.1 minutes, then returned to initial conditions and re-equilibrated for 3 minutes (total run length of 13 minutes). Sample injection volume was 8 µL. Retention times are summarized in Table 4.1.

Table 4.1. Physical and chemical properties of tested pharmaceuticals, as well as average extraction recoveries and retention times.

	Diclofenac	**Erythromycin**	**Gemfibrozil**
Chemical formula	$C_{14}H_{11}Cl_2NO_3$	$C_{37}H_{67}NO_{13}$	$C_{15}H_{22}O_3$
Molecular weight (g/mole)	296.1	733.9	250.3
Octanol-water partition coefficient (Log K_{ow})	4.51 [91]	3.06 [38]	4.77 [57]
Aqueous phase extraction recovery	97 ± 9%	117 ± 17%	98 ± 11%
Solid phase extraction recovery	75 ± 8%	56 ± 22%	68 ± 8%
UPLC retention time (minutes)	8.8	6.8	9.5

A calibration curve relating each pharmaceuticals' peak area with its nominal concentration in analytical standards was used to determine parent compounds' concentrations. Standards were prepared in both methanol and water. The instrument limits of quantification were under 10 µg/L for all compounds. The open-source software MZmine and R were used to analyze and compile mass spectra data [101, 102].

All samples were also screened for DCF, ERY, and GEM biodegradation products using a personal compound database and library (PCDL) developed from the literature (Table A.1). Degradation products are reported when mass errors were less than 5 ppm and the signal-to-noise ratio of peaks was greater than or equal to 10. The goal of this approach is not to quantify degradation products' concentrations but simply to use the presence of degradation products as

an indicator of biodegradation. The relative concentrations of aqueous degradation products were tracked over time by calculating corrected peak areas as follows:

$$Aqueous\ corrected\ peak\ area = \frac{Degradation\ product\ peak\ area \times Concentration\ factor}{Peak\ area\ of\ relevant\ 100\frac{\mu g}{L}\ standard}$$

where the "relevant standard" term refers to the peak area of the related parent compound at 100 µg/L. For example, the peak area of an aqueous ERY degradation product would be divided by the peak area of the 100 µg/L ERY standard measured during the same mass spectrometry run and multiplied by the sample's concentration factor (e.g., a 100 mL sample extracted and concentrated to 1 mL had a concentration factor of 100).

Pharmaceuticals were also extracted from granules to quantify solid phase concentrations per methods adapted from [103]. Extraction methods are summarized in Appendix A. All solid phase samples were screened for degradation products as described above. Solid phase samples were extracted in triplicate once per month and periodically evaluated for recovery using spike-recovery testing, as described above. Average recoveries are summarized in Table 4.1. Peak areas of degradation products in the solid phase were corrected as follows:

$$Solid\ corrected\ peak\ area = \frac{Degradation\ product\ peak\ area}{Peak\ area\ of\ relevant\ 100\frac{\mu g}{L}\ standard\ \times Sample\ dry\ weight\ (g)}$$

Aqueous and solid samples were periodically analyzed from the control reactor for pharmaceutical parents and degradation products. Except when noted otherwise, pharmaceuticals were not detected in any phase in the control reactor. Likewise, degradation products were generally not found in the influent to the test reactor.

Lastly, the toxicities of detected degradation products were estimated using the US Environmental Protection Agency's Toxicity Estimation Software Tool (TEST). TEST estimates chemical toxicity using quantitative structure activity relationships [104].

Bacterial Community Composition

DNA/RNA Extraction. Granules from both reactors were periodically sampled for molecular characterization of the prokaryotic microbial community using high throughput sequencing of 16S rRNA genes and transcripts. Granules were collected during the aeration phase to ensure samples were fully mixed and representative of communities in the entire reactor. Samples were stored at -80°C prior to extraction. Nucleic acids were extracted from approximately 10 granules at each time point. Extraction and analyses of replicate nucleic acid samples were beyond the scope of this study. All samples were extracted at once by bead beating in DNA/RNA Shield (Zymo Research), then DNA was purified from the lysate with the DNA Clean and Concentrator Kit (Zymo Research). RNA samples were extracted from the same lysate with the Direct-zol RNA Miniprep Kit (Zymo Research), digested with the TURBO DNA-free Kit (Invitrogen), and purified with the RNA Clean and Concentrator Kit (Zymo Research). RNA was then reverse transcribed to cDNA using the ProtoScript II First Strand cDNA Synthesis Kit (New England Biolabs). DNA and RNA concentrations were quantified with Qubit dsDNA HS and RNA HS kits (Invitrogen), respectively. For all kits listed, the manufacturer-provided protocols were followed.

Metagenome Characterization. Metagenomic sequencing of granules was conducted on granular inoculum approximately 300 days before beginning the experimentation described herein; therefore, metagenome data provides an approximation of microbe functionality within

granules (given the time between metagenome sampling and the onset of the experiment). DNA was extracted using the Zymobiomics DNA Miniprep kit and quantitated with the Qubit dsDNA kit (Invitrogen). Libraries were prepared for shotgun metagenomic sequencing on the Illumina NovaSeq platform using paired end 150bp sequencing at Novogene with a target of 15Gb of data. To quality filter fastq files, prinseq was used to remove sequences with more than 10 Ns, mean quality scores below 20, sequences shorter than 50 nt, and to trim ambiguous bases from the ends of reads. Paired end sequences were then assembled using metaSPades (v 3.15.5, [105] with kmer sizes from 21 to 99 and all reads were mapped against the resulting scaffolds using Bowtie2 [106]. The sam files were converted to bam format using samtools [107]. We binned scaffolds into putative metagenome assembled genomes (MAGs) using MetaBat2 (v 2.2.15, [108]. CheckM (v 1.2.2, [109] was used to calculate MAG quality, the relative abundance of each bin (based on the number of reads mapped to each MAG), and to construct a multigene phylogeny. Any MAG with completeness greater than 50% and with contamination above 10% was refined using Anvio (v 7.1, [110]. To classify the taxonomy of putative bins, we used GTDB-tk [111] against the v207 database release.

To gain insights into the potential functional pathways contained within the abundant MAGs, putative genes were identified using prodigal and compared to the Kyoto Encyclopedia of Genes and Genomes (KEGG) with the program KOFAM scan [112]. Pathway completeness measures were generated using KEGG Decoder [113]. This analysis was focused on MAGs with completeness over 90%, combined with MAGs that had lower completeness but made up over 1% of the community. Our analysis focused primarily on nitrogen cycling, based on previous

findings showing shifts in these pathways in reactors with pharmaceutical-exposed wastewater [114].

16S Library Preparation and Sequencing. To characterize the prokaryotic community, Phusion Hot Start II DNA polymerase (Thermo Scientific) was used to target the V4 region of the 16S rRNA gene with the primers 515F-A (GTGYCAGCMGCCGCGGTAA) and 806R-b (GGACTACVSGGGTATCTAAT). Reactions were 20 µL each with final concentrations of 0.4 mM dNTPs, 0.2 mM primers, and 1 U polymerase. Thermocycling conditions consisted of an initial denaturation at 98°C for 10 seconds followed by 30 cycles of denaturing at 98°C for 20 seconds, annealing at 60°C for 10 seconds, and elongating at 72°C for 30 seconds. A final extension was then performed at 72°C for 5 minutes. PCR products were purified with Mag-Bind TotalPure NGS beads (Omega), and samples were then barcoded with the Nextera XT Index Kit v2 Set D (Illumina). Barcoded samples were again purified with Mag-Bind beads, quantified, and pooled at equimolar concentration into a sample library containing approximately 30 ng DNA from each sample. Sequencing was performed onsite at Montana State University with the Illumina MiSeq platform using the v3 600 cycle kit. Raw sequence files were deposited to GenBank (BioProject ID PRJNA985155).

Statistics and Data Analysis. USEARCH software was used to merge forward and reverse reads, quality filter with a max score of 1, trim primer sequences, and dereplicate sequences. The UNOISE3 algorithm was used to identify zero-radius OTUs (ZOTUs) and construct an OTU table. To classify ZOTUs, we used SINTAX against a reference database of 16S sequences from the Genome Taxonomy Database (GTDB, release 202, [115]) with outgroup sequences for chloroplast and mitochondria. Sequences identified as Eukarya or with a bootstrap value less

than 70% at the phylum level were removed from downstream analyses. A phylogenetic tree was constructed using a reference maximum likelihood tree generated from full length and near-full length 16S sequences downloaded from GenBank and GTDB using RAxML [116]. MAFFT [117] was used to align the OTUs to the reference sequences; OTUs were then inserted into the reference tree with pplacer [118].

The goal of targeting both rRNA genes and transcripts (cDNA) was to examine both the total microbial community, defined as the community recovered in DNA reads, and the active microbial community, defined as ZOTUs with a ratio of 16S rRNA transcripts to rRNA genes greater than or equal to 1 [119]. Rarefied ZOTU matrices of rRNA transcripts (cDNA) and rRNA genes paired by sample were used to calculate the transcript to gene ratios and identify active OTUs across 100 rarefaction trials. To account for so-called phantom taxa, or taxa detected in rRNA but not rRNA gene sequences, values were set to 100 based on methods described in [119] prior to calculating mean values across trials. Due to the potential for bias in sequence numbers arising during cDNA transcription, DNA read numbers were used to calculate diversity indices. DNA read numbers for phantom taxa were also included in the active community. To examine differences among the community pools, non-metric multidimensional scaling ordination was used to compare the total (DNA-based), RNA-based, and active communities. Taxa were grouped at the family level to calculate changes in relative abundance over time.

To link shifts in the active microbiome with changes in nitrogen and phosphorus levels, as well as pharmaceutical degradation, we used vector fitting of effluent concentrations of DCF, ERY, and GEM using the function envfit in vegan [120]. More specifically, to examine if

specific microbial groups could be linked to the strong decline in pharmaceutical removal observed between days 5 and 17, we calculated response ratios of the active ZOTUs with greater than 0.1% relative abundance between these time points. These values ranged from -1 to 1, with 1 being a strong increase in relative abundance at day 17, and -1 being a strong decrease. Values between -0.5 and 0.5 were considered neutral. The calculated values were added to the phylogeny as a dataset within the ITOL annotation platform to examine the potential for cohesive negative or positive responses within specific clades. All statistical analyses were conducted using R software (version 4.2.2, [101] with packages vegan [120], picante [121], and phyloseq [122].

Results

Pharmaceutical Impacts on Granular Wastewater Treatment Performance

Immediately after pharmaceutical dosing to the test reactor began, nitrogen removal dropped to approximately 70% (Figure 4.1). There was a brief recovery in nitrogen removal from day 6 to 20, during which removal peaked at 93%, though removal declined thereafter and stabilized at approximately 70%. Poor nitrogen removal was due mainly to incomplete ammonia oxidation (Figure A.2). Nitrite and nitrate concentrations in both control and test reactors were approximately equal for the entire experimental duration (Figure A.3), indicating that nitrite oxidation and denitrification were minimally impacted by pharmaceutical exposure. Nitrogen removal data for the control reactor are not plotted past day 40 because the software controlling both reactors experienced an error on day 40, stopping dissolved oxygen control in the test reactor and resulting in an acid overdose to the control reactor. DO control to the test reactor was

interrupted for just 24 hours; however, the acid overdose to the control reactor caused shutdown of that reactor for 10 days. It is reasonable to expect that complete nitrogen removal would have continued in the control reactor if not for this disruption.

Phosphate removal also declined sharply in the test reactor and remained noisy for the entire experimental duration (Figure 4.1). Despite this, DOC consumption was over 90% in both reactors (Figure A.4), and most carbon continued to be consumed anaerobically in the test reactor (Figure A.5). Near-complete anaerobic carbon consumption suggests the potential activity of glycogen accumulating organisms, discussed more in the following sections.

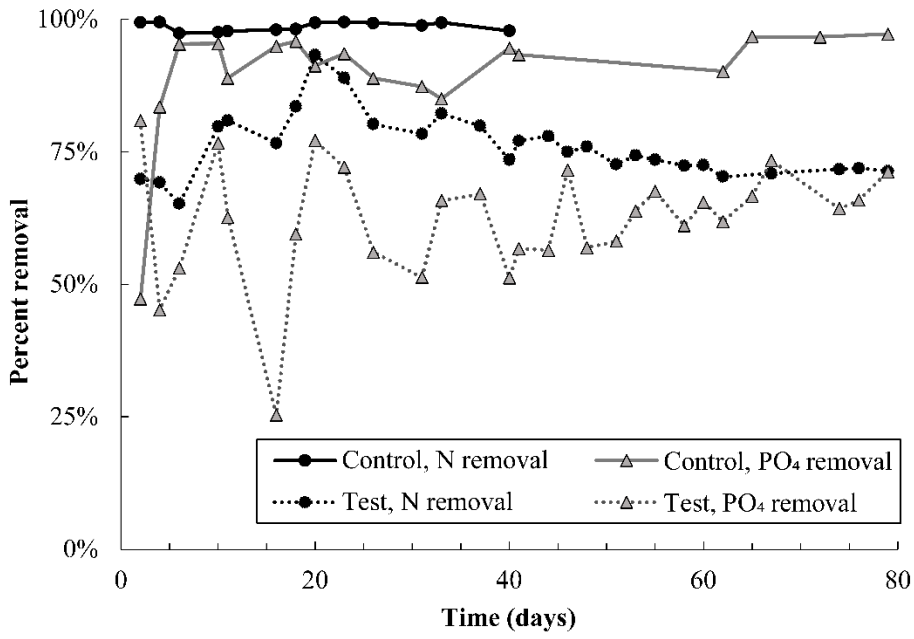

Figure 4.1. Total nitrogen and phosphate removal in the control and test SBR during the pharmaceutical dosing period. Note that N removal data in the control reactor is not plotted after day 40 because an acid overdose in the control reactor severely inhibited nitrifying populations. Given trends prior to the acid overdose, it is likely that nitrogen removal in the control would have proceeded at 100% if not for this issue. Nitrogen and phosphate removal in the test reactor averaged out at 73 ± 2% and 63 ± 6%, respectively, over the last 40 days of the experiment.

Pharmaceutical Removal

All pharmaceuticals were partially removed in the first 10-12 days of dosing, evidenced by lower effluent than influent concentrations (Figure 4.2, Figure A.6). Removal was calculated by performing a mass balance on influent and effluent concentrations at each time point (Appendix A, equations A1 and A2). Degradation products were also detected during the first 12 days (Figure 4.3). However, from day 12-23, effluent concentrations of all pharmaceuticals spiked to approximately twice influent concentrations, indicating a release of retained pharmaceuticals from the reactor. Solid phase data collected over this time frame also appear to indicate desorption of pharmaceuticals from AGS (Figure A.6). Pharmaceutical degradation is discussed in more detail in the following sections.

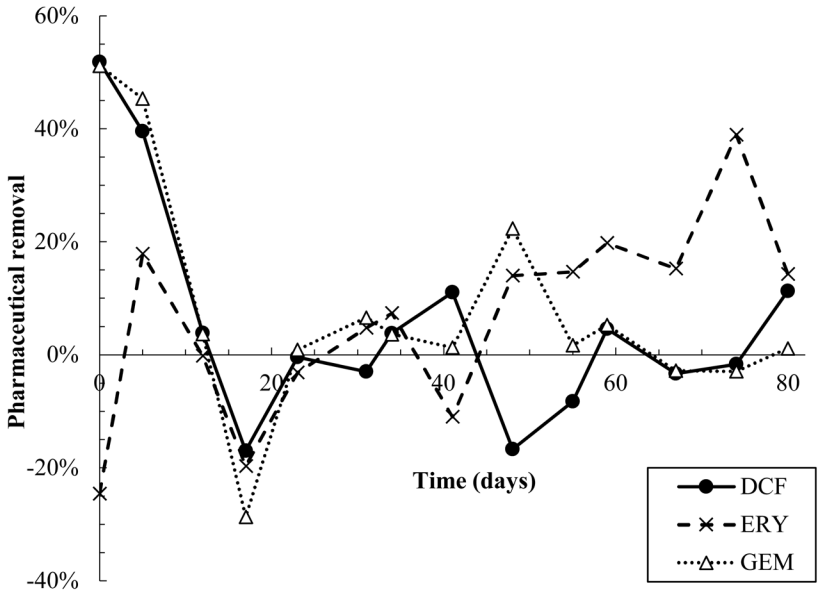

Figure 4.2. Pharmaceutical removal versus time. Removal was calculated based on a mass balance using measured influent and effluent concentrations (Appendix A equations A1 and A2). Negative removal percentages indicate that effluent concentrations were higher than predicted by the mass balance.

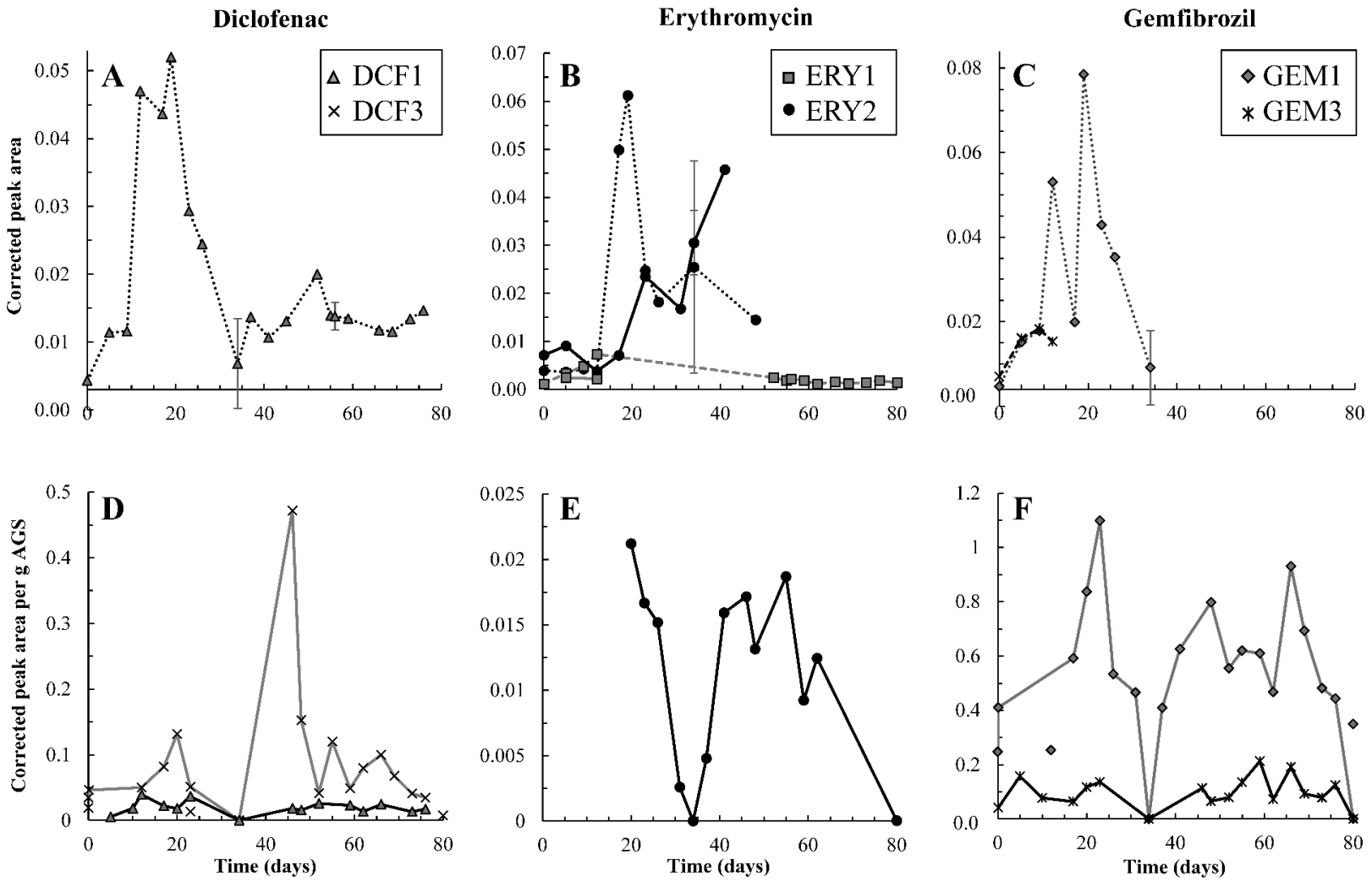

Figure 4.3. Top row, A-C: aqueous degradation products detected over time in the effluent (dashed and dotted lines) from the test reactor for DCF, ERY, and GEM, respectively. Y-axes all reflect corrected peak area but differ in scale. ERY-associated degradation products were temporarily detected in the influent (solid lines) to the test reactor. However, corrected peak areas

of both ERY-associated products were generally higher in the effluent than influent, and therefore AGS-driven biodegradation of these compounds was likely occurring. Bottom row, D-F: solid phase degradation products for DCF, ERY, and GEM, respectively. Note that y-axes differ in scale though each reflects corrected peak area per g AGS. Points not connected by a line indicate detections in control granules. DCF3 was detected three times in control granules, likely due to cross-contamination during mass spectrometry analyses. Likewise, GEM1 was detected twice in control granules. Error bars, representing standard deviation of triplicate samples, are present for both aqueous and solid data on days 34, 56, and 80, and at times are smaller than sample points. Points on these days are averages.

Diclofenac. Pharmaceutical fate was most clearly interpreted for DCF: over the first 12 days, solid phase DCF concentrations increased, while effluent concentrations remained lower than influent ones, and removal peaked at approximately 50% (Figure 4.2). The DCF degradation products hydroxy-DCF ($C_{14}H_{11}Cl_2NO_3$, "DCF1") and 1-(4-hydroxyphenyl)-2-,3-dihydro-1H-indol-2-one ($C_{14}H_{11}NO_2$, "DCF3") were also present in the aqueous and solid phases in the first 12 days (Figure 4.3). Taken together, these data indicate removal via sorption and biodegradation.

From days 17-23, desorption and a decline in biodegradation capacity likely caused DCF to spike in the effluent: on days 17 and 19, effluent concentrations peaked while solid phase DCF concentrations sharply declined (Figure A.6), suggesting desorbing DCF contributed to higher concentrations in the effluent. Likewise, aqueous phase DCF1 peaked from days 12-19 (Figure 4.3), suggesting that bacteria in AGS were less capable of converting this product to further intermediates. Solid phase peak areas of DCF1 also increased slightly over the same timeframe, likely because aqueous phase concentrations were higher and therefore increased sorption was possible.

Influent and effluent DCF concentrations were near equal from day 23 on, indicating negligible DCF removal. Interestingly, aqueous and solid phase DCF degradation products were detected for the remainder of the experiment. The presence of these products may indicate partial biodegradation, albeit not at rates significant enough to result in measurable removal.

The degradation products detected represent initial and tertiary products, according to a pathway proposed in [123]: DCF1 is formed first via mono-oxygenation. DCF1 may be present as two isomers, 4'-hydroxy-DCF and/or 5-hydroxy-DCF, but the UPLC-QToF-MS method used

herein was unable to differentiate between the two. It is most likely that DCF1 was present as the 4' isomer, as DCF3 is formed from degradation of this isomer. 4'-hydroxy-DCF is then converted to 1-(2-chloro-4-hydroxyphenyl)-3H-indol-2-one ($C_{14}H_{10}NO_2Cl$, "DCF2") via reductive dechlorination and amidation, and DCF3 is then formed via further reductive dechlorination [123]. Further degradation of DCF3 is hypothesized in [123], but intermediate structures are unknown.

Pharmaceutical degradation products may have had an inhibitory effect on bacteria in AGS; however, the impacts of many degradation products on wastewater bacteria or other environmental receptors are not well understood. Regarding the herein-detected DCF degradation products, a study by [124] showed that 4'-hydroxy-DCF inhibits ATP synthesis in rat liver mitochondria, though concentrations tested were higher than would be expected in humans and significantly higher than those in the environment. Conversely, 4'-hydroxy-DCF did not have any inhibitory impact on *Vibrio fischeri* bacteria at up to 20 mg/L [125]. The toxicity of DCF3 has not been established in the literature, therefore TEST was used. Toxicity estimates for all detected degradation products are summarized in Table A.2. In general, the predicted toxicities for detected degradation products are similar to or slightly less toxic than those for DCF, with the exception of DCF1, which is predicted to be more bioaccumulative and toxic to fathead minnows.

Erythromycin. Similar to DCF, ERY was removed in the first 12 days of dosing via both sorption and biodegradation. Effluent concentrations were lower than influent ones for the first five days, and aqueous phase degradation products were also measured at low levels over the initial 12-day period (Figure 4.2, Figure 4.3, Figure A.6). Notably, ERY removal was negative

on day zero, indicating that measured effluent concentrations were higher than those predicted by a mass balance (Figure 4.2). It is probable that negative removal on day zero is an artifact of noisy influent pharmaceutical concentrations, as discussed in the Analytical Methods – Pharmaceutical Analyses section and shown in Figure A.6. Influent ERY concentrations on day zero were likely higher than measured, given that influent concentrations then stabilize at approximately 207 ± 22 μg/L for the next 20 days. Between days 12-23, aqueous ERY degradation products then spiked, as did effluent ERY concentrations, evidenced by negative removal (Figure 4.3).

Low levels of the primary and secondary products 3-depyranosyloxy ERY ($C_{29}H_{53}NO_{10}$, "ERY1") and 7,12-dyhydroxy-6-deoxyerythronolide B ($C_{21}H_{38}O_8$, "ERY2"), respectively [126, 127], were present up to day 12, indicative of biodegradation. On days 17 and 19, ERY2 concentrations spiked in the effluent, likely indicating that conversion of this secondary product to further intermediates was no longer occurring at the same capacity. Interestingly, both products were also present in the influent (solid lines in Figure 4.3B). Influent ERY1 concentrations were lower than effluent ones, indicating that AGS contributed to formation of ERY1. ERY2 concentrations were higher in the influent than effluent and continued to increase until day 40. The presence of both ERY1 and ERY2 in the influent likely indicates photodegradation or ERY biodegradation by contaminating biomass in the influent tubing. ERY2 was also present in the solid phase throughout the test.

After day 20, effluent ERY concentrations declined to near influent ones. Approximately 19 ± 9.7% removal was sustained after day 48, perhaps due to slightly elevated solid phase concentrations over the same time (Figure 4.2, Figure A.6). The presence of aqueous and solid

phase ERY degradation products for the remaining test duration may also indicate partial removal via biodegradation.

ERY degradation pathways potentially used by wastewater bacteria and proposed in [127] and [128] hypothesize that ERY1 is formed first via cleavage of the cladinose sugar from ERY. Cladinose was not detected in this study, likely because it is readily metabolizable. ERY1 then undergoes further degradation to ERY2 via cleavage of the desosamine sugar from ERY1, and the final product of ERY degradation is 2,4,6,8,10,12-hexamethyl-3,5,6,11,12,13-hexahydroxy-9-ketopentadecanoic acid ($C_{21}H_{40}O_9$, "ERY3"). Desosamine and ERY3 were also not detected, again likely because both are readily metabolizable, or because the mass spectrometry method used was not suitable for these compounds. Although ERY removal peaked at 18% in the first 12 days of dosing, the low levels of both ERY1 and ERY2 detected in that period suggest that intermediates completed the degradation pathway and end products were fully metabolized.

The TEST-predicted toxicities of ERY1 and ERY2 are summarized in Table A.2. ERY1 and ERY2 appear to be less toxic to aquatic organisms than ERY, though both are predicted to be more toxic to rats.

Gemfibrozil. Much like DCF and ERY, GEM removal occurred due to a combination of sorption and biodegradation in the first 12 days of dosing, followed by a spike in effluent concentrations from days 12-23 (Figure 4.2). Removal was then near zero for the remainder of the test. Aqueous GEM degradation products were not detected in the effluent after day 34 (Figure 4.3). The primary and tertiary products 5-[2-(hydroxymethyl)phenoxy]-2,2-dimethylpentanoic acid ($C_{15}H_{22}O_4$, "GEM1") and 2-[(4-carboxy-4-methylpentyl)oxy]benzoic

acid ($C_{15}H_{20}O_5$, "GEM3"), respectively [129], were both measured up to day 12. GEM1 then spiked in the effluent. This pattern also mimics that seen for DCF and ERY degradation products: Primary products were converted to downstream intermediates until day 12, after which conversion stopped occurring to the same extent, causing primary products to wash out in the effluent.

The same primary and tertiary products were present in the solid phase for the entire experimental duration (Figure 4.3), which may indicate a preference of these compounds for the solid phase and/or continuous low levels of biodegradation. Regardless, biodegradation was not significant enough to impact GEM removal. GEM1 was also detected twice in control granules, likely due to carry over during mass spectrometry analyses: GEM1 was not detected in control influent or effluent, and relative solid phase concentrations were lower in control samples than test granules.

Kjeldal *et al.* (2016) isolated a GEM-degrading Bacillus species from activated sludge and proposed a degradation pathway in which GEM is first converted to GEM1 via hydroxylation [129]. GEM1 is next oxidized to 5-(2-formylphenoxy)-2,2-dimethylpentanoic acid (GEM2), which is then further oxidized to GEM3. According to the degradation pathway proposed in [129], GEM3 degradation may undergo two to three further reactions before reaching final products. Based on this, the GEM degradation observed in the first 12 days may have proceeded to approximately 50% completion, though degradation rates were insufficient for complete removal. Further GEM degradation may have also occurred, but UPLC-MS methods may not have been suited to detect other products. TEST-predicted toxicities of GEM2 and

GEM3 are summarized in Table A.2. Predicted toxicities and bioconcentration factors are generally lower for degradation products than for GEM.

Functional Potential of Granules from Shotgun Metagenomics

Metagenomic sequencing generated approximately 25 million high quality reads, resulting in a total of 19 bins with greater than 90% completeness and less than 5% contamination, and an additional 38 with completeness greater than 50% with less than 10% contamination. All MAGs were classified as members of the bacteria, including known members of glycogen accumulating organisms (GAOs) such as species in the *Competibacter* and *Contendibacter*. Phosphorus accumulating organisms (PAOs) were also present, such as species within the *Accumulibacter*. A MAG identified as a species in the *Accumulibacter* was the most abundant organism detected, at 19% of the population based on the number of raw reads that mapped to the MAG.

Despite the presence of multiple MAGs identified as known ammonia oxidizing bacteria (AOB), including *Nitrosospira* and *Nitrosomonas*, this pathway was not uncovered in the KEGG analysis of constructed MAGs, though the complete ammonia oxidation pathway was found in the total shotgun community (Figure 4.4). The scaffolds with identified ammonia monooxygenase (*amo*) genes (*amoA, amoB,* and *amoC*) were relatively short (< 6000 bp). One scaffold contained all three *amo* genes, and another scaffold contained just *amoA* and *amoC*. Based on BLAST [130], both were highly similar to sequences identified from *Nitrosomonas* species; one scaffold was similar to a MAG identified as *Nitrosomonas* from a metagenomic analysis of biofilms in wastewater treatment plants [131]. The absence of this pathway in putative AOB in the assembled MAGs could be due to the relatively low genome completeness

calculated for these taxa, as the *Nitrosomonas* MAG (Granule57, Figure 4.4) was 87% complete; however, the relative abundance of this organism was 0.66%, and was not included in the overall KEGG analysis. In addition, this MAG had the pathway for nitrite reduction and nitric oxide reduction associated with NOB. We also identified the complete pathway for hydroxylamine oxidation, the second step in nitrification, in the total community, but not in the assembled MAGs.

Nitrate reductase genes were widespread in the granule community, as seen in previous metagenomic studies of wastewater [132]. Twelve MAGs contained genes for the complete dissimilatory nitrate reduction pathway and of those, ten also contained the full nitrite oxidation pathway (Figure 4.4) including members of the *Rhodocyclaceae*, a *Competibacter,* and a MAG classified as a member of the Thermoanaerobaculia. Only a single MAG (Granule56) had the pathway for dissimilatory nitrate reduction to ammonia (DNRA), identified as a species in the Thermoanaerobaculia in the phylum Acidobacteriota, which also contained the dissimilatory nitrate reduction pathway. An organism related to the Thermoanaerobaculia was also detected in the active community, but at very low levels (< 0.1% relative abundance).

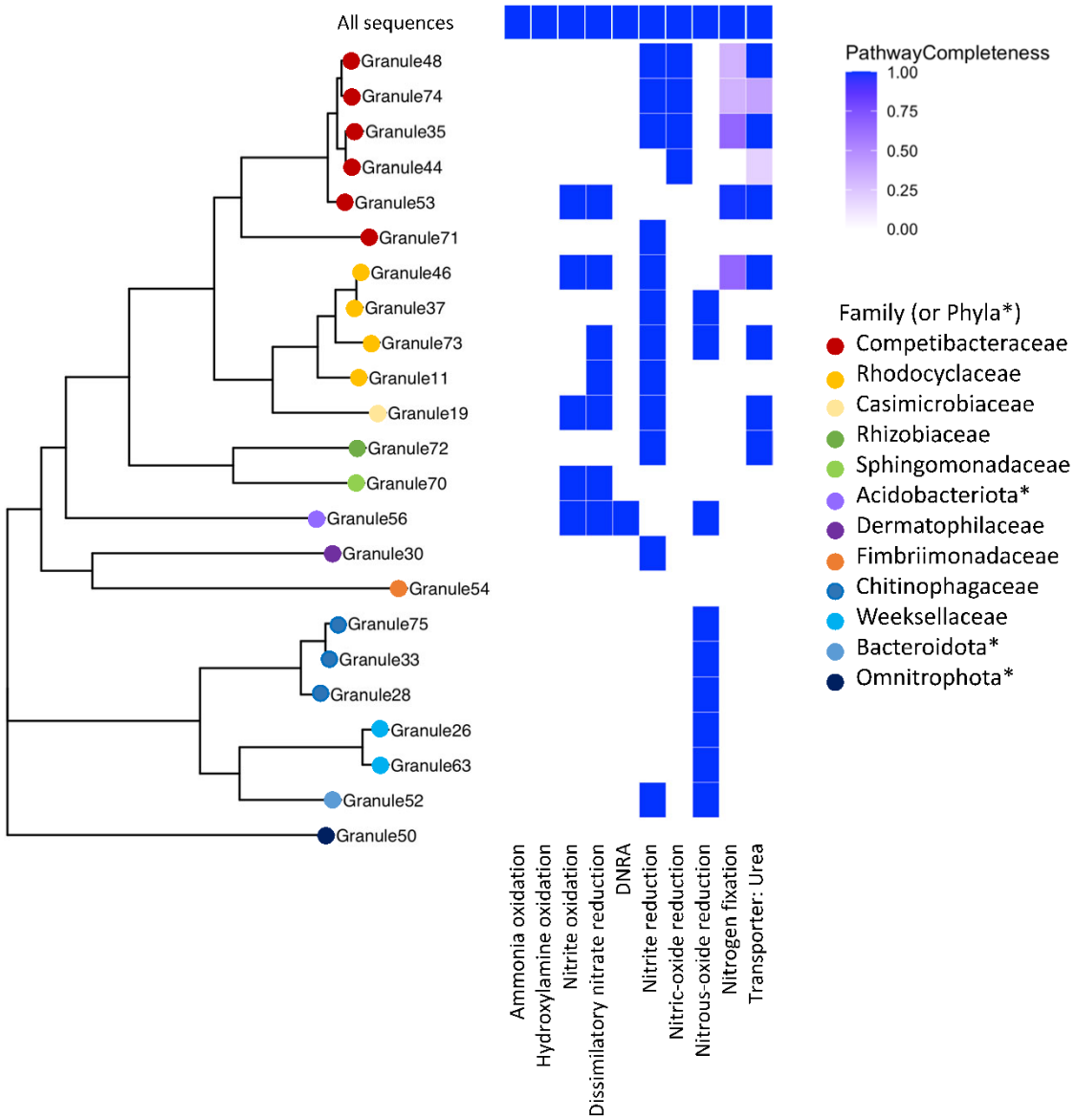

Figure 4.4. A multigene phylogeny of assembled MAGs and the level of completeness for nitrogen cycling pathways. Organisms identified from the assembled MAGs were from a range of families, with a large number in the Pseudomonadota (e.g., Competibacteraceae, Rhodocyclaceae) and the Bacteroidota. *Phyla, rather than family, are listed when the GTDB-provided family name corresponds to an uncultivated organism. None of the assembled MAGs contained the ammonia oxidation pathway, but multiple MAGs had complete denitrification pathways, primarily for dissimilatory nitrate reduction. Note that granule numbering is arbitrary and was simply used to differentiate different samples.

Active Microbial Community Response to Pharmaceuticals

Shifts in the active microbial community were evaluated using 16S sequencing of rRNA genes and transcripts throughout pharmaceutical exposure. As described in the Bacterial Community Composition section, the active microbial community was defined as ZOTUs with a ratio of 16S rRNA transcripts (i.e. cDNA) to rRNA genes greater than or equal to one. The 16S rRNA gene read numbers from ZOTUs identified as "active" were then used to calculate relative abundances within the total active community. Multidimensional ordination (Figure A.7) showed separation of the three pools (DNA, RNA, and active), but also showed separation of the treatment and control SBRs.

At day zero, the distributions of active families in both the control and test reactors were similar: *Competibacteraceae*, *Rhodocyclaceae*, and *Chitinophagaceae* were most abundant (Figure 4.5). Notably, the *Rhodocyclaceae* family includes PAOs (*Candidatus Accumulibacter)* and a potential denitrifying genus (*Zoogloea*). The role of bacteria in the *Chitinophagaceae* family is unclear—multiple OTUs matching *Niabella*, *Terrimonas,* and *Flavipsychrobacter* genera were detected, but to date, the function of these genera in AGS is unknown.

After five days, active families in the test and control SBRs diverged greatly. In the test reactor, active *Rhodocyclaceae* spiked in abundance at day five, from 14 to 46% (Figure 4.5), which may be linked with the brief recovery in phosphate removal between days four and 10 (Figure 4.1). Active *Rhodocyclaceae* then declined sharply in abundance in the test reactor for the remainder of the dosing period, stabilizing at approximately 1.5 ± 0.7% abundance for the second half of the test. In contrast, active *Rhodocyclaceae* in the control reactor were present at 10.2 ± 5% for the entire test duration.

Despite large shifts in the test reactor community, significant correlations between microbial community composition and effluent pharmaceutical concentrations were generally not found. A significant, though small, correlation between effluent GEM concentrations and the microbial community was observed ($R^2 = 0.28$, $p = 0.048$).

Despite the lack of overall correlations, when times with the largest differences in pharmaceutical removal (specifically days 5 through 17, Figure 4.2) were focused on, the strongest declines in relative abundance were concentrated within the Gammaproteobacteria and primarily in *Rhodocyclaceae* (Figure 4.5, Figure A.8). The most striking shift for any single ZOTU was observed for a sequence classified as a member of *Azonexus (*family *Rhodocyclaceae*), which made up 40% of the active community at day 5 but was absent by day 17. Large changes in relative abundance were also observed for two members of *Accumulibacter*, which were present at over 1% of the active community on day 5 but were not detected by day 17.

In contrast, positive responses were distributed across the phylogeny, with the largest shift occurring in a ZOTU identified as a *Methylotenera* species: relative abundance increased from under 0.1% at day 5 to 22% at day 17. Likewise, a ZOTU identified as a Bacteroidia species (UBA2475_sp013816615) increased from under 0.1% to 6% over the same time period. Positive shifts were also observed for members of the Chloroflexota, Gammaproteobacteria, and Acidobacteriota (Figure A.8).

We had limited success linking the ZOTUs to the organisms identified in the metagenome assemblies. Of the top ten most abundant ZOTUs in the active community, three had no close relatives in the metagenome. The most abundant active ZOTU in the test reactor

(genus *Methylotenera*, order Burkholderiales), was not detected in the assembled MAGs; however, this is likely due to the length of time elapsed between metagenome sampling and the onset of experimentation as well as the presence of pharmaceuticals. Four ZOTUs were classified as *Competibacter A denitrificans* with varying levels of confidence. The remaining ZOTUs with a close relative in the metagenome included a *Xanthomonadaceae* (genus SCMT01), a species of *Accumulibacter*, and an *Azonexus* species.

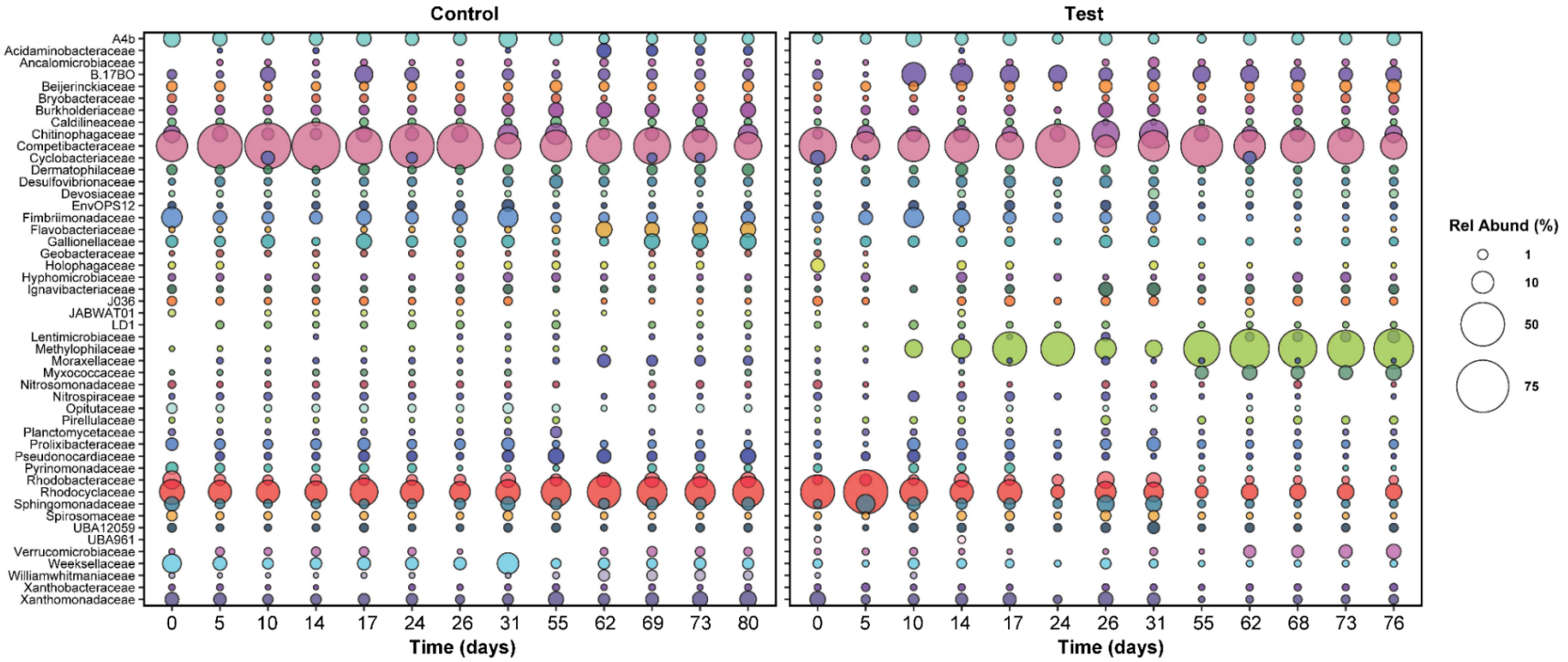

Figure 4.5. The relative abundance of active families in both reactors over time. Only families with relative abundance greater than or equal to 1% at at least one time point are plotted. Sampling times were matched across both reactors; for this reason, relative abundance data between days 31 and 55 are not plotted, since the control reactor was shut down during this time.

Discussion

Links Between Active Bacterial Community, Wastewater Treatment, and Pharmaceutical Degradation

Methylophilaceae became the dominant active family in the test reactor after day 17 and included *Methylotenera* and *Methylophilus* genera. Members of this family may have proliferated due to the presence of trace methanol in the influent from pharmaceutical dosing (0.13 mg/L influent concentration); however, some *Methylophilaceae* species can also consume acetate [133, 134], and therefore it is more likely that *Methylophilaceae* proliferated due to increased acetate availability in the aerobic phase of SBR operation (Figure A.5). Some *Methylotenera* species are also capable of aerobic denitrification [135], which may explain why nitrate did not accumulate in the test reactor. It is worth noting that this family did not appear to be affected by pharmaceuticals' presence, but also did not proliferate until after pharmaceutical removal stopped—*Methylophilaceae* were therefore likely not responsible for the pharmaceutical degradation observed in the first 12 days of the test.

Competibacteraceae was the second most abundant active family in the test reactor, at 21.8 ± 10.5% abundance over the last 40 days of exposure. Bacteria in the *Competibacteraceae* family are glycogen accumulating organisms, or GAOs, that compete with PAOs for anaerobic carbon consumption but do not aerobically consume phosphate. For this reason, their proliferation is typically linked with reduced phosphate removal [136]. It is likely that *Competibacteraceae* activity sustained anaerobic carbon consumption in the test reactor; however, it is surprising that the relative abundance of this family was lower in the test reactor than in the control reactor: active *Competibacteraceae* were present at 30.8 ± 18.6% abundance

in the control reactor, despite complete phosphate removal (Figure 4.1). It is possible that *Competibacteraceae* activity levels were similar in both reactors; the increased abundance of active *Methylophilaceae* in the test reactor may make the relative abundance of active *Competibacteraceae* appear smaller.

The relative abundance of active nitrifying families *Nitrospiraceae* and *Nitrosomonadacea* was higher in the test reactor than the control for the first 38 days of pharmaceutical exposure (Figure 4.6), which may explain why nitrogen removal briefly recovered between days zero and 20 (Figure 4.1). Nitrifier activity may also be responsible for pharmaceutical degradation in the first 12 days of the test: the ammonia monooxygenase enzyme used by both ammonia oxidizing bacteria and archaea (AOA) is known to react non-specifically with aromatic compounds, typically through an oxidation reaction [137, 138]. The primary degradation product of DCF, and all detected GEM degradation products, are formed through oxidation reactions. Aqueous GEM degradation products were not detected after day 34, approximately the same time that active nitrifier abundance dropped. Likewise, aqueous DCF1 levels fell and remained low after day 34. It is possible that decreased levels of DCF and GEM degradation products after day 34 are linked with decreased abundance of active nitrifiers over the same time period. It should be noted, however, that active *Nitrosomonadaceae* (the only AOB family detected) were not detected for most timepoints in both the control and test SBR. The lack of active AOB data, however, is contradicted by complete ammonia oxidation in the control reactor and partial ammonia oxidation in the test reactor, as well as active *Nitrospiraceae* abundance patterns over the dosing period. Several active AOA genera were also detected, which

may further explain why ammonia oxidation continued throughout dosing. AOA abundance is discussed in more detail in the next section.

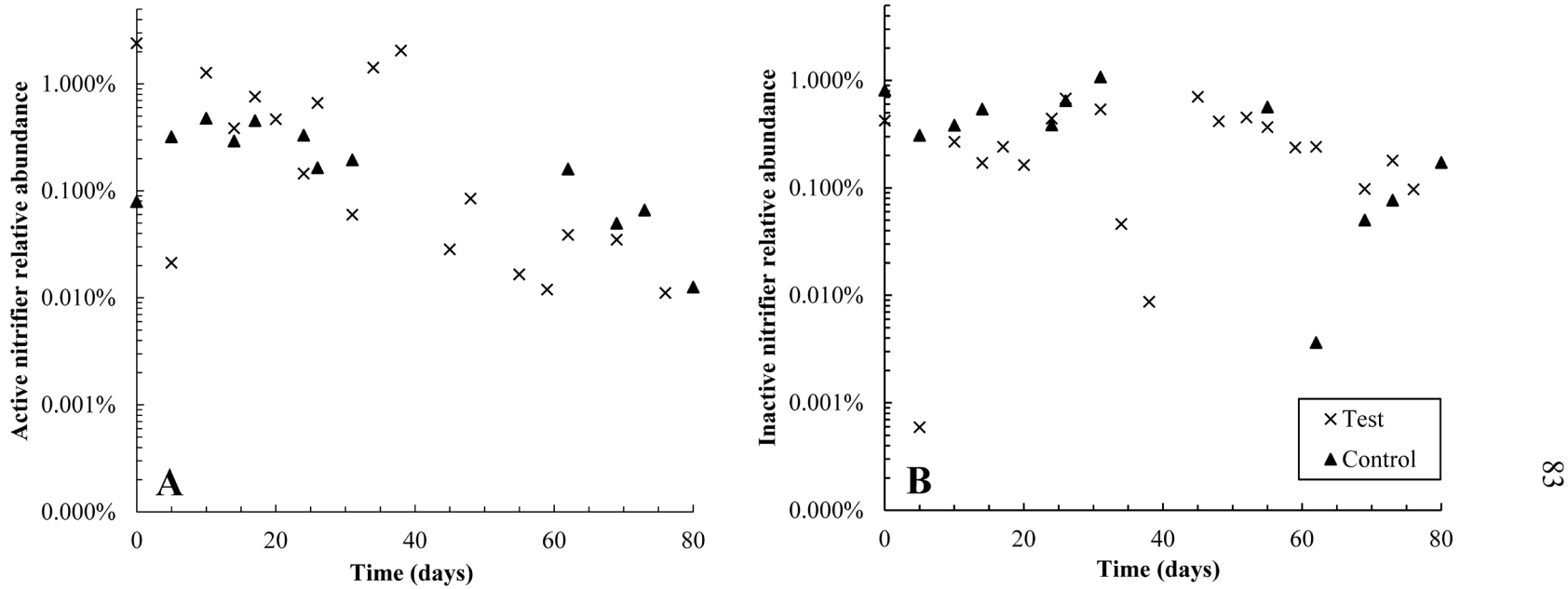

Figure 4.6. Semi-log plots of the relative abundance of active (A) and non-active (B) nitrifiers (summed *Nitrosomonadaceae* and *Nitrospiraceae* families) over time in control and test reactors. Over the first 38 days, active nitrifiers were more abundant in the test reactor than the control; however, from days 55-80, active nitrifiers were more abundant in the control SBR. Active nitrifiers also declined in relative abundance in the test reactor throughout the dosing period. The control SBR was shut down from days 40-50 and therefore data is not available in that timeframe; this is also likely why active nitrifiers in the control reactor are present at slightly lower relative abundances in the second half of the experiment than the first. Inactive nitrifiers were present at similar levels in both reactors throughout the test.

Patterns in Taxonomic Shifts in Microbial Communities

The addition of pharmaceutical compounds led to strong shifts in the microbial community and concomitant reductions in nitrogen and phosphorus removal. Based on the assessment of potential functional pathways, no high-quality MAGs were found with the ammonia oxidation pathway. Although AOB, such as *Nitrosomonas,* were detected in both the shotgun metagenomic and metabarcoding datasets, we were unable to construct a MAG with over 90% completeness, which limited our ability to determine the role of these organisms. However, despite their limited abundance overall, it is likely that *Nitrosomonas* is the main driver of ammonia oxidation in the reactors, given their presence in seed granules and the homology of the identified functional genes.

Several archaeal taxa were also found in the metabarcoding dataset though archaea were not detected in the granule metagenome. Archaea detected were primarily species within the *Thermoproteota,* including members of the order *Nitrosophaerales*. *Nitrosophaerales* contains numerous AOA, such as *Nitrosotenuis* and *Nitrosocaldus* genera. AOA have been posited to be important for the oxidation of ammonia to nitrite in commercial wastewater treatment plants [139], though a study by [140] found that AOA dominated in smaller scale treatment plants while AOB dominated in commercial ones. The authors hypothesized that AOA may be more sensitive to the toxic compounds more frequently measured in larger scale treatment plants.

Although archaea made up less than 1% of the sequences identified, 47 ZOTUs were identified as active taxa. We focused primarily on abundant taxa, but the ability of rare organisms to drive ecosystem function is well documented [141]; for example, rare taxa may be particularly important in pollutant degradation. The large shifts in relative abundance of

wastewater-treating taxa, such as *Rhodocyclaceae* and *Methylophilaceae* (Figure 4.5), suggest that additional studies in which microbe functionality is explored could provide important insights into community interactions that might otherwise be overlooked.

Conclusions

Lab-grown AGS was exposed to three commonly found, but relatively unstudied pharmaceuticals at approximately 150 µg/L each. The fate of each pharmaceutical and its degradation products in the aqueous and solid phases were monitored, and pharmaceutical impacts on wastewater treatment performance and microbial communities were evaluated.

All pharmaceuticals were partially removed via both biodegradation and sorption in the first 12 days of the study. Biodegradation capacity then declined irreversibly, indicated by washout of degradation products, declining production, and negligible pharmaceutical removal. Exposure to the pharmaceutical mixture negatively impacted wastewater treatment efficacy and the relative abundance of active wastewater treating families. Nitrogen and phosphate removal declined to approximately 73% and 63%, respectively, though carbon removal was not impacted. Declining nitrogen removal was due mainly to inhibited ammonia oxidation and likely also related to the declining abundance of active nitrifiers. Similarly, active *Rhodocyclaceae* declined in abundance in the test reactor, which likely contributed to poor phosphate removal.

Funding

This research was supported by Montana INBRE, which is funded by the National Institute of General Medical Sciences division of the National Institutes of Health under Award

Number P20GM103474. The content is solely the responsibility of the authors and does not necessarily represent the official views of the National Institutes of Health.

Acknowledgements

The authors would like to thank staff at the Mass Spectrometry Facility at Montana State University (MSU) for training and assistance. Funding for the Proteomics, Metabolomics and Mass Spectrometry Facility used in this publication was made possible in part by the MJ Murdock Charitable Trust, the National Institute of General Medical Sciences of the National Institutes of Health under Award Numbers P20GM103474 and S10OD28650, and the MSU Office of Research, Economic Development and Graduate Education.

Declaration of Competing Interests

The authors have no relevant financial or non-financial interests to disclose.

CHAPTER FIVE

PHARMACEUTICAL IMPACTS ON AEROBIC GRANULAR SLUDGE MORPHOLOGY AND POTENTIAL IMPLICATIONS FOR ABIOTIC REMOVAL

Contribution of Authors and Co-Authors

Manuscript in Chapter 5

Author: Kylie B. Bodle

Contributions: Designed and conducted study. Collected and analyzed data, wrote and revised manuscript.

Co-Author: Catherine M. Kirkland

Contributions: Helped conceive and design study, aided in data interpretation, aided in revision of the manuscript and provided comments.

Manuscript Information

Kylie B. Bodle, Catherine M. Kirkland

Chemosphere

Status of Manuscript:
☐ Prepared for submission to a peer-reviewed journal
☐ Officially submitted to a peer-reviewed journal
☐ Accepted by a peer-reviewed journal
☒ Published in a peer-reviewed journal

Elsevier
Vol. 350
https://doi.org/10.1016/j.chemosphere.2024.141187

Abstract

The goal of this study was to investigate abiotic pharmaceutical removal and abiotic pharmaceutical effects on aerobic granular sludge morphology. For 80 days, a pharmaceutical mixture containing approximately 150 µg/L each of diclofenac, erythromycin, and gemfibrozil was fed to an aerobic granular sludge sequencing batch reactor and granule characteristics were compared with those from a control reactor. Aqueous and solid phase pharmaceutical concentrations were monitored and staining was used to assess changes in biofilm structures. Solid phase pharmaceutical concentrations were elevated over the first 12 days of dosing; however, they then dropped, indicative of desorption. The lipid content in pharmaceutical-exposed granules declined by approximately half over the dosing period, though the relative concentrations of other key biofilm components (proteins, alpha-, and beta-polysaccharides) did not change. Batch experiments were conducted to try to find an explanation for the desorption observed, but reduced solid phase pharmaceutical concentrations could not be linked with the presence of common wastewater constituents such as ammonia or phosphate. Sorption of all three compounds was modelled best by the Henry isotherm, indicating that, even at 150 µg/L, granules' sorption site coverage was incomplete. Altogether, this study demonstrates that simplified batch systems may not accurately represent the complex abiotic processes occurring in flow-through, biotic systems.

Introduction

Pharmaceuticals are increasingly found in the environment, due in part to release from wastewater treatment plants, which are typically not designed to treat such compounds. Though

environmental pharmaceutical concentrations are currently low (ng/L to µg/L levels), concentrations are likely to increase until sustainable treatment technologies are developed and implemented. Existing technologies, such as activated carbon or advanced oxidation processes, are non-regenerating and expensive [142], and therefore improved treatment technologies are worthy of investigation.

One such emerging treatment technology is aerobic granular sludge (AGS). AGS consists of diverse communities of wastewater bacteria that self-aggregate into dense, spherical biofilm granules up to several millimeters in diameter. Oxygen gradients throughout AGS enable nitrifying, denitrifying, and phosphate accumulating organisms to coexist in a single granule, thus allowing complete treatment of phosphorus, organic carbon, and nitrogen species in a single reactor. The variety of extracellular polymeric substances (EPS) secreted by bacteria in AGS provide a protective diffusive boundary, enhancing the resilience of AGS during exposure to toxic substances [1]. The complex EPS in granules may also provide a sorptive medium for pharmaceutical removal, which, unlike conventional sorptive materials, would self-regenerate with bacterial growth [3, 4]. Literature studies thus far indicate that AGS largely removes pharmaceuticals via sorption (e.g. [4, 32]); however, much remains unknown about the extent and breadth of pharmaceuticals AGS may be able to remove.

The goal of this study was to focus on abiotic pharmaceutical removal and abiotic pharmaceutical effects on AGS biofilm structures. The extent of each pharmaceutical's partitioning to solid and aqueous phases was documented, and the effects of the pharmaceutical mixture on the spatial distribution and fractions of EPS throughout exposure were tracked. Biotic

impacts of the pharmaceutical mixture on AGS are discussed in [143] in order to allow more detailed discussion of abiotic effects herein.

Notably, relative to the number of studies on pharmaceutical impacts on AGS, very few quantify sorption via pharmaceutical extraction from solids [44, 144]: most only quantify aqueous pharmaceutical concentrations (e.g., [4, 84]); some also extrapolate aqueous measurements from batch adsorption experiments to those observed in sequencing batch reactors (SBRs) [3, 32, 47]. It has been demonstrated that pharmaceuticals sorb to various lab supplies [81, 100], and therefore it is important to determine the portion of pharmaceuticals truly removed by AGS via extraction from solids.

Furthermore, though multiple studies evaluate pharmaceutical impacts on protein-to-polysaccharide ratios in AGS (e.g., [4, 88]), none track spatial changes, or effects on lipids or polysaccharide form (alpha vs. beta). It is generally widely accepted that more stable granules have higher protein-to-polysaccharide ratios [145]; however, the role of lipids is poorly understood, as are the roles of alpha- versus beta-polysaccharides. Alpha-polysaccharides may act as a carbon source during starvation [18] whereas beta-polysaccharides may confer structural rigidity, but are likely not biodegradable [146]. Tracking changes in EPS components throughout pharmaceutical dosing, therefore, may provide important insights about how these biopolymers contribute to granules' structure and function.

Three common pharmaceuticals were selected for use in this study. Pharmaceutical compounds were selected based on their prevalence in the environment and their scarcity in AGS literature studies (less than three) at the time of experimental design. Diclofenac (DCF) is a non-steroidal anti-inflammatory drug (NSAID) that is both ingested and applied topically, thus

presenting multiple routes of entry to wastewater. DCF is poorly removed in conventional treatment systems, and numerous studies have documented its harmful effects at environmental concentrations (e.g., [26, 147]). Erythromycin (ERY) is a macrolide antibiotic used in both human and veterinary medicine that has been implicated in proliferation of antibiotic resistance genes and shown to bioaccumulate in numerous aquatic species [38, 43]. Lastly, gemfibrozil (GEM) is a fibrate, or lipid regulator, that has been detected in wastewater influents at up to 64 µg/L [57]. It has been shown to act as an endocrine disruptor in multiple aquatic species [62]. All three compounds are generally detected at less than 10 µg/L in surface waters, but concentrations in influents to wastewater treatment plants are typically much higher—over 50 µg/L DCF, for example, has been measured [26, 38, 80, 148]. This study therefore provides important information on the abiotic fate and effects of three frequently detected, but relatively unstudied, pharmaceuticals on AGS.

Methods

Sequencing Batch Reactor Operation

AGS sequencing batch reactor operation is detailed in [143]. In brief, two identical glass laboratory-scale sequencing batch reactors (SBRs) with a working volume of 3.4 L were used to grow AGS. Repeating three-hour SBR cycles consisted of 72 minutes anaerobic feed from the bottom of the reactor, 100 minutes aeration at approximately 5 L/min gas flow, three minutes settling, and five minutes effluent discharge. Approximately 50% of the reactor liquid was withdrawn in each cycle, resulting in a hydraulic residence time (HRT) of 6.4 hours. The solids residence time (SRT) was controlled at 25 ± 5 days, resulting in near-constant biomass concentrations in both reactors of 24.5 ± 1 g/L total suspended solids.

LabVIEW software (National Instruments) controlled pH (7.0 ± 0.3) and dissolved oxygen (DO, 1.75 ± 0.25 mg/L) during the aeration phase, and pH, DO, and temperature data were collected continuously for the entire experiment. The influent concentration of sodium acetate was 10.3 mM; otherwise influent media were identical to those described in [89]. In brief, influent concentrations of ammonium and phosphate were approximately 60 mg/L; influent organic carbon was approximately 250 mg/L for an organic loading rate of 2.5 g C/L*d. Influent media are detailed in Table B.1 in Appendix B. AGS from an AquaNereda® treatment plant in Utrecht, The Netherlands was used to seed both reactors, and each was operated for over 300 days at steady state prior to beginning experimentation.

Pharmaceuticals were dosed to the test reactor for 80 days: 46 mL of pharmaceutical media were combined with the influent medium, resulting in an influent concentration of approximately 150 µg/L of each pharmaceutical. Influent samples were taken from a sampling port in the tubing located at the base of the reactor (Figure B.1) and were extracted and quantified per methods in the Analytical Methods section. The pharmaceutical media consisted of two stock solutions: 17.86 mg/L each of diclofenac sodium (Acros Organics) and gemfibrozil (Acros Organics) in nanopure water ("DG solution"), and 35.8 mg/L erythromycin (TCI Chemicals) in nanopure water ("ERY solution"). ERY solution was fed separate from DG solution because results discussed in [100] showed varying sorption of each pharmaceutical to different tubing types; therefore ERY solution was pumped into the reactor using silicone tubing (Masterflex) and DG solution was pumped into the reactor using PharmaPure tubing (Masterflex). Despite different pharmaceutical stock solution concentrations, influent concentrations were stable at approximately 150 µg/L of each pharmaceutical. This influent

concentration was selected for testing because 150 μg/L was the minimum concentration of pharmaceuticals that could be consistently dosed to the test reactor without significant losses from sorption.

Stock solutions of each individual pharmaceutical were prepared at 10 g/L first in methanol and then diluted into water. Twenty-three mL of each solution were delivered with the influent medium (Figure B.1); therefore approximately 0.13 mg/L methanol was also present in the combined influent stream. The pharmaceutical media were protected from light to prevent photolytic degradation and prepared fresh every 8-10 days.

Analytical Methods

Influent and effluent samples from the control and test reactors were regularly taken and filtered through 0.45 μm regenerated cellulose filters prior to analyses for ammonia, nitrite, nitrate, and phosphate. Effluent samples were taken from the SBR cycle immediately prior to influent samples, to prevent reduced influent volumes from impacting effluent sample characteristics. Ammonia was quantified with Hach kit TNT 832 and a Hach DR 3900 spectrophotometer, equivalent to US EPA Method 350.1. A Dionex ICS-1100 anion chromatography system equipped with an IonPac AS22 RFIC column (4 x 250 mm) and IonPac guard column (4 x 50 mm) was used to quantify other anions listed.

Granule size distributions were determined via sieving. Total and volatile suspended solids (TSS and VSS respectively) were determined following standard methods [149]. Sludge volume index was determined after 3 minutes (SVI_3) of settling by reading a graduated scale placed on the reactor column.

Aqueous influent and effluent samples were prepared for mass spectrometry (MS) analyses by solid phase extraction (SPE) as detailed in [143]. In short, 100 mL influent or effluent sample were prepared for solid phase extraction by filtering with a 1.5 μm glass fiber filter (Hach). Samples were then loaded on preconditioned Waters Oasis HLB cartridges (30 mg, 20 mL) at 10 mL/min using a vacuum manifold system. Loaded cartridges were washed, dried, and frozen at -18ºC until elution (no more than 14 days). Influent and effluent pharmaceutical samples were periodically taken in duplicate to assess extraction recovery, as detailed in [143], and average recoveries are summarized in Table B.2. To assess accuracy but prevent excessive disruption to the reactor, triplicate influent and effluent samples were taken once per month.

Pharmaceuticals were also extracted from granules per methods adapted from [103]. In short, approximately 40 mL (2 g wet weight) of granules were sampled during aeration to ensure samples were completely mixed. Samples were filtered, split in half, weighed, and crushed. Moisture fractions in half of the sample were determined by drying. The remaining wet half of the sample was sonicated in 5 mL methanol in a glass centrifuge tube for 15 minutes, then centrifuged at 1600 xg for 8 minutes. The supernatant was transferred to a clean glass test tube, and sonication and centrifugation were repeated with 2 mL methanol followed by 2 ml acetone. Supernatants were combined after each centrifugation and evaporated down to approximately 2 mL under a gentle nitrogen stream at 40°C. The remaining supernatant was then diluted with 150 mL nanopure water and extracted as described above. Solid-phase samples were extracted in triplicate once per month and periodically evaluated for recovery using spike-recovery testing, as described above. Average recoveries are summarized in Table B.2. To confirm pharmaceuticals

were absent from the control reactor, aqueous and solid samples from the control were also periodically analyzed.

All pharmaceutical quantification and detection were performed with an Acquity I Class Plus ultra-performance liquid chromatograph (UPLC) coupled to a Waters Synapt XS quadrupole time-of-flight mass spectrometer (QToF-MS) in positive ion mode. Chromatographic analysis methods were adapted from [92] and are detailed in [143]. The open-source software Mzmine and R were used to analyze and compile mass spectra data [101, 102].

Batch Experiments

The goal of batch experiments was twofold: (1) identify if phosphate and/or ammonia concentrations impacted the sorptive capacity of AGS; and (2) determine if sorption of each pharmaceutical followed monolayer (Langmuir) or multilayer (Freundlich) models. To that end, batch experiments were conducted in HEPES buffer with varying concentrations of ammonia, phosphate, and pharmaceuticals as well as at varying pH (Table 5.1). For each condition, four glass bottles (triplicate samples plus one control) were prepared with 50 mL each of 30 mM HEPES buffer and 0.1 wt% sodium azide (Fisher) to prevent pharmaceutical biodegradation. Macro- and micro-nutrients were also present at concentrations identical to those in the influent, described in [89], excepting sodium acetate, which was not added. Sodium acetate was absent from solution to mimic conditions near the middle or end of the settled granule bed during SBRs' anaerobic fill phase. AGS was added to each sample, excepting the controls, at approximately 9.5 g/L TSS, and samples were shaken at 150 RPM at room temperature for six hours, roughly equal to the SBR HRT. Periodically throughout the experiment, aqueous samples were filtered with 0.45 μm regenerated cellulose syringe filters and stored at 4°C for no longer than one week.

Samples were analyzed via UPLC-QtoF-MS directly (ie., without extraction), via methods detailed in the Analytical Methods section.

Data from isotherm experiments were fit to linearized versions of the Langmuir and Freundlich isotherms (Equations 1 and 2, respectively) [150]. The Langmuir isotherm assumes monolayer sorption across homogeneous sites. In contrast, the Freundlich isotherm assumes that sorption sites are heterogeneous and reflects multilayer sorption [150]. In all equations, q_e is the equilibrium amount of adsorbed pharmaceutical in µg/g TSS and C_e is the equilibrium aqueous contaminant concentration in µg/L. For the Langmuir isotherm, q_{max} is the maximum adsorption capacity of the biomass (µg/g TSS) and K_L is the empirical Langmuir constant in L/µg. For the Freundlich isotherm, K_F is the Freundlich capacity factor (L/g TSS) and n is the adsorption intensity [150]. Intensity values less than one indicate that solute affinity for the sorbent decreases with increased loading; n = 1 indicates constant affinity for the sorbent, and n > 1 indicates increased affinity with higher loading [151]. Intensity factors equal to one may also simply indicate that the adsorbate concentrations tested are low enough to fall in the Henry isotherm region (Equation 3), in which q_e increases linearly with C_e, sorption site coverage is incomplete, and therefore only monolayer sorption is possible [151].

$$\frac{C_e}{q_e} = \frac{1}{q_{max}} C_e + \frac{1}{K_L q_{max}} \tag{1}$$

$$\log(q_e) = \frac{1}{n} \log(C_e) + \log(K_F) \tag{2}$$

$$q_e = K_H C_e \tag{3}$$

Table 5.1. Batch sorption experiment conditions. All concentrations listed are approximate and were measured immediately after adding AGS. High NH_3 and PO_4 concentrations were selected based on their average concentrations at the end of the fill phase in both reactors, as concentrations of each anion peaked at this point in SBR operation. Anaerobic phosphate release by phosphate accumulating organisms resulted in approximately 700 mg/L PO_4 at the end of the fill phase; dilution of the influent medium with liquid remaining in the SBR resulted in NH_3 concentrations of approximately 30 mg/L.

Experiment description	**Condition**	**Initial PO_4 concentration (mg/L)**	**Initial NH_3 concentration (mg/L)**	**pH**	**Pharmaceutical concentration (µg/L)**
Effects of elevated NH_3 or PO_4 on sorptive capacity	Acidic pH	0	0	6	200
	Neutral pH	0	0	7	
	High PO_4	700	0		
	High NH_3	8	30		
Isotherm test	100 µg/L pharm. mix	0	0	7	100
	300 µg/L				300
	400 µg/L				400
	500 µg/L				500

Microscopic Analyses

To assess pharmaceutical impacts on the distribution of major EPS components in AGS, granule samples from both reactors were sampled and fixed approximately every two weeks, and stained for proteins, lipids, and alpha- and beta-polysaccharides according to methods in [17]. Granules were then cut into 30 µm sections with a cryotome and sections from the approximate center of granules (~300 µm from granule surface) were imaged with an inverted Leica DMI8 Stellaris confocal laser scanning microscope (CLSM). Imaris imaging software was used to determine the relative biovolumes of proteins, lipids, and polysaccharides in each granule section, and the fraction of each component relative to the total section biovolume was calculated. The total biovolume of the granule section was estimated by over-thresholding the

biovolume of the transmitted light image such that the entire biovolume of the granule section was calculated. Multiple EPS components overlaid each other in each granule section, and therefore component fractions sum to over 100%. Triplicate slices from the same granule, as well as triplicate slices from different granules, were analyzed to assess variability.

Results

The goal of this study was to focus on abiotic pharmaceutical removal and abiotic interactions between pharmaceuticals and AGS biofilm structures. For that reason, we limit our discussion of pharmaceutical inhibition of conventional wastewater treatment to the effects that elevated concentrations of conventional wastewater analytes may have had on granules' sorptive capacity. More detail on inhibition of wastewater treatment by DCF, ERY, and GEM can be found in [143]. In brief, phosphate removal in the test reactor declined to approximately 60% throughout dosing, and nitrogen removal declined to approximately 70%. Poor nitrogen removal was due mainly to 25% less ammonia oxidation in the test reactor [143]. Likewise, although changes in granular structure may have been driven by bacterial responses to pharmaceutical exposure, we focus on the effects that structural changes may have had on abiotic pharmaceutical removal. A more detailed discussion of the effects of pharmaceuticals on bacteria in AGS can be found in [143].

Reactor Performance

Effluent concentrations of ammonia and phosphate increased in the test reactor within two days of starting pharmaceutical dosing: ammonia increased from non-detection (below 2.4 mg/L) to 30 mg/L, and phosphate from approximately 5 mg/L to 16 mg/L (Figure 5.1). From day

6 to 20, effluent ammonia concentrations decreased in the test SBR, reaching a minimum of 5.5 mg/L. Concentrations then steadily increased until day 62 before stabilizing at 24.7 ± 4.7 mg/L for the remaining 20 days of the experiment. Effluent phosphate concentrations were unstable throughout the experimental duration but stabilized somewhat at 36 ± 11 mg/L for the last 40 days. In contrast, in the control reactor effluent ammonia remained below detection limits; effluent phosphate concentrations were 6.7 ± 3.6 mg/L on average.

It is important to note that the software controlling both reactors experienced an error on day 40: DO control in the test reactor was briefly interrupted, causing minimal impact; however, acid was overdosed to the control reactor, causing shutdown of that reactor for 10 days. For this reason, effluent ammonia data from the control reactor are not plotted past day 40 in Figure 5.1, as the acid overdose in that reactor inhibited the activity of ammonia oxidizing bacteria. It is likely that effluent ammonia concentrations in the control reactor would have remained below detection levels for the remainder of the experiment if not for this issue.

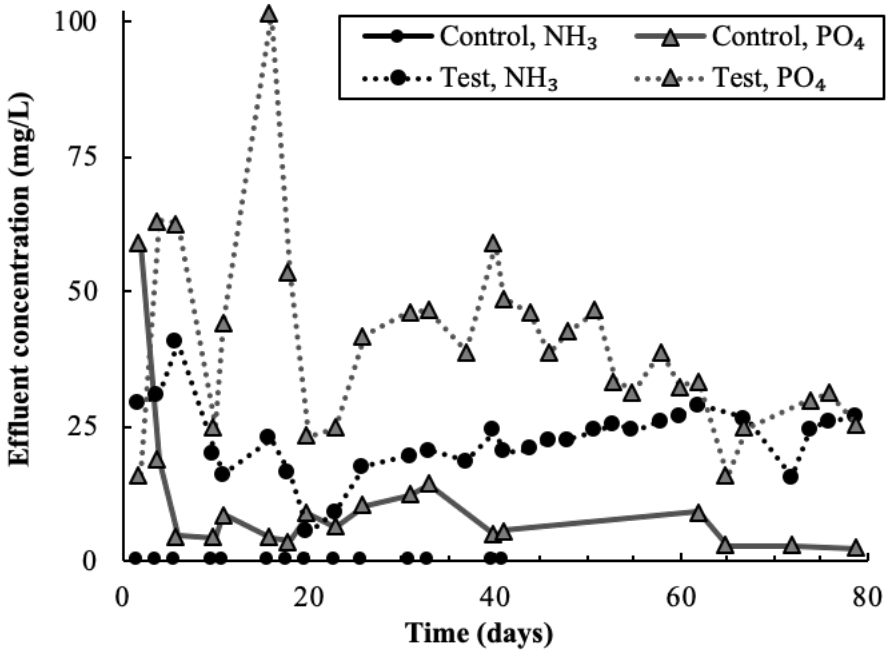

Figure 5.1. Effluent concentrations of ammonia and phosphate from the control and test reactors. Control effluent ammonia concentrations are not plotted past day 40 for reasons discussed in the text. Influent concentrations of both ammonia and phosphate were approximately 60 mg/L. Note that effluent phosphate concentrations peak above this value due to the activity of phosphate accumulating organisms, which release phosphate during the anaerobic phase of SBR operation.

Batch Experiments / Adsorption Isotherms

Sorption of all pharmaceuticals was modeled well by both the Henry and Freundlich isotherms (Figure 5.2). Isotherm coefficients and R^2 values are summarized in Table 5.2. Sorption data fit to the monolayer Langmuir isotherm are not shown, as R^2 values indicated poor fit of the data to the model ($R^2 < 0.7$). Given that sorption data were modeled slightly better by the Henry isotherm than Freundlich, it is likely that the pharmaceutical concentrations tested were low enough that sorption sites remained available at equilibrium, thereby allowing monolayer sorption only. We can conclude with relative confidence that all sorption isotherm samples reached equilibrium within six hours, as a t-test indicated that each replicate's sorbed pharmaceutical concentrations at three and six hours were not significantly different ($p > 0.05$).

Intensity values predicted by the Freundlich isotherm were also approximately equal to one (n = 0.76-0.85, Table 5.2), which may further indicate that the tested concentrations were not high enough to conclusively determine if mono- or multilayer sorption of the tested pharmaceuticals is possible. Experiments with higher pharmaceutical concentrations were not conducted, as results at higher concentrations would not be relevant to either the SBR experiment described herein or environmental conditions.

Sorption capacity was well-predicted by log K_{ow} values (listed in Table B.2) at the pharmaceutical concentrations tested: sorbed GEM concentrations were consistently highest, followed by DCF, then ERY. Interestingly, the equilibrium concentrations of sorbed pharmaceuticals observed in the batch experiments were over an order of magnitude higher than those measured in the test SBR. In the sample set with conditions most like those in the test SBR ("High NH_3" batch experiment, Table 5.1), granules sorbed 8.1 ± 0.8 µg DCF, 5.1 ± 0.5 µg ERY, and 21 ± 1.7 µg GEM per g TSS after six hours. Batch experiments in which ammonia and phosphate concentrations were varied did not show a significant relationship between granules' sorptive capacities and ammonia or phosphate levels and are discussed in more detail in the Discussion section.

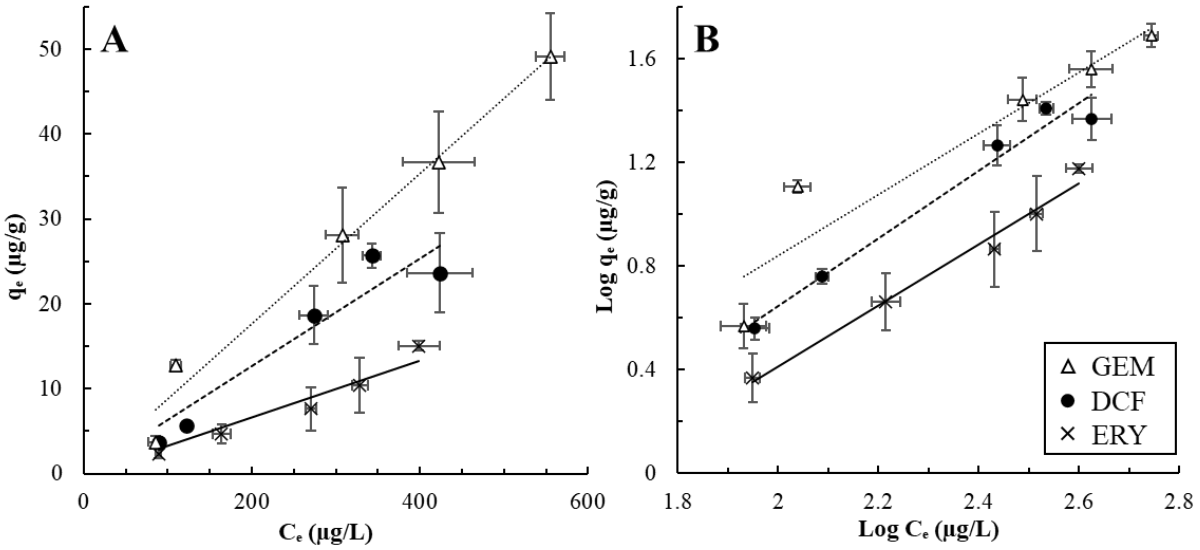

Figure 5.2. Batch adsorption data fit to (A) Henry and (B) Freundlich isotherms. Error bars all indicate standard deviation of triplicate samples and at times are smaller than sample points. Error bars in the x-direction indicate the standard deviation of C_e values for triplicates; those in the y-direction indicate the standard deviation of q_e values.

Table 5.2. Fitted constants and R^2 values for the Henry and Freundlich isotherms for each pharmaceutical.

	Henry		**Freundlich**		
	K_H **(L/g TSS)**	R^2	K_F **(L/g TSS)**	n	R^2
DCF	0.063	0.98	0.0105	0.763	0.97
ERY	0.033	0.99	0.0111	0.846	0.98
GEM	0.089	0.99	0.0304	0.848	0.89

Pharmaceutical Fate

All pharmaceuticals were partially removed in the first 12 days of dosing (Figure 5.3, Figure B.2); removal then dropped to approximately zero for the remainder of the test, excepting ERY, which stabilized somewhat at 19 ± 10% removal between days 48-80. Removal was calculated based on a mass balance using measured influent and effluent concentrations of each pharmaceutical; equations B1 and B2 in Appendix B describe this calculation. Between days 12-

23, sorbed pharmaceuticals appeared to be released from the solid phase and washed out of the reactor, evidenced by effluent concentrations that exceeded influent ones, negative removal, and declining solid phase concentrations (Figure 5.3). Pharmaceutical biodegradation was monitored but is not discussed here; details can be found in [143].

Diclofenac. The abiotic mechanisms driving pharmaceutical removal and release were most clearly interpreted for DCF: over the first 12 days of dosing, solid phase DCF concentrations increased, the same time frame in which DCF removal was greater than zero (Figure 5.3, Figure B.2). Solid phase DCF concentrations then dropped sharply from day 12-31, roughly the same time in which effluent concentrations exceeded influent ones. Taken together, this suggests desorbing DCF contributed to higher effluent concentrations. This pattern was seen again from days 37-55: solid phase concentrations increased by approximately 0.1 μg/g between days 37-46, then dropped by roughly the same amount over days 46-55. DCF removal and release again occurred over roughly the same timeframes, respectively. For the remainder of the test, DCF removal was negligible and solid phase concentrations averaged out at 0.26 ± 0.03 μg/g.

Erythromycin. ERY concentrations followed patterns similar to those observed for DCF. Removal occurred in the first 5 days, evidenced by lower effluent than influent concentrations (Figure 5.3, Figure B.2). Solid phase ERY concentrations also increased during this time. On days 9 and 12, influent and effluent concentrations were near equal, corresponding with a dip in solid phase concentrations. Then, from days 12-23, effluent ERY concentrations spiked, despite solid phase ERY concentrations increasing from 0.14 μg/g on day 12 to 0.52 μg/g on day 20. It is possible that solid concentrations spiked because effluent concentrations were higher, and

therefore there was more ERY available for sorption. However, the reasons for increased effluent concentrations are unclear. Perhaps actual influent concentrations were higher than measured—the noise observed in all influent pharmaceutical concentrations is likely due to the constant sorption and desorption of each pharmaceutical within influent tubing. The periodic flow conditions that are characteristic of sequencing batch reactor systems also likely exacerbated noisy influent pharmaceutical concentrations.

After day 23, influent and effluent ERY concentrations were near equal and removal was negligible until day 48, after which removal remained fairly constant at 19.5 ± 9.7% for the remainder of the test. Solid phase ERY concentrations were also elevated during this period compared to the first half of the test, at 0.3 ± 0.04 µg/g, versus 0.23 ± 0.11 µg/g over the first 46 days.

Gemfibrozil. Much like DCF and ERY, GEM removal occurred in the first 12 days of dosing, during which solid phase GEM concentrations also increased (Figure 5.3, Figure B.2). GEM concentrations then spiked in the effluent from days 12-23. GEM did not appear to significantly desorb from the granules within the timeframe that effluent GEM concentrations spiked, and so it is again difficult to identify what caused effluent concentrations to increase. It is possible that sampling frequency was insufficient to adequately document GEM desorption, as solid phase GEM concentrations briefly dropped at day 17. Influent concentrations may have also been higher than measured. After day 23, GEM removal was negligible. Solid phase concentrations remained near constant at 0.14 ± 0.04 µg/g.

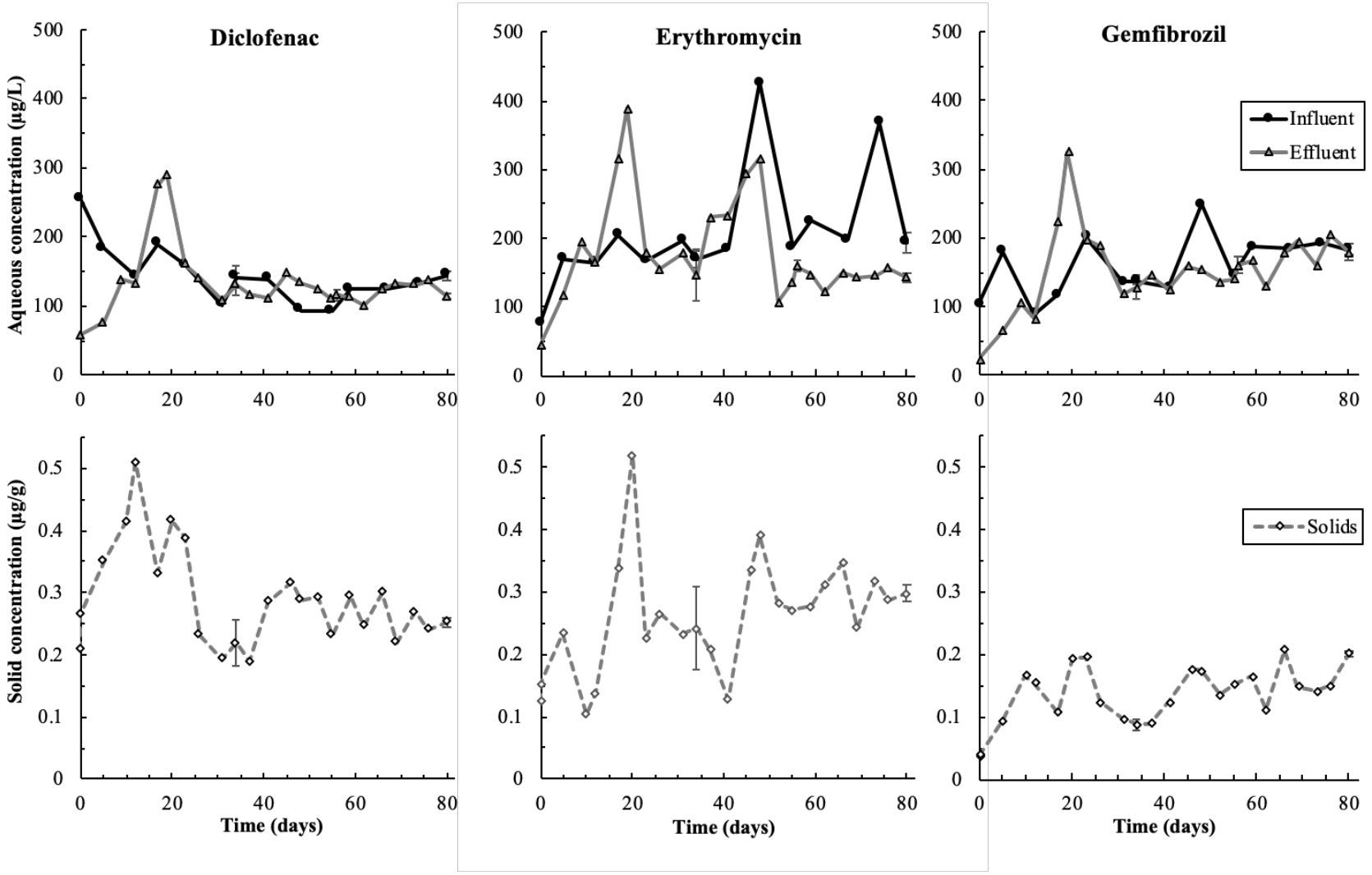

Figure 5.3. Pharmaceutical concentrations in the aqueous (top row) and solid phase (bottom row) over time. Error bars represent the standard deviation of triplicate samples and are present on days 34, 56, and 80 for aqueous samples and days 34 and 80 for solid samples; points on these days are averages. Data in this image were originally published in [143] and are shown here with permission from the authors.

Changes in Morphology

On the first day of pharmaceutical dosing, granules from both reactors had similar EPS compositions: each 30 μm section contained approximately 50% proteins, 20% lipids, and 35-45% each of alpha- and beta-polysaccharides (Table 5.3). Note that multiple components overlay each other (Figure 5.4, Figure B.3, Figure B.4), and since the fraction of each component is calculated relative to the biovolume of the whole granule section, EPS component fractions sum to over 100%. EPS component distributions in control granules did not change ($p > 0.05$) over the experimental period, but the lipid fraction in test granules declined linearly with time, from 20% at day 0 to 9% at day 80 (Figure B.5). The spatial distribution of lipids in test granules also changed: at day zero ("t0"), lipids were present in the granule interior and along the edges of the granule section (Figure 5.4). By day 38, lipids were no longer present in the granule interior, and the lipid boundary at the edge of the granule dwindled from approximately 200 μm at its thickest point on day zero to just 90 μm. On day 80, the lipid barrier was approximately 60 μm at its thickest point.

Protein, alpha-, and beta-polysaccharide (PS) fractions did not change significantly with time in test granules. A t-test confirmed that, excepting lipids, all other EPS components were present at similar distributions in both control and test granules at day zero and day 80 ($p > 0.05$, Table 5.3, Figure B.5).

Table 5.3. Average fractions of EPS components in 30 μm granule sections throughout the experiment. Values were calculated using granule sections taken from the approximate center of three different granules. One-tailed p-values were calculated from two-sample t-tests assuming unequal variance ($\alpha = 0.05$) and reflect comparisons of t0 and t80 values. Note that fractions sum to over 1 for reasons discussed in the text.

	Control			**Test**		
	t0	**t80**	**P-value**	**t0**	**t80**	**P-value**
Proteins	0.52 ± 0.13	0.55 ± 0.07	0.37	0.46 ± 0.16	0.42 ± 0.08	0.38
Lipids	0.23 ± 0.03	0.26 ± 0.06	0.28	***0.19 ± 0.04***	***0.09 ± 0.005***	***0.03***
α-PS	0.45 ± 0.12	0.46 ± 0.05	0.47	0.34 ± 0.13	0.37 ± 0.09	0.35
β-PS	0.47 ± 0.11	0.34 ± 0.06	0.08	0.34 ± 0.13	0.24 ± 0.01	0.15

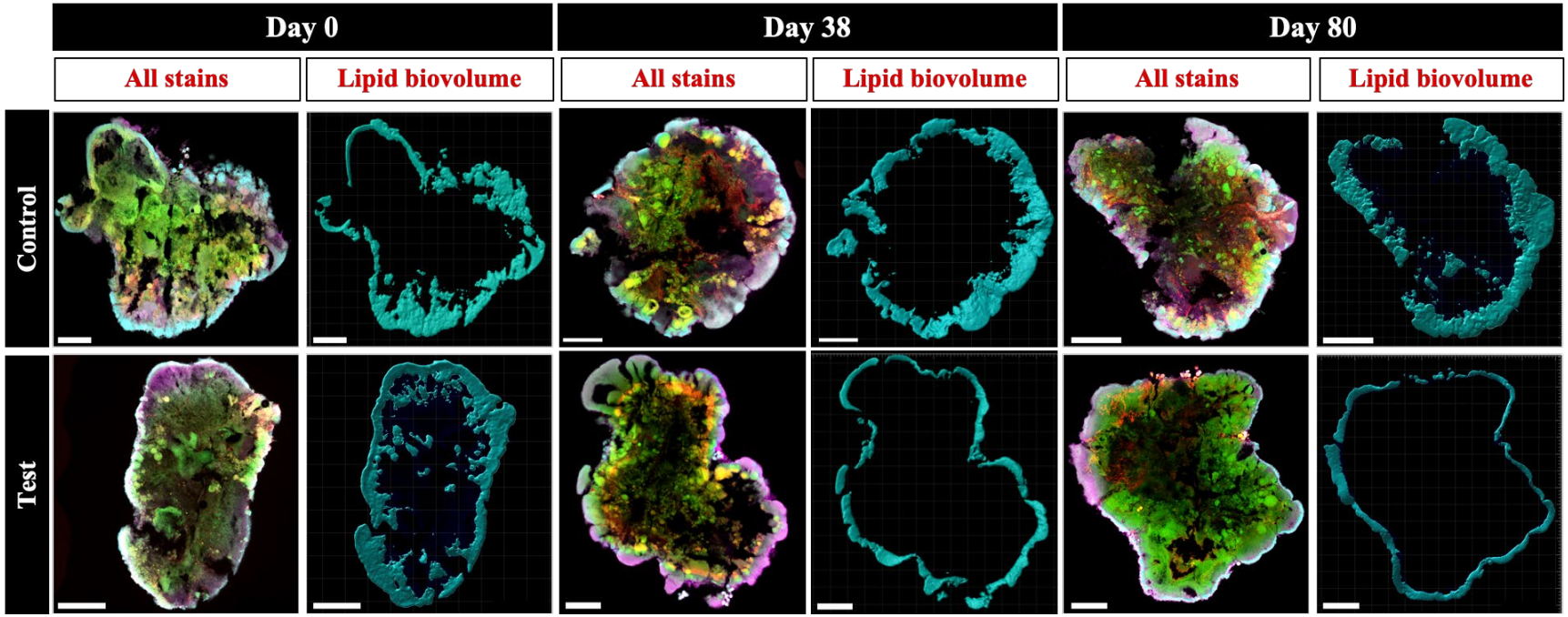

Figure 5.4. EPS component distributions in control and test granules over time. Green indicates proteins (fluorescein isothiocyanate stain); blue, lipids (nile red); red, alpha-PS (concanavalin A); pink, beta-PS (calcofluor white). All scale bars are 200 μm.

Sludge volume index (SVI) is an indication of AGS density and settling capacity, where lower values mean denser sludge and the timescale of the measurement reflects how rapidly the sludge settles. SVI_3, measured after three minutes of settling time, doubled in the test reactor throughout the dosing period: test granules' SVI_3 increased linearly from 11.2 mL/g at day zero to 22.8 mL/g at day 80 (Figure B.6). Although SVI_3 values for the control reactor are not plotted past day 40 (due to the software error described previously), control reactor SVI_3 values likely would have remained within the range of values measured over the first half of the experiment (11.7 ± 1.9 mL/g). In the 120-day period immediately prior to beginning experimentation, granules' SVI_3 values were near constant at 11.5 ± 1.4 mL/g; it is therefore practical to assume that control granules' SVI_3 would have remained within this range. The software error also caused test SBR SVI_3 values to peak on days 40 and 41 before returning to more consistent values. Interestingly, the distribution of granule sizes did not appear to change significantly over time in either reactor (Figure B.7).

Discussion

Pharmaceutical Sorption in Batch Versus SBR

The spike in effluent concentrations measured for all pharmaceuticals from days 12-23 can tentatively be linked with pharmaceutical desorption from granules, evidenced by declining solid phase concentrations over roughly the same timeframe (Figure 5.3). Between days 12 and 23, solid phase DCF declined from 0.51 µg/g to 0.38 µg/g. Although solid phase ERY concentrations increased from days 12-20, they then sharply dropped from 0.52 µg/g to 0.23 µg/g. Likewise, solid phase GEM concentrations declined between days 12-17, from 0.15 µg/g to 0.11 µg/g, before increasing again to 0.19 µg/g. It is likely that all declines in solid phase

concentrations contributed to higher effluent concentrations. However, the reasons for this desorption event are unclear. It is worth noting that, also between days 10 and 23, effluent concentrations of ammonia dropped, and those of phosphate spiked (Figure 5.1). Plots of solid phase pharmaceutical concentrations versus effluent ammonia and phosphate over the forementioned timeframe show a weakly negative relationship (Figure B.8)—in other words, higher sorbed concentrations were measured when both ammonia and phosphate were low. It is therefore tempting to link ammonia and phosphate concentrations with sorptive capacity.

Unfortunately, batch experiments in which ammonia and phosphate concentrations were varied did not conclusively show a relationship between either compound and granules' sorptive capacity (Figure 5.5). ERY and GEM sorption were elevated at higher phosphate concentrations, a result that conflicts with results from the test SBR and the literature: elevated phosphate concentrations are known to encourage desorption of organic carbon from soils, as well as outcompete organic matter for sorption sites [152]. DCF sorption at high phosphate concentrations was equal to that in samples without phosphate ($p = 0.24$). Likewise, ammonia concentrations did not appear to impact DCF and ERY sorption, as samples with and without ammonia had similar sorbed concentrations ($p > 0.05$). GEM sorption was lowest in pH 7 samples without ammonia, which also contradicts results from the test SBR.

Only pH appeared to have a consistent effect on sorptive capacity, and the effects of pH aligned well with each compound's pKa (Table B.2). Both DCF and GEM are weakly acidic; therefore, as pH decreases, both compounds become less soluble, resulting in better sorption. Conversely, ERY is weakly basic and therefore becomes more soluble as pH decreases, resulting in less sorption, as was also observed in batch experiments (Figure 5.5). Given that the pH in

both SBRs was maintained and recorded at 7.0 ± 0.3 throughout dosing, it is unlikely that pH changes dramatically impacted granules' sorptive capacity, and therefore the reason for desorption between days 12-23 remains uncertain. Likewise, both reactors remained at 23 ± 1°C, and therefore it is unlikely that temperature changes impacted granules' sorptive capacity.

Lastly, batch experiment results also did not accurately predict granules' sorptive capacity in the test SBR. Though sorption increased with each pharmaceutical's K_{ow} value in batch experiments, the opposite was true in the test SBR: GEM sorption was lowest and ERY was highest. Likewise, sorbed pharmaceutical concentrations in the test SBR ranged from 16-130 times lower than those measured in batch experiments with similar initial pharmaceutical concentrations. However, even if granules in the test reactor were capable of binding pharmaceuticals at batch levels, sorptive capacities would be met in under one day (eight SBR cycles) of dosing: DCF and ERY sorption capacity would be met within three SBR cycles, and GEM sorption capacity within seven cycles. Calculations are provided in Appendix B.

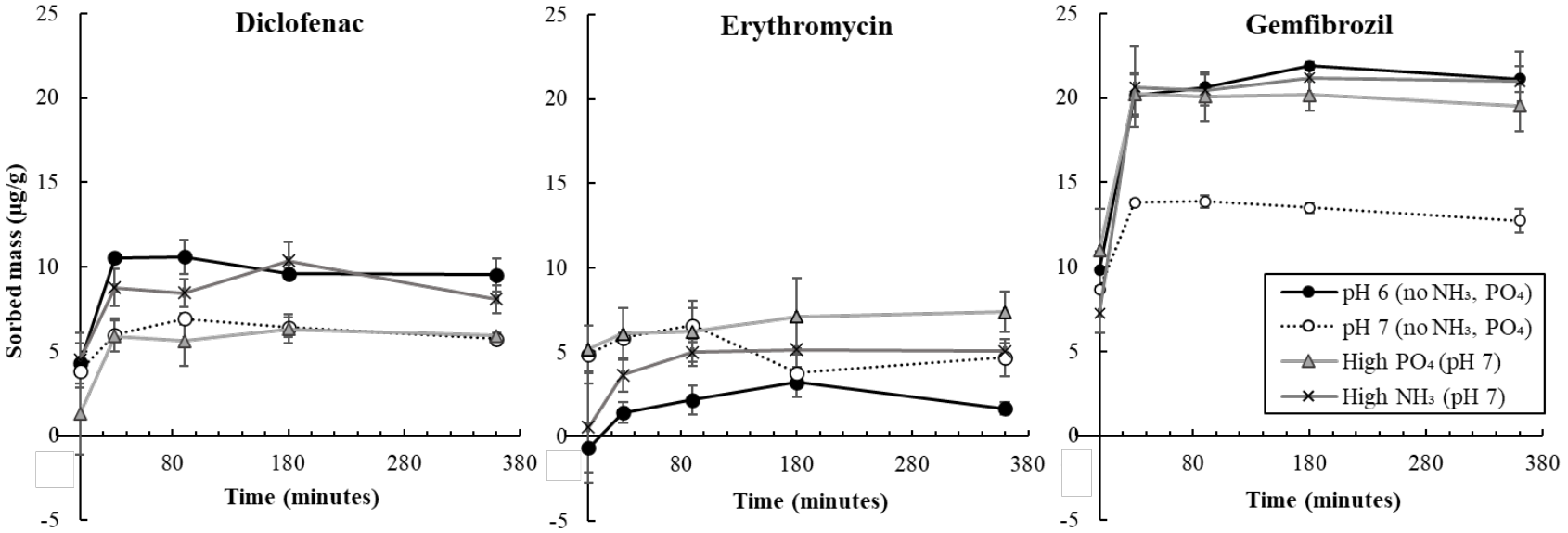

Figure 5.5. Sorbed masses of DCF, ERY, and GEM in batch tests versus time (based on a mass balance from aqueous measurements). Error bars indicate the standard deviation of triplicate samples and are at times smaller than sample points.

It is possible that lower TSS concentrations in batch encouraged greater pharmaceutical sorption per unit mass. TSS in the SBRs was over two times higher than that in batch tests (approximately 24.5 g/L versus 9.5 g/L, respectively). Unfortunately, batch experiments with TSS concentrations closer to those in the SBRs were not possible due to limited amounts of non-pharmaceutical exposed granules. However, the different modes by which granules were exposed to pharmaceuticals in batch and SBR tests may help explain this observation. Granules in the SBR were fed pharmaceuticals in a plug flow fashion; therefore, granules at the bottom of the reactor were fed higher pharmaceutical doses per unit TSS, more analogous to batch conditions.

Following this reasoning and using the average SVI_3 of control granules (11.7 mL/g), the mass of TSS used in batch tests equates to a settled volume of approximately 5.5 mL of granules in the test SBR. It is possible that, in the beginning of the experiment, the bottom 5-10 mL of granules in the SBR were sorbing pharmaceuticals at levels similar to those in batch. However, because a 40 mL completely mixed granule sample was taken during aeration, this sample would not necessarily reflect those high concentrations. Settled granule volumes in the SBR were approximately 1 L; high solid phase concentrations in 10 mL of granules would thus be greatly diluted by lower concentrations in the remaining volume. Nevertheless, as dosing continued, the densest granules at the bottom of the reactor would theoretically become saturated, allowing sorption to granules in the layers above, until all granules had sorbed pharmaceuticals at concentrations like those in batch tests. This hypothesis may explain why solid phase pharmaceutical concentrations increased until approximately day 12 (20 for ERY, Figure 5.3), rather than reaching equilibrium in six hours as was observed in batch tests. However, granules'

lower sorption capacity in the SBR remains unexplained, as well as the reasons for desorption between days 12-23.

Altogether, it seems likely that either the conditions in batch tests, or the short timeframe over which batch tests were conducted, could not accurately mimic complexity in the SBR. Batch test results may represent the first six hours of pharmaceutical sorptive behavior in the SBR; unfortunately, we do not have corresponding solid phase samples from the SBR to corroborate this. Likewise, pharmaceutical degradation products (discussed in [143]) or intermediate metabolites may have impacted granules' sorptive capacities; the lack of aeration or the sodium azide used to inactivate bacteria during batch experiments may have also impacted sorption. Limited studies have shown that sodium azide can react with the analytes of interest in sorption studies, thereby reducing aqueous concentrations and resulting in overestimated sorption capacities [153, 154]. This likely did not occur in experiments described herein, as pharmaceutical concentrations in control samples remained stable throughout batch experiments. Other studies have shown that sodium azide can impact the external surface area of sorbents and increase anion exchange capacity, thereby also artificially inflating sorptive capacity [155]. Sorption batch experiments with autoclaved AGS or without sodium azide were attempted; in both cases, however, pharmaceutical degradation products were detected and increased over time. For that reason, results from these experiments are not reported.

In summation, we can only conclude that results from six-hour batch tests cannot be extrapolated to explain behavior in the test SBR. The timescales of the two experiments are vastly different—six hours versus 80 days. Similarly, the difference in physical scale and operating conditions between the two systems means that samples collected from the batch tests

were more likely to be representative than those collected from the test SBR. Thus, while sorptive behavior similar to that observed in the batch tests may have occurred in the test SBR, there is insufficient resolution in the test SBR data to confirm that behavior due to the differences in physical and temporal scales between the two systems.

Potential Impacts of Declining Lipid Content on Sorptive Capacity and SVI_3

The log K_{ow} of all three pharmaceuticals indicates a preference of each for dissolution in lipids (Table B.2). It is possible that pharmaceutical-lipid partitioning lowered the lipid content in test granules, thereby reducing sites for pharmaceutical sorption. This may have resulted in a feedback loop of sorts: as lipids declined, but pharmaceutical dosing continued, pharmaceuticals would likely be encouraged to bind to those remaining lipids at a greater density. This increased density of pharmaceuticals would in turn further reduce lipids, and so on, resulting in reductions in both lipid content and pharmaceutical sorption capacity. GEM partitioning to lipids may have particularly stimulated lipids' decline: in humans, GEM stimulates production of extracellular lipoprotein lipase, a triglyceride-degrading enzyme [156]. Numerous bacterial genera can produce this enzyme [157], likewise, it is well-known that bacteria in AGS and conventional activated sludge utilize lipases to break down and consume lipids in influent wastewater [12, 158, 159]. Limited studies have shown that GEM exposure can inhibit fatty acid synthesis in bacteria [160, 161] or impact lipid metabolism in general [162]. This may explain why lipids declined in test granules: continued consumption of EPS-associated lipids, combined with inhibited synthesis, would result in lower lipid concentrations. Lower lipid concentrations, in turn, may have allowed less sorption.

To our knowledge, no studies exist on DCF effects on bacterial lipid metabolism. There are multiple studies on the impacts of ERY on lipase production by the acne-associated genera *Propionibacterium*. Most observed that ERY decreased lipase production [163-165]. It is unclear, however, if ERY has the same impact on wastewater bacteria, and this impact would not explain the decline in lipids observed here.

It is also difficult to link the linear decline in lipid concentrations (Figure B.5, $R^2 = 0.94$) throughout dosing with the abrupt drop in solid phase pharmaceutical concentrations observed between days 12-23. Abrupt changes in both lipid content and solid phase pharmaceutical concentrations would more clearly indicate a link between the two. It is possible that there is a lipid threshold below which sorption of DCF, ERY, and GEM is significantly less favorable: solid phase pharmaceutical concentrations dropped between days 12-40, approximately, over which lipids declined from 17 ± 2% to 13 ± 6%. However, a t-test on lipid concentrations over this timeframe found that this decline in lipids was not statistically significant ($p = 0.18$). Furthermore, lipids continued to decline over the experimental duration, whereas solid phase pharmaceutical concentrations approached fairly constant values: from days 46-80, solid phase concentrations for DCF, ERY, and GEM were 0.27 ± 0.03, 0.3 ± 0.04, and 0.16 ± 0.03 μg/g, respectively. Taken together, it is not possible to conclude whether lipid content impacted pharmaceutical sorption. It is likely that pharmaceutical exposure reduced lipid content, but whether this fed back to result in declining solid phase pharmaceutical concentrations remains unclear.

The increased sorption capacity measured in batch tests may also be linked with lipid concentrations. Control granules, which contained twice the lipids of test granules at day 80

(Table 5.3), were used in these tests. Perhaps increased lipid concentrations, combined with batch test conditions and the short timeframe over which tests were conducted, resulted in higher sorption measurements. Batch tests using granules with decreasing lipid concentrations were beyond the scope of this work but would aid in determining the extent to which lipids and sorption capacity are linked.

Over the experimental duration, test granules' SVI_3 doubled, from 11.2 to 22.8 mL/g (Figure B.6). Perhaps relatedly, lipid content halved. This is likely coincidental, as multiple studies have shown that higher protein-to-polysaccharide ratios, not lipid content, are correlated with lower SVIs [145, 166, 167]. To our knowledge, just one study exists in which SVI and lipid content in granules were monitored and a correlation between the two was not observed [168]. Given that granule sizes (Figure B.7) and protein and polysaccharide fractions (Table 5.3) in test granule sections did not change significantly, it is difficult to determine what specifically caused the increase in SVI_3.

Conclusions

This study explored the abiotic fate of three common pharmaceuticals—DCF, ERY, and GEM—throughout dosing in an AGS SBR. Pharmaceutical effects on granular morphology were also tracked. For the first 12 days of dosing, pharmaceutical removal occurred and sorbed pharmaceutical concentrations increased; however, pharmaceuticals then desorbed and effluent concentrations spiked. The reasons for this desorption event could not be explained by changing ammonia or phosphate concentrations in the reactor. Sorption of all pharmaceuticals was modelled well by the Henry isotherm, but sorption capacities measured in batch experiments greatly exceeded those measured in the test SBR. The lipid content in granules decreased linearly

throughout exposure, which may be linked with declining sorptive capacity and increasing SVI_3, though further studies are needed to verify this relationship. Pharmaceuticals remained sorbed to AGS throughout dosing, albeit at smaller concentrations, and removal was negligible after day 12.

Funding

This research was supported by Montana INBRE, which is funded by the National Institute of General Medical Sciences division of the National Institutes of Health under Award Number P20GM103474. The content is solely the responsibility of the authors and does not necessarily represent the official views of the National Institutes of Health.

Acknowledgements

The authors would like to thank staff at the Mass Spectrometry Facility at Montana State University (MSU) for training and assistance. Funding for the Proteomics, Metabolomics and Mass Spectrometry Facility used in this publication was made possible in part by the MJ Murdock Charitable Trust, the National Institute of General Medical Sciences of the National Institutes of Health under Award Numbers P20GM103474 and S10OD28650, and the MSU Office of Research, Economic Development and Graduate Education.

Declaration of Competing Interests

The authors have no relevant financial or non-financial interests to disclose.

CHAPTER SIX

ENVIRONMENTALLY-GROWN AEROBIC GRANULAR SLUDGE RESPONSE TO PHARMACEUTICALS: IMPACTS ON WASTEWATER TREAMENT EFFICACY, ACTIVE MICROBIAL COMMUNITIES, AND PHARMACEUTICAL FATE

Contribution of Authors and Co-Authors

Manuscript in Chapter 6

Author: Kylie B. Bodle

Contributions: Designed and conducted study. Collected and analyzed data, wrote and revised manuscript.

Co-Author: Catherine M. Kirkland

Contributions: Helped conceive and design study, aided in data interpretation, aided in revision of the manuscript and provided comments.

Manuscript Information

Kylie B. Bodle, Catherine M. Kirkland

Journal of Environmental Management

Status of Manuscript:
☐ Prepared for submission to a peer-reviewed journal
☒ Officially submitted to a peer-reviewed journal
☐ Accepted by a peer-reviewed journal
☐ Published in a peer-reviewed journal

Elsevier
Submitted March 5, 2024

Abstract

This study assessed environmentally-grown aerobic granular sludge performance during exposure to a 60 µg/L pharmaceutical mixture. The pharmaceuticals diclofenac, erythromycin, and gemfibrozil were fed to a test sequencing batch reactor for approximately 70 days, and changes in wastewater treatment efficacy, granular structures, and active microbial communities were monitored and compared with that of a control reactor. Pharmaceutical fates were also evaluated. Phosphate removal was uninhibited, but nitrogen removal was inhibited by approximately 60% and due mainly to decreased ammonia oxidation—likely because active *Nitrosomonadaceae* were lower in abundance in the test reactor than the control. Granule structures were not impacted by pharmaceuticals. Neither diclofenac nor erythromycin were consistently removed by over 20%, but gemfibrozil removal via biodegradation reached 100%. Active bacteria belonging to the *Xanthomonadaceae* family and Anaerolineae and Ignavibacteria classes (specifically uncultured families J111 and OLB5, respectively) increased in abundance in the test reactor at approximately the same time as gemfibrozil removal increased. Elevated relative abundances were sustained thereafter, leading us to hypothesize that these families may have driven gemfibrozil degradation. This study is one of the first to utilize environmentally-grown granules rather than lab-grown ones, and therefore provides important information about the response of granules cultivated outside of a lab environment.

Introduction

Pharmaceutical concentrations in natural water bodies, soils, and other environmental media are increasing across the globe. This poses risks to both human and animal health, as

many pharmaceuticals can have toxic effects on fish, birds, and small mammals, as well as contribute to the proliferation of antibiotic resistance genes in bacteria [24, 76]. Effluent discharge from wastewater treatment plants is a major vector by which pharmaceuticals enter the environment, as many pharmaceuticals are not biodegradable under conventional wastewater treatment conditions [24]. Current technologies capable of pharmaceutical removal, such as membrane filtration or advanced oxidation processes, are expensive and do not self-regenerate [142, 169]. For this reason, it is essential to investigate improved methods of wastewater treatment.

One such technology that thus far has shown promise at treating both pharmaceuticals and conventional wastewater contaminants is aerobic granular sludge, or AGS [3, 32]. AGS is an emerging biofilm-based technology in which wastewater bacteria self-aggregate into spheres several millimeters in diameter. Oxygen gradients throughout granules allow nitrifying, denitrifying, and phosphate accumulating organisms to coexist, thereby allowing complete wastewater treatment in a single reactor. Additionally, extracellular polymeric substances (EPS) secreted by bacteria in AGS create a protective, diffusive barrier between bacteria and toxins, such as pharmaceuticals, which enhances bacterial resilience, AGS density, and biomass retention [1, 2].

Multiple studies have shown that AGS is capable of simultaneously treating conventional wastewater contaminants while removing pharmaceuticals via a mixture of sorption and biodegradation (e.g., [3, 32, 34]. Currently, however, almost all published studies utilize granules grown in a lab environment: conventional activated sludge (CAS) is typically used to seed lab-scale sequencing batch reactors, and experimentation is conducted on granules grown from CAS

on synthetic wastewater after 30 days or longer (e.g., [3, 32, 34, 46, 84, 170]. It has been shown that wastewater composition impacts AGS microbial communities and structures [13, 171]; likewise, AGS grown in full-scale treatment plants is exposed to a much more diverse body of substrates than lab-grown AGS [12], and therefore may be better able to degrade complex substrates such as pharmaceuticals. Since all of these factors are likely to have a major impact on AGS' capacity for pharmaceutical removal, it is crucial to investigate how environmentally-grown granules respond to pharmaceuticals—studies of this nature provide important information about how accurately lab-grown granules model the behavior of environmentally-grown AGS.

In this study, three frequently-detected but relatively unstudied (fewer than three studies on each compound were available at the time of study design) pharmaceuticals were dosed into a lab-scale reactor containing AGS from a full-scale treatment plant. Diclofenac (DCF), erythromycin (ERY), and gemfibrozil (GEM) are often detected in the environment at concentrations up to 10 μg/L, and in wastewater treatment plant influents concentrations as high as 64 μg/L have been measured [26, 38, 57]. DCF is a non-steroidal anti-inflammatory compound that is typically removed by less than 40% during conventional treatment [50], and has been shown to act synergistically with antibiotics to prevent biofilm formation [53]. A macrolide antibiotic used in both human and veterinary medicine, ERY has been shown to bioaccumulate in aquatic organisms and contribute to antibiotic resistance gene proliferation [38, 43]. Lastly, GEM is a commonly used fibrate that has been shown to disrupt the endocrine systems of multiple aquatic organisms [62]. Limited results suggest it may also reduce lipid concentrations in lab-grown AGS [172].

The objectives of this study were four-fold: (1) track pharmaceutical impacts on conventional wastewater treatment efficacy; (2) investigate pharmaceutical fate in both the aqueous and solid (sorbed) phases by tracking parent compound and degradation product levels in each phase; (3) evaluate pharmaceutical impacts on AGS structures by tracking changes in EPS macromolecule distributions, granule sizes, and density; and (4) assess changes in active microbial community composition throughout pharmaceutical dosing. Few studies confirm pharmaceutical sorption via extraction from solids, nor is degradation product detection commonly used to confirm biodegradation. Both methods provide important information about the extents of pharmaceutical removal and conversion. Likewise, though high protein-to-polysaccharide ratios are well-known to contribute to granules' stability [4], the roles of lipids and specific polysaccharide forms (alpha versus beta) are not well understood. Improved understanding of pharmaceutical effects on these components may aid overall understanding of the role of these biopolymers in AGS' structure and function. Lastly, much remains unknown regarding the links between active microbial communities in AGS and pharmaceutical removal. Shifts in the abundance of active microbial populations and potential correlations between wastewater treatment efficacy and pharmaceutical biodegradation were therefore given particular attention.

Methods

SBR Operation

Two sequencing batch reactors (SBRs) were seeded with approximately 1 L each (settled volume) of granules sampled from the AquaNereda® demonstration plant in Rockford, IL. Granule samples were shipped overnight on ice and, upon delivery, immediately added to both

SBRs. Both reactors had an internal diameter of 60 mm and working volume of 3.4 L. SBRs were operated in repeating three-hour cycles: 65 minutes anaerobic feed, 100 minutes aeration, 10 minutes settling, and 5 minutes effluent discharge from a port 47 cm above the bottom flange. The settling time was gradually reduced to 5 minutes over the first 4 weeks of SBR operation to allow granules to adapt to the new environment, prevent washout of valuable biomass, and maintain selection pressure for denser granules. Approximately 50% of liquid in each SBR was withdrawn during each cycle, resulting in a 6.4-hour hydraulic residence time. LabVIEW software (National Instruments) was used to maintain the pH and dissolved oxygen (DO) concentration during aeration, at 8.0 ± 0.2 and 3.7 ± 0.3 mg/L, respectively. Pump operation was automated using an automatic timer (Chrontrol).

Influent synthetic wastewater medium consisted of a mixture of two media diluted with deionized water. Medium A contained 1.13 g/L $NaC_3H_5O_2$, 0.27 g/L $MgSO_4*7H_2O$, 0.11 g/L KCl, and 8.8 g/L $NaHCO_3$. Medium B contained 0.87 g/L NH_4Cl, 0.11 g/L K_2HPO_4, 0.18 g/L KH_2PO_4, and 10 mL/L of trace element solution, as described in [173]. Influent media concentrations were based on average influent data from the Rockford plant and adapted from recipes described in [89] and [174]. The use of real wastewater as influent medium was unfortunately beyond the scope of this study, due to safety concerns and laboratory limitations. 150 mL of each medium was combined with 1.3 L deionized water to result in final influent concentrations of approximately 27 mg/L NH_3 and 17 mg/L PO_4. Sodium propionate concentrations in medium A were gradually increased from 1.13 g/L to 2.83 g/L over the first 10 days of the experiment to reach a final influent organic carbon concentration of 100 mg/L.

Propionate concentrations were increased in this fashion to ensure that all organic carbon was consumed during the anaerobic feed phase of SBR operation.

After inoculation, both SBRs were operated for 24 hours to provide a brief acclimation period for biomass. Pharmaceutical dosing then began to the test reactor: approximately 21 mL of a stock solution containing 3.95 mg/L each of diclofenac and gemfibrozil ("DG solution", both Acros Organics) was fed with the influent medium. Twenty-one mL of a separate solution ("ERY") containing 3.95 mg/L erythromycin (TCI Chemicals) was also fed with the influent medium. Approximately 60 µg/L of each pharmaceutical was present in the final combined influent stream. This influent concentration was selected because it represented realistic, if slightly elevated, pharmaceutical concentrations measured in wastewater treatment plant influents across the globe [26, 38, 57]. Individual stock solutions of each pharmaceutical were prepared first at 10 g/L in methanol, then diluted into nanopure water to obtain the forementioned concentrations. Pharmaceutical media were protected from light and prepared fresh every 8-10 days.

The three pharmaceuticals were not all mixed into one solution because prior results, documented in [100], showed that each sorbed to lab materials with different affinities. To mitigate pharmaceutical losses to tubing, DG solution was pumped through PharmaPure tubing and ERY solution through silicone tubing (both Masterflex). However, ERY concentrations in the influent were lower than expected for the first 20 days, likely due to sorption to influent tubing or tubing connections, and therefore the ERY stock solution concentration was increased to 8.95 mg/L on day 24. Prior to this change, influent ERY concentrations were 12.9 ± 1 µg/L;

thereafter, concentrations increased to 76.3 ± 19.5 µg/L. Influent samples were taken from a sampling port at the base of the reactor, shown in Appendix C Figure C.1.

Analytical Methods

Wastewater Analytes and Pharmaceuticals. Influent and effluent samples were regularly taken from both reactors for analyses of ammonia, nitrite, nitrate, phosphate, and dissolved organic carbon. Samples were filtered through 0.45 µm regenerated cellulose filters prior to analyses. Hach kit TNT 832 and a Hach DR 3900 spectrophotometer, equivalent to US EPA Method 350.1, were used to quantify ammonia. A Dionex ICS-1100 anion chromatography system equipped with an IonPac AS22 RFIC column (4 x 250 mm) and IonPac guard column (4 x 50 mm) was used to quantify the other anions listed. A SKALAR Formacs^{HT} Total Organic Carbon analyzer system was used to quantify dissolved organic carbon (DOC), defined as that which could pass through a 0.45 µm filter.

Granule size distributions were determined via sieving. Total and volatile suspended solids (TSS and VSS respectively) were determined following standard methods [149]. A graduated scale on the reactor column was used to determine sludge volume index after 10 minutes (SVI_{10}) of settling. Although the settling time was gradually reduced to 5 minutes over the first 4 weeks of experimentation, SVI_{10} was monitored throughout dosing to ensure consistency throughout the experimental duration. SVI_{10} was used as an indicator of biomass density and settling capacity, with lower values indicating denser, faster-settling sludge.

Mass spectrometry was used for quantification and identification of aqueous and solid phase pharmaceutical compounds and degradation products. Prior to analyses, aqueous influent and effluent samples were extracted as detailed in [143]. In brief, 50 mL influent or 100 mL

effluent was filtered through a 1.5 µm glass fiber filter (Hach), then loaded on preconditioned Waters Oasis HLB cartridges (30 mg, 20 mL) using a vacuum manifold. Loaded cartridges were washed and dried per manufacturer guidelines and frozen at -20°C until elution (no longer than 2 weeks). Once per week, influent and effluent samples were taken in duplicate to assess extraction recovery with spike-recovery tests (as described in [143] and in Appendix C, Equation C1). Average recoveries of each pharmaceutical are summarized in Table C.1. To assess accuracy but prevent excessive disruption to the reactor, triplicate influent and effluent samples were taken once per month.

Once per week, pharmaceuticals were also extracted from granules sampled from the test reactor. Extraction methods were adapted from [103]; in brief, approximately 2 g wet weight (5 mL settled volume) AGS were sampled during aeration. Samples were filtered to remove excess moisture and approximately 0.25 g (wet weight) of the sample was dried to determine the moisture fraction of the sample. The remaining sample mass was crushed with a spatula before transferring to a glass centrifuge tube. Samples were sonicated for 15 minutes with 5 mL methanol, centrifuged at 1600 xg for 8 minutes, and the supernatant was then transferred to a clean glass test tube. This process was repeated with 2 mL methanol followed by 2 mL acetone. Supernatants were pooled after each centrifuge step and evaporated down to approximately 5 mL under a gentle nitrogen stream. The remaining sample was then filtered through a 0.45 µm regenerated cellulose filter, diluted into 150 mL deionized water, and extracted with HLB cartridges as described above. At the beginning and end of the experiment, solid phase samples were extracted in triplicate. Every other week, spike-recovery testing was used to assess extraction recovery (Equation C1). Pharmaceuticals were also extracted from granules prior to

beginning dosing, to determine if DCF, ERY, and/or GEM were already present in the biomass. Aqueous and solid phase samples from the control reactor were also extracted once per month to confirm pharmaceuticals' absence.

An Acquity I Class Plus ultra-performance liquid chromatograph (UPLC) coupled to a Waters Synapt XS quadrupole time-of-flight mass spectrometer (QToF-MS) in positive ion mode was used for pharmaceutical quantification and detection. Chromatographic analysis methods were adapted from [92] and are detailed in [143]. The open-source software MZmine and R were used to analyze and compile mass spectra data [101, 102].

Lastly, all samples were screened for DCF, ERY, and GEM biodegradation products using a personal compound database and library (PCDL) developed from the literature (Table C.2). Degradation products were detected when the signal-to-noise ratio of peaks was greater than or equal to 10 and mass errors were less than 5 ppm. The goal of this approach was not to quantify degradation products' concentrations, but simply to use the presence of degradation products as an indicator of relative levels of biodegradation. "Corrected peak areas" of both aqueous and solid phase degradation products are therefore reported here as a proxy for concentration; equations S2 and S3 described in the SI were used to calculate these values.

Microscopy. Pharmaceutical impacts on the distribution of major EPS components in AGS were assessed using the staining scheme described in [17, 172]. Approximately once per week, granules from both reactors were fixed with 4% paraformaldehyde and stained for proteins, lipids, and alpha- and beta-polysaccharides per methods in [17]. Stained granules were cryosectioned into 30 μm slices and sections near the center (~700 μm from the granule surface) were imaged with an inverted Leica DMI8 Stellaris confocal laser scanning microscope (CLSM).

Imaris imaging software was used to determine the relative biovolumes of proteins, lipids, and polysaccharides in each granule section, and the fraction of each component relative to the total section biovolume was calculated. The total biovolume of the granule section was estimated by over-thresholding the biovolume of the transmitted light image such that the entire biovolume of the granule section was calculated. Multiple EPS components overlaid each other in each granule section, and therefore component fractions sum to over 100%. Triplicate slices from the same granule, as well as triplicate slices from different granules, were analyzed to assess variability.

Bacterial Community Composition

DNA/RNA Extraction. Granules from both reactors were periodically sampled for molecular characterization of the prokaryotic microbial community using high throughput sequencing of 16S rRNA genes and transcripts, using methods identical to those described in [143]. In brief, biomass was collected during aeration to obtain a completely mixed sample, and samples were stored at -80°C prior to extraction. Nucleic acids were extracted from approximately 5 granules and 100 µL flocs at each time point. Samples were extracted via bead beating in DNA/RNA Shield (Zymo Research). DNA was purified from the lysate with the DNA Clean and Concentrator Kit (Zymo Research). RNA samples were extracted from the same lysate using the Direct-zol RNA Miniprep Kit (Zymo Research), digested with the TURBO DNA-free Kit (Invitrogen), and purified with the RNA Clean and Concentrator Kit (Zymo Research). The ProtoScript II First Strand cDNA Synthesis Kit (New England Biolabs) was used to reverse transcribe RNA to cDNA. Qubit dsDNA HS and RNA HS kits (Invitrogen) were used to quantify DNA and RNA concentrations, respectively. Manufacturer-provided protocols were

followed for all kits listed. Extraction and analyses of replicate nucleic acid samples at each time point were beyond the scope of this study.

16S Library Preparation and Sequencing. 16S library preparation followed methods identical to those in [143]. In brief, Phusion Hot Start II DNA polymerase (Thermo Scientific) was used to target the V4 region of 16S rRNA genes ("rDNA") and transcripts (cDNA) with the primers 515F-A (GTGYCAGCMGCCGCGGTAA) and 806R-b (GGACTACVSGGGTATCTAAT). Reaction ingredients and thermocycling conditions are detailed in [143]. Mag-Bind TotalPure NGS beads (Omega) were used to purify PCR products; samples were then barcoded with the Nextera XT Index Kit v2 Set D (Illumina). Barcoded samples were again purified with Mag-Bind beads, quantified, and pooled into a sample library containing approximately 30 ng DNA from each sample. Sequencing was performed onsite at Montana State University with the Illumina MiSeq platform using the v3 600 cycle kit. Raw sequence files were deposited to the NIH's Sequence Read Archive under ID PRJNA1081863.

Statistics and Data Analysis. As detailed in [143], USEARCH software was used to merge forward and reverse reads, quality filter with a max score of 1, trim primer sequences, and dereplicate sequences. Zero-radius OTUs (ZOTUs) were identified with the UNOISE3 algorithm, and an OTU table was then constructed. To classify ZOTUs, SINTAX was used against a reference database of 16S sequences from the Genome Taxonomy Database (GTDB, release 202, [115]) with outgroup sequences for chloroplast and mitochondria. Sequences identified as Eukarya or with a bootstrap value less than 70% at the phylum level were removed from downstream analyses.

rDNA was targeted to examine the total microbial community. rRNA transcripts (cDNA) were targeted to examine the active microbial community, defined as ZOTUs with a ratio of 16S rRNA transcripts to rDNA greater than or equal to 1 [119]. ZOTU matrices were rarefied 100 times using using R software (version 4.3.2, [101]) with packages mirlyn [175], vegan [120], and phyloseq [122]. Counts were then averaged across all 100 trials; this rarefied matrix was used to calculate transcript to gene ratios. "Phantom taxa", or taxa detected in rRNA but not rDNA, were accounted for by setting ratios to 100 based on methods described in [119]. To mitigate biases in sequence numbers that may have arisen during cDNA transcription, rDNA read numbers were used to calculate relative abundances within the active community. Since rDNA read numbers for phantom taxa were zero, rRNA read numbers were used to approximately track changes in the "phantom community". Taxa were grouped at the family level to calculate changes in relative abundance or read numbers over time.

Results and Discussion

Wastewater Treatment Performance

Preliminary experiments in which environmentally-grown AGS was cultivated in the lab showed that granules took 30 days or longer to adapt to the new environment, evidenced by incomplete nitrogen and phosphate removal. Ammonia oxidation was particularly inhibited. Since the goal of this experiment was to track the response of environmentally-grown granules to pharmaceuticals, we chose to forego this 30-plus-day adaptation period in order to utilize granules that were not yet changed by lab conditions. For this reason, percent inhibition of nitrogen and phosphate removal in the test reactor relative to the control reactor (Equations C4-C6) was used to characterize how pharmaceutical dosing impacted granules' wastewater

treatment capacity (Figure 6.1). Percent removal of nitrogen and phosphate in the control and test SBRs is shown in Appendix C, Figure C.2.

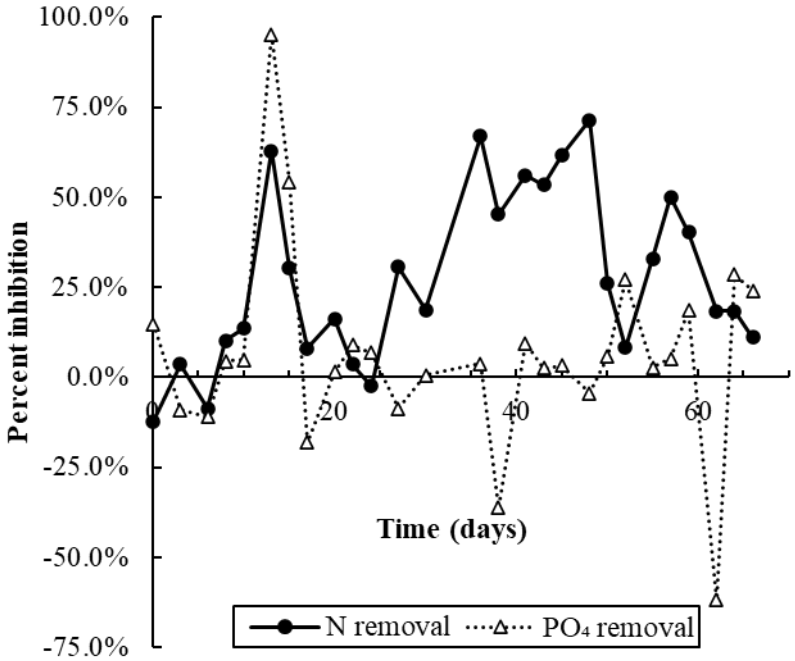

Figure 6.1. Percent inhibition of nitrogen and phosphate removal versus time. Percent inhibition values below zero indicate that removal of nitrogen or phosphate was higher in the test reactor than the control. Phosphate removal was largely uninhibited throughout dosing; nitrogen removal was particularly inhibited between days 27-48.

Inhibition of phosphate removal remained near zero throughout the dosing period, except days 13-17 (Figure 6.1). Poor phosphate removal in the test reactor over this period was likely due to a biomass washout that occurred on day 13: from days 0-13, biomass in both SBRs consisted of a mixture of granules and flocs. For an unknown reason, on day 13, all flocs in the test SBR washed out, leaving behind only granular biomass. No operational errors occurred on day 13. It is possible that pharmaceutical dosing in some way contributed to the biomass washout, but a similar washout event was also observed during preliminary experiments without

pharmaceuticals. It seems more likely that this washout was simply some artifact of environmentally-grown biomass adjusting to the lab environment.

Nitrogen removal inhibition spiked between days 13-17, likely also due to the biomass washout on day 13. After a brief drop in inhibition between days 17-24, inhibition increased and was sustained at 59 ± 9.5% between days 36-48. Poor nitrogen removal was largely due to incomplete ammonia oxidation (Figure C.3). Nitrite and nitrate removal in both SBRs was similar and near 100% for the duration of the experiment, which suggests that both processes were minimally impacted by pharmaceutical exposure (Figure C.3, Figure C.4). DOC removal in both reactors was also near complete and mainly occurred anaerobically (Figure C.5), which, combined with near-complete phosphate removal data (Figure C.2), suggests that most carbon was consumed by phosphate accumulating organisms (PAOs). PAO activity is discussed in more detail in the following sections.

Pharmaceutical Fate and Removal

Figure 6.2 shows pharmaceutical removal versus time in the test SBR. Removal of both DCF and ERY was generally less than 20% throughout the experiment, but GEM removal stabilized at 100% after day 36. Removals less than 0% indicate that measured effluent concentrations were higher than those predicted by a mass balance (Equations C4-C5). Pharmaceutical sorption to influent tubing is likely the main reason for negative removal values: SBR systems operated periodically, with pharmaceutical media stagnant in influent tubes for 110 minutes before flowing again for 70 minutes. Changes in flow likely impacted sorption rates, and therefore influent samples taken for a fraction of the influent flow time might reflect large or small losses from sorption. The most accurate representation of influent concentrations would

have been obtained by sampling the entire influent volume; however, this would have greatly disrupted the experiment. Removal values below zero should be interpreted as 0% removal.

Pharmaceutical fate and biodegradation are discussed in more detail in the following sections. Pharmaceutical parents or degradation products were not detected in any aqueous or solid phase samples from the control SBR, excepting the AGS inoculum, which had background parent concentrations of 0.04, 0.03, and 0.02 μg/g DCF, ERY, and GEM, respectively (Figure 6.3).

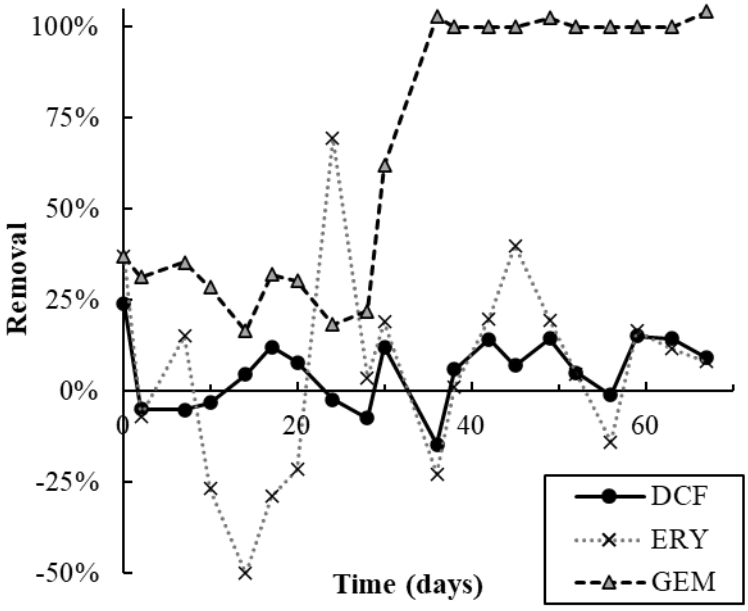

Figure 6.2. Pharmaceutical removal in the test SBR. Removals below zero signify that effluent concentrations were higher than those predicted by a mass balance and should be interpreted as 0% removal.

Diclofenac. DCF removal remained below 15% after the second day of the 67-day experiment (Figure 6.2). Despite this, some degradation occurred, evidenced by the presence of aqueous phase degradation products in the effluent (Figure 6.4). The DCF degradation products hydroxy-DCF ("DCF1", $C_{14}H_{11}Cl_2NO_3$) and hydroxy-DCF-quinone imine ("DCF2",

$C_{14}H_9Cl_2NO_3$) were detected throughout dosing. DCF1 is formed initially during DCF biodegradation, and may be present as either 4'-hydroxy-DCF or 5-hydroxy-DCF [123]. The mass spectrometry method used herein was unable to differentiate between the two isomers. Per pathways proposed in [123] and [176], DCF2 is formed from degradation of 5-hydroxy-DCF or DCF-lactam. DCF-lactam was not detected in this study; it may have been present, but the extraction and/or quantification methods used were unable to detect it. Given that both products were only detected in the effluent from the test SBR, it is likely that both were formed by bacteria in AGS. DCF degradation to further intermediates may have also occurred, but other degradation products were not detected, again potentially because the extraction/quantification methods used were not suited for detection of these compounds.

Background solid phase DCF concentrations in the granular inoculum were approximately 0.04 µg/g (Figure 6.3); concentrations then increased to 0.3 µg/g on day 14, after which they dropped to approximately 0.1 µg/g. The sharp drop in DCF concentrations after day 14 was likely due to the floc washout mentioned earlier. An analysis of pharmaceutical partitioning to all biomass, versus just flocs, showed that flocs bound approximately 40% of the total DCF sorbed (Figure C.6). Since flocs washed out on day 13, but solid phase concentrations peaked on day 14, it is possible that the increased aqueous DCF availability temporarily enhanced sorption to AGS. It is also possible that solid phase DCF concentrations were highest on day 13, and that measurements on day 14 actually reflect a drop from this prior peak, which the sampling frequency was unable to capture.

Solid phase DCF concentrations again increased between days 36-63, which may have contributed to the sustained, albeit slight, removal (9.4 ± 5.6%) over this time period (Figure

6.2). Despite this, solid phase concentrations and removal were not strongly correlated (R^2 = 0.5), which may indicate that sorption was not a major contributor to DCF removal. It is also possible, however, that sorption was a precursor to biodegradation: increasing sorbed concentrations may have provided bacteria in AGS with more access to pharmaceuticals, consequently allowing increased degradation. This theory may explain why, for example, solid phase DCF concentrations increased up to day 14 (Figure 6.3), then dropped while degradation product levels spiked (Figure 6.4). This theory may also explain the fluctuations in DCF sorption and degradation product levels throughout the experiment.

On the final day of the experiment (day 67), aqueous pharmaceutical concentrations and degradation product levels were monitored throughout one SBR cycle (Figure 6.5, Figure 6.6). Figure 6.5 shows that some loss of DCF occurred during the fill phase, evidenced by lower concentrations at the end of the fill phase (70 minutes) than those predicted by a mass balance (closed symbols at zero minutes). Concentrations then declined by approximately 10 µg/L in the first third of the aeration phase (70-103 minutes). Throughout the rest of the SBR cycle, DCF concentrations increased, with effluent concentrations near equal to those at the end of fill (45 and 41 µg/L, respectively). The decline and subsequent increase in aqueous DCF concentrations throughout the cycle suggests sorption in the first 100 minutes followed by desorption in the remaining 80 minutes. Changing solid phase concentrations were not measured throughout a single cycle, however, as the removal of biomass would have caused too much disruption to the reactor, so it is not possible to confirm this hypothesis.

As shown in Figure 6.6, neither DCF1 nor DCF2 were detected in the influent, which confirms that these products were solely formed within the test SBR. DCF1 levels were high at

the end of the fill phase, perhaps indicating DCF degradation during the anaerobic phase of SBR operation. DCF1 levels then declined throughout aeration while DCF2 levels increased, which indicates that bacteria were aerobically converting DCF1 to DCF2. Despite evidence of degradation, removal on day 67 was just 9.1%. Given that sorption during aeration appeared to be temporary, and that removal did not appear to correlate with solid phase DCF concentrations, it seems likely that biodegradation was the main cause of DCF removal.

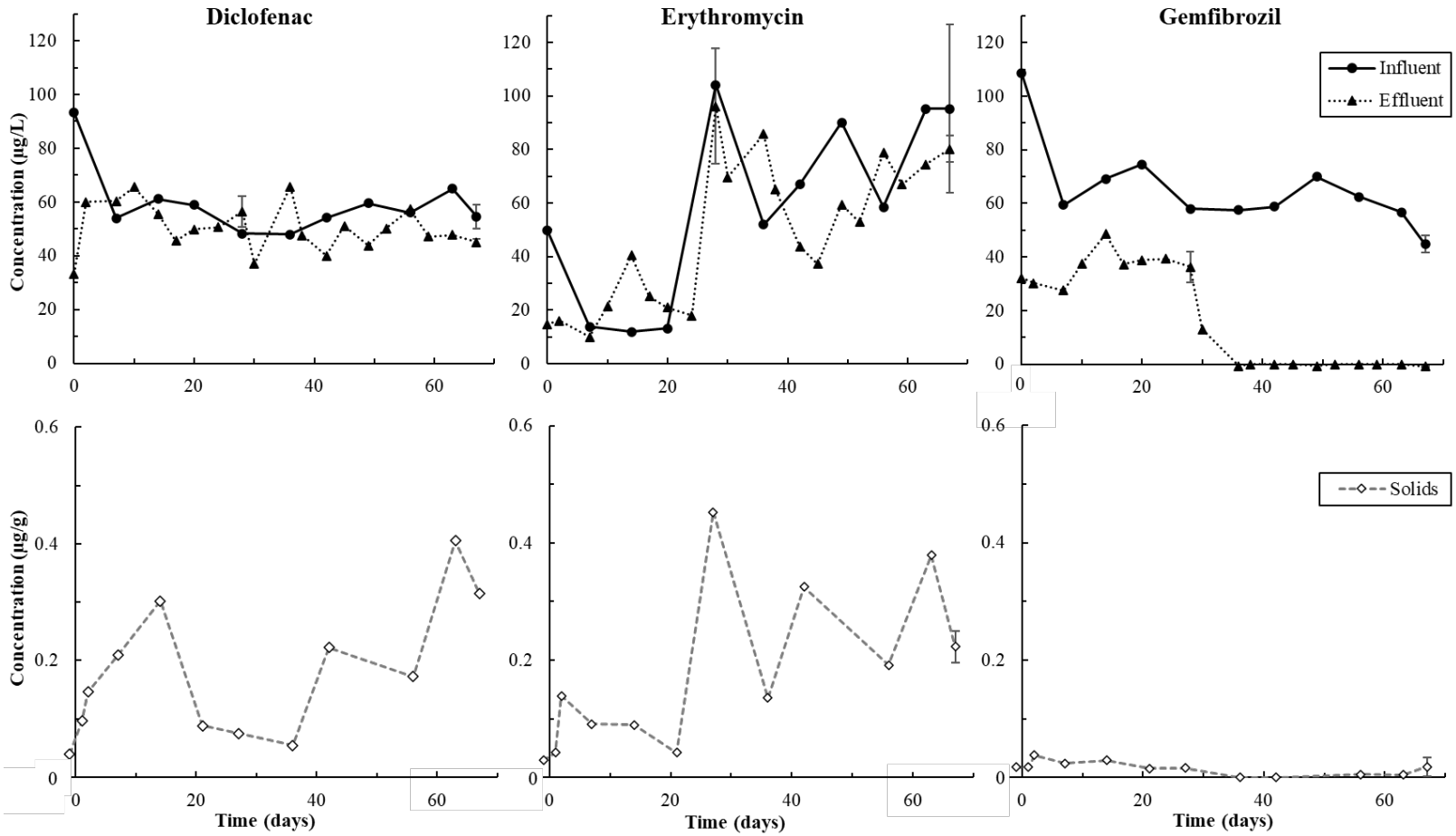

Figure 6.3. Influent and effluent pharmaceutical concentrations (top row) and solid phase pharmaceutical concentrations (bottom row) versus time. Error bars are present on days 28 and 67 for aqueous samples and day 67 for solid phase samples and reflect the standard deviation of triplicate sample extractions; values on these days are averages. Solid phase concentrations at day "-1" indicate background pharmaceutical concentrations in the granules.

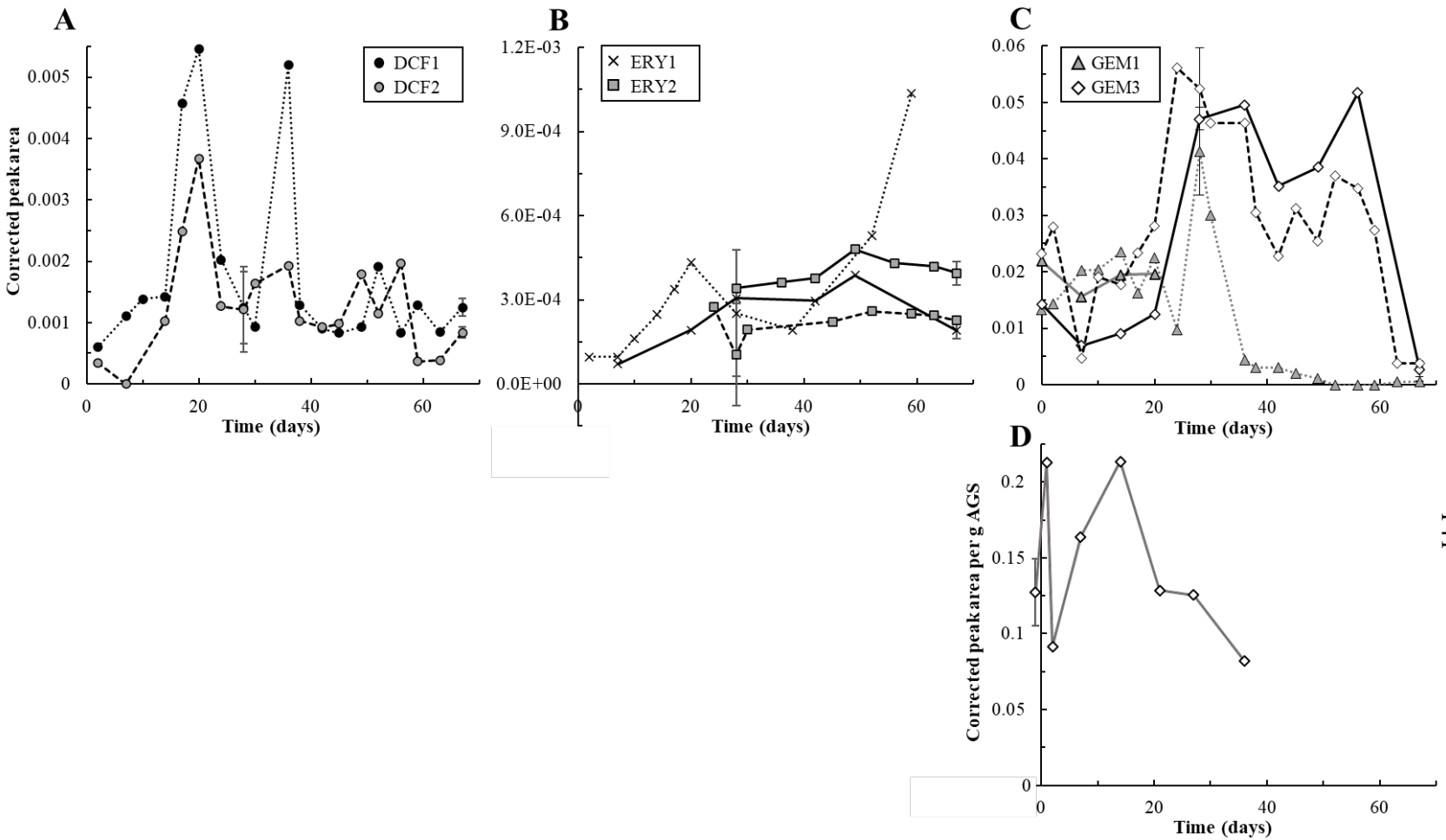

Figure 6.4. A-C: Aqueous phase degradation products versus time. Dashed or dotted lines indicate products detected in the effluent; solid lines indicate those found in the influent. Note that all y-axis scales are different, though all reflect corrected peak area. Error bars are present on days 28 and 67 and indicate the standard deviation of triplicate samples; bars may be smaller than sample points. D: Solid phase GEM degradation products. Solid phase DCF and ERY degradation products were not detected throughout the experiment.

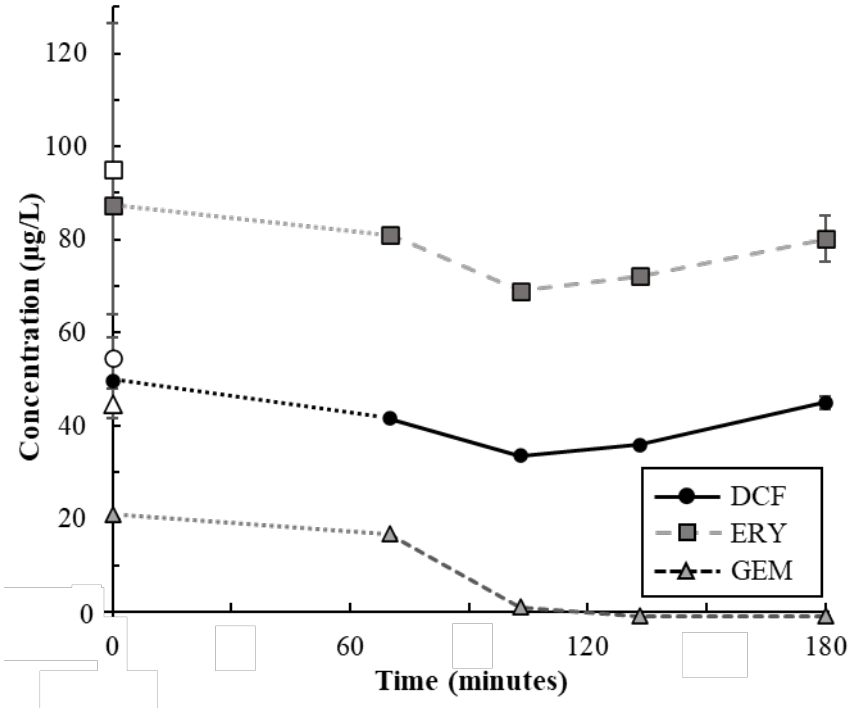

Figure 6.5. Aqueous parent pharmaceutical concentrations throughout a single SBR cycle on the final day of the experiment (day 67). Open symbols at time zero indicate influent concentrations. Filled symbols at time zero indicate mass-balance predicted final concentrations in the reactor at the end of the fill phase (calculated with Equation C4). The actual concentration measured at the end of the fill phase is shown at 70 minutes. Concentrations at 180 minutes reflect those in the effluent. Error bars on influent and effluent points reflect the standard deviation of triplicate samples and are smaller than sample points for some pharmaceuticals.

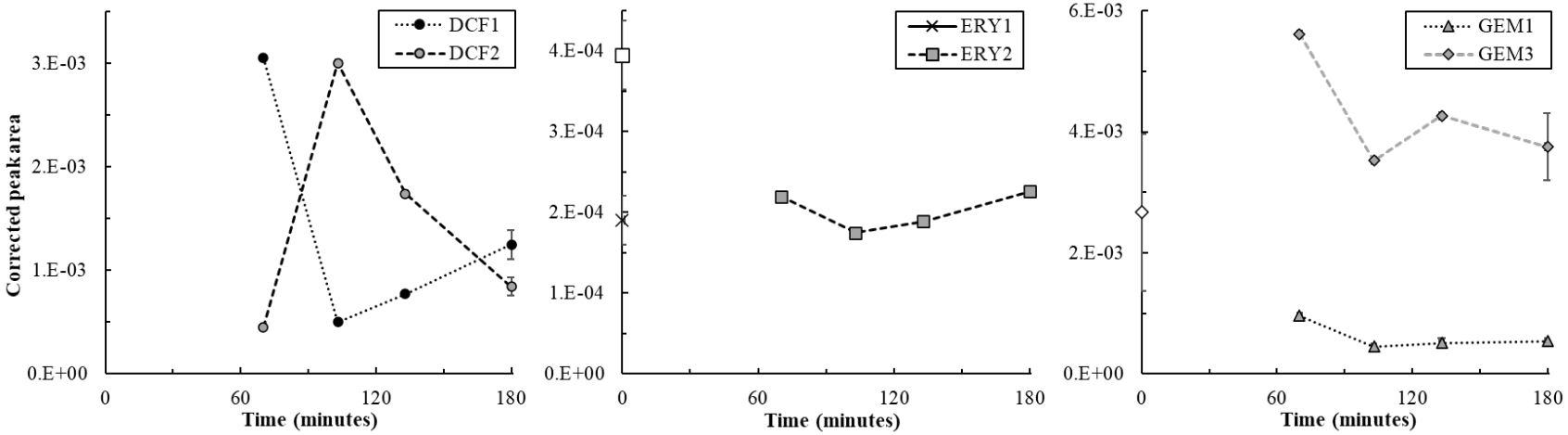

Figure 6.6. Aqueous phase degradation products detected throughout one SBR cycle on day 67. Open symbols at time zero for ERY1, ERY2, and GEM 3 indicate the presence of these degradation products in the influent. Note that y-axis scales are not equivalent, though all reflect corrected peak areas. Error bars on influent and effluent points reflect the standard deviation of triplicate samples and are smaller than sample points for some compounds.

Erythromycin. ERY removal was generally under 20% in the test SBR (Figure 6.2). As described previously, influent ERY concentrations were lower than intended for the first 24 days of dosing. Immediately after increasing influent ERY concentrations on day 24, removal peaked at 69%, likely due to increased ERY availability and thereby increased sorption—solid phase data in Figure 6.3 reflect this, as sorbed ERY concentrations peaked at 0.45 µg/g AGS on day 27. ERY removal remained variable thereafter, and appeared to coincide with increases and decreases in solid phase concentrations. For example, removal declined at roughly the same times solid phase concentrations declined (e.g., between days 27-36), and removal increased when solid phase concentrations increased (e.g., between days 36-42; Figure 6.2, Figure 6.3). Solid phase ERY concentrations may have fluctuated because approximately 80% of sorbed ERY was bound to flocs (Figure C.6); therefore, small changes in floc concentrations would have had large impacts on the sorption capacity of all biomass in the test SBR.

ERY degradation products were detected in the influent and effluent to the test reactor throughout dosing (Figure 6.4). “ERY1”, or 3-depyranosyloxy ERY ($C_{29}H_{53}NO_{10}$) and “ERY2” (7,12-dyhydroxy-6-deoxyerythronolide B, $C_{21}H_{38}O_8$) are primary and secondary metabolites of ERY degradation, per degradation pathways proposed in [126] and [127]. Prior to increasing the influent ERY concentration, only ERY1 was detected. ERY1 levels increased in both the influent and effluent between days 0-24; levels in the effluent were slightly higher than those in the influent, which may indicate that AGS activity contributed to the formation of this metabolite. Per the literature, ERY1 is only formed via biodegradation [126-128, 177] or advanced oxidation processes with both ozone and ultraviolet light or ozone and hydrogen peroxide [178]. It is therefore unlikely that light exposure alone, occurring when ERY medium flowed through

influent tubing to the test SBR, caused formation of ERY1. Biofilm growth was occasionally observed in the influent tubing and may be the reason ERY1 was detected in the influent.

On the same day that influent ERY concentrations increased, ERY2 was detected in the effluent. It is possible that this product was present in the effluent prior to day 24, but at levels below detection limits. Increased influent ERY concentrations may have encouraged ERY2 production at higher levels. On day 28, ERY2 was also detected in the influent; for the remainder of the experiment, ERY2 was detected in the influent at higher levels than the effluent.

Altogether, the presence of both degradation products throughout dosing indicates some degree of ERY biodegradation. However, because both products were present in the influent, it is difficult to determine the extent to which AGS contributed to the formation of either. More ERY1 formation may have occurred within the SBR than in the influent, but, since this compound is an intermediate, its conversion to further end products would prevent accumulation in the SBR. This is also the case for ERY2: it may have been produced at higher levels in the SBR than in the influent, but its conversion to other end products would also result in lower effluent levels. Altogether, ERY removal was likely due to a combination of biodegradation and sorption.

Aqueous ERY concentrations throughout a single cycle exhibited trends similar to those for DCF (Figure 6.5). Some ERY loss was observed anaerobically, as concentrations at 70 minutes were 6 µg/L lower than those predicted by a mass balance (closed symbols at zero minutes). In the first third of aeration, concentrations declined further, then, by the end of the cycle, returned to approximately the same level they were at 70 minutes. This pattern again suggests sorption followed by desorption. Figure 6.6 shows that ERY1 was only detected in the

influent on day 67. The lack of ERY1 detection at any other point in the SBR cycle may indicate that ERY1 was not formed, or that its conversion to other intermediates was efficient enough to prevent detectable levels from accumulating. ERY2 levels in the influent were double those at the end of the fill phase, which indicates anaerobic consumption of ERY2. ERY2 levels declined most between 70-103 minutes, likely indicating consumption during the first third of aeration. Levels then increased throughout the rest of the cycle, which may indicate that ERY1 conversion to ERY2 was proceeding faster than ERY2 consumption, or that ERY2 consumption had declined.

Gemfibrozil. GEM was the only pharmaceutical successfully removed in the test SBR and appeared to undergo removal exclusively via biodegradation. Between days 0-28, removal was near-constant at 28 ± 7%; it increased to 100% between days 28-36 and was sustained at 100% for the remainder of the experiment (Figure 6.2). Solid phase GEM concentrations remained very low throughout dosing—0.02 ± 0.009 μg/g over the first 28 days—and were lowest after removal reached 100% (Figure 6.3). Solid phase GEM concentration patterns may again indicate sorption as a precursor for biodegradation: solid concentrations slowly declined as biodegradation improved (days 0-36) and were not detected after removal became sustained at 100%. In other words, solid phase GEM may have been detected over the first 36 days because biodegradation was incomplete; after biodegradation became complete, GEM may have been biodegraded at the same rate that it sorbed.

Likewise, GEM degradation products were detected throughout dosing (Figure 6.4). Per biodegradation pathways proposed in [129] and [179], the primary and tertiary products "GEM1" ($C_{15}H_{22}O_4$, 5-[2-(hydroxymethyl)phenoxy]-2,2-dimethylpentanoic acid) and "GEM3"

($C_{15}H_{20}O_5$, 2-[(4-carboxy-4-methylpentyl)oxy]benzoic acid) were detected in the aqueous phase for the duration of the experiment; GEM3 was detected in the solid phase until day 36 (Figure 6.4). Other GEM intermediates may have been present but were not detectable using the extraction or quantification methods described herein.

GEM1 was present in the influent and effluent at similar levels until day 20. It is likely that contaminating biomass in the influent line contributed to GEM1 formation there. After day 20, however, GEM1 was only detected in the effluent, and levels spiked on day 28 before declining. Altogether, this indicates that this metabolite was formed due to interactions with AGS, and that increased removal from day 28 on likely corresponded with increased degradation, evidenced by elevated GEM1 levels. Declining GEM1 levels after day 28 indicate efficient conversion of GEM1 to further intermediates.

Between days 0-28, GEM3 levels in the effluent were higher than those in the influent, which suggests greater GEM conversion in the SBR. At roughly the same time that GEM removal increased, effluent GEM3 levels spiked, which further confirms the idea that GEM removal was due mainly to biodegradation: bacteria in AGS were forming more degradation products, indicative of greater degradation. Effluent GEM3 levels slowly declined after day 24, while complete GEM removal proceeded, suggesting improved conversion of GEM3 to further intermediates. Curiously, influent GEM3 levels also spiked at the same time that GEM removal began to increase (day 28). The reasons for this are unclear. Perhaps a 28-day period was needed for bacteria in both the influent and the SBR to adjust to experimental conditions, and after this lag, increased degradation efficacy was possible. The one-way valve located at the base of the SBR (Figure C.1) may also have leaked slightly during influent sampling, allowing some GEM3

in the SBR to backflow into the influent sample. GEM3 has not been documented in the literature as a product of photodegradation, so its presence is likely due to bacteria in the influent tubing. Regardless, influent and effluent GEM concentrations confirm that the majority of GEM removal occurred in the SBR, not in the influent tubing.

GEM concentrations monitored throughout a single SBR cycle further confirmed that GEM biodegradation occurred in the test reactor and was mostly an aerobic process (Figure 6.5). Concentrations at the end of the fill phase were approximately 5 μg/L less than those predicted by a mass balance, indicating some anaerobic removal. In the first 33 minutes of aeration, GEM concentrations declined to just 1 μg/L, and GEM was not detected after 66 minutes of aeration. GEM1 and GEM3 levels were both highest after filling, indicative of anaerobic production but reduced conversion. Levels of both metabolites dropped most in the first third of aeration, then remained near constant for the remainder of the cycle. This pattern demonstrates efficient conversion of the two metabolites to further intermediates while near-complete GEM removal occurred; after GEM was gone from solution, it appears that metabolite conversion also slowed or stopped, as both GEM1 and GEM3 levels did not change considerably. It is worth noting that the levels of these metabolites on day 67 were significantly lower than levels at previous time points (Figure 6.4), and therefore it is possible that bacterial conversion of these metabolites was limited at such low concentrations.

AGS Structural Characteristics

Biomass concentrations in both the control and test SBRs did not change significantly throughout the experiment: TSS and VSS in both reactors were near constant at 6.2 ± 0.7 g/L and 5.4 ± 0.6 g/L, respectively. Likewise, SVI_{10} values for biomass in the control and test SBRs were

fairly equal to each other throughout dosing (Figure C.7). The SVI_{10} of biomass in the test SBR dropped sharply after flocs washed out on day 13; however, SVI_{10} values then increased between days 15-27 to reach values near equal to those of biomass in the control reactor. SVI_{10} values then remained near-constant and equivalent to each other in both reactors, which suggests that pharmaceutical exposure did not majorly impact test biomass' SVI_{10}.

Although biomass in both reactors had similar settling characteristics and density, evidenced by SVI_{10}, granule size distributions were distinct. Until day 43, approximately 55% of all VSS in the control SBR consisted of large granules (> 2 mm diameter, Figure C.8). Small granules (< 1 mm diameter) were the second-most abundant, making up approximately 25% of all VSS, followed by medium granules (1-2 mm diameter), at approximately 20%. In contrast, the size distributions of biomass in the test reactor were more variable. The effects of the floc washout on day 13 were evident: the proportion of large granules increased to nearly 70% of all VSS, whereas small granules dropped to just 8%. Small granules then began to proliferate, likely causing large granules to decrease in relative proportion—large granules were just 22% of all VSS on day 66. Medium granules gradually increased in proportion, from 17% at day zero to 33% at day 66, and small granules eventually became the dominant biomass size in the test SBR, reaching 45% of VSS on day 66. Interestingly, despite different distributions for most of the experiment, granule size distributions in the test and control SBRs became near equal between days 57-66. Small granules in both SBRs became most abundant and large granules least abundant.

Despite differing size distributions, the EPS composition in both control and test granules remained largely similar over time (Figure 6.7 , Figure C.9). At day zero, granules consisted of

approximately 55% proteins, 25% lipids, 20% alpha-polysaccharides, and 40% beta-polysaccharides. The average EPS compositions of granules at the end of the test is provided in Table 6.1. A two-sample t-test assuming unequal variance was used to compare the fractions of each major EPS component in control granules at day 0 and 66, and a significant difference was not found for any component ($p > 0.05$). Likewise, EPS fractions in control and test granules at day 66 were compared, and no significant differences were found. Only beta-polysaccharide fractions in test granules at day 66 were found to be significantly different from those at day 0 ($p = 0.04$); however, this p-value barely meets the criteria for significance and is more likely an artifact of noise in test granules' composition. Since beta-polysaccharide fractions declined in both control and test granules over time, and since beta-PS fractions in control and test granules at day 66 were not significantly different, it seems more likely that beta-PS fractions changed as granules adapted to the lab environment, not due to pharmaceutical exposure.

Altogether, changes to physical granule characteristics present a somewhat conflicting picture of pharmaceutical impacts on granule structures. TSS, VSS, and SVI_{10} values for biomass in both the control and test SBRs were near equal to each other throughout the entire experiment. Likewise, EPS component distributions were similar for control and test AGS over time. Despite this, granule size distributions differed between SBRs for most of the experiment. Given the similarities between other granule characteristics, we conclude that pharmaceutical exposure was not the reason for differences in granule size distributions. Instead, the floc washout on day 13 appears to have driven test granules to more quickly attain size distributions that control biomass also attained, albeit more slowly. In other words, AGS adaptation to the lab environment, not pharmaceutical exposure, appeared to result in increased formation of small, dense granules,

evidenced by decreasing SVI_{10} and sustained suspended solids and EPS component concentrations.

Table 6.1. Average fractions of EPS components in granules at day zero and day 66. Note that multiple components overlay each other, and therefore fractions sum to greater than 1. Values were calculated using 30 μm sections taken from the center of three different granules.

	Day 0 (AGS inoculum)	**Control, day 66**	**Test, day 66**
Proteins	0.56 ± 0.1	0.56 ± 0.08	0.58 ± 0.05
Lipids	0.25 ± 0.06	0.27 ± 0.04	0.25 ± 0.06
α-polysaccharides	0.19 ± 0.09	0.21 ± 0.07	0.19 ± 0.03
β-polysaccharides	0.41 ± 0.04	0.35 ± 0.09	0.27 ± 0.08

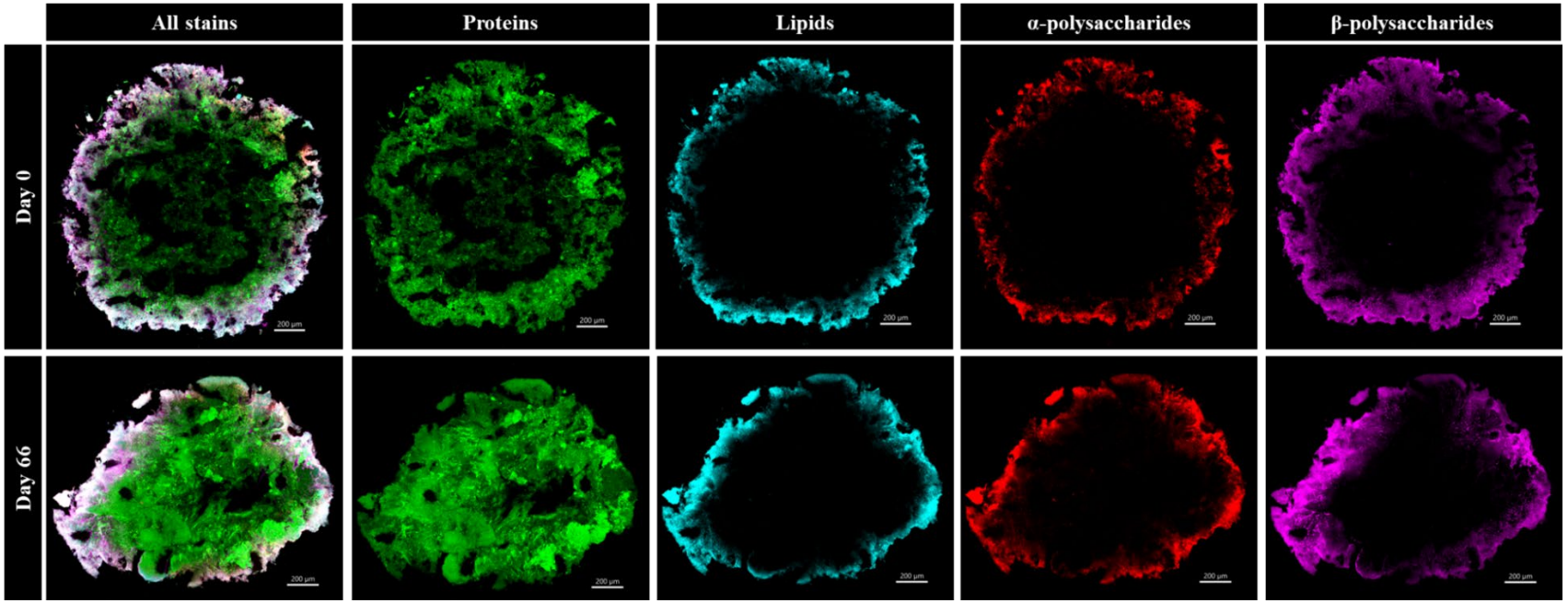

Figure 6.7. EPS component distributions in test granules at day zero (top row) and day 66 (bottom row). All scale bars are 200 µm. Statistically significant changes in fractions of each component were not found, excepting beta-polysaccharides, which decreased from 0.41 ± 0.04 of the total section biovolume at day zero to 0.27 ± 0.08 on day 66 ($p = 0.04$). Notably, beta-polysaccharide fractions in control granules also decreased to 0.35 ± 0.09—a concentration that was not statistically significantly different from beta-PS fractions in test granules at day 66. For this reason, declines in beta-PS fractions in test granules may be a consequence of AGS adaptation to the lab environment, not pharmaceutical exposure.

Active Microbial Community Shifts and Potential Links with Wastewater Treatment and Pharmaceutical Degradation

Shifts in the active microbial community were tracked via sequencing of 16S rRNA genes and transcripts. Figure 6.8 shows changes in the relative abundance of active taxa, grouped at the family level, in both reactors versus time. As described previously, potential contributions of phantom taxa, i.e., taxa with detected rRNA but undetected rDNA, were accounted for by plotting the rRNA counts of these taxa versus time (Figure 6.9). Counts were grouped at the family level, and only families for which 25% of samples contained over 50 counts were plotted. It is important to emphasize that different rRNA counts should only be compared over time within the same family, not between different families. For example, higher rRNA counts for *Rhodocyclaceae* than *Rhizobiales* do not necessarily indicate that *Rhodocyclaceae* was more active, as biases in rRNA transcription and sequencing may have aided in the overall detection of *Rhodocyclaceae* rRNA sequences. However, declines in *Rhodocyclaceae* rRNA counts over time likely indicate declines in activity of this family.

The active and phantom communities were analyzed in this fashion because many key bacterial families, such as the ammonia oxidizers *Nitrosomonadaceae*, were frequently detected as phantoms. Taxa belonging to the *Nitrosomonadaceae* were detected 835 times in the sample set; of these, nearly 30% were phantoms. On average, 35 ± 17% of active taxa detected in each sample were phantoms. Neglecting these data would inhibit our ability to gain important insights about the control and test SBR microbiomes. For example, active *Nitrosomonadaceae* were consistently present at very low relative abundances in both SBRs—typically less than 0.4% (Figure 6.8). Despite this, ammonia oxidation fluctuated in both reactors, but higher removal was

generally correlated with increasing rRNA counts for phantom taxa (Figure C.3, Figure 6.9). Evaluation of rRNA count data provides an explanation for fluctuating ammonia oxidation data that would otherwise not exist.

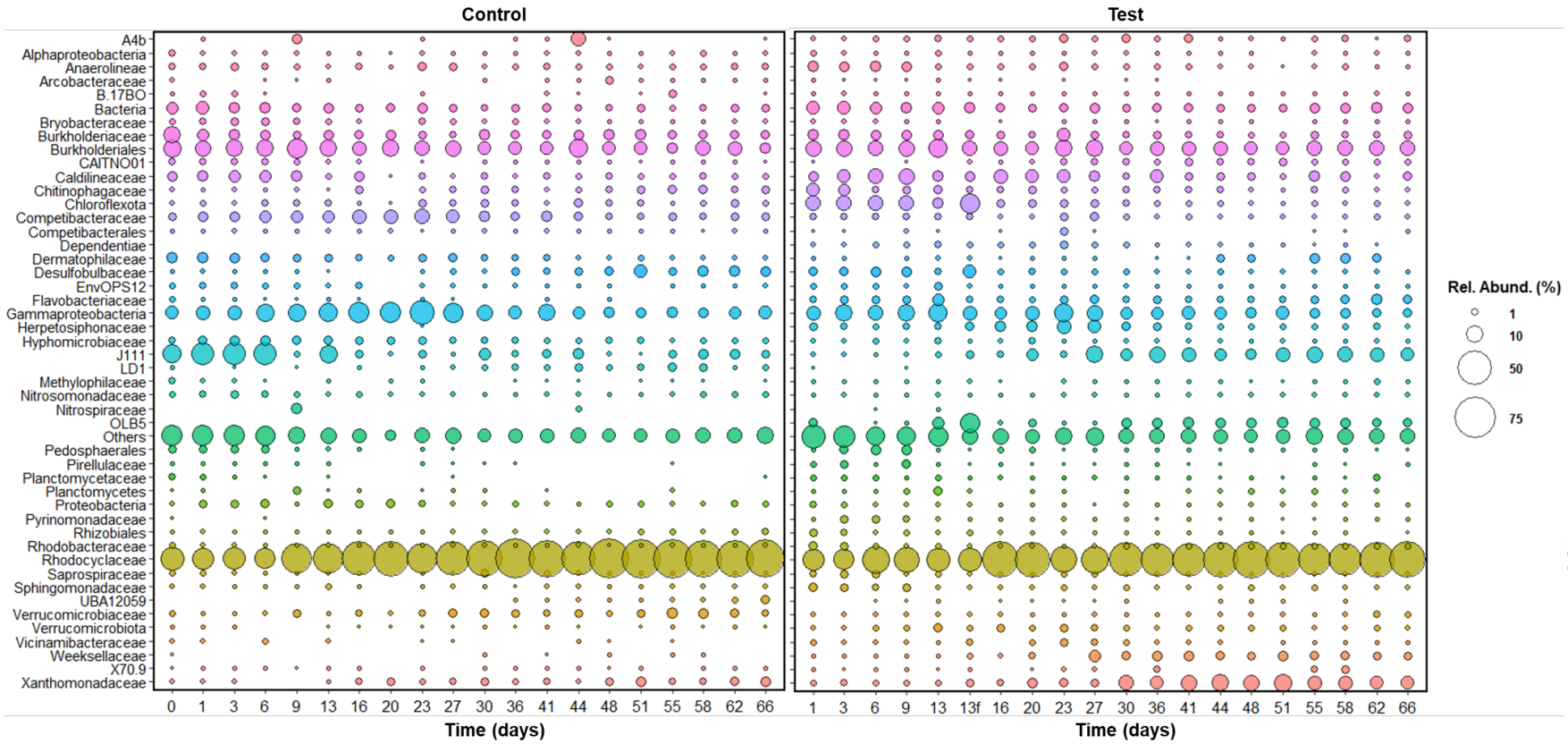

Figure 6.8. Relative abundances of active families versus time. Only families with relative abundance greater than or equal to 1% at at least one time point are plotted. ZOTUs that could not be classified at the family level with over 70% confidence were grouped by the next highest taxonomy level at which they could be confidently classified. The Control time zero sample reflects characteristics of the granular inoculum; the Test sample at time "13f" reflects characteristics of a sample of the floc washout that occurred on day 13. Families for which relative abundance was less than 1% were summed and are grouped as "Others" at each time point.

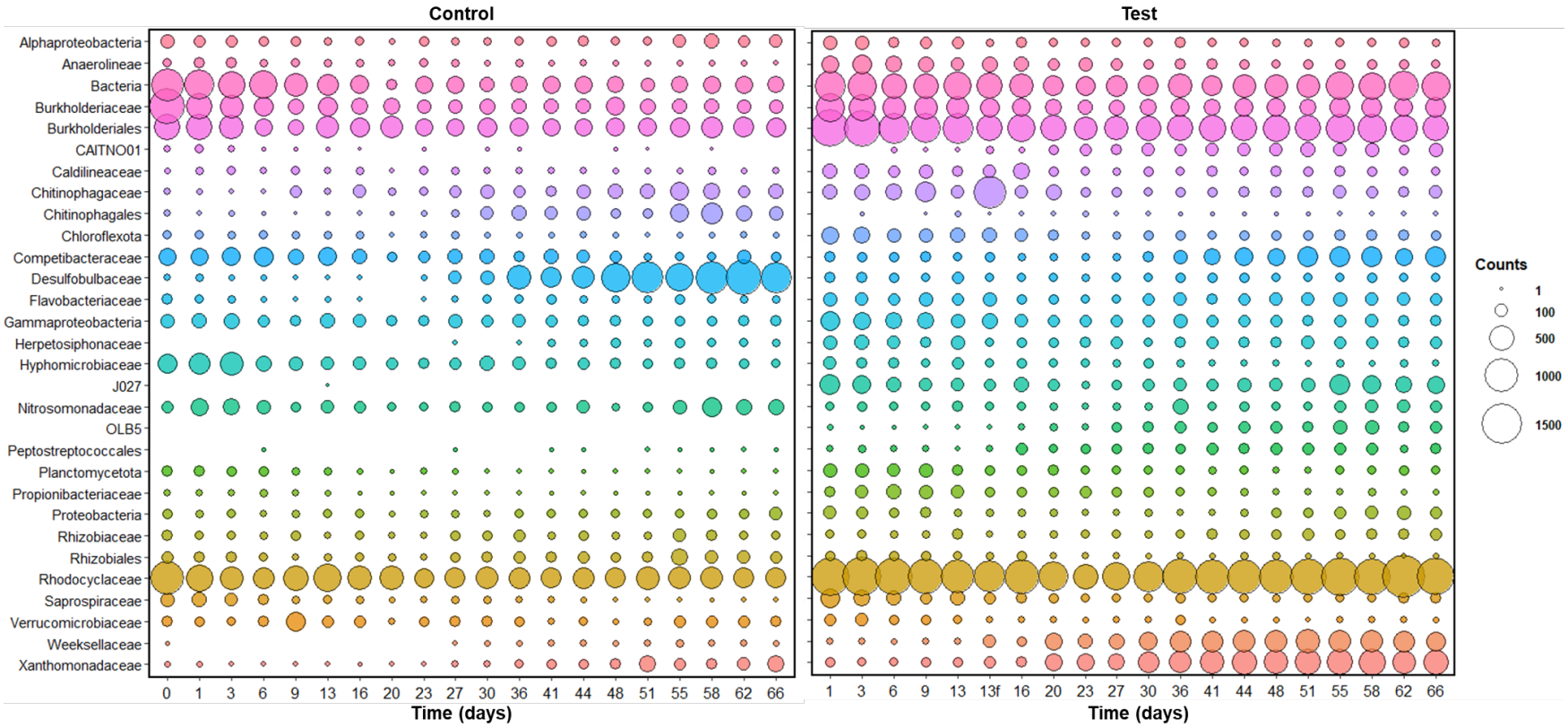

Figure 6.9. rRNA counts for phantom taxa, grouped at the family level, plotted versus time. Counts are only plotted for families in which over 50 counts occurred in at least 25% of samples. Taxa that could not be classified at the family level with over 70% confidence were grouped by the next highest taxonomy level at which they could be confidently classified. The Control time zero sample reflects characteristics of the granular inoculum; the Test sample at time "13f" reflects characteristics of a sample of the floc washout that occurred on day 13.

Active communities in both reactors were fairly similar throughout the experiment: *Rhodocyclaceae* and *Burkholderiaceae* genera and bacteria that could be not classified past the Burkholderiales order were consistently most abundant. Active species' richness also remained relatively constant in both SBRs, at 1570 ± 270 ZOTUs (Figure C.10). It was anticipated that richness would decline as AGS adapted to the lab environment, or as pharmaceutical exposure selectively enriched for pharmaceutical-tolerant species in the test SBR, but a significant trend was not observed.

Active *Rhodocyclaceae* in both SBRs included many taxa belonging to PAOs; many studies have found that PAO abundance in AGS is essential for granule stability (e.g., [89, 180]). The presence of active PAOs likely explains why test and control granules had similar structural characteristics, such as SVI_{10}, as PAOs are known to increase granules' density [181]. Sustained phosphate removal in both SBRs was also likely due to the continuous presence of active PAOs. *Rhodocyclaceae* also included multiple taxa belonging to *Zoogloea*, a denitrifying genus, and *Propionivibrio aalborgensis*, a glycogen accumulating species [182]. The sustained presence of both genera likely also contributed to AGS stability, as *Zoogloea* are biofilm-formers and *Propionivibrio* are dense and slow-growing [182, 183]. Furthermore, previous studies in which active *Rhodocyclaceae* declined during pharmaceutical dosing to AGS documented increases in granules' SVI and declines in lipid content [143, 172], changes that were not observed here.

Interestingly, active communities in the test SBR were relatively unaffected by the floc washout on day 13 or the increased ERY dosage that began on day 24 (Figure 6.8). The floc washout did not contain a significant portion of active nitrifiers (*Nitrosomonadaceae* or *Nitrospiraceae*) or PAOs (*Rhodocyclaceae*), and the relative abundance of these families

remained constant after the washout. In fact, active *Nitrospiraceae* were rarely detected in both SBRs, although nitrite oxidation was complete throughout dosing (Figure C.3, Figure C.4). Phantom activity levels, as rRNA counts, were also unchanged immediately following the floc washout, suggesting that activity within phantom families was unaffected. These data, however, do not explain why phosphate removal declined between days 13-17, or why ammonia oxidation declined in the test SBR after day 13 (Figure 6.1, Figure C.3). Instead, because rRNA counts for phantom *Nitrosomonadaceae* were consistently lower in the test reactor than in the control, the data suggest that pharmaceutical exposure reduced *Nitrosomonadaceae* activity. Declining ammonia removal at the same time as the floc washout may have been coincidental. There is not sufficient resolution in microbial community data to determine the reason for the temporary decline in phosphate removal between days 13-17.

To identify potential pharmaceutical-degrading organisms, we evaluated enrichments in active families that occurred in the test reactor but not in the control. Curiously, active bacteria belonging to the family J111 (order 4572-78, class Anaerolineae) were abundant at approximately 20% in both the granular inoculum and in the control SBR for the first six days of the experiment but were less than 1% abundant in the test SBR until day 20. Somewhat similarly, active bacteria belonging to the family OLB5 (order SJA-28, class Ignavibacteria) were not detected at all in the control SBR but were found in all but one sample from the test SBR and increased in relative abundance over time (Figure 6.8). rRNA counts for taxa belonging to this family also increased with time (Figure 6.9), which suggests that activity increased. It is possible that both families contributed to GEM degradation, since they increased in relative abundance and activity near day 36, the same day that GEM removal reached 100% (Figure 6.2). Notably,

bacteria within Anaerolineae and Ignavibacteria are anaerobic [184, 185], but most GEM degradation occurred during SBR aeration (Figure 6.5). If these families were responsible for GEM degradation, they were likely located deep within granules where oxygen penetration was minimal.

The relative abundance and rRNA counts for active *Xanthomonadaceae* in the test SBR also increased after day 30, perhaps also indicative of a link between this family and GEM degradation. *Xanthomonadaceae* taxa belonging to *Pseudoxanthomonas* were identified; bacteria in this genus have been shown to aerobically degrade various aromatic compounds [186, 187].

Active *Rhodocyclaceae* also included two genera associated with anaerobic aromatic degradation: *Azonexus* and *Sulfuritalea* [188, 189]. Plots of relative abundances and rRNA counts for the forementioned genera are shown in Figure C.11. The relative abundance of active *Azonexus* species was slightly higher in the test reactor than the control, though populations in both SBRs were typically under 0.25%. Similarly, active *Sulfuritalea* species were generally more abundant in the test SBR, though populations in both were less than 0.2% of the total active population.

rRNA counts for phantom taxa, however, better demonstrated differences in activity levels between the control and test reactors. After day 20, *Azonexus* rRNA counts remained 2-10 times higher in the test SBR than the control, indicating higher activity of these species in the test reactor. *Sulfuritalea* species' counts were lower in the test SBR than the control until day 20, at which point counts in the two reactors diverged: rRNA counts for *Sulfuritalea* in the control SBR approached zero, whereas counts in the test SBR approximately doubled. Taken together, both

genera may have contributed to the small amounts of anaerobic pharmaceutical biodegradation observed throughout dosing.

Lastly, the relative abundance of active *Competibacteraceae*, glycogen accumulating organisms known to compete with PAOs for anaerobic carbon consumption, remained relatively constant below 6% in both SBRs throughout the experiment. However, while rRNA counts for this family decreased over time in the control SBR, counts increased in the test SBR. It is possible that, over a longer pharmaceutical dosing period, increased activity of this family may have led to increased relative abundance in the test SBR and potential declines in phosphate removal efficacy.

Conclusions

The impacts of three common pharmaceuticals on environmentally-grown AGS were evaluated in a lab setting. Granules were able to sustain phosphate removal throughout dosing, but ammonia oxidation was inhibited in the test SBR, likely due to the reduced activity of *Nitrosomonadaceae* bacteria in that reactor. Pharmaceuticals did not appear to impact granules' structural characteristics, perhaps due to the sustained abundance of active *Rhodocyclaceae* genera. Neither DCF nor ERY were consistently removed by more than 20%, but after approximately 30 days, GEM was 100% removed. GEM removal increases coincided with increases in the relative abundance and rRNA counts for J111, OLB5, and *Xanthomonadaceae* families. Since bacteria belonging to the J111 and OLB5 families (Anaerolineae and Ignavibacteria classes, respectively) are likely anaerobic, it is possible that the pharmaceutical degradation observed here would not have been observed in experiments with lab-grown granules: environmentally-grown granules tend to be larger and more diverse than lab-grown

granules [172, 190], thus providing conditions more conducive to the activity of these families. Furthermore, neither family was detected at over 1% relative abundance in a similar study utilizing lab-grown granules; GEM removal was also not observed in that study [143]. This study therefore provides important information about the behavior and characteristics of environmentally-grown granules that studies with lab-grown granules may not be able to capture.

Funding

This research was supported by Montana INBRE, which is funded by the National Institute of General Medical Sciences division of the National Institutes of Health under Award Number P20GM103474. The content is solely the responsibility of the authors and does not necessarily represent the official views of the National Institutes of Health.

Acknowledgements

The authors would like to thank staff at the AquaNereda® demonstration plant in Rockford, IL for sample provision and troubleshooting advice. Thanks also to staff at the Mass Spectrometry Facility at Montana State University (MSU) for training and assistance. Funding for the Proteomics, Metabolomics and Mass Spectrometry Facility used in this publication was made possible in part by the MJ Murdock Charitable Trust, the National Institute of General Medical Sciences of the National Institutes of Health under Award Numbers P20GM103474 and S10OD28650, and the MSU Office of Research, Economic Development and Graduate Education.

Declaration of Competing Interests

The authors have no relevant financial or non-financial interests to disclose.

CHAPTER SEVEN

CONCLUSIONS AND FUTURE WORK

Conclusions: Lab- Versus Environmentally-Grown AGS

The research presented in this dissertation contributes to the understanding of aerobic granular sludge-driven removal of pharmaceuticals. Pharmaceutical impacts on wastewater treatment efficacy, AGS biofilm structures, and active communities within AGS were examined. The fates of the dosed pharmaceuticals in the solid and aqueous phases were also investigated.

Perhaps most importantly, care was taken throughout this research to utilize lab materials that minimized pharmaceutical losses during dosing, as detailed in Chapter 3. We found that it was surprisingly difficult to ensure that fed pharmaceutical concentrations matched the intended dose and were even more shocked to see this issue all but ignored in the literature. Given the growing presence of pharmaceuticals in the environment, and thus the need to study removal techniques for these compounds in the lab, it is essential that studies accurately identify where removal is occurring. We found that pharmaceutical partitioning to various lab supply materials was significant. Studies that do not consider this form of loss may greatly overestimate pharmaceutical removal rates and then attribute these rates to the wrong mechanism. As discussed in Chapter 3, numerous AGS studies that reported pharmaceutical removals over 75% (with some testing pharmaceutical concentrations over 5 mg/L) did not report the lab materials used or appear to consider losses to other materials (e.g., [4, 11, 88]). It is possible that we would have also observed significantly higher pharmaceutical removal, and falsely attributed this to interactions with AGS, had we not accounted for losses to other lab supplies.

As discussed in Chapters 4-6, AGS was capable of pharmaceutical removal to some extent in all studies. However, removal depended on the pharmaceutical compound itself and varied throughout time. In Chapter 4, pharmaceuticals were partially removed by lab-grown granules over the first 12 days of experimentation via both sorption and biodegradation. For an unknown reason, pharmaceuticals then desorbed from granules, and removal remained near-zero for the remainder of the experiment. Pharmaceutical biodegradation also declined irreversibly after the first 12 days, evidenced by the washout of degradation products. It is possible that the pharmaceutical dose of 150 µg/L was simply too toxic to microorganisms for removal to continue; this may explain why, as detailed in Chapter 6, 100% GEM removal was possible at approximately half the dose (60 µg/L). DCF and ERY removal fractions were also higher in the study in Chapter 6.

The different pharmaceutical doses utilized in research in Chapters 4 and 6 may also explain why wastewater treatment was inhibited to different degrees in both studies. Phosphate removal by environmentally-grown AGS (60 µg/L pharmaceutical dose) was not inhibited at all during pharmaceutical exposure; in contrast, phosphate removal by lab-grown AGS (150 µg/L pharmaceutical dose) declined to approximately 60%. Ammonia oxidation was the most inhibited nitrogen conversion process in both studies, though AOB were more inhibited in environmentally-grown granules than they were in lab-grown ones. It is important to note, however, that many factors other than pharmaceutical dose may have impacted wastewater treatment efficacy in both studies—media composition and concentrations differed, as well as biomass concentrations.

Shifts in active microbial community composition were strongly linked with wastewater treatment performance in both studies. Active AOB declined in relative abundance in both lab- and environmentally-grown granules, which explains poor ammonia oxidation during both studies. In contrast, the PAO-containing family *Rhodocyclaceae* declined in relative abundance during experimentation with lab granules but remained present and active at near-constant levels throughout testing on environmentally-grown AGS. Again, fluctuations in relative abundance of this family can be linked with phosphate removal efficacy in both studies.

Potential pharmaceutical-degrading families were difficult to identify in the study in Chapter 4, given the temporary nature of degradation in that study. It seems likely that *Nitrosomonadaceae* genera played a role in the temporary pharmaceutical removal observed: higher relative abundances of active *Nitrosomonadaceae* concurred with elevated pharmaceutical removals. As described in Chapter 4 and detailed elsewhere (e.g., [138, 191]), the non-specific ammonia monooxygenase enzyme utilized by AOB is known to react via oxidation with numerous aromatic compounds, such as pharmaceuticals. Declines in active AOB abundance likewise corresponded with declining pharmaceutical degradation in that study.

In contrast, several potential pharmaceutical-degrading families and genera were identified in the study with environmentally-grown AGS. Potential aerobic pharmaceutical degradation may have been performed by active *Xanthomonadaceae*, which increased in relative abundance and activity in the test SBR. Anaerobic degradation may have been performed by *Azonexus* or *Sulfuritalea* species, or bacteria within the uncultivated families J111 and OLB5. It's possible that these microbes were active solely due to their presence in fresh, environmentally-grown AGS inoculum; it's also possible that these microbes were present in

lab-grown AGS, but the pharmaceutical dose used in the lab-grown AGS study prevented proliferation of these populations to detectable levels.

The forementioned microbes may also only be capable of pharmaceutical degradation when living in environmental AGS. Most pharmaceutical degradation occurred during SBR aeration, but most identified potential pharmaceutical degraders are anaerobic. If these populations were responsible for degradation, they would need to be located deep within granules, where oxygen penetration was sufficiently limited. This may only be possible in environmentally-grown AGS, which tends to be larger and more diverse than lab-grown AGS [172, 190].

Lastly, pharmaceutical impacts to AGS biofilm structures varied, as detailed in Chapters 5-6. Again, these different impacts may be attributed to the cultivation conditions of the granules themselves (lab versus full-scale WWTP), or to the pharmaceutical doses and/or active microbial communities. As detailed in Chapter 5, the lipid layer in lab-grown granules significantly declined throughout dosing. Declining lipid content may have reduced granules' sorption capacity and may have occurred due to the presence of GEM: GEM can stimulate lipase production in humans and can impact lipid metabolism in bacteria [156, 162]. However, active *Rhodocyclaceae* also declined in that study, and as discussed in Chapter 6, *Rhodocyclaceae* may play an essential role in granule stability and structure [181]. The sustained abundance of this family in environmentally-grown AGS, coupled with stable biofilm macromolecule concentrations throughout dosing, may indicate that these organisms—not pharmaceutical exposure directly—are responsible for changes to AGS structures. Instead, the higher

pharmaceutical dose used in the lab-granule study may have inhibited *Rhodocyclaceae* activity, causing declining lipids.

Altogether, research in the dissertation showed that aerobic granular sludge is capable of pharmaceutical removal while treating wastewater. The dominant removal mechanism appeared to be biodegradation, as sorption was temporary, highly variable, and poorly predicted by batch tests with inactivated AGS (detailed in Chapter 5). Degradation products from all three compounds were detected in all studies throughout dosing, but removal was most successful with environmentally-grown AGS, which was capable of 100% GEM biodegradation after 36 days. Findings from this research demonstrate that both the pharmaceutical dose and cultivation environment likely have complex, multifaceted impacts on granules' microbial communities, wastewater treatment capacity, and pharmaceutical removal efficacy. The most promising results were obtained under conditions more closely resembling those in the real world, which essentially summarizes the potential of AGS as a pharmaceutical treatment technology: under environmentally-relevant conditions, AGS can enhance pharmaceutical removal while treating wastewater.

Recommendations for Future Work

Research in this dissertation repeatedly shows that AGS is capable of at least some pharmaceutical removal. These enticing glimpses of partial or temporary removal beg the question—how can AGS systems be optimized such that total pharmaceutical removal occurs? Furthermore, given that pharmaceutical contamination in wastewater treatment plants consists of complex, ever-changing mixtures of compounds at constantly varying concentrations, how can AGS systems be engineered to treat such nebulous contaminant mixtures? To accurately answer

this question, experimental conditions that closely mimic those of the real world must be used. Future research must continue to investigate the effects of complex pharmaceutical mixtures at trace concentrations on AGS, with a focus on the role of different bacterial populations in pharmaceutical degradation. If key populations that enhance AGS stability and pharmaceutical removal can be identified, reactor operation and growth conditions that aid in enrichment of these organisms should be studied.

The complex interplay between AGS biofilm components and microbial populations may never be fully understood, but future research should also seek to determine how granule enrichment in certain biofilm components (e.g., lipids or beta-polysaccharides) can be used to support the activity of key wastewater- or pharmaceutical-treating populations, and vice versa. Bioprocess engineering designs and operating conditions that facilitate proliferation of specific EPS should also be investigated. Limited studies have shown, for example, that aeration intensity strongly affects protein-to-polysaccharide ratios in AGS and microbial communities [192, 193]. Future research should take these findings one step further by investigating how bioprocess engineering can be utilized to enhance pharmaceutical removal.

Much remains unknown about pharmaceutical degradation products in general—not only are the compounds formed during pharmaceutical degradation largely unidentified, their potential toxic impacts are poorly understood. Pharmaceutical degradation pathways and end products need better characterization so that scientists can determine if a parent pharmaceutical is truly degraded to an inert form. The effects of complex mixtures of degradation products on various environmental receptors also require further study. The impacts of these mixtures on

AGS should also be explored, and the potential chronic effects of these mixtures on wastewater treatment efficacy and parent pharmaceutical removal also requires research.

In any large project, there are likely to be findings that warrant further investigation but cannot be pursued due to various constraints—in this case, time and budget prevented me from chasing these leads. I am concluding this dissertation by presenting results from two such tests because I believe each demonstrates the promise of AGS and the remaining wealth of knowledge to be gained.

Most promisingly, batch tests with starved AGS showed complete removal of all three pharmaceuticals at up to a 500 μg/L starting concentration (Figure 7.1). The methods used for this experiment are detailed in Appendix D. In brief, lab-grown AGS that was stored at 4°C in spent media for several months was exposed to pharmaceutical mixtures at varying concentrations, with no exogenous carbon or nitrogen sources. Degradation products for all three compounds were detected and were produced and consumed in patterns that suggested conversion to further end products (Figure D.2, Figure D.3). Altogether, results from this preliminary experiment hinted that perhaps bacteria in AGS could be coerced to perform more complete pharmaceutical removal after periods of starvation or in the absence of other nutrients. Furthermore, this pattern was repeated in several other preliminary batch tests. Perhaps starved AGS could be used as a "polishing step" at the end of conventional wastewater treatment to provide further pharmaceutical removal.

SBR operation could also potentially be adjusted to facilitate granule "starvation" and thereby encourage greater pharmaceutical degradation. In a functioning SBR, nearly all nutrients are consumed by the end of the aeration phase. Extending the length of aeration, relative to the

anaerobic feed phase, may therefore provide starvation conditions similar to those in batch tests described above, resulting in enhanced pharmaceutical removal. Future research should investigate if addition of this "starvation" phase to the SBR cycle can enhance pharmaceutical removal and assess the time and conditions necessary for complete removal. For example, post-starvation, bacteria may require more time to return to treatment of conventional contaminants. How might this impact the timing of feed and aeration phases? Anaerobic starvation conditions may also be needed, post-aeration, for pharmaceutical degradation, which will require mixing methods other than aeration. Lastly, the length of the starvation period required for complete pharmaceutical degradation is unknown. Altogether, future research should consider how SBR phases could be tailored to enhance pharmaceutical removal, guided by the idea that starvation conditions appear to encourage biodegradation.

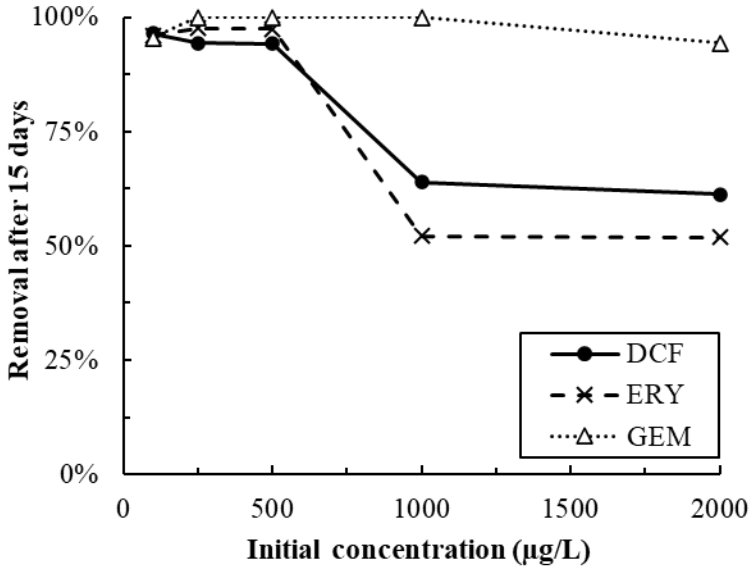

Figure 7.1. Pharmaceutical removal after 15 days versus initial dosed concentration in starved granule batch tests. AGS were capable of near-complete biodegradation (> 90% removal) of all three compounds at up to a 500 µg/L starting concentration. GEM was at least 95% biodegraded at up to a 2 mg/L starting concentration.

Microscopy-focused experiments using fluorescence in situ hybridization (FISH, described in more detail in Appendix D) also present an area for further investigation. I had hoped to use fluorescent labeling of key wastewater-treating bacteria in granule sections as a complement to 16S rRNA and rDNA analyses, but unfortunately time constraints and method development issues prevented this. I was particularly curious about how bacteria in AGS may shift spatially during pharmaceutical exposure, and if these shifts could be used to explain increases or decreases in active populations. For example, if strictly aerobic bacteria such as *Nitrosomonadaceae* relocated deeper within the granule during pharmaceutical exposure, this shift might explain decreases in active populations, as oxygen would be more limited with depth. This spatial shift might also explain declining ammonia oxidation. Different microbial distributions in lab- and environmentally-grown granules might also help explain varying treatment capacities; insights in this area also might be useful in future work related to reactor engineering or growth condition optimization.

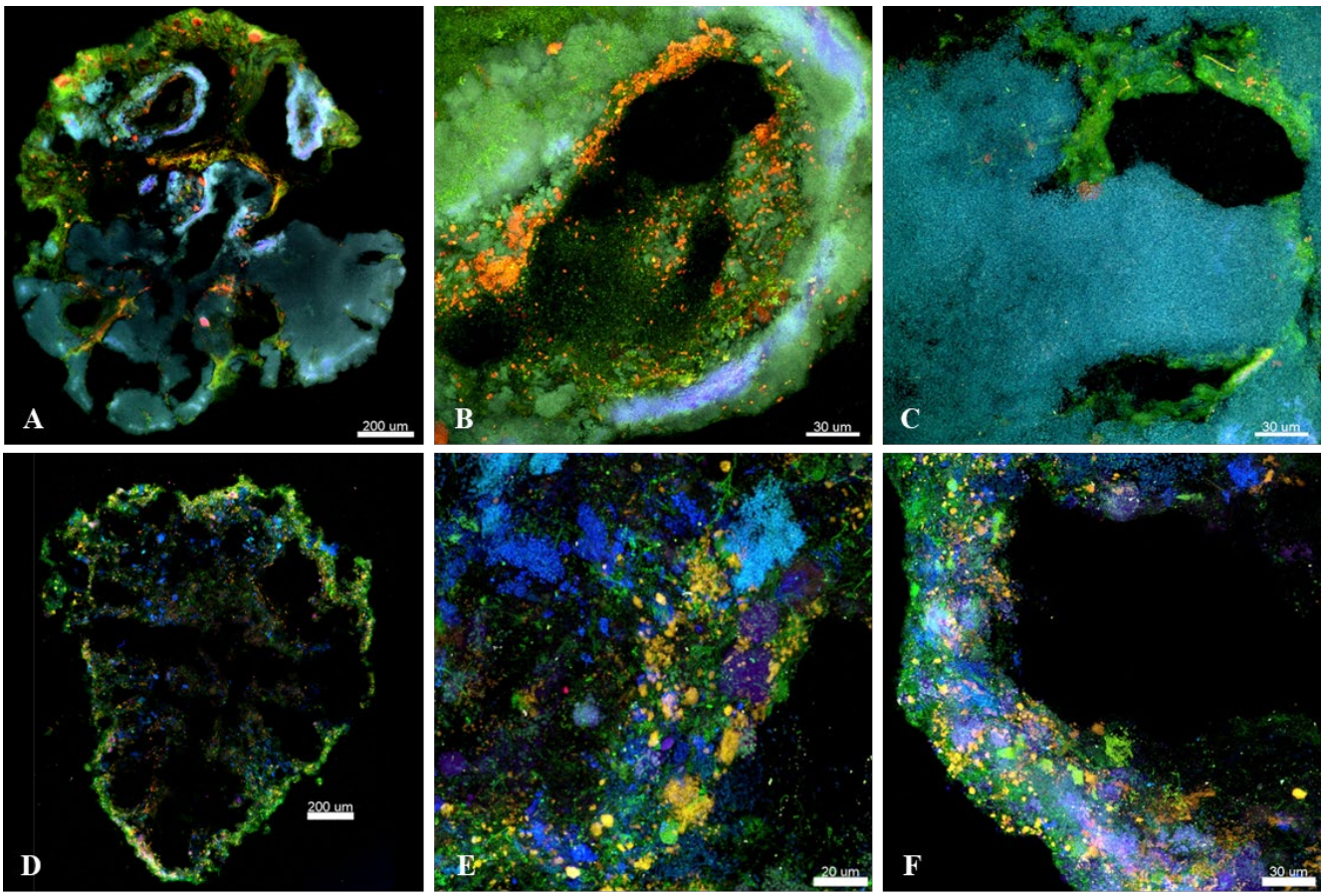

Figure 7.2. FISH images of lab-grown (A-C) and environmentally-grown (D-F) AGS. Figures A and D show the whole granule section at 10x magnification; Figures B, C, E, and F are images collected at 100x magnification of different areas of the granules shown in A and D. Color key: green, all bacteria; blue, PAOs; red/orange, nitrifiers; lavender, GAOs.

Figure 7.2 shows a successful FISH analysis conducted on granules that were not exposed to pharmaceuticals. Notably, the lab-grown granule is much more homogeneous and stratified and consists mostly of PAOs (in blue). Nitrifiers (in red) cluster near pores, where oxygen is likely to be more plentiful. In contrast, the environmentally-grown granule is much more heterogeneous and appears “emptier” than the lab-grown granule. All tagged bacterial species appear to coexist as a mixture with each other. This analysis shows that cultivation

conditions result in different bacterial distributions; it is therefore likely that pharmaceutical exposure would also cause spatial shifts.

In conclusion, aerobic granular sludge is a promising biotechnology for pharmaceutical removal from wastewater. Its ability to both biodegrade and sorb three pharmaceuticals has been demonstrated in this dissertation. Potential pharmaceutical-degrading families were identified, and future research should investigate methods to enrich such populations more efficiently in AGS. Further research on optimization of AGS-driven pharmaceutical removal is also essential. Pharmaceutical contamination in the environment is likely to increase with population growth; water scarcity is likewise projected to increase. Both factors will cause pharmaceutical concentrations in water to increase. Improved treatment methods are therefore vital. Research in this dissertation demonstrates that pharmaceutical removal using aerobic granular sludge shows promise and is worthy of further investigation.

CUMULATIVE REFERENCES CITED

1. Adav, S.S., et al., Aerobic granular sludge: Recent advances. Biotechnology Advances, 2008. 26(5): p. 411-423.

2. Bessa, V.S., et al., Biological removal processes in aerobic granular sludge exposed to diclofenac. Environmental Technology, 2021: p. 1-14.

3. Kent, J. and J.H. Tay, Treatment of 17α-ethinylestradiol, 4-nonylphenol, and carbamazepine in wastewater using an aerobic granular sludge sequencing batch reactor. Science of The Total Environment, 2019. 652: p. 1270-1278.

4. Kong, Q., et al., Characterization of the extracellular polymeric substances and microbial community of aerobic granulation sludge exposed to cefalexin. International Biodeterioration & Biodegradation, 2015. 102: p. 375-382.

5. Wang, S. and C.K. Gunsch, Effects of selected pharmaceutically active compounds on the ammonia oxidizing bacterium Nitrosomonas europaea. Chemosphere, 2011. 82(4): p. 565-572.

6. Dokianakis, S.N., M.E. Kornaros, and G. Lyberatos, On the effect of pharmaceuticals on bacterial nitrite oxidation. Water Science and Technology, 2004. 50(5): p. 341-346.

7. Zhao, J., et al., Diclofenac inhibited the biological phosphorus removal: Performance and mechanism. Chemosphere, 2020. 243: p. 125380.

8. Deo, R.P., Pharmaceuticals in the Surface Water of the USA: A Review. Current Environmental Health Reports, 2014. 1(2): p. 113-122.

9. Benotti, M.J., et al., Pharmaceuticals and Endocrine Disrupting Compounds in U.S. Drinking Water. Environmental Science & Technology, 2009. 43(3): p. 597-603.

10. Bexfield, L.M., et al., Hormones and Pharmaceuticals in Groundwater Used As a Source of Drinking Water Across the United States. Environmental Science & Technology, 2019. 53(6): p. 2950-2960.

11. Rodriguez-Sanchez, A., et al., Performance and bacterial community structure of a granular autotrophic nitrogen removal bioreactor amended with high antibiotic concentrations. Chemical Engineering Journal, 2017. 325: p. 257-269.

12. Toja Ortega, S., M. Pronk, and M.K. de Kreuk, Anaerobic hydrolysis of complex substrates in full-scale aerobic granular sludge: enzymatic activity determined in different sludge fractions. Appl Microbiol Biotechnol, 2021. 105(14-15): p. 6073-6086.

13. Kirkland, C.M., et al., Characterizing the structure of aerobic granular sludge using ultra-high field magnetic resonance. Water Science and Technology, 2020. 82(4): p. 627-639.

14. Wilén, B.M., et al., The mechanisms of granulation of activated sludge in wastewater treatment, its optimization, and impact on effluent quality. Appl Microbiol Biotechnol, 2018. 102(12): p. 5005-5020.

15. Tchobanoglous, G., et al., Wastewater Engineering: Treatment and Resource Recovery. 5 ed, ed. M.E. Inc. 2014: McGraw-Hill Education.

16. Donlan, R.M., Biofilms: microbial life on surfaces. Emerg Infect Dis, 2002. 8(9): p. 881-90.

17. Chen, M.-Y., et al., Staining of extracellular polymeric substances and cells in bioaggregates. Applied Microbiology and Biotechnology, 2007. 75(2): p. 467-474.

18. Adav, S.S., D.-J. Lee, and J.-H. Tay, Extracellular polymeric substances and structural stability of aerobic granule. Water Research, 2008. 42(6): p. 1644-1650.

19. Adav, S.S., et al., Aerobic granular sludge: Recent advances. Biotechnology Advances, 2008. 26(5): p. 411-423.

20. de Sousa Rollemberg, S.L., et al., Aerobic granular sludge: Cultivation parameters and removal mechanisms. Bioresource Technology, 2018. 270: p. 678-688.

21. Ndon, U.J., Analysis and kinetics of the sequencing batch reactors. Environmental engineering science, 2007. 24(4): p. 505-514.

22. Chen, Y., et al., Smart energy savings for aeration control in wastewater treatment. Energy Reports, 2022. 8: p. 1711-1721.

23. Murshid, S., et al., A review on biofilm-based reactors for wastewater treatment: Recent advancements in biofilm carriers, kinetics, reactors, economics, and future perspectives. Science of The Total Environment, 2023. 892: p. 164796.

24. Kim, S. and D.S. Aga, Potential Ecological and Human Health Impacts of Antibiotics and Antibiotic-Resistant Bacteria from Wastewater Treatment Plants. Journal of Toxicology and Environmental Health, Part B, 2007. 10(8): p. 559-573.

25. Calisto, V. and V.I. Esteves, Psychiatric pharmaceuticals in the environment. Chemosphere, 2009. 77(10): p. 1257-1274.

26. Sathishkumar, P., et al., Occurrence, interactive effects and ecological risk of diclofenac in environmental compartments and biota - a review. Science of The Total Environment, 2020. 698: p. 134057.

27. Murack, P.J., J. Parrish, and T.P. Barry, Effects of progesterone on sperm motility in fathead minnow (Pimephales promelas). Aquatic Toxicology, 2011. 104(1): p. 121-125.

28. Gonzalez-Pleiter, M., et al., Toxicity of five antibiotics and their mixtures towards photosynthetic aquatic organisms: implications for environmental risk assessment. Water Res, 2013. 47(6): p. 2050-64.

29. Chopra, S. and D. Kumar, Ibuprofen as an emerging organic contaminant in environment, distribution and remediation. Heliyon, 2020. 6(6): p. e04087-e04087.

30. Kummerová, M., et al., Possible ecological risk of two pharmaceuticals diclofenac and paracetamol demonstrated on a model plant Lemna minor. J Hazard Mater, 2016. 302: p. 351-361.

31. Świacka, K., et al., Toxic effects of NSAIDs in non-target species: A review from the perspective of the aquatic environment. Environmental Pollution, 2021. 273: p. 115891.

32. Wang, X.C., et al., Removal of tetracycline by aerobic granular sludge and its bacterial community dynamics in SBR. RSC Advances, 2018. 8(33): p. 18284-18293.

33. Zheng, X.-y., et al., A comparative adsorption study: 17β-estradiol onto aerobic granular sludge and activated sludge. Environmental Technology, 2016. 37(1): p. 136-144.

34. Moreira, I.S., et al., Removal of fluoxetine and its effects in the performance of an aerobic granular sludge sequential batch reactor. Journal of Hazardous Materials, 2015. 287: p. 93-101.

35. Information, N.C.f.B. PubChem Compound Summary for CID 3033, Diclofenac. 2022; Available from: https://pubchem.ncbi.nlm.nih.gov/compound/Diclofenac.

36. Information, N.C.f.B. PubChem Compound Summary for CID 3463, Gemfibrozil. 2022; Available from: https://pubchem.ncbi.nlm.nih.gov/compound/Gemfibrozil.

37. Information, N.C.f.B. PubChem Compound Summary for CID 12560, Erythromycin. 2022; Available from: https://pubchem.ncbi.nlm.nih.gov/compound/Erythromycin.

38. Schafhauser, B.H., et al., Global review and analysis of erythromycin in the environment: Occurrence, bioaccumulation and antibiotic resistance hazards. Environmental Pollution, 2018. 238: p. 440-451.

39. Focazio, M.J., et al., A national reconnaissance for pharmaceuticals and other organic wastewater contaminants in the United States — II) Untreated drinking water sources. Science of The Total Environment, 2008. 402(2): p. 201-216.

40. Jessick, A., Detection, fate, and bioavailability of erythromycin in environmental matrices, in Toxicology. 2010, Iowa State University. p. 98.

41. Godfrey, E., W.W. Woessner, and M.J. Benotti, Pharmaceuticals in On-Site Sewage Effluent and Ground Water, Western Montana. Groundwater, 2007. 45(3): p. 263-271.

42. Icopini, G., T. Swinney, and A. English, Occurrence and Distribution of Organic Wastewater Contaminants in Waters of the Gallatin Valley, Gallatin County, Montana. 2016, Gallatin Local Water Quality District, Montana Bureau of Mines and Geology.

43. Fan, C. and J. He, Proliferation of antibiotic resistance genes in microbial consortia of sequencing batch reactors (SBRs) upon exposure to trace erythromycin or erythromycin-H2O. Water Research, 2011. 45(10): p. 3098-3106.

44. Wang, S., et al., Piggery wastewater treatment by aerobic granular sludge: Granulation process and antibiotics and antibiotic-resistant bacteria removal and transport. Bioresource Technology, 2019. 273: p. 350-357.

45. Pasquini, L., et al., Impact of certain household micropollutants on bacterial behavior. Toxicity tests/study of extracellular polymeric substances in sludge. Science of the Total Environment, 2013. 463: p. 355-365.

46. Margot, J., et al., Role of ammonia-oxidizing bacteria in micropollutant removal from wastewater with aerobic granular sludge. Water Science and Technology, 2015. 73(3): p. 564-575.

47. Yu, Z., et al., Enhancement of PPCPs removal by shaped microbial community of aerobic granular sludge under condition of low C/N ratio influent. Journal of Hazardous Materials, 2020. 394: p. 122583.

48. Database, C.D. The Top Drugs of 2021. 2024; Available from: https://clincalc.com/DrugStats/Top300Drugs.aspx.

49. Hui, X., et al., In vivo bioavailability and metabolism of topical diclofenac lotion in human volunteers. Pharm Res, 1998. 15(10): p. 1589-95.

50. Paxéus, N., Removal of selected non-steroidal anti-inflammatory drugs (NSAIDs), gemfibrozil, carbamazepine, b-blockers, trimethoprim and triclosan in conventional wastewater treatment plants in five EU countries and their discharge to the aquatic environment. Water Science and Technology, 2004. 50(5): p. 253-260.

51. Spongberg, A.L. and J.D. Witter, Pharmaceutical compounds in the wastewater process stream in Northwest Ohio. Science of The Total Environment, 2008. 397(1): p. 148-157.

52. Chan, E.W.L., et al., Synergistic effect of non-steroidal anti-inflammatory drugs (NSAIDs) on antibacterial activity of cefuroxime and chloramphenicol against methicillin-resistant Staphylococcus aureus. Journal of Global Antimicrobial Resistance, 2017. 10: p. 70-74.

53. Pawar, H.V., et al., Comparison of in vitro antibacterial activity of streptomycin-diclofenac loaded composite biomaterial dressings with commercial silver based

antimicrobial wound dressings. International Journal of Biological Macromolecules, 2019. 121: p. 191-199.

54. van Dijk, E.J.H., M. Pronk, and M.C.M. van Loosdrecht, Controlling effluent suspended solids in the aerobic granular sludge process. Water Research, 2018. 147: p. 50-59.

55. Falås, P., et al., Suspended biofilm carrier and activated sludge removal of acidic pharmaceuticals. Water Research, 2012. 46(4): p. 1167-1175.

56. Parke-Davis, P.I. LOPID (Gemfibrozil Tablets, USP). 2017 [cited 2022; Available from: https://www.accessdata.fda.gov/drugsatfda_docs/label/2017/018422s056lbl.pdf.

57. Fang, Y., et al., Occurrence, fate, and persistence of gemfibrozil in water and soil. Environmental Toxicology and Chemistry, 2012. 31(3): p. 550-555.

58. Luo, Y., et al., A review on the occurrence of micropollutants in the aquatic environment and their fate and removal during wastewater treatment. Science of The Total Environment, 2014. 473-474: p. 619-641.

59. Miller, K. and J. Meek, Helena Valley Ground Water: Pharmaceuticals, Personal Care Products, Endocrine Disruptors (PPCPs), and Microbial Indicators of Fecal Contamination. 2006, Montana Department of Environmental Quality.

60. Sui, Q., et al., Occurrence, sources and fate of pharmaceuticals and personal care products in the groundwater: A review. Emerging Contaminants, 2015. 1(1): p. 14-24.

61. Schmidt, W., et al., Effects of the pharmaceuticals gemfibrozil and diclofenac on the marine mussel (Mytilus spp.) and their comparison with standardized toxicity tests. Mar Pollut Bull, 2011. 62(7): p. 1389-95.

62. Zurita, J.L., et al., Toxicological effects of the lipid regulator gemfibrozil in four aquatic systems. Aquat Toxicol, 2007. 81(1): p. 106-15.

63. Inyang, M., et al., Biotransformation of trace organic compounds by activated sludge from a biological nutrient removal treatment system. Bioresource Technology, 2016. 216: p. 778-784.

64. Bluck, L. and D.A. Volmer, The Role of Naturally Occurring Stable Isotopes in Mass Spectrometry, Part I: The Theory. Spectroscopy (Springf), 2009. 23(10): p. 36.

65. Loos, M., et al., Accelerated Isotope Fine Structure Calculation Using Pruned Transition Trees. Analytical Chemistry, 2015. 87(11): p. 5738-5744.

66. Elliott, A.D., Confocal Microscopy: Principles and Modern Practices. Curr Protoc Cytom, 2020. 92(1): p. e68.

67. Mitreva, M., 8 - The Microbiome in Infectious Diseases, in Infectious Diseases (Fourth Edition), J. Cohen, W.G. Powderly, and S.M. Opal, Editors. 2017, Elsevier. p. 68-74.e2.

68. Illumina, High-Speed, Multiplexed 16S Microbial Sequencing on the MiSeq® System. 2014.

69. Dabney, J., M. Meyer, and S. Pääbo, Ancient DNA damage. Cold Spring Harb Perspect Biol, 2013. 5(7).

70. Okshevsky, M., V.R. Regina, and R.L. Meyer, Extracellular DNA as a target for biofilm control. Current Opinion in Biotechnology, 2015. 33: p. 73-80.

71. Jones, S.E. and J.T. Lennon, Dormancy contributes to the maintenance of microbial diversity. Proceedings of the National Academy of Sciences, 2010. 107(13): p. 5881-5886.

72. Bowsher, A.W., P.J. Kearns, and A. Shade, 16S rRNA/rRNA Gene Ratios and Cell Activity Staining Reveal Consistent Patterns of Microbial Activity in Plant-Associated Soil. Msystems, 2019. 4(2).

73. Blazewicz, S.J., et al., Evaluating rRNA as an indicator of microbial activity in environmental communities: limitations and uses. The ISME Journal, 2013. 7(11): p. 2061-2068.

74. Verwilt, J., P. Mestdagh, and J. Vandesompele, Artifacts and biases of the reverse transcription reaction in RNA sequencing. Rna, 2023. 29(7): p. 889-897.

75. Klein, A.M., et al., Molecular Evidence for Metabolically Active Bacteria in the Atmosphere. Frontiers in Microbiology, 2016. 7.

76. Xia, K., et al., Occurrence and Fate of Pharmaceuticals and Personal Care Products (PPCPs) in Biosolids. Journal of Environmental Quality, 2005. 34(1): p. 91-104.

77. Boonnorat, J., et al., Effect of hydraulic retention time on micropollutant biodegradation in activated sludge system augmented with acclimatized sludge treating low-micropollutants wastewater. Chemosphere, 2019. 230: p. 606-615.

78. Tay, S.T.-L., et al., Rapid cultivation of stable aerobic phenol-degrading granules using acetate-fed granules as microbial seed. Journal of Biotechnology, 2005. 115(4): p. 387-395.

79. English, A., T. Crone, and G. Icopini, Assessment and Distribution of Pharmaceuticals and Endocrine Disruptors in Wastewater, Ground Water and Surface Waters of the Gallatin Valley, Gallatin County, Montana. 2009, Gallatin Local Water Quality District, Montana Bureau of Mines and Geology.

80. Louvet, J.N., et al., Adverse effects of erythromycin on the structure and chemistry of activated sludge. Environmental Pollution, 2010. 158(3): p. 688-693.

81. Hebig, K.H., et al., Impact of materials used in lab and field experiments on the recovery of organic micropollutants. Science of The Total Environment, 2014. 473-474: p. 125-131.

82. Amorim, C.L., et al., Treatment of a simulated wastewater amended with a chiral pharmaceuticals mixture by an aerobic granular sludge sequencing batch reactor. International Biodeterioration & Biodegradation, 2016. 115: p. 277-285.

83. Kang, A.J., et al., Removal of antibiotic sulfamethoxazole by anoxic/anaerobic/oxic granular and suspended activated sludge processes. Bioresource Technology, 2018. 251: p. 151-157.

84. Zhao, X., et al., Remediation of pharmaceuticals and personal care products using an aerobic granular sludge sequencing bioreactor and microbial community profiling using Solexa sequencing technology analysis. Bioresource Technology, 2015. 179: p. 104-112.

85. Zhu, L., et al., The stability of aerobic granular sludge under 4-chloroaniline shock in a sequential air-lift bioreactor (SABR). Bioresource Technology, 2013. 140: p. 126-130.

86. Amorim, C.L., et al., Performance of aerobic granular sludge in a sequencing batch bioreactor exposed to ofloxacin, norfloxacin and ciprofloxacin. Water Research, 2014. 50: p. 101-13.

87. Muñoz-Palazon, B., et al., Total and Metabolically Active Microbial Community of Aerobic Granular Sludge Systems Operated in Sequential Batch Reactors: Effect of Pharmaceutical Compounds. Toxics, 2021. 9(5).

88. Wang, L., et al., Analysis of aerobic granules under the toxic effect of ampicillin in sequencing batch reactors: Performance and microbial community. Journal of Environmental Management, 2017. 204(Pt 1): p. 152-159.

89. de Kreuk, M.K. and M.C.M. van Loosdrecht, Selection of slow growing organisms as a means for improving aerobic granular sludge stability. Water Science and Technology, 2004. 49(11-12): p. 9-17.

90. Skube, M.K., et al., Study of physicochemical parameters affecting the release of diclofenac sodium from lipophilic matrix tablets. Acta Chim. Slov, 2004. 51.

91. Avdeef, A., et al., Determination of liposomal membrane-water partition coefficients of ionizable drugs. Pharmaceutical research, 1998. 15(2): p. 209-215.

92. Sodré, F.F. and T.R. Sampaio, Development and application of a SPE-LC-QTOF method for the quantification of micropollutants of emerging concern in drinking waters from the Brazilian capital. Emerging Contaminants, 2020. 6: p. 72-81.

93. Camacho-Muñoz, D., et al., An affordable method for the simultaneous determination of the most studied pharmaceutical compounds as wastewater and surface water pollutants. J Sep Sci, 2009. 32(18): p. 3064-73.

94. Chen, Y., et al., Occurrence and environmental implications of pharmaceuticals in Chinese municipal sewage sludge. Chemosphere, 2012. 93(9): p. 1765-1772.

95. Spongberg, A. and J. Witter, Pharmaceutical Compounds in the Wastewater Process Stream in Northwest Ohio. The Science of the total environment, 2008. 397: p. 148-57.

96. McKeen, L.W., Fluoropolymers, in Film Properties of Plastics and Elastomers (Third Edition), L.W. McKeen, Editor. 2012, William Andrew Publishing: Boston. p. 255-313.

97. Yang, X., et al., Surface functional groups of carbon-based adsorbents and their roles in the removal of heavy metals from aqueous solutions: A critical review. Chem Eng J, 2019. 366: p. 608-621.

98. Kose, H., The effects of physical factors on the adsorption of synthetic organic compounds by activated carbons and activated carbon fibers, in Environmental Engineering and Earth Science. 2010, Clemson.

99. Bernot, M.J., et al., A national reconnaissance of trace organic compounds (TOCs) in United States lotic ecosystems. Science of The Total Environment, 2016. 572: p. 422-433.

100. Bodle, K.B., M.R. Pernat, and C.M. Kirkland, Pharmaceutical Sorption to Lab Materials May Overestimate Rates of Removal in Lab-Scale Bioreactors. Water, Air, & Soil Pollution, 2022. 233(12): p. 505.

101. RStudioTeam. a language and environment for statistical computing. 2009 2009; Available from: https://cir.nii.ac.jp/crid/1570854175843385600.

102. Pluskal, T., et al., MZmine 2: modular framework for processing, visualizing, and analyzing mass spectrometry-based molecular profile data. BMC Bioinformatics, 2010. 11: p. 395.

103. Martin, J., et al., Multi-residue method for the analysis of pharmaceutical compounds in sewage sludge, compost and sediments by sonication-assisted extraction and LC determination. J Sep Sci, 2010. 33(12): p. 1760-6.

104. Martin, T.M., et al., Toxicity Estimation Software Tool. 2020, US EPA: Cincinnati, OH.

105. Nurk, S., et al., metaSPAdes: a new versatile metagenomic assembler. Genome Res, 2017. 27(5): p. 824-834.

106. Langmead, B. and S.L. Salzberg, Fast gapped-read alignment with Bowtie 2. Nature Methods, 2012. 9(4): p. 357-359.

107. Li, H., et al., The Sequence Alignment/Map format and SAMtools. Bioinformatics, 2009. 25(16): p. 2078-9.

108. Kang, D.D., et al., MetaBAT 2: an adaptive binning algorithm for robust and efficient genome reconstruction from metagenome assemblies. PeerJ, 2019. 7: p. e7359.

109. Parks, D.H., et al., CheckM: assessing the quality of microbial genomes recovered from isolates, single cells, and metagenomes. Genome Res, 2015. 25(7): p. 1043-55.

110. Eren, A.M., et al., Anvi'o: an advanced analysis and visualization platform for 'omics data. PeerJ, 2015. 3: p. e1319.

111. Chaumeil, P.-A., et al., GTDB-Tk: a toolkit to classify genomes with the Genome Taxonomy Database. Bioinformatics, 2019. 36(6): p. 1925-1927.

112. Aramaki, T., et al., KofamKOALA: KEGG Ortholog assignment based on profile HMM and adaptive score threshold. Bioinformatics, 2019. 36(7): p. 2251-2252.

113. Graham, E.D., J.F. Heidelberg, and B.J. Tully, Potential for primary productivity in a globally-distributed bacterial phototroph. The ISME Journal, 2018. 12(7): p. 1861-1866.

114. Jiang, Y., X. Shi, and H.Y. Ng, Aerobic granular sludge systems for treating hypersaline pharmaceutical wastewater: Start-up, long-term performances and metabolic function. Journal of Hazardous Materials, 2021. 412: p. 125229.

115. Parks, D.H., et al., GTDB: an ongoing census of bacterial and archaeal diversity through a phylogenetically consistent, rank normalized and complete genome-based taxonomy. Nucleic Acids Research, 2021. 50(D1): p. D785-D794.

116. Stamatakis, A., RAxML version 8: a tool for phylogenetic analysis and post-analysis of large phylogenies. Bioinformatics, 2014. 30(9): p. 1312-1313.

117. Katoh, K. and D.M. Standley, MAFFT Multiple Sequence Alignment Software Version 7: Improvements in Performance and Usability. Molecular Biology and Evolution, 2013. 30(4): p. 772-780.

118. Matsen, F.A., R.B. Kodner, and E.V. Armbrust, pplacer: linear time maximum-likelihood and Bayesian phylogenetic placement of sequences onto a fixed reference tree. BMC Bioinformatics, 2010. 11(1): p. 538.

119. Bowsher, A.W., P.J. Kearns, and A. Shade, 16S rRNA/rRNA Gene Ratios and Cell Activity Staining Reveal Consistent Patterns of Microbial Activity in Plant-Associated Soil. mSystems, 2019. 4(2): p. e00003-19.

120. Oksanen, J., Vegan : community ecology package. http://vegan.r-forge.r-project.org/, 2010.

121. Kembel, S.W., et al., Picante: R tools for integrating phylogenies and ecology. Bioinformatics, 2010. 26(11): p. 1463-1464.

122. McMurdie, P.J. and S. Holmes, phyloseq: An R Package for Reproducible Interactive Analysis and Graphics of Microbiome Census Data. PLOS ONE, 2013. 8(4): p. e61217.

123. Jewell, K.S., et al., Transformation of diclofenac in hybrid biofilm–activated sludge processes. Water Research, 2016. 105: p. 559-567.

124. Syed, M., C. Skonberg, and S.H. Hansen, Mitochondrial toxicity of diclofenac and its metabolites via inhibition of oxidative phosphorylation (ATP synthesis) in rat liver mitochondria: Possible role in drug induced liver injury (DILI). Toxicology in Vitro, 2016. 31: p. 93-102.

125. Grandclément, C., et al., Biological Removal and Fate Assessment of Diclofenac Using Bacillus subtilis and Brevibacillus laterosporus Strains and Ecotoxicological Effects of Diclofenac and 4′-Hydroxy-diclofenac. Journal of Chemistry, 2020. 2020: p. 9789420.

126. Llorca, M., et al., Identification of new transformation products during enzymatic treatment of tetracycline and erythromycin antibiotics at laboratory scale by an on-line turbulent flow liquid-chromatography coupled to a high resolution mass spectrometer LTQ-Orbitrap. Chemosphere, 2015. 119: p. 90-98.

127. Ren, J., et al., Isolation and identification of a novel erythromycin-degrading fungus, Curvularia sp. RJJ-5, and its degradation pathway. FEMS Microbiol Lett, 2021. 368(1).

128. Ren, J., et al., Characterization of the erythromycin degradation pathway and related enzyme in Rhodococcus gordoniae rjjtx-2. Journal of Cleaner Production, 2022. 379: p. 134758.

129. Kjeldal, H., et al., Genomic, Proteomic, and Metabolite Characterization of Gemfibrozil-Degrading Organism Bacillus sp. GeD10. Environmental Science & Technology, 2016. 50(2): p. 744-755.

130. Altschul, S.F., et al., Basic local alignment search tool. J Mol Biol, 1990. 215(3): p. 403-10.

131. Suarez, C., et al., Disturbance-based management of ecosystem services and disservices in partial nitritation-anammox biofilms. NPJ Biofilms Microbiomes, 2022. 8(1): p. 47.

132. Singleton, C.M., et al., Connecting structure to function with the recovery of over 1000 high-quality metagenome-assembled genomes from activated sludge using long-read sequencing. Nature Communications, 2021. 12(1): p. 2009.

133. Jenkins, O., D. Byrom, and D. Jones, Methylophilus: a New Genus of Methanol-Utilizing Bacteria. International Journal of Systematic and Evolutionary Microbiology, 1987. 37(4): p. 446-448.

134. Dedysh, S.N., C. Knief, and P.F. Dunfield, Methylocella species are facultatively methanotrophic. J Bacteriol, 2005. 187(13): p. 4665-70.

135. Mustakhimov, I., et al., Insights into Denitrification in Methylotenera mobilis from Denitrification Pathway and Methanol Metabolism Mutants. Journal of Bacteriology, 2013. 195(10): p. 2207-2211.

136. McIlroy, S.J., et al., 'Candidatus Competibacter'-lineage genomes retrieved from metagenomes reveal functional metabolic diversity. Isme j, 2014. 8(3): p. 613-624.

137. Keener, W.K. and D.J. Arp, Transformations of Aromatic Compounds by Nitrosomonas europaea. Applied and Environmental Microbiology, 1994. 60(6): p. 1914-1920.

138. Schatteman, A., et al., Hydrazines as Substrates and Inhibitors of the Archaeal Ammonia Oxidation Pathway. Appl Environ Microbiol, 2022. 88(8): p. e0247021.

139. Limpiyakorn, T., et al., amoA-encoding archaea in wastewater treatment plants: a review. Applied Microbiology and Biotechnology, 2013. 97(4): p. 1425-1439.

140. Bai, Y., et al., Abundance of ammonia-oxidizing bacteria and archaea in industrial and domestic wastewater treatment systems. FEMS Microbiol Ecol, 2012. 80(2): p. 323-30.

141. Jousset, A., et al., Where less may be more: how the rare biosphere pulls ecosystems strings. The ISME Journal, 2017. 11(4): p. 853-862.

142. Westerhoff, P., et al., Fate of Endocrine-Disruptor, Pharmaceutical, and Personal Care Product Chemicals during Simulated Drinking Water Treatment Processes. Environmental Science & Technology, 2005. 39(17): p. 6649-6663.

143. Bodle, K.B., et al., Treatment performance and microbial community structure in an aerobic granular sludge sequencing batch reactor amended with diclofenac, erythromycin, and gemfibrozil. Frontiers in Microbiomes, 2023. 2(1242895).

144. Mendes Barros, A.R., et al., Effects of the antibiotics trimethoprim (TMP) and sulfamethoxazole (SMX) on granulation, microbiology, and performance of aerobic granular sludge systems. Chemosphere, 2021. 262: p. 127840.

145. Zhang, L., et al., Role of extracellular protein in the formation and stability of aerobic granules. Enzyme and Microbial Technology, 2007. 41(5): p. 551-557.

146. Wang, Z.-W., Y. Liu, and J.-H. Tay, Distribution of EPS and cell surface hydrophobicity in aerobic granules. Applied Microbiology and Biotechnology, 2005. 69(4): p. 469-473.

147. Triebskorn, R., et al., Toxic effects of the non-steroidal anti-inflammatory drug diclofenac: Part II. Cytological effects in liver, kidney, gills and intestine of rainbow trout (Oncorhynchus mykiss). Aquatic Toxicology, 2004. 68(2): p. 151-166.

148. Araujo, L., et al., Persistence of gemfibrozil, naproxen and mefenamic acid in natural waters. Environmental Chemistry Letters, 2011. 9(1): p. 13-18.

149. APHA and AWWA, Standard Methods for the Examination of Water and Wastewater, 20. 1998, American Public Health Association: Washington, DC.

150. Kalam, S., et al., Surfactant Adsorption Isotherms: A Review. ACS Omega, 2021. 6(48): p. 32342-32348.

151. Pignatello, J.J., Sorption of organic chemicals in soil, in Encyclopedia of Soils in the Environment (Second Edition), M.J. Goss and M. Oliver, Editors. 2023, Academic Press: Oxford. p. 315-326.

152. Spohn, M., et al., Sorption and desorption of organic matter in soils as affected by phosphate. Geoderma, 2022. 405: p. 115377.

153. Chefetz, B., et al., Interactions of sodium azide with triazine herbicides: Effect on sorption to soils. Chemosphere, 2006. 65(2): p. 352-357.

154. Ro, K.S., K.H. Chung, and J.W. Robinson, Chemical transformation of atrazine with sodium azide. Journal of Environmental Science and Health . Part A: Environmental Science and Engineering and Toxicology, 1995. 30(2): p. 321-332.

155. Klimenko, N.A., T.V. Polyakova, and L.A. Savchina, Influence of sodium azide on the removal of fulvic acids by activated carbon. Journal of Water Chemistry and Technology, 2010. 32(6): p. 329-335.

156. Rodriguez, B. and R. Correa, Gemfibrozil, ed. StatPearls. 2022: StatPearls Publishing.

157. Chandra, P., et al., Microbial lipases and their industrial applications: a comprehensive review. Microbial Cell Factories, 2020. 19(1): p. 169.

158. Toja Ortega, S., M. Pronk, and M.K. de Kreuk Effect of an Increased Particulate COD Load on the Aerobic Granular Sludge Process: A Full Scale Study. Processes, 2021. 9, DOI: 10.3390/pr9081472.

159. Gessesse, A., et al., Lipase and protease extraction from activated sludge. Water Research, 2003. 37(15): p. 3652-3657.

160. Reich-Slotky, R., et al., Gemfibrozil inhibits Legionella pneumophila and Mycobacterium tuberculosis enoyl coenzyme A reductases and blocks intracellular growth of these bacteria in macrophages. J Bacteriol, 2009. 191(16): p. 5262-71.

161. Serra-Compte, A., et al., Fluvial biofilms exposed to desiccation and pharmaceutical pollution: New insights using metabolomics. Science of The Total Environment, 2018. 618: p. 1382-1388.

162. Yergeau, E., et al., Metatranscriptomic Analysis of the Response of River Biofilms to Pharmaceutical Products, Using Anonymous DNA Microarrays. Applied and Environmental Microbiology, 2010. 76(16): p. 5432-5439.

163. Strauss, J.S. and A.M. Stranieri, Acne treatment with topical erythromycin and zinc: Effect on Propionibacterium acnes and free fatty acid composition. Journal of the American Academy of Dermatology, 1984. 11(1): p. 86-89.

164. Hellgren, L. and J. Vincent, Erythromycin Stearate in Acne vulgaris: Its Effect on the Skin Surface Lipids and on the Activity of Purified Pancreatic Lipase. Dermatology, 1978. 156(2): p. 105-110.

165. Webster, G.F., K.J. McGinley, and J.J. Leyden, Inhibition of lipase production in Propionibacterium acnes by sub-minimal-inhibitory concentrations of tetracycline and erythromycin. British Journal of Dermatology, 1981. 104(4): p. 453-457.

166. McSwain, B.S., et al., Composition and distribution of extracellular polymeric substances in aerobic flocs and granular sludge. Appl Environ Microbiol, 2005. 71(2): p. 1051-7.

167. Deng, S., L. Wang, and H. Su, Role and influence of extracellular polymeric substances on the preparation of aerobic granular sludge. Journal of Environmental Management, 2016. 173: p. 49-54.

168. Meng, F., et al., Application of aerobic granules-continuous flow reactor for saline wastewater treatment: Granular stability, lipid production and symbiotic relationship between bacteria and algae. Bioresource Technology, 2020. 295: p. 122291.

169. Żyłła, R., et al. Impact of Polymer Membrane Properties on the Removal of Pharmaceuticals. Membranes, 2022. 12, DOI: 10.3390/membranes12020150.

170. Kang, A.J., et al., Variation in bacterial community structure of aerobic granular and suspended activated sludge in the presence of the antibiotic sulfamethoxazole. Bioresource Technology, 2018. 261: p. 322-328.

171. Fan, X.-Y., et al., Shifts in bacterial community composition and abundance of nitrifiers during aerobic granulation in two nitrifying sequencing batch reactors. Bioresource Technology, 2018. 251: p. 99-107.

172. Bodle, K.B. and C.M. Kirkland, Pharmaceutical impacts on aerobic granular sludge morphology and potential implications for abiotic removal. Chemosphere, 2024: p. 141187.

173. Vishniac, W. and M. Santer, The thiobacilli. Bacteriological reviews, 1957. 21(3): p. 195-213.

174. Lochmatter, S., G. Gonzalez-Gil, and C. Holliger, Optimized aeration strategies for nitrogen and phosphorus removal with aerobic granular sludge. Water Research, 2013. 47(16): p. 6187-6197.

175. Cameron, E.S., et al., Enhancing diversity analysis by repeatedly rarefying next generation sequencing data describing microbial communities. Scientific Reports, 2021. 11(1): p. 22302.

176. Ramesh, M. and V.P. Bharatam, Formation of a Toxic Quinoneimine Metabolite from Diclofenac: A Quantum Chemical Study. Drug Metabolism Letters, 2019. 13(1): p. 64-76.

177. Ren, J., et al., Biodegradation efficiency and mechanism of erythromycin degradation by Paracoccus versutus W7. Journal of Environmental Management, 2023. 332: p. 117372.

178. Luiz, D.B., et al., Identification of Degradation Products of Erythromycin A Arising from Ozone and Advanced Oxidation Process Treatment. Water Environment Research, 2010. 82(9): p. 797-805.

179. Kang, S.-I., et al., Rapid oxidation of ring methyl groups is the primary mechanism of biotransformation of gemfibrozil by the fungus Cunninghamella elegans. Archives of Microbiology, 2009. 191(6): p. 509-517.

180. Cheng, L., et al., Effects of feeding mode on the formation and stability of aerobic granular sludge under combined antibiotic stress. Chemical Engineering Journal, 2023. 475: p. 145996.

181. Oshiki, M., et al., Separation of PHA-accumulating cells in activated sludge based on differences in buoyant density. The Journal of General and Applied Microbiology, 2010. 56(2): p. 163-167.

182. Albertsen, M., et al., “Candidatus Propionivibrio aalborgensis”: A Novel Glycogen Accumulating Organism Abundant in Full-Scale Enhanced Biological Phosphorus Removal Plants. Frontiers in Microbiology, 2016. 7.

183. Parsons, A.B. and P.R. Dugan, Production of extracellular polysaccharide matrix by Zoogloea ramigera. Appl Microbiol, 1971. 21(4): p. 657-61.

184. Yamada, T., et al., Anaerolinea thermolimosa sp. nov., Levilinea saccharolytica gen. nov., sp. nov. and Leptolinea tardivitalis gen. nov., sp. nov., novel filamentous anaerobes, and description of the new classes Anaerolineae classis nov. and Caldilineae classis nov. in the bacterial phylum Chloroflexi. International Journal of Systematic and Evolutionary Microbiology, 2006. 56(6): p. 1331-1340.

185. Kadnikov, V.V., et al., Microbial Life in the Deep Subsurface Aquifer Illuminated by Metagenomics. Frontiers in Microbiology, 2020. 11.

186. Kim, J.M., et al., Influence of Soil Components on the Biodegradation of Benzene, Toluene, Ethylbenzene, and o-, m-, and p-Xylenes by the Newly Isolated Bacterium Pseudoxanthomonas spadix BD-a59. Applied and Environmental Microbiology, 2008. 74(23): p. 7313-7320.

187. Wang, G.L., et al., Pseudoxanthomonas jiangsuensis sp. nov., a DDT-degrading bacterium isolated from a long-term DDT-polluted soil. Curr Microbiol, 2011. 62(6): p. 1760-6.

188. Reinhold-Hurek, B. and T. Hurek, The Genera Azoarcus, Azovibrio, Azospira and Azonexus, in The Prokaryotes: Volume 5: Proteobacteria: Alpha and Beta Subclasses, M. Dworkin, et al., Editors. 2006, Springer New York: New York, NY. p. 873-891.

189. Sperfeld, M., G. Diekert, and S. Studenik, Anaerobic aromatic compound degradation in Sulfuritalea hydrogenivorans sk43H. FEMS Microbiol Ecol, 2019. 95(1).

190. Li, A.-j., et al., Microbial population dynamics during aerobic sludge granulation at different organic loading rates. Water Research, 2008. 42(13): p. 3552-3560.

191. Keener, W.K. and D.J. Arp, Transformations of Aromatic-Compounds by Nitrosomonas-Europaea. Applied and Environmental Microbiology, 1994. 60(6): p. 1914-1920.

192. Zhang, Z., et al., Gradient reduced aeration in an enhanced aerobic granular sludge process optimizes the dominant microbial community and its function. Environmental Science: Water Research & Technology, 2018. 4(5): p. 680-688.

193. Cydzik-Kwiatkowska, A., et al., Microbial structure and nitrogen compound conversions in aerobic granular sludge reactors with non-aeration phases and acetate pulse feeding. Environmental Science and Pollution Research, 2016. 23(24): p. 24857-24870.

194. Wei, L., et al., Transformation of erythromycin during secondary effluent soil aquifer recharging: Removal contribution and degradation path. Journal of Environmental Sciences, 2017. 51: p. 173-180.

195. Kosjek, T., et al., Metabolism studies of diclofenac and clofibric acid in activated sludge bioreactors using liquid chromatography with quadrupole – time-of-flight mass spectrometry. Journal of Hydrology, 2009. 372(1): p. 109-117.

196. Nielsen, P.H., H. Daims, and H. Lemmer, FISH Handbook for Biological Wastewater Treatment. 2009: IWA Publishing.

197. Behnam, F., et al., A straightforward DOPE (double labeling of oligonucleotide probes)-FISH (fluorescence in situ hybridization) method for simultaneous multicolor detection of six microbial populations. Applied and environmental microbiology, 2012. 78(15): p. 5138-5142.

198. Amann, R.I., L. Krumholz, and D.A. Stahl, Fluorescent-oligonucleotide probing of whole cells for determinative, phylogenetic, and environmental studies in microbiology. J Bacteriol, 1990. 172(2): p. 762-70.

199. Daims, H., et al., The domain-specific probe EUB338 is insufficient for the detection of all Bacteria: development and evaluation of a more comprehensive probe set. Syst Appl Microbiol, 1999. 22(3): p. 434-44.

200. Mobarry, B.K., et al., Phylogenetic probes for analyzing abundance and spatial organization of nitrifying bacteria. Appl Environ Microbiol, 1996. 62(6): p. 2156-62.

201. Daims, H., et al., In situ characterization of Nitrospira-like nitrite-oxidizing bacteria active in wastewater treatment plants. Appl Environ Microbiol, 2001. 67(11): p. 5273-84.

202. Wagner, M., et al., In situ analysis of nitrifying bacteria in sewage treatment plants. Water Science and Technology, 1996. 34(1): p. 237-244.

203. Crocetti, G.R., et al., Identification of polyphosphate-accumulating organisms and design of 16S rRNA-directed probes for their detection and quantitation. Appl Environ Microbiol, 2000. 66(3): p. 1175-82.

204. Kong, Y., et al., Diversity and distribution of a deeply branched novel proteobacterial group found in anaerobic-aerobic activated sludge processes. Environ Microbiol, 2002. 4(11): p. 753-7.

205. Crocetti, G.R., et al., Glycogen-accumulating organisms in laboratory-scale and full-scale wastewater treatment processes. Microbiology (Reading), 2002. 148(Pt 11): p. 3353-3364.

APPENDICES

APPENDIX A

SUPPLEMENTARY MATERIALS FOR CHAPTER 4

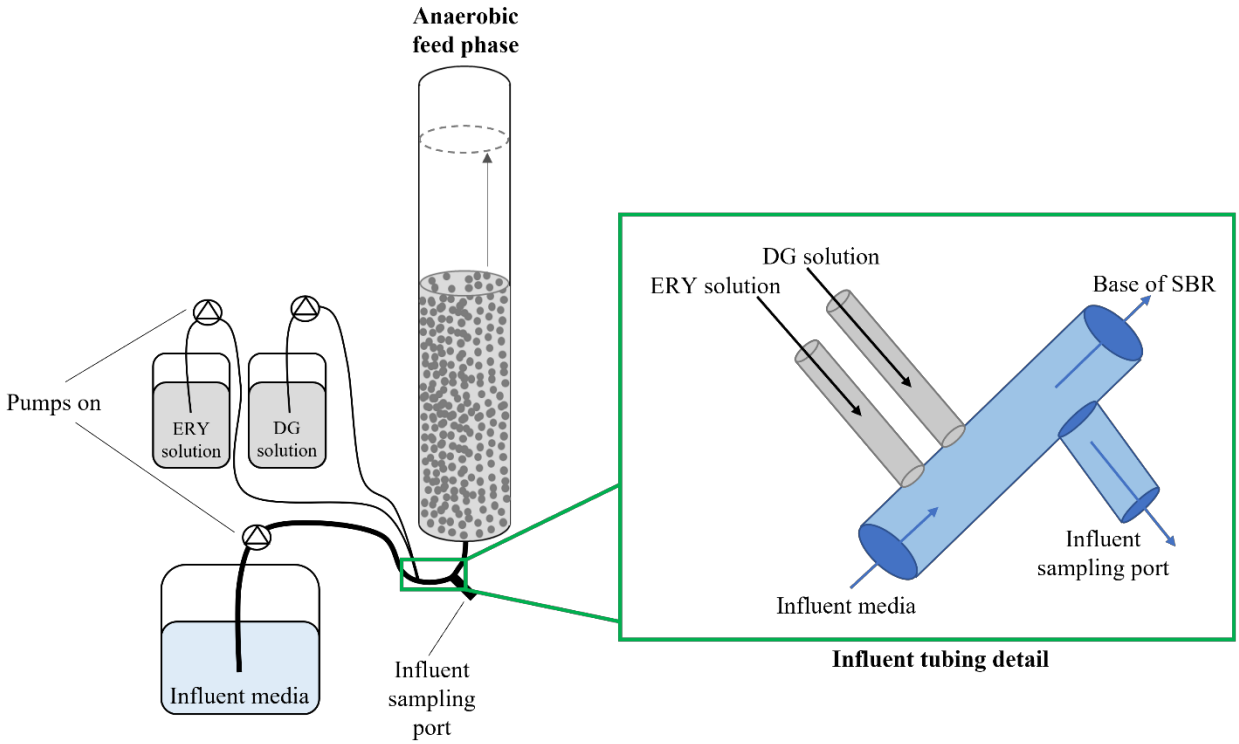

Figure A.1. Schematic of the sampling port from which influent samples were taken. During the anaerobic feed phase, the influent sampling port tubing was briefly unclamped to allow collection of samples for influent pharmaceutical and nutrient concentrations.

Table A.1. Suspected degradation products screened for in all samples. This PCDL was constructed after reviewing relevant literature. Not all compounds listed were detected (indicated by "-"). Compounds with the same residence time could not be distinguished from one another and therefore were not reported. Both sodium and hydrogen adducts of gemfibrozil degradation products were often detected; for samples in which both adducts were present, peak areas were summed together and this total area was corrected as described in the main article.

Parent compound	Formula	Adduct	m/z	Retention time (min)	Source
ERY	$C_{21}H_{38}O_8$	M+H	419.2639	8.07	[127]
	$C_8H_{16}O_4$		177.1121	-	
	$C_8H_{17}NO_3$		176.1281	-	
	$C_{29}H_{53}NO_{10}$		576.3742	5.5	[126, 127]
	$C_{21}H_{40}O_9$		437.2745	8.7	[127, 194]
	$C_6H_{14}NO$		117.1148	-	[194]
	$C_8H_{16}NO_2$		135.1254	-	
	$C_{29}H_{50}O_{10}$		559.3477	7.1	
DCF	$C_{14}H_{11}Cl_2NO_3$	M+H	312.0189	7.84	[26]
	$C_6H_4Cl_2$		146.9763	-	
	$C_{13}H_9Cl_2NO_2$		282.0083	8.83	[123]
	$C_{14}H_9Cl_2NO_3$		310.0035	7.1	
	$C_{14}H_{11}NO_2$		226.0856	10.07	
	$C_{12}H_9Cl_2NO_3$		286.0031	-	
	$C_{12}H_{11}Cl_2NO_3$		288.0191	-	
	$C_{14}H_{10}NO_2Cl$		260.0467	-	
	$C_{14}H_9Cl_2NO_2$		294.0082	-	
	$C_{13}H_9Cl_2NO_3$		298.0032	-	
	$C_{11}H_9Cl_2NO_3$		274.0032	-	
	$C_{10}H_7Cl_2NO_2$		243.9922	-	
	$C_{14}H_{10}Cl_2NO$		279.0212	8.83	[195]
	$C_{13}H_{10}Cl_2N$		251.0263	8.83	
GEM	$C_{15}H_{22}O_4$	M+H	267.1591	8.6	[129]
	$C_{15}H_{21}O_4$		266.1513	7.78	
	$C_{15}H_{20}O_5$		281.1384	8.83	
	$C_8H_8O_3$		153.0546	-	
	$C_7H_8O_2$		125.0597	-	
	$C_7H_{12}O_4$		161.0808	-	
	$C_6H_6O_4$		143.0339	9.52	
	C_5HO_3		109.9998	-	

	$C_{15}H_{22}O_4$	M+Na	289.1413	8	
	$C_{15}H_{21}O_4$		288.1335	-	
	$C_{15}H_{20}O_5$		303.1206	8.5	
	$C_8H_8O_3$		175.0368	-	
	$C_7H_8O_2$		147.0419	11.64	
	$C_7H_{12}O_4$		183.063	-	
	$C_6H_6O_4$		165.0161	5.1	
	C_5HO_3		131.982	11.65	

Supplementary Methods – Pharmaceutical Extraction from Granules

Pharmaceuticals were extracted from granules to quantify solid phase concentrations per methods adapted from [103]. In brief, granule samples were split in half, weighed, and crushed. Moisture fractions in half of the sample were determined by drying. The remaining wet half of the sample was sonicated in 5 mL methanol in a glass centrifuge tube for 15 minutes, then centrifuged at 1600 xg for 8 minutes. Supernatant was collected and transferred to a clean glass test tube. Sonication and centrifugation were then repeated with 2 mL methanol followed by 2 ml acetone. Supernatants were collected and combined after each centrifugation, then evaporated down to approximately 2 mL under a gentle nitrogen stream at 40°C. The remaining supernatant was then diluted with 150 mL nanopure water and extracted as described in the main text.

Removal Calculation for All Analytes (Pharmaceuticals and Nutrients)

$$Theoretical\ effluent\ concentration = \frac{(Influent \times 1.6L) + (Effluent \times 1.8L)}{3.4\ L} \quad \text{(A1)}$$

$$\%\ Removal = \left(1 - \frac{Effluent}{Effluent_{theoretical}}\right) \times 100\% \quad \text{(A2)}$$

Results

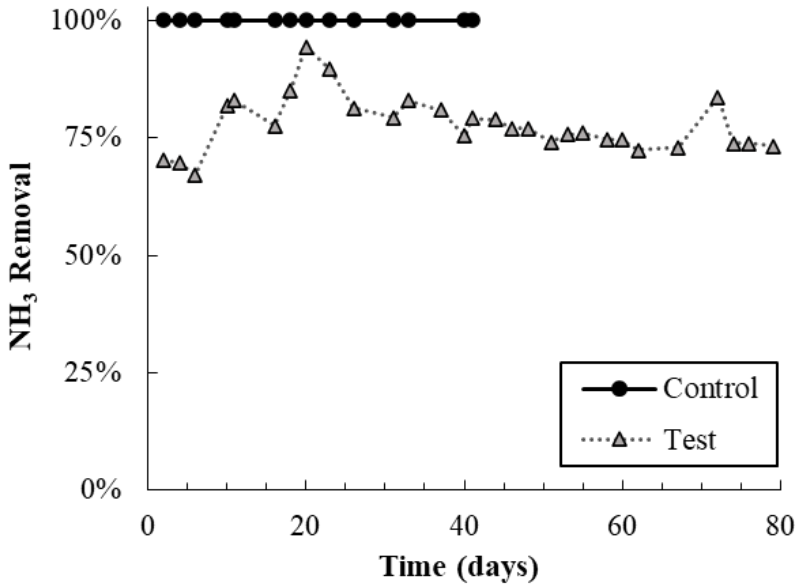

Figure A.2. Ammonia removal throughout the dosing period in the control and test reactor. Ammonia concentrations in the control reactor are not reported after day 40 due to a reactor operation issue, discussed in the main article body. Ammonia oxidation in the test reactor was the most inhibited nitrogen removal process—nitrite oxidation and denitrification proceeded at levels near equal to those in the control reactor, evidenced by equivalent nitrite and nitrate concentrations in both reactors (Figure A.3).

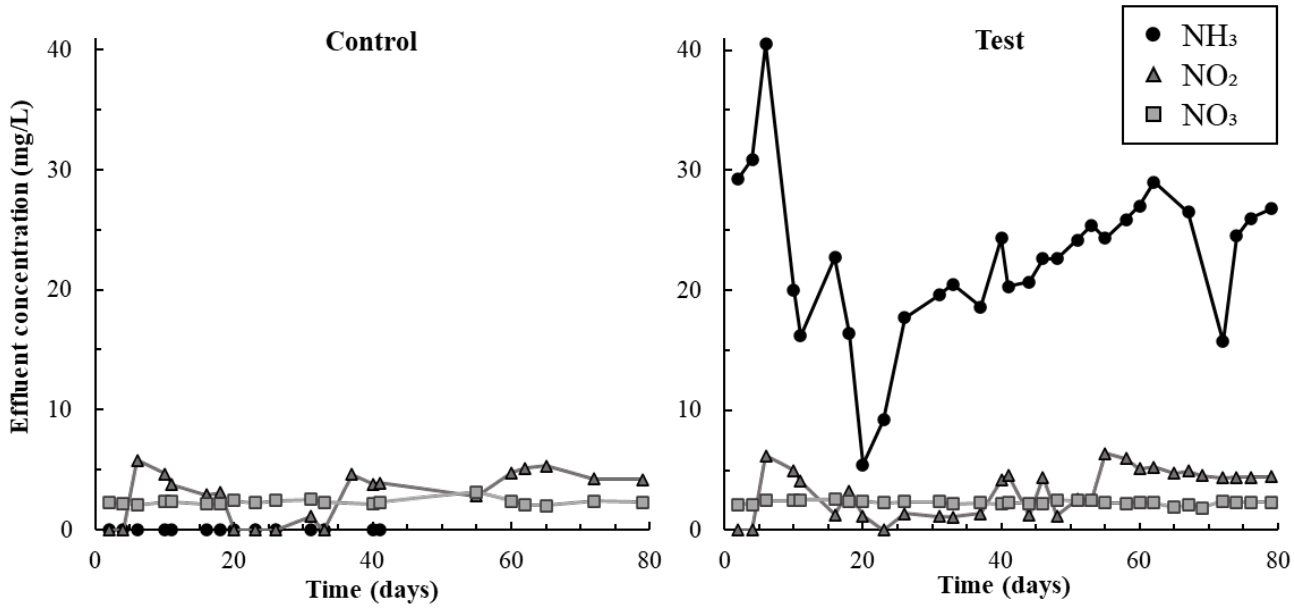

Figure A.3. Effluent concentrations of ammonia (NH_3), nitrite (NO_2), and nitrate (NO_3) versus time in the control and test reactors. Effluent ammonia concentrations are not reported past day 40 in the control reactor for reasons discussed previously (see Figure A.2 caption).

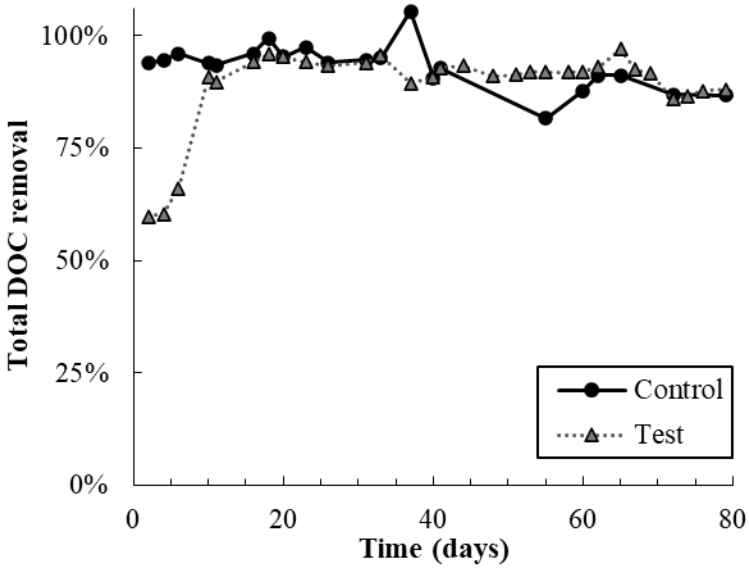

Figure A.4. Total dissolved organic carbon (DOC) removal throughout the dosing period in both SBRs. Note that excess DOC was accidentally fed in the first 10 days, resulting in lower DOC removal by the test reactor.

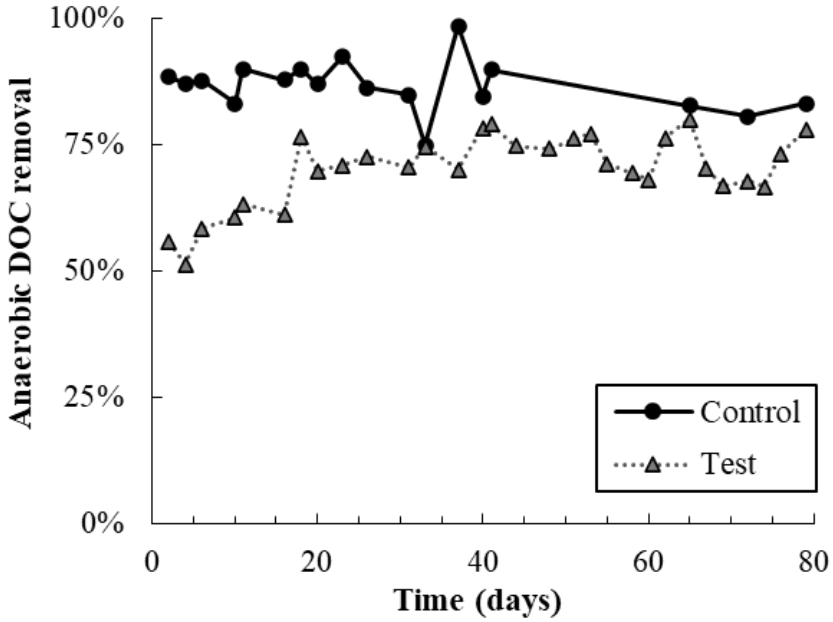

Figure A.5. DOC consumption in the anaerobic feed phase of reactor operation. Though more DOC was consumed anaerobically in the control reactor than the test, most DOC consumption in the test SBR continued to occur anaerobically (70 ± 7%).

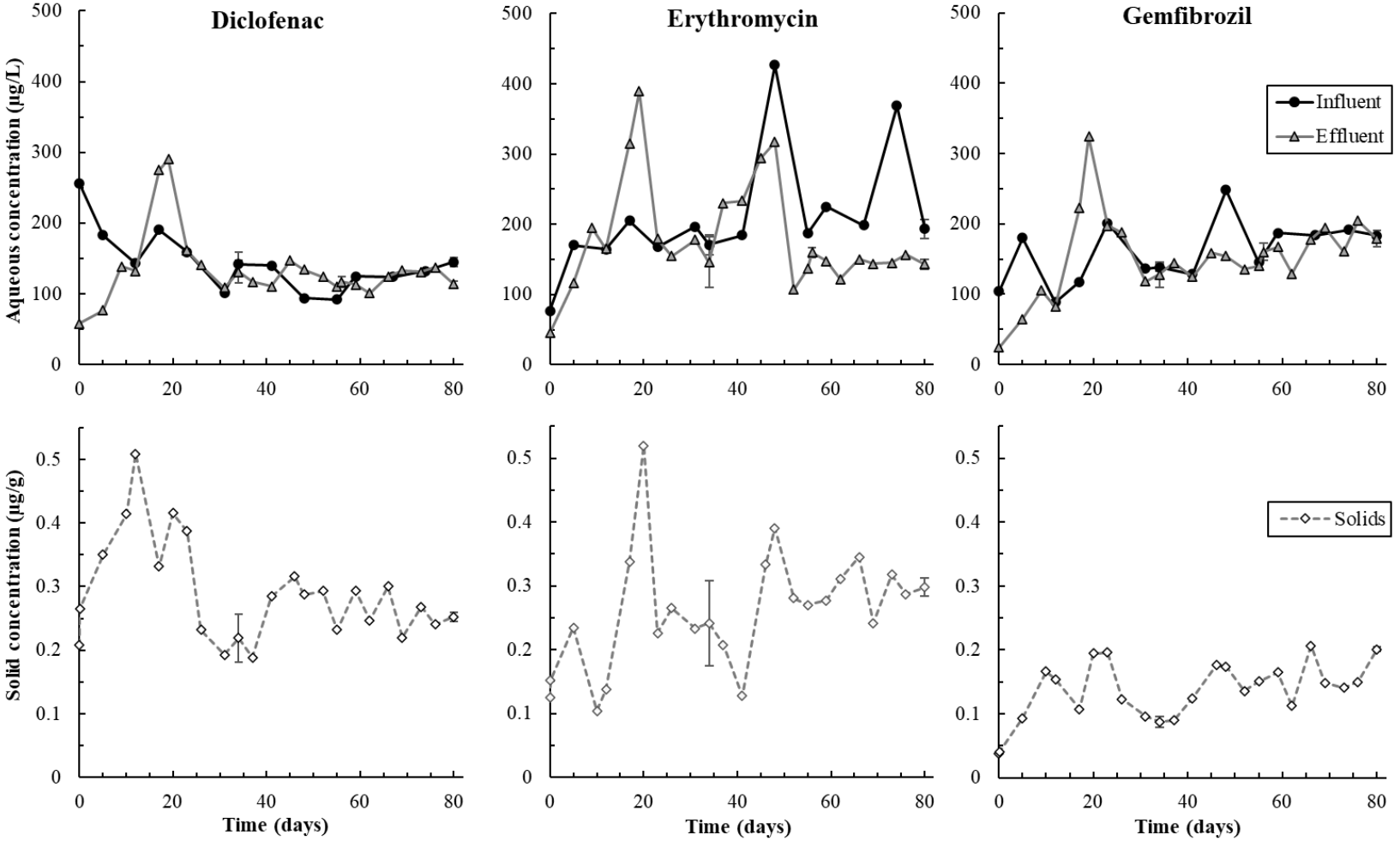

Figure A.6. Parent pharmaceutical concentrations in the aqueous (top row) and solid phase (bottom row) over time. Error bars represent the standard deviation of triplicate samples and are present on days 34, 56, and 80; points on these days are averages.

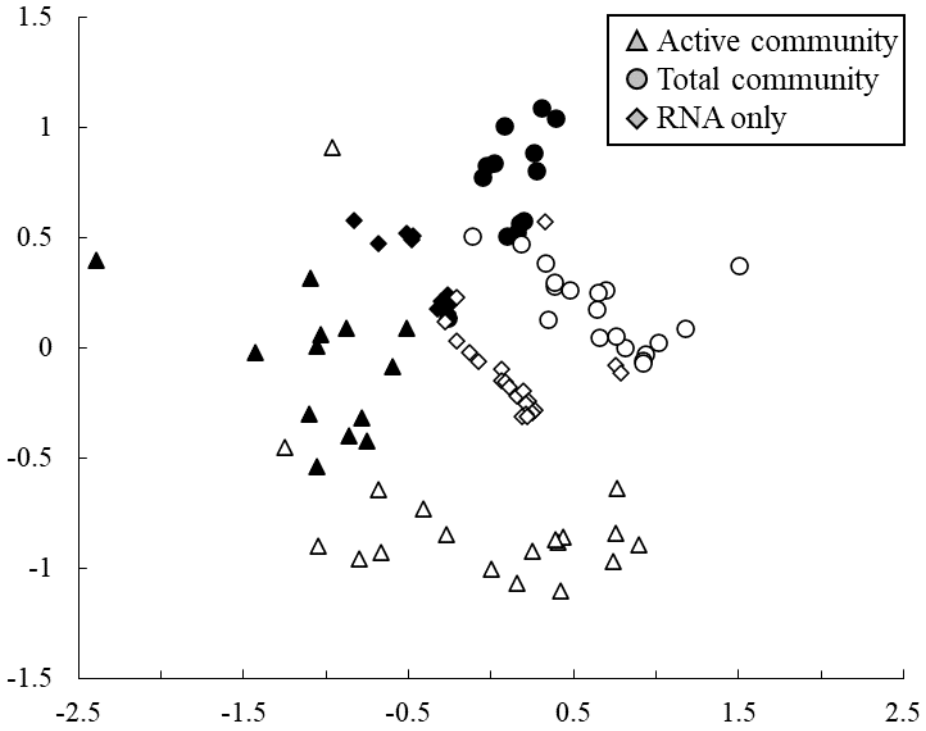

Figure A.7. Non-metric multidimensional ordination of community similarity for the control (closed symbol) and test (open symbol) communities. The active community is delineated based on rRNA transcript to gene ratios (triangle symbols); the total community on DNA reads (circles); and lastly the total RNA pool is shown with diamond symbols.

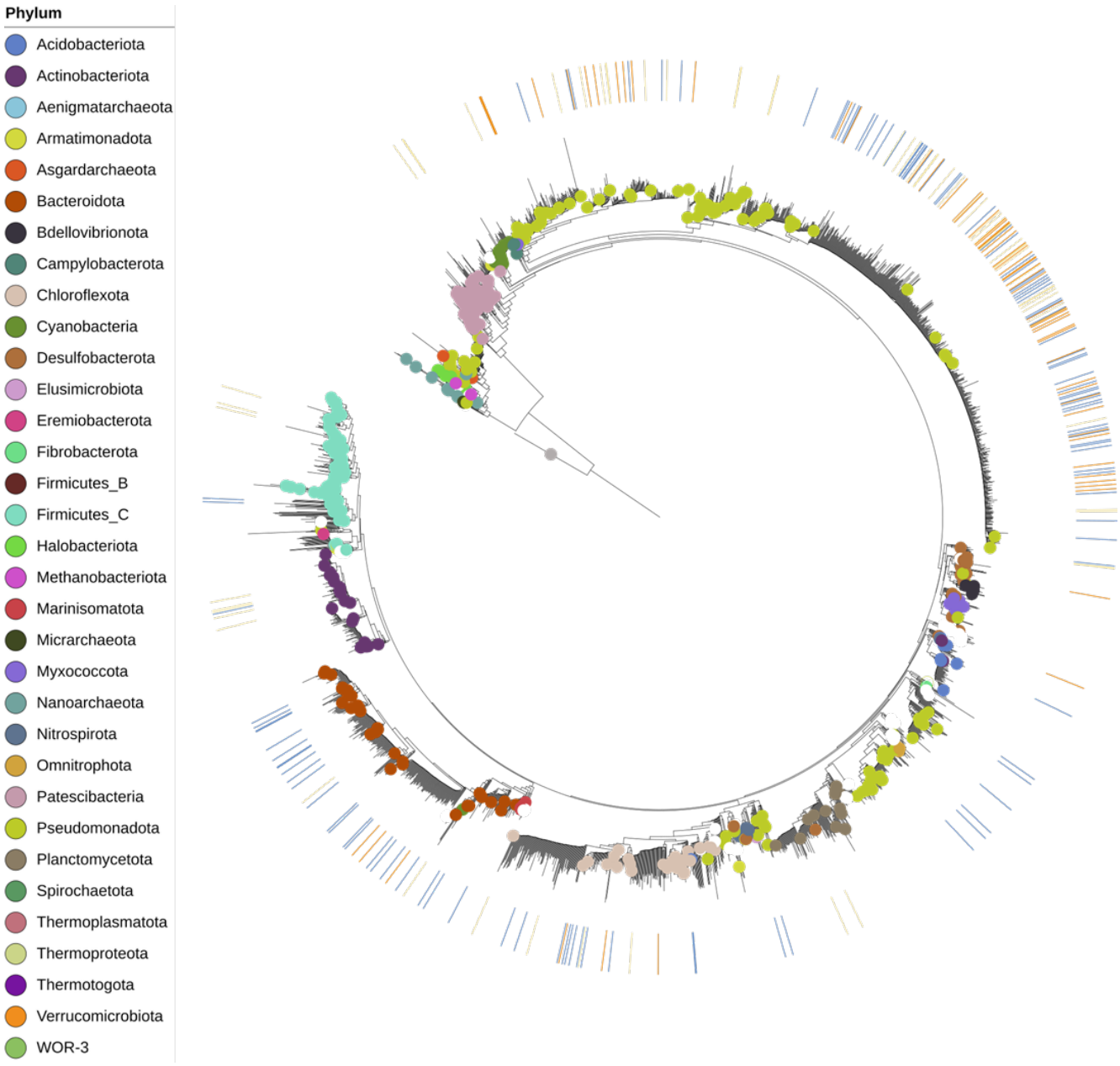

Figure A.8. Phylogenetic tree of reference 16S sequences downloaded from GTDB (v 202) with environmental ZOTUs inserted into the tree. Reference taxa are identified with colored symbols. The ring active taxa show negative (orange), neutral (beige), or positive (blue) responses between sampling day 5 and 17, when removal of all pharmaceuticals showed a sharp decline.

Table A.2. Predicted toxicity of detected degradation products using EPA TEST software. A higher resolution version of this table can be found at https://www.frontiersin.org/articles/10.3389/frmbi.2023.1242895/full#supplementary-material

Colors indicate prediction confidence - key provided below table				**Values predicted with EPA TEST software**					**Mean Absolute Error (MAE) values**				
Name	**Formula**	**Structure**	**SMILES**	**Fathead minnow LC50 (96 hr, mg/L)**	**Daphnia magna LC50 (48 hr, mg/L)**	**Oral rat LD50 (mg/kg)**	**Bioconcentration factor**	**Solubility at 25°C (mg/L)**	**Fathead minnow LC50 (96 hr, mg/L)**	**Daphnia magna LC50 (48 hr, mg/L)**	**Oral rat LD50 (mg/kg)**	**Bioconcentration factor**	**Solubility at 25°C (mg/L)**
Diclofenac	$C_{14}H_{11}Cl_2NO_2$	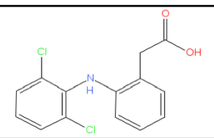	C1=CC=C(C(=C1)CC(=O)O)NC2=C(C=CC=C2Cl)Cl	0.4	3.5	244.02	26.94	5.27	0.508	0.012	0.376	0.476	0.764
DCF1 (4'-hydroxy-DCF)	$C_{14}H_{11}Cl_2NO_3$	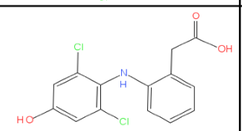	O=C(O)CC=1C=CC=CC1NC=2C(Cl)=CC(O)=CC2Cl	0.18	4.41	256.65	11.49	24.1	0.499	0.742	0.445	0.464	0.739
DCF1b (5-hydroxy-DCF)	$C_{14}H_{11}Cl_2NO_3$	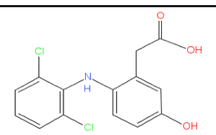	O=C(O)CC1=CC(O)=CC=C1NC=2C(Cl)=CC=CC2Cl	0.35	2.64	268	10.21	22.6	0.499	0.742	0.409	0.464	0.78
DCF3	$C_{14}H_{11}NO_2$	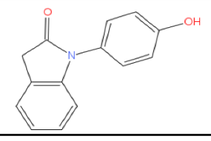	O=C1N(C2=CC=C(O)C=C2)C=3C=CC=CC3C1	2.52	9.04	604.81	31.07	35.3	0.282	0.551	0.355	0.418	0.701
Erythromycin	$C_{37}H_{67}NO_{13}$	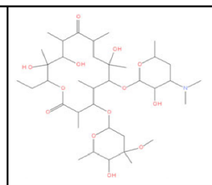	O=C1OC(CC)C(O)(C)C(O)C(C(=O)C(C)CC(O)(C)C(OC2OC(C)CC(N(C)C)C2O)C(C)C(OC3OC(C)C(O)C(OC)(C)C3)C1C)C	n/a	180.36	3097.82	n/a	387.93	n/a	0.349	0.333	n/a	0.958
ERY1	$C_{29}H_{53}NO_{10}$	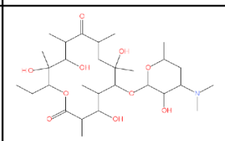	CC1C(C(C(CC)OC(C(C)C(C(C(C(CC(C1=O)C)(C)O)OC2C(C(CC(C)O2)[N](C)C)O)C)O)=O)(C)O)O	0.0659	303.22	2815.8	n/a	619.27	0.921	0.606	0.318	n/a	0.91
ERY2	$C_{21}H_{38}O_8$	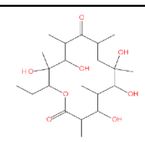	CC1C(C(C(CC)OC(C(C)C(C(C(C(CC(C1=O)C)(C)O)O)C)O)=O)(C)O)O	29.73	249.33	1895.94	n/a	1017.46	0.966	0.922	0.443	n/a	0.667
Gemfibrozil	$C_{15}H_{22}O_3$	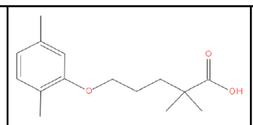	CC1=CC(=C(C=C1)C)OCCCC(C)(C)C(=O)O	3.89	5.13	469.56	16.11	17.16	0.809	0.929	0.449	0.706	0.62
GEM1	$C_{15}H_{22}O_4$	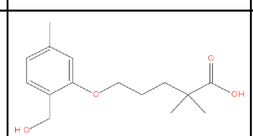	O=C(O)C(C)(C)CCCOC1=CC(=CC=C1CO)C	3.23	17.38	1966.36	5.48	193.84	0.809	0.934	0.246	0.588	0.49
GEM3	$C_{15}H_{20}O_5$	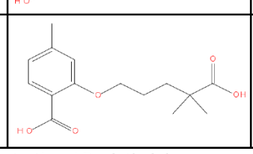	O=C(O)C1=CC=C(C=C1OCCCC(C(=O)O)(C)C)C	8.13	n/a	1652.79	1.6	211.95	0.809	n/a	0.196	0.648	0.31

LC = lethal concentration, LD = lethal dose
n/a = insufficient similar chemical data available; no predication can be made

Fathead minnow LC50 (96 hr, mg/L)	Aq. conc'n at which 50% of exposed fathead minnows die after 96 hours
Daphnia magna LC50 (48 hr, mg/L)	Aq. conc'n at which 50% of exposed D. magna (planktonic crustacean) die after 48 hrs
Oral rat LD50 (mg/kg)	Amt of chemical in mg/kg body weight that is lethal to 50% of rats after injestion
Bioconcentration factor	Ratio of the chemical conc'n in fish to that in water at steady state

Color key:	**MAE = Mean Absolute Error**
MAE < 0.2	Mean absolute errors for similar chemicals (similarity ≥ 0.5) in the training set are reported, except when experimental values were available for the queried chemical. In that case, the MAE for similar chemicals from the test set is reported. For more details, please see Martin, T.M., et al., Toxicity Estimation Software Tool. 2020, US EPA.
MAE 0.2 - 0.4	
MAE 0.4 - 0.6	
MAE 0.6 - 0.8	
MAE > 0.8	

APPENDIX B

SUPPLEMENTARY MATERIALS FOR CHAPTER 5

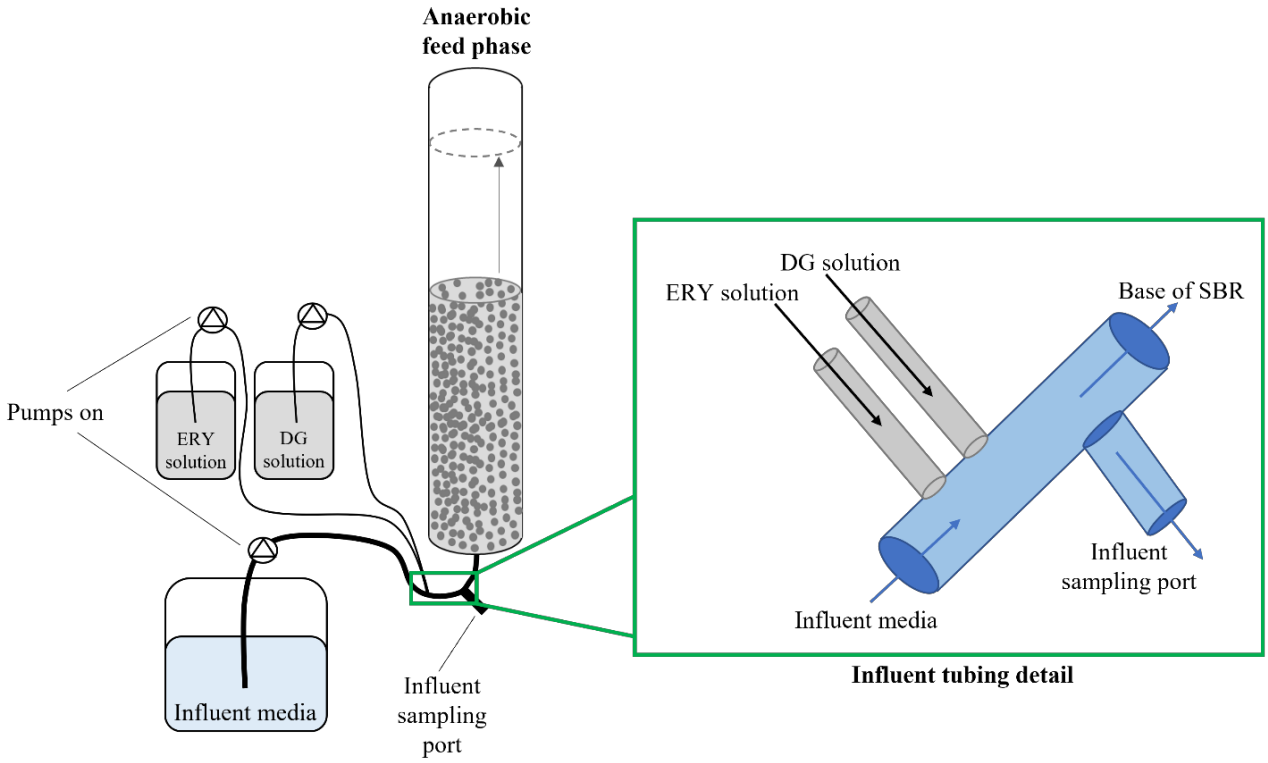

Figure B.1. Schematic of the sampling port from which influent samples were taken. During the anaerobic feed phase, the influent sampling port tubing was briefly unclamped to allow collection of samples for influent pharmaceuticals and nutrient concentrations.

Recovery Calculation for Pharmaceuticals

$$Recovery = \frac{Prespike\ concentration - unspiked\ concentration}{Postspike\ concentration - unspiked\ concentration}$$

Table B.1. The composition of the influent media, adapted from [89].

Compound	Concentration (mg/L)	Compound	Concentration (mg/L):
$C_2H_3NaO_2$	851.1	$ZnSO_4 * H_2O$	20.6
$MgSO_4 * 7H_2O$	85.5	$CaCl_2$	5.2
KCl	33.6	$MnCl_2 * 7H_2O$	4.7
NH_4Cl	176.5	$FeSO_4 * 7H_2O$	4.7
K_2HPO_4	35.9	$(NH_4)_6Mo_7O_{24} * 4H_2O$	1.0
KH_2PO_4	56.1	$CuSO_4 * 5H_2O$	1.5
EDTA	46.9	$CoCl_2 * 6H2O$	1.5

Table B.2. Physical and chemical properties of tested pharmaceuticals, as well as average extraction recoveries and retention times.

	Diclofenac	**Erythromycin**	**Gemfibrozil**
Chemical formula	$C_{14}H_{11}Cl_2NO_3$	$C_{37}H_{67}NO_{13}$	$C_{15}H_{22}O_3$
Molecular weight (g/mole)	296.1	733.9	250.3
Octanol-water partition coefficient (Log K_{ow})	4.51 [91]	3.06 [38]	4.77 [57]
Acid dissociation constant (pKa)	3.99 [91]	8.89 [38]	4.7 [57]
Aqueous phase extraction recovery	97 ± 9%	117 ± 17%	98 ± 11%
Solid phase extraction recovery	75 ± 8%	56 ± 22%	68 ± 8%
UPLC retention time (minutes)	8.8	6.8	9.5

Removal Calculation for All Analytes (Pharmaceuticals and Nutrients)

$$Theoretical\ effluent\ concentration = \frac{(Influent \times 1.6L) + (Effluent \times 1.8L)}{3.4\ L} \quad \text{(B1)}$$

$$\%\ Removal = \left(1 - \frac{Effluent}{Effluent_{theoretical}}\right) \times 100\% \quad \text{(B2)}$$

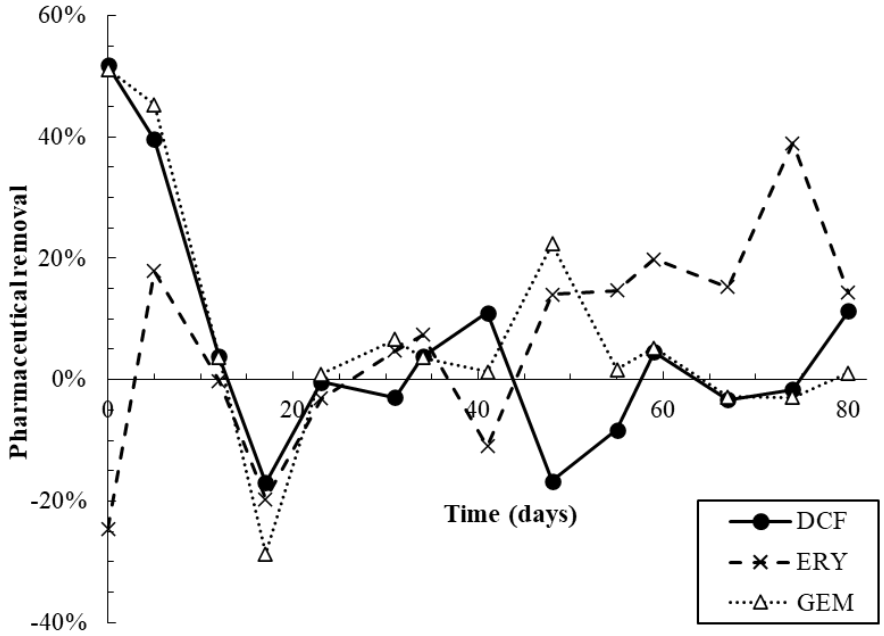

Figure B.2. Pharmaceutical removal versus time. Removal was calculated using equations S1 and S2. Removal percentages below zero indicate that effluent concentrations were higher than predicted by the mass balance. Data in this figure were originally published in [143] and are shown here with permission.

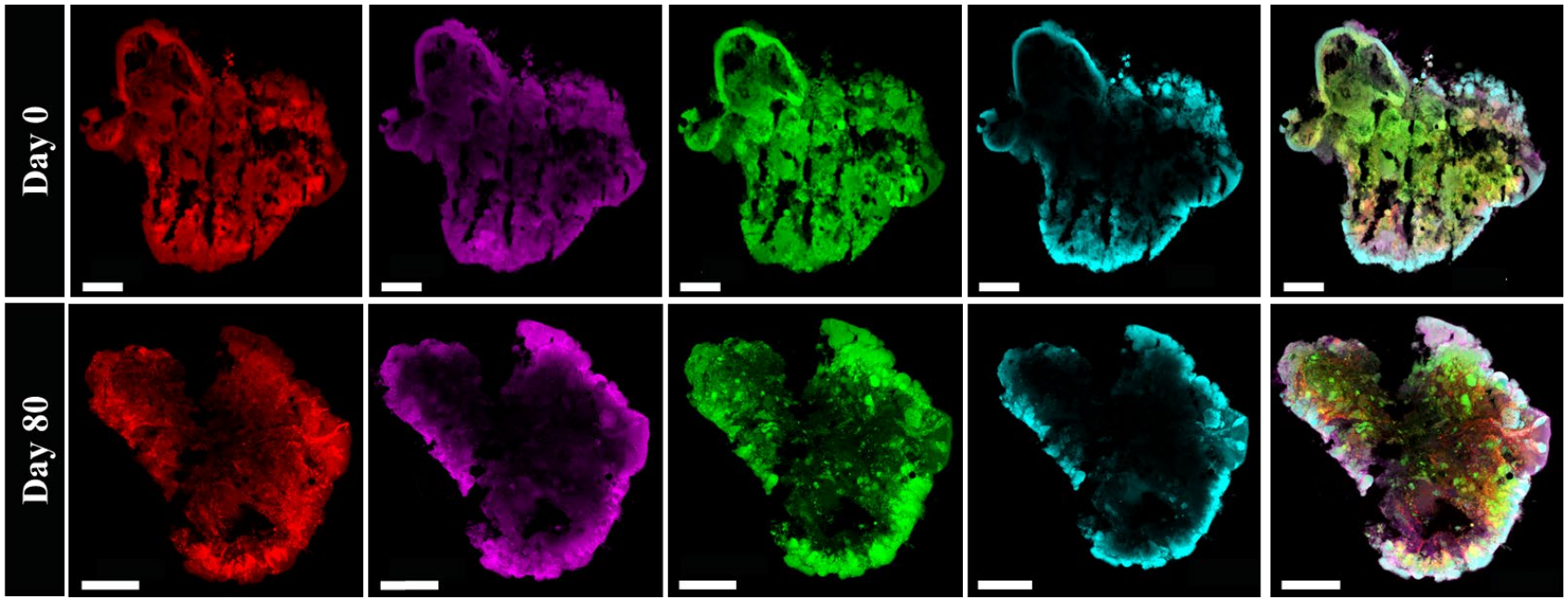

Figure B.3. Individual images of each EPS stain for a **control** granule at day 0 (top row) and day 80 (bottom row). From left to right: Red, alpha-polysaccharides; pink, beta-polysaccharides; green, proteins; blue; lipids; far right, the combined image of all stains. All scale bars are 200 μm.

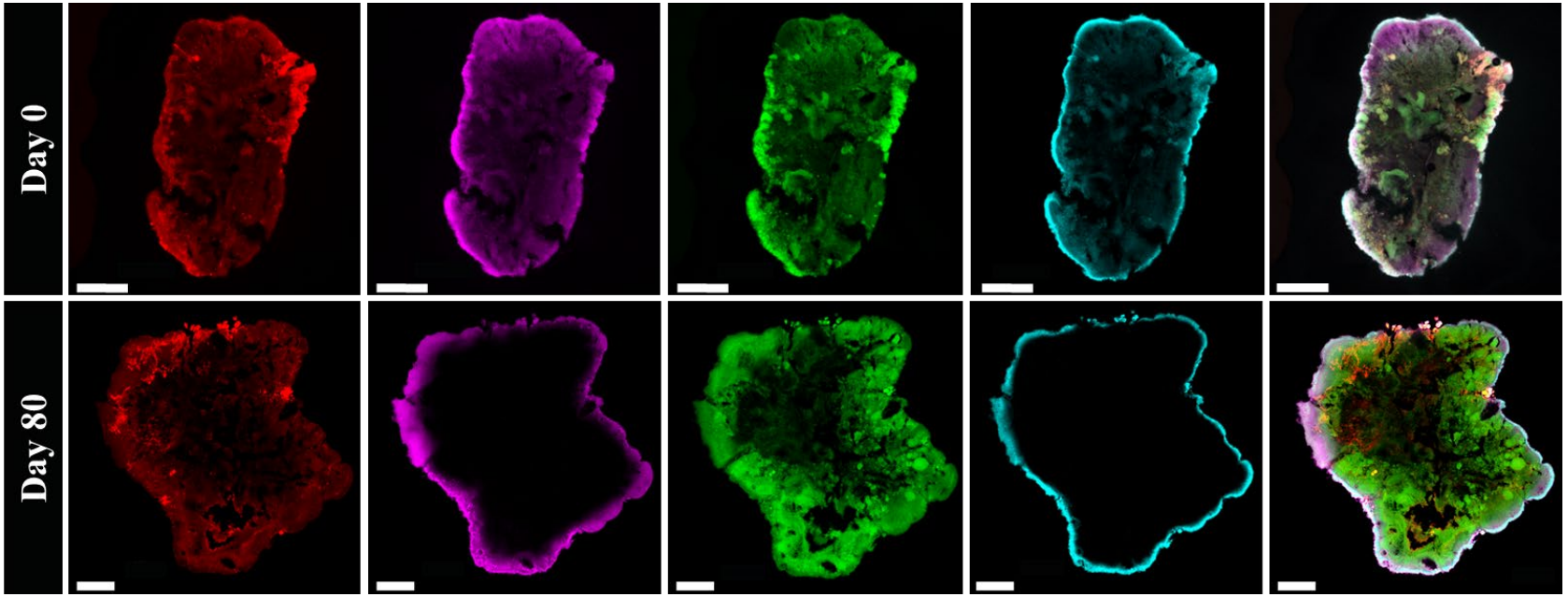

Figure B.4. Individual images of each EPS stain for a **test** granule at day 0 (top row) and day 80 (bottom row). From left to right: Red, alpha-polysaccharides; pink, beta-polysaccharides; green, proteins; blue; lipids; far right, combined image of all stains. All scale bars are 200 μm.

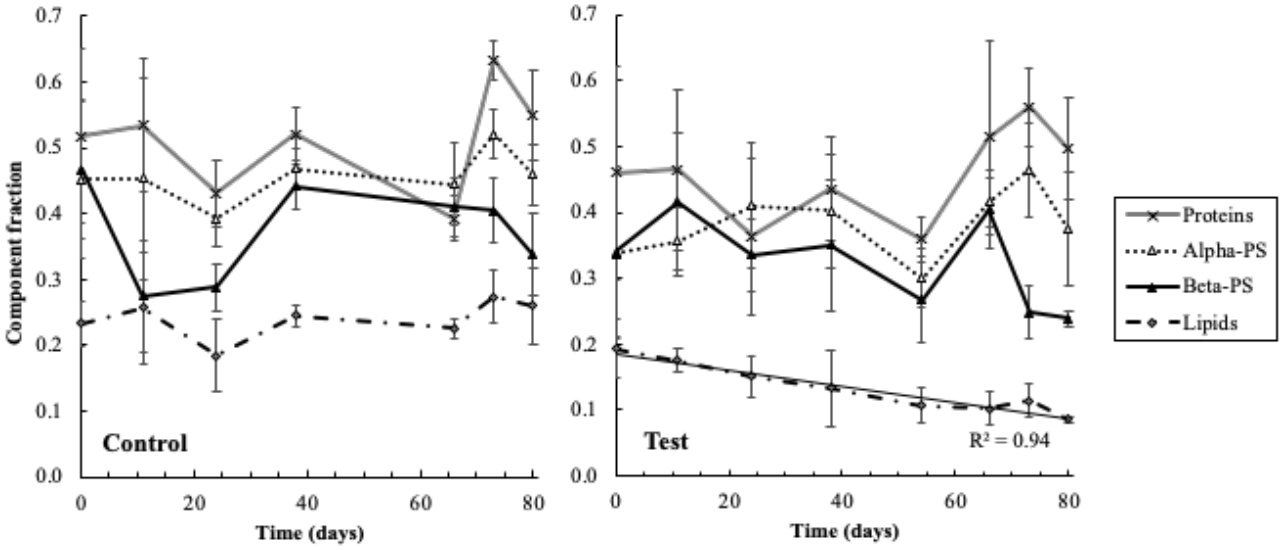

Figure B.5. Average fractions of various EPS components in granule sections versus time. Error bars represent the standard deviation of sections from triplicate granules. Triplicate sections from the same granule were also analyzed for each EPS component, and average values and standard deviations were similar to those plotted here at each time point (data not shown). Lipid concentrations in test granules declined linearly over time, evidenced by the linear trendline $R^2 > 0.9$.

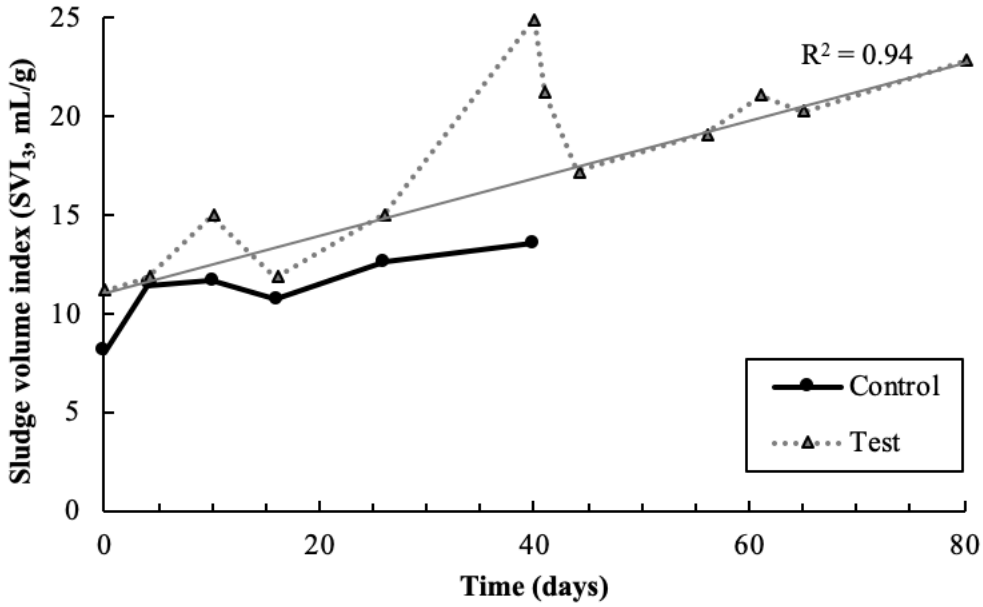

Figure B.6. Sludge volume index versus time in both control and test reactors. The SVI_3 of AGS in the test reactor increased linearly over the 80-day exposure period, excepting the two points in which SBR-controlling software experienced an error (days 40 and 41, discussed in more detail in the main body of the text). Control AGS SVI_3 remained constant at approximately 12 mL/g.

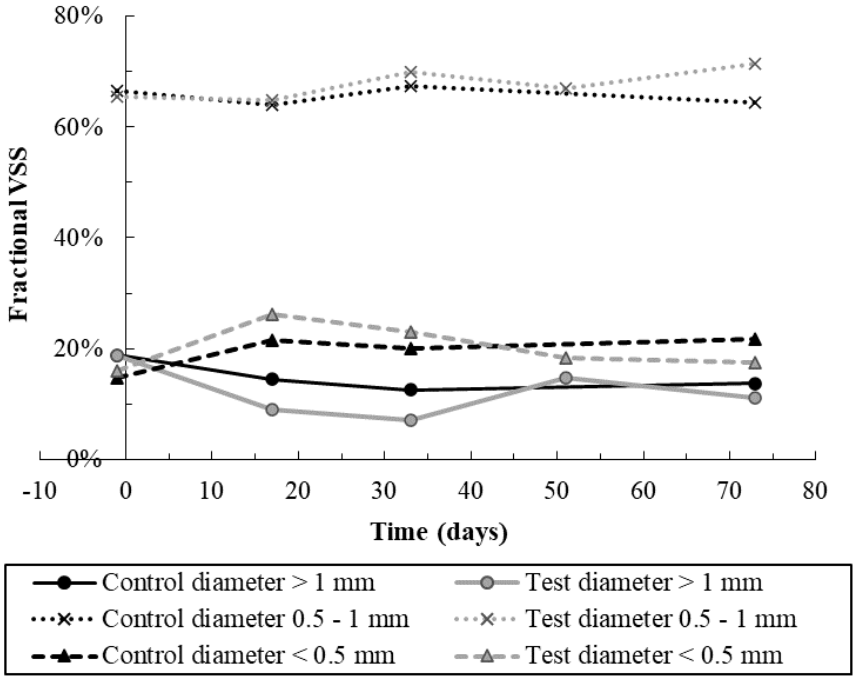

Figure B.7. Granule size fractions versus time in both reactors. 10 mL AGS was sieved, and sieved portions were analyzed for VSS. "Fractional VSS" was calculated by dividing the VSS in each size bin by the total sample VSS. Sample points at t(-1) indicate samples taken from both reactors immediately before beginning pharmaceutical dosing.

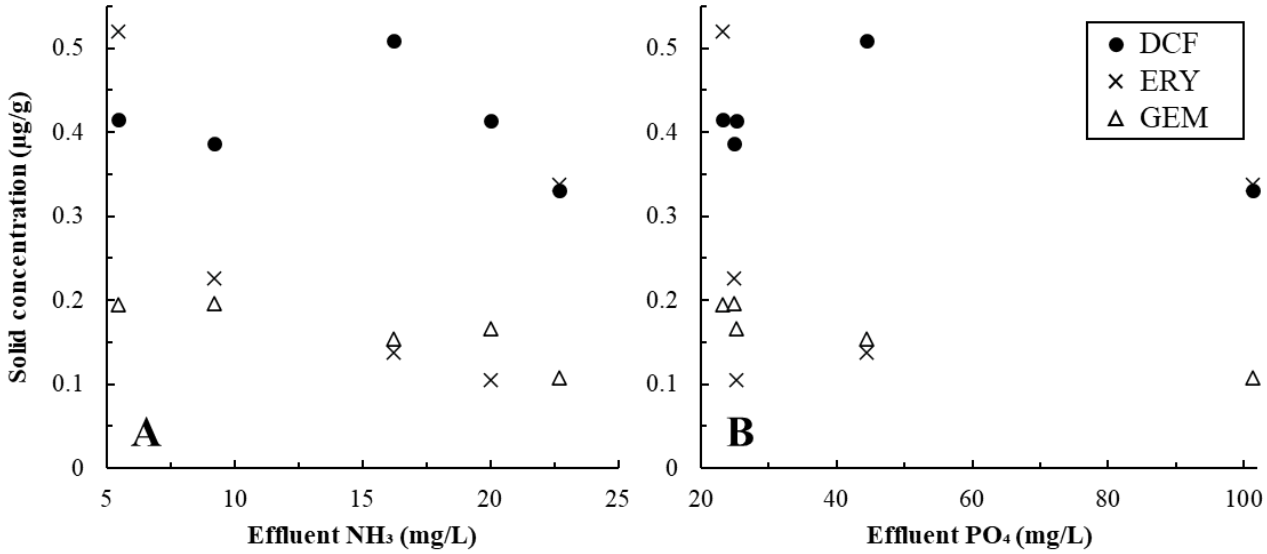

Figure B.8. Solid phase pharmaceutical concentrations versus effluent (A) ammonia and (B) phosphate concentrations over days 10-23 only.

Test SBR Sorption Capacity Calculations

Key Terms.

C_{Inf}	Influent pharmaceutical concentration, approximately 150 µg/L each compound
V_{Inf}	Influent volume, 1.6 L per cycle
TSS	Average total suspended solids in the test SBR, approximately 21.8 g/L; total reactor volume is 3.4 L
$Q_{DCF};\ Q_{ERY};\ Q_{GEM}$	Equilibrium amounts of adsorbed DCF, ERY, and GEM (µg/g TSS) in batch tests at pH 7 with 200 µg/L of each pharmaceutical initially, approximately 30 mg/L ammonia, and 8 mg/L phosphate
M_{cycle}	Pharmaceutical mass dosed per cycle (8 SBR cycles/day)
$M_{DCF};\ M_{ERY};\ M_{GEM}$	Maximum pharmaceutical mass that granules can sorb, given reactor TSS and Q values for each pharmaceutical
$n_{DCF}; n_{ERY}; n_{GEM}$	Number of SBR cycles possible before granules' sorptive capacity is reached for each pharmaceutical (assuming all influent pharmaceuticals sorb to AGS and effluent concentrations are zero)

Calculations.

$$M_{cycle} = C_{Inf} * V_{Inf} = 150\frac{\mu g}{L} * 1.6\frac{L}{cycle} = 240\frac{\mu g}{cycle}$$

$$M_{DCF} = TSS * 3.4\ L *\ Q_{DCF} = 21.8\frac{g}{L} * 3.4\ L * 8.1\frac{\mu g\ DCF}{g} = 601.6\ \mu g\ DCF$$

$$M_{ERY} = TSS * 3.4\ L *\ Q_{ERY} = 21.8\frac{g}{L} * 3.4\ L * 5.1\frac{\mu g\ ERY}{g} = 375.7\ \mu g\ ERY$$

$$M_{GEM} = TSS * 3.4L * Q_{GEM} = 21.8\frac{g}{L} * 3.4\ L * 21\ \frac{\mu g\ GEM}{g} = 1558.7\ \mu g\ GEM$$

$$n_{DCF} = \frac{M_{DCF}}{M_{cycle}} = \frac{426.2\ \mu g\ DCF}{240\ \mu g/cycle} = 2.5\ cycles$$

$$n_{ERY} = \frac{M_{ERY}}{M_{cycle}} = \frac{347.8\ \mu g\ ERY}{240\ \mu g/cycle} = 1.6\ cycles$$

$$n_{GEM} = \frac{M_{ERY}}{M_{cycle}} = \frac{947.3\ \mu g\ GEM}{240\ \mu g/cycle} = 6.5\ cycles$$

APPENDIX C

SUPPLEMENTARY MATERIALS FOR CHAPTER 6

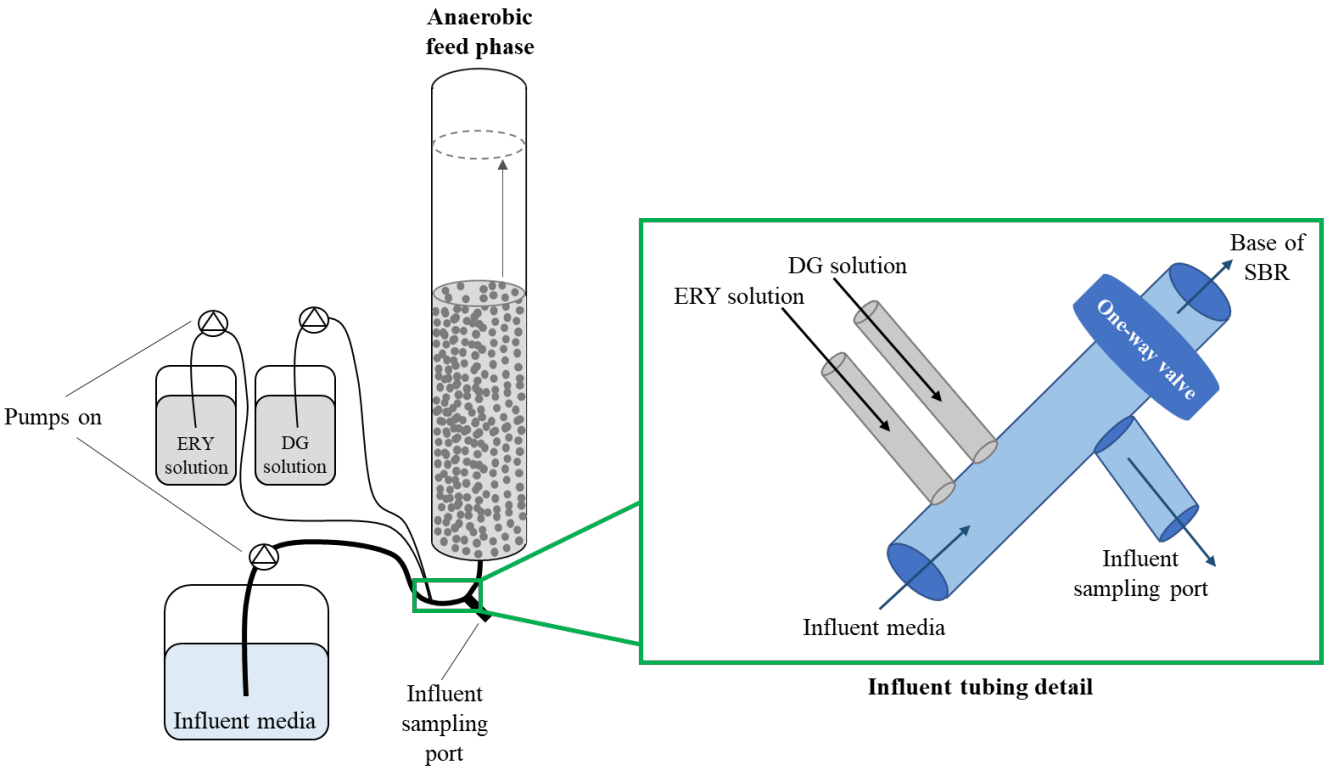

Figure C.1. Schematic of the sampling port from which influent samples were taken. During the anaerobic feed phase, the influent sampling port tubing was briefly unclamped to allow collection of samples for influent pharmaceutical and nutrient concentrations.

Table C.1. Physical and chemical properties of tested pharmaceuticals, as well as average extraction recoveries, retention times, and quantification limits. The method for recovery assessment is detailed below.

	Diclofenac	**Erythromycin**	**Gemfibrozil**
Chemical formula	$C_{14}H_{11}Cl_2NO_3$	$C_{37}H_{67}NO_{13}$	$C_{15}H_{22}O_3$
Molecular weight (g/mole)	296.1	733.9	250.3
Octanol-water partition coefficient (Log K_{ow})	4.51 [91]	3.06 [38]	4.77 [57]
Acid dissociation constant (pKa)	3.99 [91]	8.89 [38]	4.7 [57]
Aqueous phase extraction recovery	71 ± 14%	31 ± 5%	69 ± 6%
Solid phase extraction recovery	42 ± 2%	52 ± 7%	50 ± 8%
UPLC retention time (minutes)	8.9	6.9	9.5
UPLC-QTOF-MS quantification limit (µg/L)	< 2.5		

Spike-Recovery Testing

One sample from each duplicate set was pre-spiked with pharmaceutical stock solution to a final nominal concentration of 20 µg/L prior to extraction. After extraction, the unspiked sample was split in half, and one half was post-spiked to a final nominal concentration equal to 20 µg/L multiplied by each samples' concentration factor. Recovery was then determined using Equation C1:

$$Recovery = \frac{Prespike\ concentration - unspiked\ concentration}{Postspike\ concentration - unspiked\ concentration} \quad \text{(C1)}$$

Table C.2. Suspected degradation products screened for in all samples. This PCDL was constructed after reviewing relevant literature. Not all compounds listed were detected (indicated by "-"). Compounds with the same residence time could not be distinguished from one another and therefore were not reported. Both sodium and hydrogen adducts of gemfibrozil degradation products were often detected; for samples in which both adducts were present, peak areas were summed together and this total area was corrected as described below.

Parent compound	Formula	Adduct	m/z	Retention time (min)	Source
ERY	$C_{21}H_{38}O_8$	M+H	419.2639	8.1	[127]
	$C_8H_{16}O_4$		177.1121	-	
	$C_8H_{17}NO_3$		176.1281	-	
	$C_{29}H_{53}NO_{10}$		576.3742	5.5	[126, 127]
	$C_{21}H_{40}O_9$		437.2745	8.7	[127, 194]
	$C_6H_{14}NO$		117.1148	-	[194]
	$C_8H_{16}NO_2$		135.1254	-	
	$C_{29}H_{50}O_{10}$		559.3477	7.1	
DCF	$C_{14}H_{11}Cl_2NO_3$	M+H	312.0189	7.8	[26]
	$C_6H_4Cl_2$		146.9763	-	
	$C_{13}H_9Cl_2NO_2$		282.0083	8.8	[123]
	$C_{14}H_9Cl_2NO_3$		310.0035	7.5	
	$C_{14}H_{11}NO_2$		226.0856	10.1	
	$C_{12}H_9Cl_2NO_3$		286.0031	-	
	$C_{12}H_{11}Cl_2NO_3$		288.0191	-	

	$C_{14}H_{10}NO_2Cl$		260.0467	-	
	$C_{14}H_9Cl_2NO_2$		294.0082	-	
	$C_{13}H_9Cl_2NO_3$		298.0032	-	
	$C_{11}H_9Cl_2NO_3$		274.0032	-	
	$C_{10}H_7Cl_2NO_2$		243.9922	-	
	$C_{14}H_{10}Cl_2NO$		279.0212	8.8	[195]
	$C_{13}H_{10}Cl_2N$		251.0263	8.8	
GEM	$C_{15}H_{22}O_4$	M+H	267.1591	8.5	[129]
	$C_{15}H_{21}O_4$		266.1513	7.8	
	$C_{15}H_{20}O_5$		281.1384	8.7	
	$C_8H_8O_3$		153.0546	-	
	$C_7H_8O_2$		125.0597	-	
	$C_7H_{12}O_4$		161.0808	-	
	$C_6H_6O_4$		143.0339	9.5	
	C_5HO_3		109.9998	-	
	$C_{15}H_{22}O_4$	M+Na	289.1413	8.5	
	$C_{15}H_{21}O_4$		288.1335	-	
	$C_{15}H_{20}O_5$		303.1206	8.5	
	$C_8H_8O_3$		175.0368	-	
	$C_7H_8O_2$		147.0419	11.6	
	$C_7H_{12}O_4$		183.063	-	
	$C_6H_6O_4$		165.0161	5.1	
	C_5HO_3		131.982	11.7	

"Corrected Peak Area" Calculations for Degradation Products

As stated in the main text, degradation products were tracked simply as an indicator of biodegradation. For this reason, determining the actual concentrations of degradation products was beyond the scope of this work; instead, we tracked changes in peak area versus time. To account for slight variations in the relationship between standards' peak areas and concentrations in different mass spectrometry runs, the peak areas of all degradation products were corrected by the peak area of the relevant 100 µg/L standard. For example, the peak area of an aqueous ERY degradation product would be divided by the peak area of the 100 µg/L ERY standard measured

during the same mass spectrometry run, then multiplied by the sample's concentration factor (Equation C2). The peak areas of degradation products detected in solid phase samples were corrected in the same fashion but were also corrected by the sample's dry weight (Equation C3).

$$Aqueous\ corrected\ peak\ area = \frac{Degradation\ product\ peak\ area \times Concentration\ factor}{Peak\ area\ of\ relevant\ 100\frac{\mu g}{L}\ standard} \quad \text{(C2)}$$

$$Solid\ corrected\ peak\ area = \frac{Degradation\ product\ peak\ area}{Peak\ area\ of\ relevant\ 100\frac{\mu g}{L}\ standard\ \times Sample\ dry\ weight\ (g)} \quad \text{(C3)}$$

Removal Calculations for All Analytes

$$Theoretical\ effluent\ concentration = \frac{(Influent \times 1.6L) + (Effluent \times 1.8L)}{3.4\ L} \quad \text{(C4)}$$

$$\%\ Removal = \left(1 - \frac{Effluent}{Effluent_{theoretical}}\right) \times 100\% \quad \text{(C5)}$$

$$\%\ Inhibition = \frac{\%\ Removal_{control} - \%\ Removal_{test}}{\%\ Removal_{control}} \quad \text{(C6)}$$

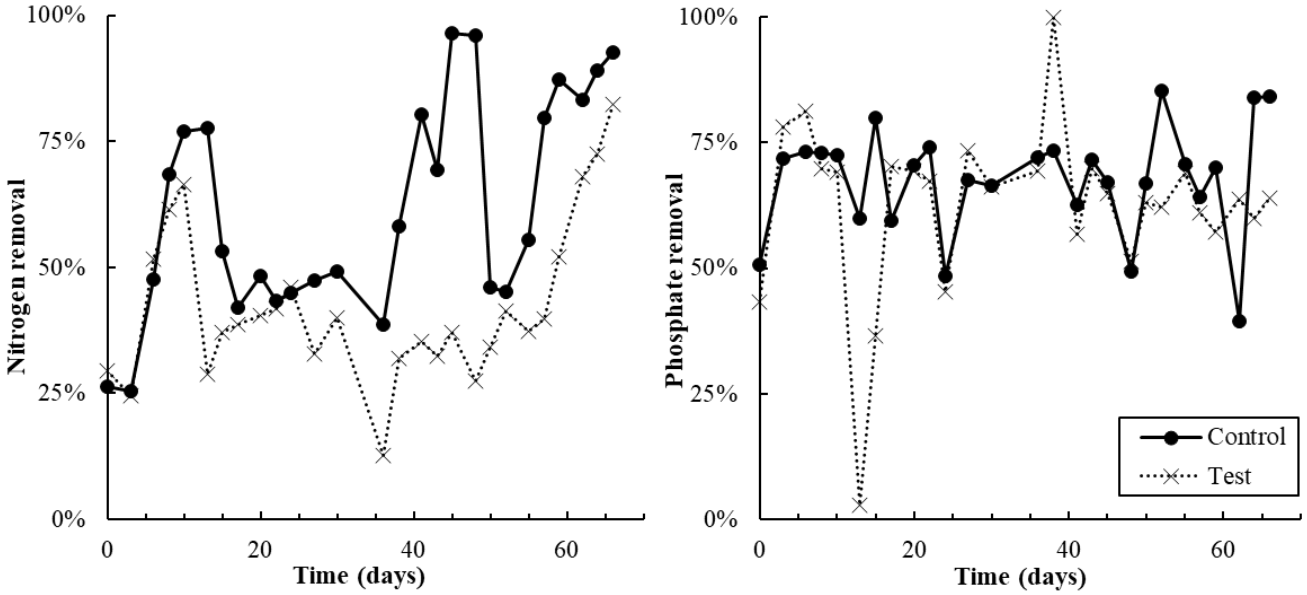

Figure C.2. Left, nitrogen removal; right, phosphate removal in the control and test reactors versus time.

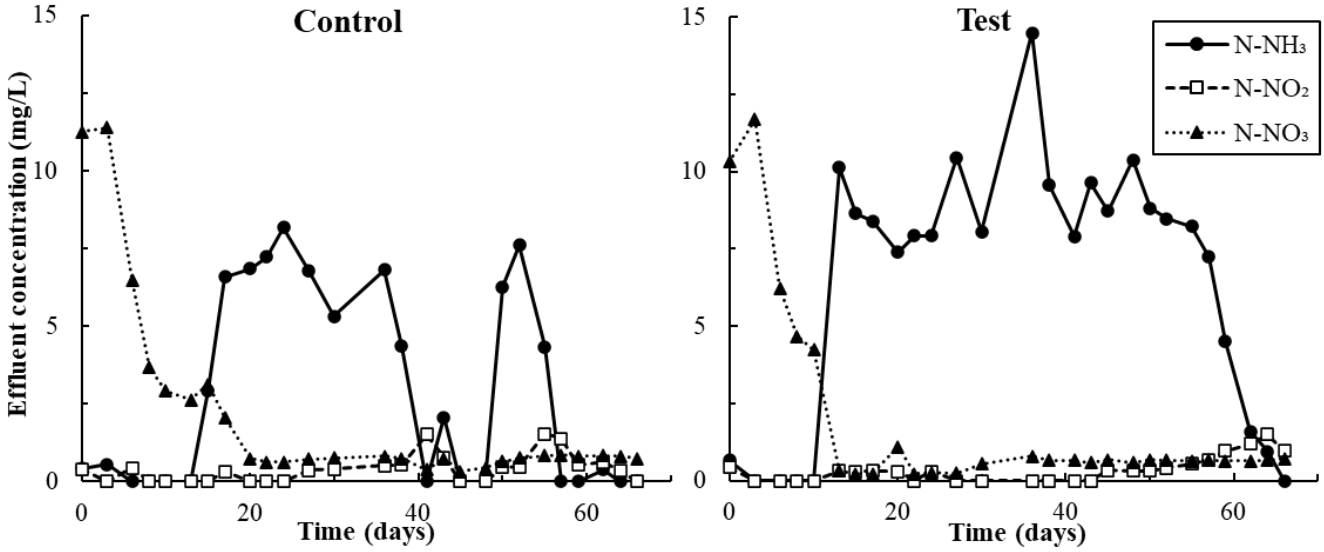

Figure C.3. Effluent concentrations of ammonia-, nitrite-, and nitrate-nitrogen in the control and test reactors. Compounds are plotted as nitrogen to aid data visualization. Effluent nitrate was high in both SBRs over the first 10 days while organic carbon dosing was below 100 mg/L in the influent.

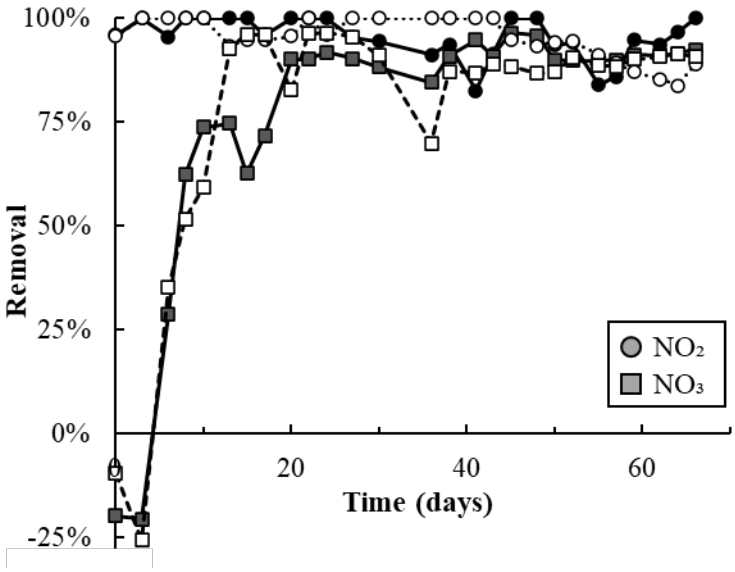

Figure C.4. Nitrite and nitrate removal in the control and test SBRs. Control data is plotted with solid symbols and lines, test data with open symbols and dashed lines. A mass balance on the ammonia consumed was used to predict nitrite production. Predicted nitrite concentrations and effluent nitrite values were used to calculate nitrite removal and predict nitrate concentrations; effluent and predicted nitrate values were used to calculate nitrate removal.

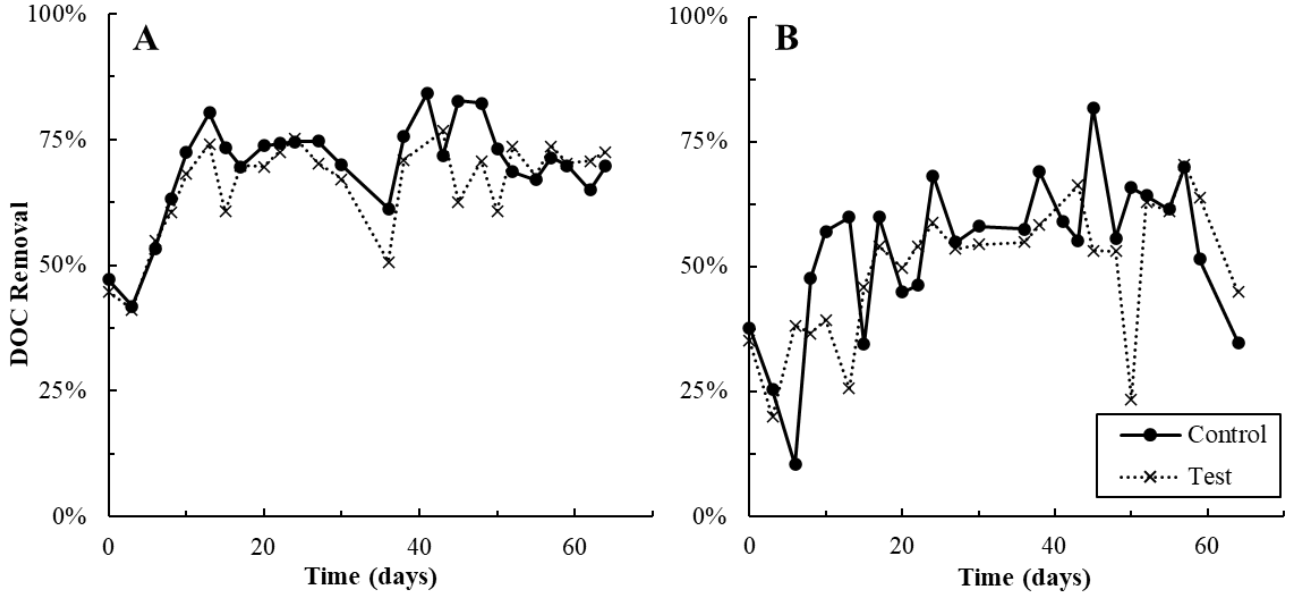

Figure C.5. A: Total dissolved organic carbon (DOC) removal in both reactors. B: Anaerobic DOC removal. Approximately 20% of the influent carbon was fed as EDTA in the trace nutrient solution; EDTA is typically recalcitrant to biodegradation and therefore total DOC removals near 80% reflect almost complete removal of all biodegradable organic carbon. Most of the DOC fed was removed anaerobically after day 10.

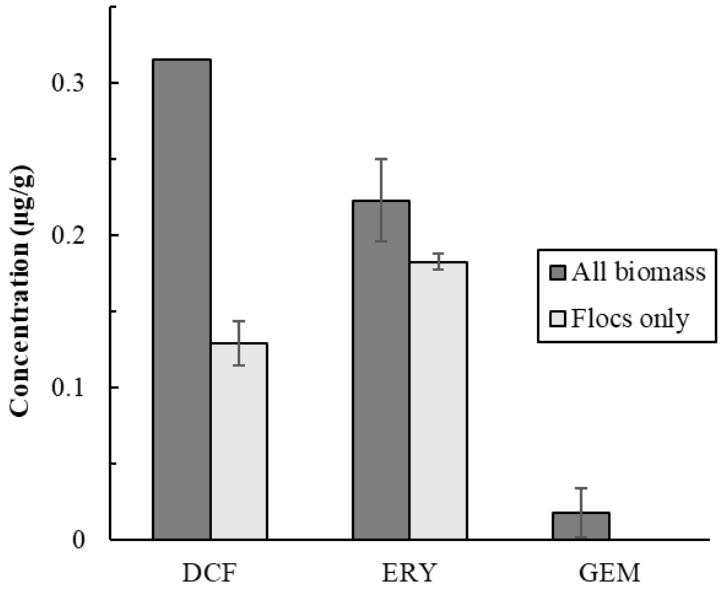

Figure C.6. Pharmaceutical concentrations bound to all biomass (AGS and floc mixture) and just flocs (i.e., biomass that passed through a 0.2 mm sieve). Error bars represent the standard deviation of triplicate samples. An error bar is not present for all biomass for DCF because of an error during the mass spectrometry run of one triplicate; ERY and GEM could be quantified from this sample, but DCF could not. DCF all biomass data therefore represents the average of duplicate samples. GEM concentrations in all floc samples were below detection.

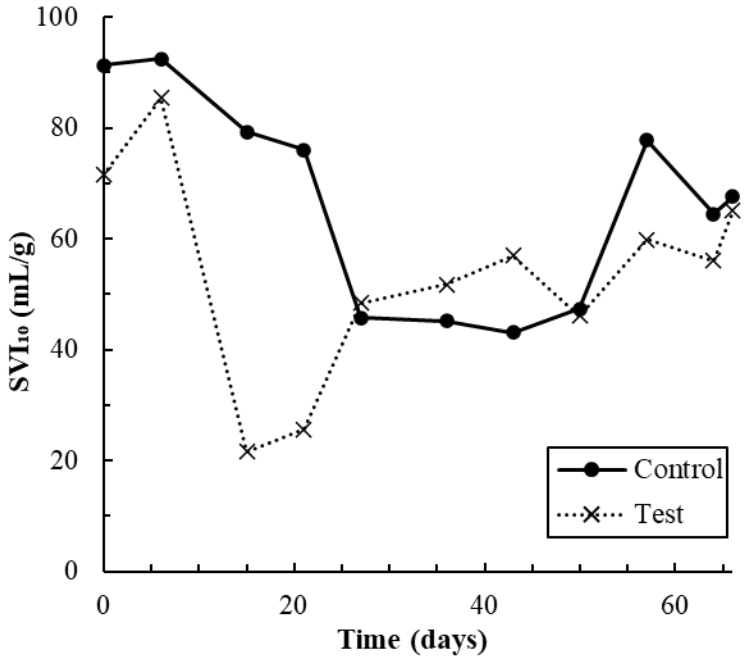

Figure C.7. Sludge volume index of biomass in both reactors measured after 10 minutes of settling (SVI_{10}) versus time. The large drop in SVI_{10} for biomass in the test SBR between days 6-15 is due to the floc washout that occurred on day 13. Notably, control biomass' SVI_{10} also dropped between days 0-27, and the SVI_{10} of biomass in both SBRs was equal on day 27. Both control and test biomass' SVI_{10} values remained near equal for the remainder of the experiment.

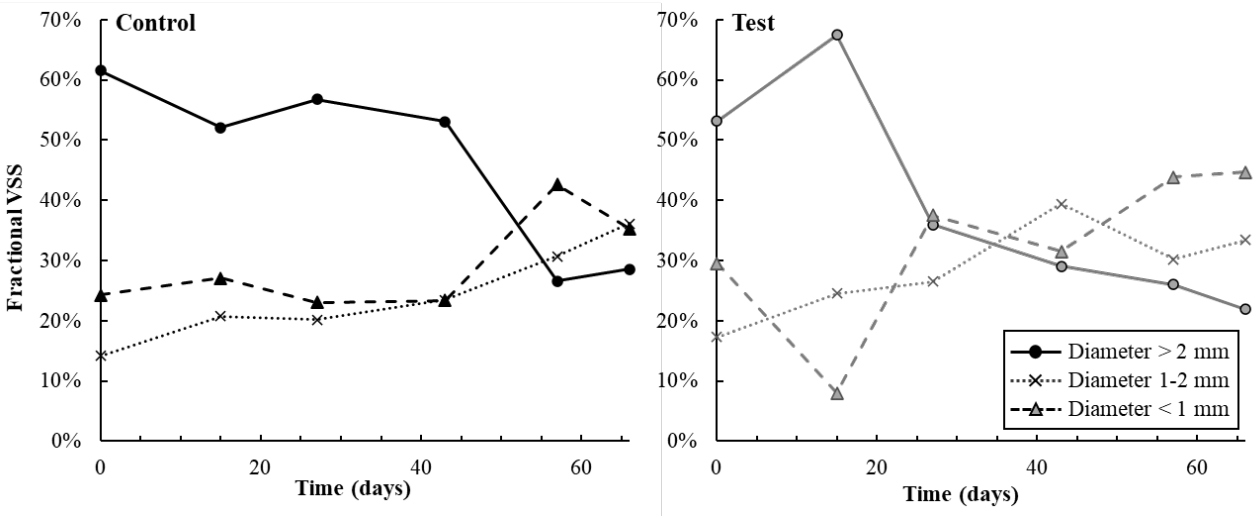

Figure C.8. Granule size distributions, as a fraction of the summed VSS of the sample, versus time in the control and test reactors.

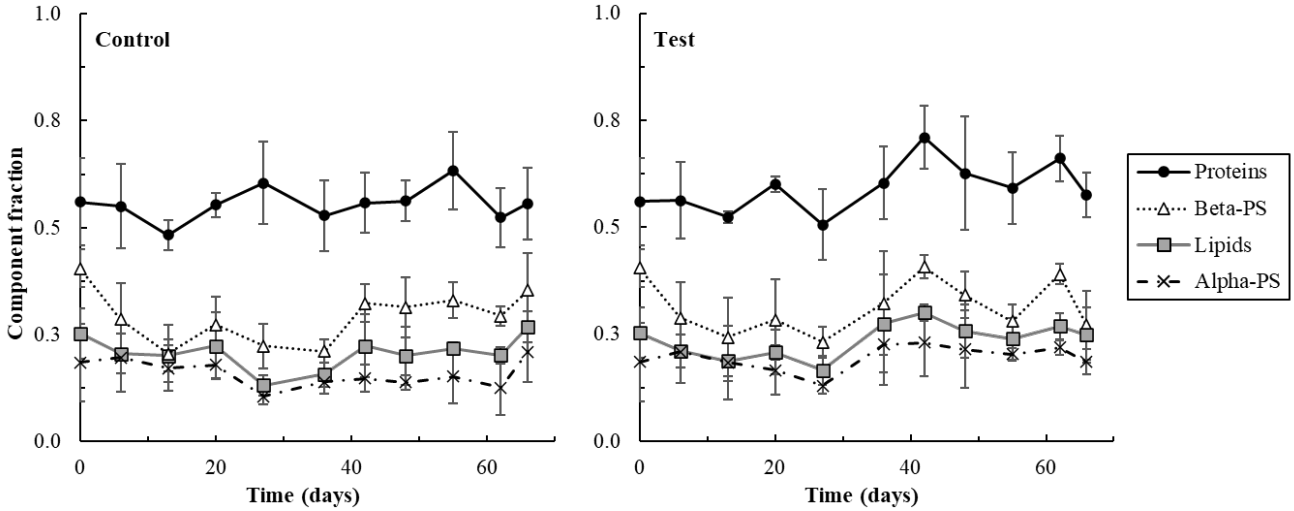

Figure C.9. Average fractions of various EPS components in granule sections versus time. Error bars represent the standard deviation of sections from triplicate granules. Triplicate sections from the same granule were also periodically analyzed for each EPS component and data followed trends similar to those shown above.

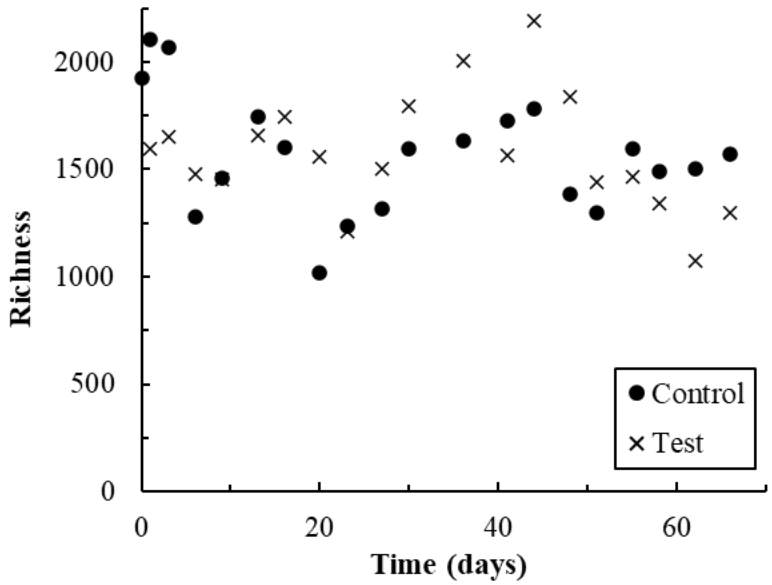

Figure C.10. Species' richness (as the number of active OTUs, or those with an rRNA to rDNA ratio greater than or equal to one) versus time in both SBRs.

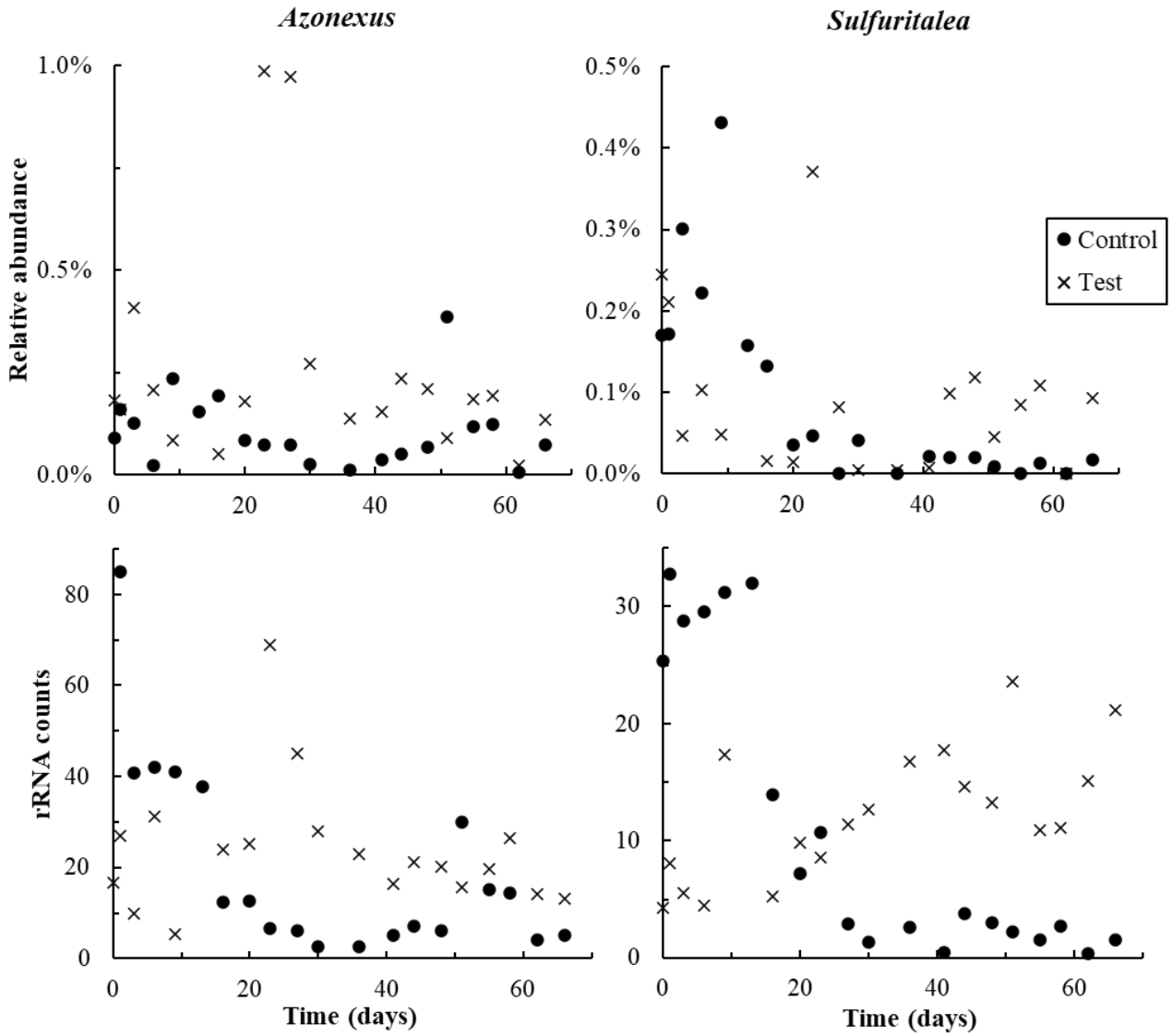

Figure C.11. Top row: the relative abundance of active *Azonexus* and *Sulfuritalea* species versus time in both SBRs. Bottom row: rRNA counts for phantom taxa belonging to *Azonexus* (left) and *Sulfuritalea* species (right) versus time. Note that y-axis scales differ for all plots to improve data visualization.

APPENDIX D

MISC. METHODS USED IN PRELIMINARY EXPERIMENTS

Starved AGS Batch Tests

Lab-grown AGS were stored in spent media at 4°C for 3-4 months before use in starved granule batch tests. Batch tests included DCF, ERY, and GEM as a mixture at 100, 250, 500, 1000, or 2000 µg/L each. For each condition, four glass bottles (triplicate samples plus one control) were prepared with 100 mL each of 30 mM HEPES buffer, pH 7.8. Thirty mL (settled volume) of starved AGS was added to all samples except controls to obtain a TSS concentration of approximately 13 g/L. Samples were shaken at 150 RPM at room temperature for 15 days. Periodically throughout the experiment, aqueous samples were filtered with 0.45 µm regenerated cellulose syringe filters and stored at 4°C for no longer than one week. Samples were analyzed via UPLC-QtoF-MS directly (ie., without extraction), via methods detailed in Chapter 2. Final samples taken on day 15 were extracted per methods in Chapter 2 to confirm that concentrations were below detection limits. Degradation products were also identified as described in Chapter 3.

TSS and VSS were evaluated with standard methods [149] at the beginning and end of the experiment and were on average 13.2 ± 2.1 g/L TSS (11.3 ± 1.8 g/L VSS) at day zero and 13.2 ± 1.4 g/L TSS (10.4 ± 1.1 g/L VSS) on day 10. Suspended solids concentrations on day 15 were not evaluated.

Average pharmaceutical concentrations versus time in all batch samples and controls are shown in Figure D.1. Data points at “t-2” reflect average concentrations in samples, prior to AGS inoculation, without any loss to the syringe filter; data points at “t-1” also reflect concentrations in media prior to AGS addition but after losses to the filter material. This analysis was performed to account for pharmaceutical losses to the syringe filter material.

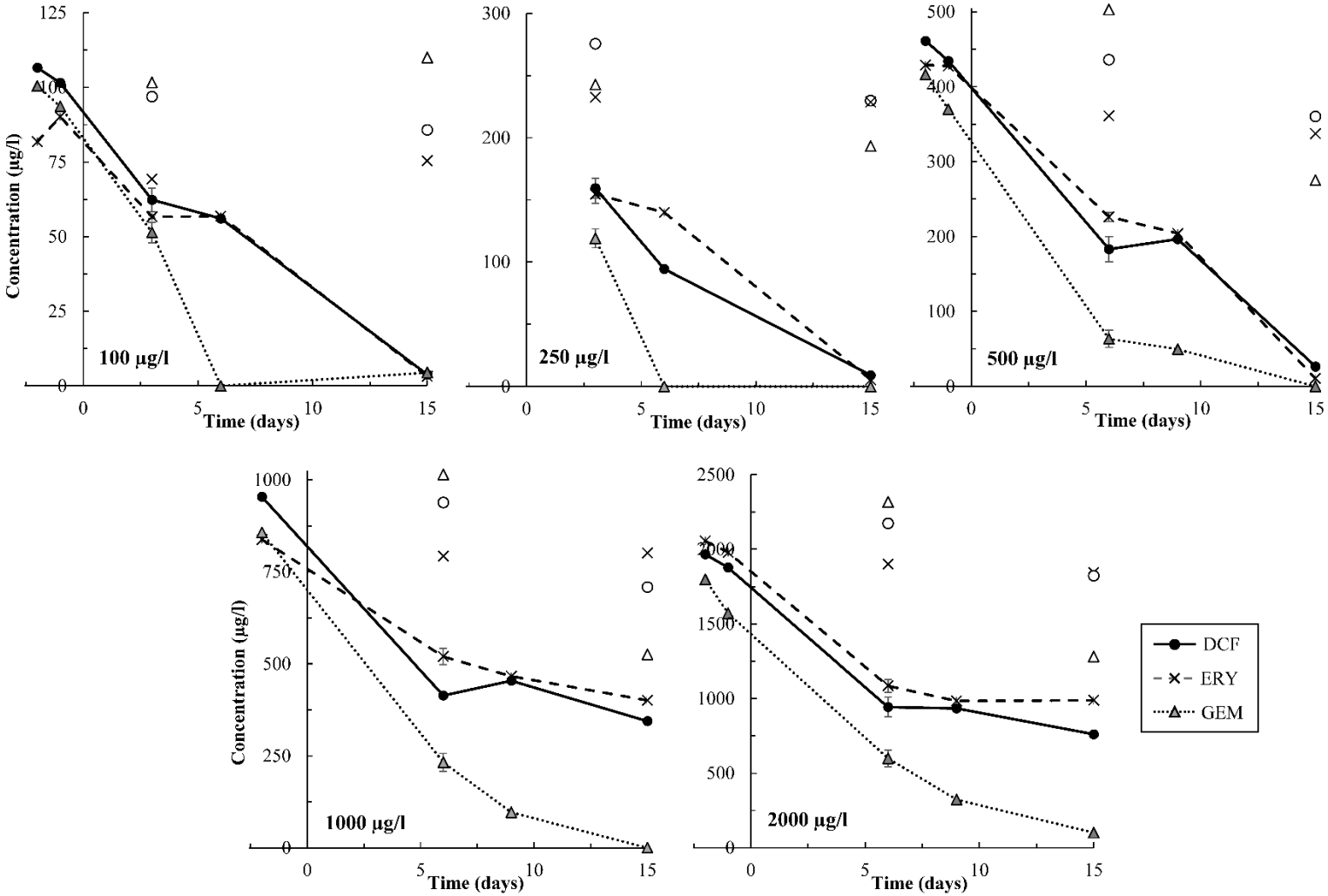

Figure D.1. Starved AGS batch tests results at all pharmaceutical concentrations. Open symbols with no connecting line indicate control samples. Sample data at "t-2" and "t-1" reflects the concentration in bottles without any loss to filter material or AGS as described in the text. These samples were not analyzed from the 250 ug/L triplicates simply to reduce the number of analyses needed.

Figure D.2 shows degradation products that were only detected on the last day of the test (day 15). ERY degradation proceeded furthest in samples with up to 500 µg/L ERY, evidenced by the presence of ERY2 as well as ERY1. This concurs with the complete ERY removal observed in these samples by day 15 (Figure D.1). DCF1 levels increased with the starting DCF dose. It is possible that DCF1 levels were significantly lower in samples with up to 500 µg/L DCF because DCF was completely removed in all of these samples, which suggests bacteria were capable of more complete degradation of DCF1 as well.

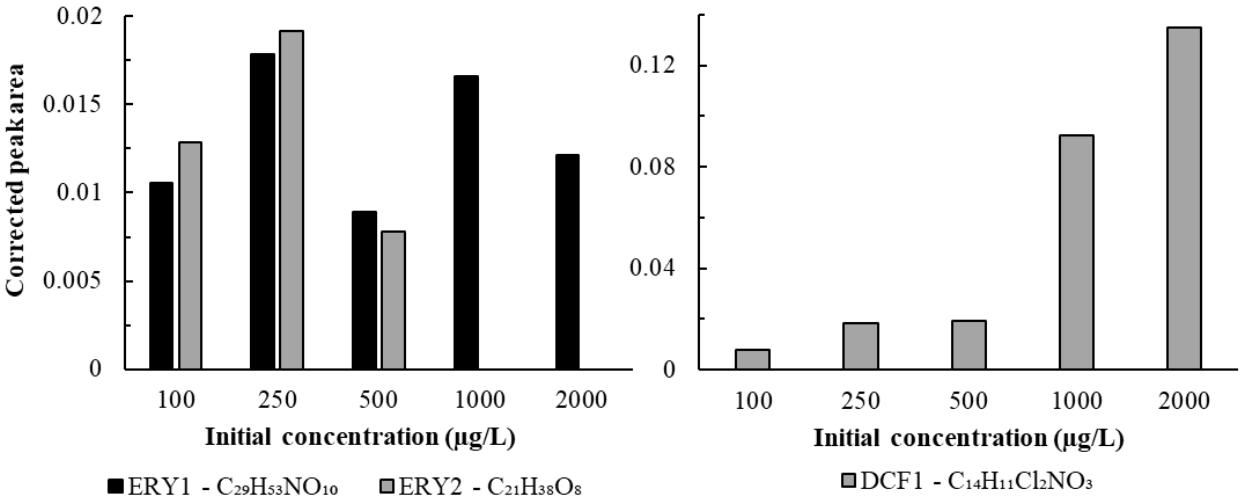

Figure D.2. Degradation products only detected on day 15 in starved AGS batch tests. Left, ERY-associated degradation products; right, DCF-associated degradation products. Note that y-axes both show corrected peak area but differ in scale. More detail on all molecules is provided in Chapters 4 and 6.

Only GEM degradation products were detected at multiple timepoints, as shown in Figure D.3. Relative concentrations of GEM3 increased with initial GEM concentrations, suggesting that more degradation products were formed with higher GEM doses. GEM5, or 4-methylcatechol, was only detected in this specific study, and is the fifth product formed per the degradation pathway proposed in [129]. Given the complete GEM removal observed under all

conditions in this test, and near-zero levels of GEM5 on day 15, we hypothesize that degradation of GEM5 to further intermediates likely occurred. These results indicate that GEM degradation in this test proceeded further than in any studies in Chapters 4-6, as only products associated with the third step in GEM degradation (GEM3) were detected in those studies.

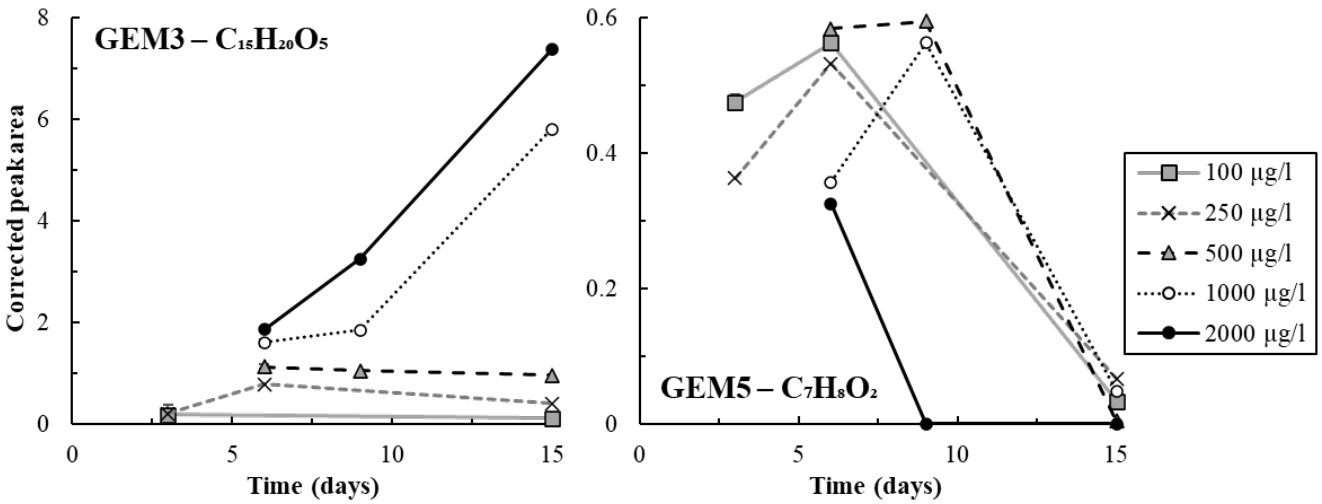

Figure D.3. GEM degradation products detected over time in starved AGS batch tests. Y-axes differ in scale, but both show corrected peak areas. GEM3 is discussed in more detail in Chapters 4 and 6; GEM5 was only detected in this study and is discussed in more detail in the above text.

Fluorescence in situ Hybridization (FISH)

FISH utilizes fluorescence principles similar to staining (discussed in Chapter 2); however, rather than binding a fluorophore to specific macromolecules, fluorophores pre-bound to DNA sequences are used to visualize specific bacteria. In short, a singled-stranded rDNA sequence tagged with a fluorophore ("probe") is introduced to the sample (in this case, a ~30 µm granule section on a microscope slide) in the presence of a precise mixture of salts, buffers, and formamide. Samples are pretreated to preserve morphology and permeabilize cell wells, which allows probes to enter cells. The rDNA probe then hybridizes to a complementary sequence of ribosomal RNA (rRNA) in the sample. Probes are designed to bind to rRNA sequences unique to

certain bacteria and can be specific down to the species level. After hybridization for several hours, unbound probes are washed out of the sample, and the sample can be visualized with CLSM.

rRNA-targeted probes were used in this research because their brightness increases in proportion to the number of ribosomes—cells that were active prior to preservation will have more ribosomes, resulting in more probe binding, and thus a brighter fluorescent signal. In contrast, DNA-targeted probes bind to complimentary DNA sequences, which will allow detection of any cells containing the complimentary DNA sequence. DNA is much more stable than rRNA, therefore usage of DNA-targeted probes will result in visualization of all cells containing complimentary sequences in the sample, active or not. As our goal was to track the effects of pharmaceuticals on active bacteria in AGS, rRNA-targeted probes were used. Table D.1 lists all probes used; methods are detailed in [196].

Table D.1. FISH probes used in preliminary experiments, discussed in Chapter 7. *Indicates dual-labelled probe as described in [197].

Mixture	Probe	Target	Fluorophore	Sequence (5' – 3')	Reference
EUB mix	EUB i	Most bacteria	Fluos	GCT GCC TCC CGT AGG AGT	[198]
	EUB ii	*Planctomycetes*		GCA GCC ACC CGT AGG TGT	[199]
	EUB iii	*Verrucomicrobiales*		GCT GCC ACC CGT AGG TGT	[199]
Nitrifier mix	NSO 1225	Betaproteobacterial ammonia oxidizing bacteria (AOB)	Cy3	CGC CAT TGT ATT ACG TGT GA	[200]
	Ntspa662	*Nitrospira* (NOB)		GGA ATT CCG CGC TCC TCT	[201]
	NIT3	*Nitrobacter* (NOB)		CCT GTG CTC CAT GCT CCG	[202]
PAO mix	PAO462	Most *Candidatus* Accumulibacter phosphatis	Cy5	CCG TCA TCT ACW CAG GGT ATT AAC	[203]
	PAO651	Most *Accumulibacter*		CCC TCT GCC AAA CTC CAG	[203]
	PAO846	Most *Accumulibacter*		GTT AGC TAC GGC ACT AAA AGG	[203]
GAO mix	GB_G2	Some *Competibacter*	Cy3-Cy5*	TTC CCC AGA TGT CAA GGC	[204]
	GAOQ989	Some *Competibacter*		TTC CCC GGA TGT CAA GGC	[205]
	GAOQ431	Some *Competibacter*		TCC CCG CCT AAA GGG CTT	[205]

APPENDIX E

LABVIEW PROGRAM CODE USED FOR SBR CONTROL

Please see the attached LabVIEW file, titled “App_E_KBodle_AGS_SBR.vi”.